AD-A162 706 PHANTOM DOSIMETRY CALCULATIONS FOR USE IN RADIATION EFFECTS CORRELATIONS(U) SCIENCE APPLICATIONS INC SCHAUMBURG IL D C KAUL ET AL. 30 JUL 84 SAI-84-1706 1/2

UNCLASSIFIED DNA-TR-83-51 DNA001-83-C-0187 F/G 6/18 NL

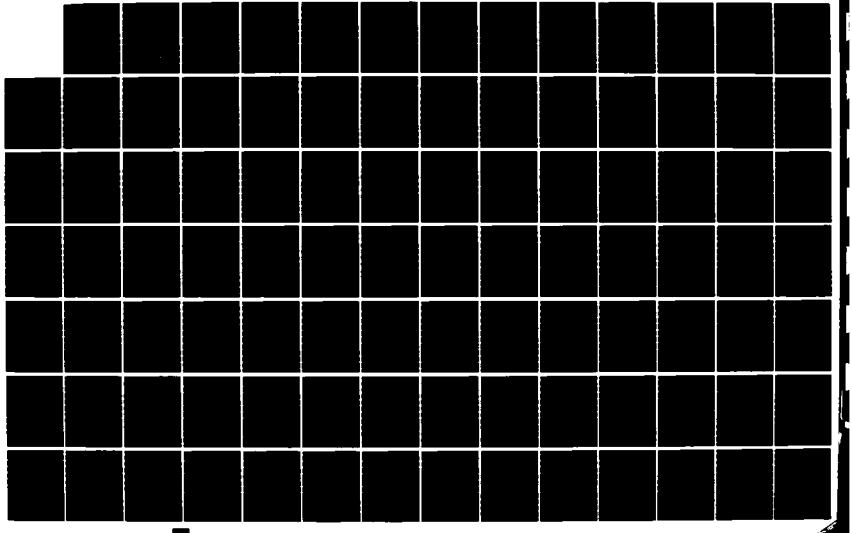

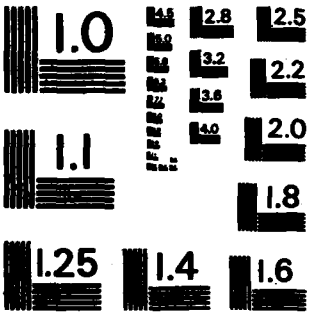

MICROCOPY RESOLUTION TEST CHART
NATIONAL BUREAU OF STANDARDS-1963-A

AD-A162 706

E 301 852

(2)

DNA-TR-83-51

PHANTOM DOSIMETRY CALCULATIONS FOR USE IN RADIATION EFFECTS CORRELATIONS

Dean C. Kaul
James A. Roberts
Stephen D. Egbert
Science Applications, Inc.
One Woodfield Place Building
1701 E. Woodfield Road
Schaumburg, IL 60195-5160

30 July 1984

Technical Report

CONTRACT No. DNA 001-83-C-0187

Approved for public release;
distribution is unlimited.

THIS WORK WAS SPONSORED BY THE DEFENSE NUCLEAR AGENCY
UNDER RDT&E RMSS CODE B350083466 U99QMXMK00056 H2590D.

DTIC FILE COPY

Prepared for
Director
DEFENSE NUCLEAR AGENCY
Washington, DC 20305-1000

DTIC
ELECTE
DEC 19 1985
S D
B

85

Destroy this report when it is no longer needed. Do not return to sender.

PLEASE NOTIFY THE DEFENSE NUCLEAR AGENCY, ATTN: STTI, WASHINGTON, DC 20305-1000, IF YOUR ADDRESS IS INCORRECT, IF YOU WISH IT DELETED FROM THE DISTRIBUTION LIST, OR IF THE ADDRESSEE IS NO LONGER EMPLOYED BY YOUR ORGANIZATION.

UNCLASSIFIED
SECURITY CLASSIFICATION OF THIS PAGE

REPORT DOCUMENTATION PAGE

1a REPORT SECURITY CLASSIFICATION UNCLASSIFIED	1b RESTRICTIVE MARKINGS
2a SECURITY CLASSIFICATION AUTHORITY	3 DISTRIBUTION / AVAILABILITY OF REPORT Approved for public release; distribution is unlimited.
2b DECLASSIFICATION / DOWNGRADING SCHEDULE N/A since UNCLASSIFIED	
4 PERFORMING ORGANIZATION REPORT NUMBER(S) SAI-84/1706	5 MONITORING ORGANIZATION REPORT NUMBER(S) DNA-TR-83-51
6a NAME OF PERFORMING ORGANIZATION Science Applications, Inc 6b OFFICE SYMBOL (If applicable)	7a NAME OF MONITORING ORGANIZATION Director Defense Nuclear Agency
6c ADDRESS (City, State, and ZIP Code) 1 Woodfield Place Building 1701 E. Woodfield Road Schaumburg, IL 60195-5160	7b ADDRESS (City, State, and ZIP Code) Washington, DC 20305-1000
8a NAME OF FUNDING / SPONSORING ORGANIZATION 8b OFFICE SYMBOL (If applicable)	9 PROCUREMENT INSTRUMENT IDENTIFICATION NUMBER DNA 001-83-C-0187
8c ADDRESS (City, State, and ZIP Code)	10 SOURCE OF FUNDING NUMBERS PROGRAM ELEMENT NO: 62715H; PROJECT NO: U99QMXM; TASK NO: K; WORK UNIT ACCESSION NO: DH006904

11 TITLE (Include Security Classification)
PHANTOM DOSIMETRY CALCULATIONS FOR USE IN RADIATION EFFECTS CORRELATIONS

12 PERSONAL AUTHOR(S) Dean C. Kaul, James A. Roberts, Stephen D. Egbert

13a TYPE OF REPORT	13b TIME COVERED	14 DATE OF REPORT (Year Month Day)	15 PAGE COUNT
Technical Report	FROM 830401 TO 840730	1984 July 30	168

16 SUPPLEMENTARY NOTATION
This work was sponsored by the Defense Nuclear Agency under RDT&E RMSS Code B350083466 U99QMXMK00056 H2590D.

17 COSATI CODES			18 SUBJECT TERMS (Continue on reverse if necessary and identify by block number)		
FIELD	GROUP	SUB-GROUP	Phantom	Gamma Ray	Macaca Mulatta
6	18		Dosimetry	Neutron	Radiation Transport
20	8		KERMA	Rhesus Monkey	TRIGA REACTOR

19 ABSTRACT (Continue on reverse if necessary and identify by block number)

Models corresponding to an adult Rhesus Monkey and a simple analogue have been created in combinatorial geometry for use in Monte Carlo radiation transport calculations. The complex monkey phantom is based on anatomical measurements of a sectioned cadaver. The simple phantom is cylindrical with a sperical head. Adjoint Monte Carlo calculations were performed to obtain the energy-and angle-differential adjoint fluence for the mid-head, mid-thorax locations in both phantoms and active marrow in the complex monkey phantom. The results have also been convoluted with free-field spectra for two TRIGA reactor exposure room configurations at the Armed Forces Radiobiological Research Institute, using the VCS code system. Comparisons are made between calculated and measured KERMA values in the simple phantom. Good agreement is obtained. However, it is found that good agreement cannot be obtained using simple scalar coupling.

20 DISTRIBUTION / AVAILABILITY OF ABSTRACT	21 ABSTRACT SECURITY CLASSIFICATION	
☐ UNCLASSIFIED/UNLIMITED ☒ SAME AS RPT ☐ DTIC USERS	UNCLASSIFIED	
22a NAME OF RESPONSIBLE INDIVIDUAL Betty L. Fox	22b TELEPHONE (Include Area Code) (202) 325-7042	22c OFFICE SYMBOL DNA/STTI

DD FORM 1473, 84 MAR — 83 APR edition may be used until exhausted. All other editions are obsolete.

SECURITY CLASSIFICATION OF THIS PAGE
UNCLASSIFIED

18. SUBJECT TERMS (Continued)

Morse	Mid-Head	Adjoint Monte Carlo
VCS	Mid-Thorax	
Monte Carlo	Active Marrow	

PREFACE

This research was conducted according to the principles enunciated in the "Guide for Laboratory Animal Facilities and Care," prepared by the National Academy of Sciences, National Research Council.

Accession For
NTIS GRA&I ☑
DTIC TAB ☐
Unannounced ☐
Justification
By
Distribution/
Availability Codes
Dist | Avail and/or Special
A-1

QUALITY INSPECTED 3

TABLE OF CONTENTS

LIST OF ILLUSTRATIONS

LIST OF TABLES

SECTION 1

INTRODUCTION

Since the mid 60's, extensive studies have been carried out by the Armed Forces Radiobiological Research Institute (AFRRI) and other military organizations to examine the effects of intermediate to high doses of ionizing radiation on mammals. The intent of these studies has been to acquire information on lower order mammals, which might be extrapolated to man. Particularly extensive studies have been carried out using the rhesus monkey (Macaca mulatta) and the AFRRI TRIGA reactor exposure facility. The purpose of the work described in this report is to duplicate these studies by analytical means. This is done in order to provide spectral detail not available from common integral measurement techniques and to obtain dosimetry data for locations not amenable to measurements.

Studies of effects of ionizing radiation on the rhesus monkey have involved post-exposure performance testing and assessments of mortality incidence. These effects have been correlated with dosimetric quantities which are thought to be relevant to the effect in question if not to have a causal relationship. Dose to the mid-head has generally been associated with degradation in performance or with incapacitation, while dose to a point at the mid-thorax has generally been associated with mortality incidence.

It is generally recognized that the threshold dose which has a causal relationship to mammalian mortality is that which is deposited in the active marrow.[1] It has also been theorized that incapacitation may be related to some dose other than mid-head. Of course the reason why the mid-head and mid-thorax doses have remained in vogue for correlation purposes is that they represent well defined and relatively unambiguous locations at which all types of measurements can be conveniently made. On the other hand it would require a distribution of detectors throughout an accurate phantom or cadaver to measure dose to marrow. Such experiments are difficult and inconvenient to perform and are restrictive as to the types of detectors that can be used, due to size limitations.

PREVIOUS PAGE IS BLANK

Because of the practical limitations on dose measurements, analytical methods for obtaining the dosimetric quantities of interest have been examined with some success. In an earlier study[2] neutron and gamma spectra were obtained in simple geometries by experimental and analytical means and compared. In the study described herein this work has been extended to include analysis of radiation transmission within a detailed rhesus monkey phantom.

The phantom has been developed based on anatomical measurements of a rhesus monkey cadaver. These measurements have been incorporated into a three-dimensional mathematical model through the use of combinatorial geometry. This is a system by which complex objects may be constructed analytically through the combination of simple shapes. Combinatorial geometry is interpreted for radiation transport analysis using the three-dimensional Monte Carlo code MORSE.[3]

Calculations of the transport of neutron and gamma radiation within the monkey phantom due to such radiation externally incident on the phantom, particularly that of the AFRRI TRIGA reactor, have been performed and are described herein. The calculations include the mid-head, mid-thorax and active marrow as analytical detector locations with exposure in two TRIGA exposure room configurations. A companion set of calculations for the mid-head and mid-thorax locations has been performed for a simple phantom. This has been done in order to allow validation and verification of the analytical method by means of comparison with experiment.

The balance of this report describes the development of the realistic (complex) rhesus monkey phantom and its simple analogue. It also describes the calculations of radiation transport in the complex and simple phantom and presents the results in graphical and tabular form. Finally, the report describes the results of validation and verification studies of these calculated values as performed to date.

SECTION 2

RHESUS MONKEY PHANTOM

This section of the report describes the development of specifications for a complex three-dimensional rhesus monkey phantom and its simple analogue.

2.1 Complex Geometry Phantom

Science Applications, Inc., has developed a complex computational model of an adult rhesus monkey in three dimensions, including detailed representations of lung, skeletal and soft tissue. The model has been produced using the combinatorial geometry module of the MORSE Monte Carlo radiation transport code and is represented pictorially herein using the GIFT code.[4] Combinatorial geometry is a system for representing complex shapes by means of combinations of simple shapes or "bodies" understood individually by the computer program. The bodies are assembled into regions, such as the lungs, skeleton and soft tissue of an anthropomorphic phantom. Certain limitations apply to this process which should be explained to the reader before describing the model and its basis. First, the process of computing radiation transport through the model media requires that the crossing of all boundaries between bodies be accounted for. This must be done in order for the code to know the location of the radiation particle and also to know the nature of the material through which it has passed. Such an accounting process is time consuming. Thus, in order for the transport program to operate efficiently the number of bodies which are used to represent an object should be kept to a minimum consistent with a reasonable level of physical accuracy. Second, the shapes of the bodies understood in combinatorial geometry have some limitations. The most important of these are 1) that an ellipsoid must be rotational about one axis and 2) that elliptical cylinders and truncated elliptical cones must have their upper and lower bases in proportion to one another, i.e., the ratio of the minor to major axis must be the same for the upper and lower bases. With these limitations in mind the monkey phantom model can now be described.

2.1.1 Phantom Dimensions

The monkey phantom has been developed based on anatomical measurements of a rhesus monkey cadaver. Such measurements were made from true scale photographs portraying the upper surfaces of lateral cross sections of the monkey, taken at approximately 3 cm intervals. Dimensions of the monkey, taken before and after sectioning, are given in Tables 1 and 2, along with equivalent values from the phantom model.

The model was designed to correspond to the plan view of the photographed sections and the sum of their thicknesses. Consequently, given the effect of roundoff error and irregular sections, the model is two centimeters shorter, crown to tailbone, than the measurement of the intact subject. The lengths of the limbs were modeled to correspond to internal measurements, joint to joint, and are similar to but not exactly the same as the limb lengths measured externally. Hands and feet have been omitted from the model, since they represent little mass and contain little material of dosimetric interest. The partial body lengths are approximate, particularly since the model has no explicitly designated chin or mandible. Instead, the base of the chin in the model has been taken to be the top of the neck, and the crown-mandible length is taken to the maximum minor diameter of the elliptical head of the model.

The model is slightly smaller than the prototype subject based on the external dimensions, including circumferences of the torso at two points. However, comparisons of the principal dimensions of the individual sections with those of the model indicate very close agreement between the two. The locations of these sections are depicted in Figures 1 (frontal view, Azimuth 0.0^{o}, Elevation 0.0^{o})) and 2 (side view, Azimuth 90^{o}, Elevation 0.0^{o}). They are described in terms of their height above the pad or the rump of the monkey, and are given as width (distance side to side) and depth (mid-sagital) dimensions normal to the length of the animal.

Views of the cross sectional surfaces, looking downward from the level of the section (Azimuth 0.0^{o}, Elevation 90.0^{o}), are provided in Figures 3 through 19, which correspond to each of the sections listed in Table 2. It can be seen from

the Figures that the torso of the model is made up of concentric cylinders and cones, some elliptical. The shoulder region is constructed using additional elliptical cones which overlap those which make up the torso.

Figures 20 through 23 show various views of the phantom. The phantom posture and orientation of the limbs have been designed to correspond to those of the monkey in a restraint chair.

Figures 3 through 19 also show skeletal and lung detail corresponding to that found in the section photographs. The three dimensional representation of this detail is shown in Figures 24 through 27.

The volumes of the lungs, skeletal and soft tissue regions are 124, 370, and 4768 cubic centimeters, respectively, as determined by GIFT. Assuming that densities of equivalent human regions apply to the monkey (lung: 0.296, skeleton: 1.40 and soft tissue: 1.04 g/cc[5]) the total mass of the model is 5.513 kg. This mass is consistent with rhesus monkeys of the general dimensions of the study subject as reported in published data.[6] According to these data, a monkey of 36 to 42 months in age, having length (head/buttocks) of 47.4 cm, may be expected to have a mass of 5.2 kilograms. The subject monkey is between 51 and 53 cm in length, having other dimensions on a similar scale relative to that published and, thus, may be expected to have a slightly larger mass, as is indeed the case.

Although the 5.5 kilogram mass can be justified as representative of the particular monkey being modeled based on available cadaver data, it is nevertheless at the high end for experimental subjects used at AFRRI as shown in Table 3. Therefore, SAI was directed by the sponsor to adjust the mass of the monkey to be approximately 3.4 kg, which is near the middle of the size range of subjects previously used at AFRRI and more of typical of modern subjects. After studying data on the rhesus monkey anatomy, as referred to previously, it was confirmed that the linear dimensions of the monkey were proportional to the cube root of the mass. The only complication in this was the fact that the proportionality for the head was found to differ from that of the remainder of the monkey in that head displayed less size variation with monkey mass. Constants of proportionality were determined for both monkey regions based on the two monkey

Table 1. Specifications of subject, as measured prior to sectioning, and model

Description		Measure (cm) Subject	Model
Top of Crown - Tailbone		53	51
Tip of Finger - Point of Elbow		23	14 (ulna)
Elbow - Humeral/Scapula Joint		16	13 (humerus)
Point of Ankle - Knee		17	15 (tibia)
Knee - Pelvis		13	14 (femur)
Base of Chin - Mid Pelvis		33	32
Crown - Lower Edge of Mandible		11	9 (head minor dia.)
Abdominal Circumference	Upper (Chest)	39	36 @ Z = 25.5 cm*
	Lower (Waist)	33	31 @ Z = 13.5 cm*
Mass (Kg)		4.0	5.5

*relative to pad (seat)

Table 2. Dimensions of section upper surfaces

Height above pad (cm)	Dimensions (cm) Subject Width	Subject Depth	Model Width	Model Depth
3	9.1	5.3	9.1	6.8
6	11.3	8.5	11.5	8.5
9	12.0	10.0	11.5	9.5
12	10.8	9.6	11.5	9.5
15	10.5	10.6	10.3	10.3
18	11.2	11.4	11.0	11.0
21	11.9	11.8	11.8	11.8
24	11.5	11.5	11.6	11.6
27	11.1	11.5	11.4	11.4
30	11.8	11.4	11.2	11.2
33 @ mid depth	11.5	10.9	11.0	11.0
33 max	15.2		13.4	
37 @ mid depth	12.1	8.2	12.2	8.1
37 max	13.2		12.8	
40 @ mid depth	8.0	5.5	8.4	6.
40 max	9.3		9.0	
42	no data available		4.5	4.5
45	8.0	11.5	7.9	9.8
48	8.5	10.0	7.9	9.8
50	5.0	6.5	5.4	5.6
Total Section Thickness	51		51	

Table 3. Specifications of age and mass for rhesus monkeys used in AFRRI experiments, 1966 to 1973

Report No.	No. of Subjects	Age Range (Mo.)	Mass (Kg.)
SR66-2	131	24 - 48	3.0 - 5.3
SP66-23	190	24 - 60	3.1 - 5.5
SR68-16	6	*	3.8 - 5.6
SR69-1	6	*	4.3 - 5.7
SR69-2	6	*	3.2 - 4.9
SR69-8	6	*	4.1 - 5.7
SR69-9	6	41 - 67	4.9 - 6.0
SR69-14	6	46 (mean)	4.7 - 5.9
SR69-18	30	*	3.0 - 5.0
SR69-21	14	*	3.5 - 5.0
SR70-7	7	*	4.2 - 5.2
SR70-11	71	*	3.0 - 5.0
SR71-3	14	18 - 48	2.7 - 4.6
SR71-6	10	30 (mean)	2.5 - 3.7
SR71-10	6	*	3.0 - 5.0
SR72-14	8	*	*
SR72-19	85	18 - 50	2.1 - 5.3
SR73-1	88	15 - 51	2.4 - 5.3
Subject-weighted average mass range:			2.7 - 5.3

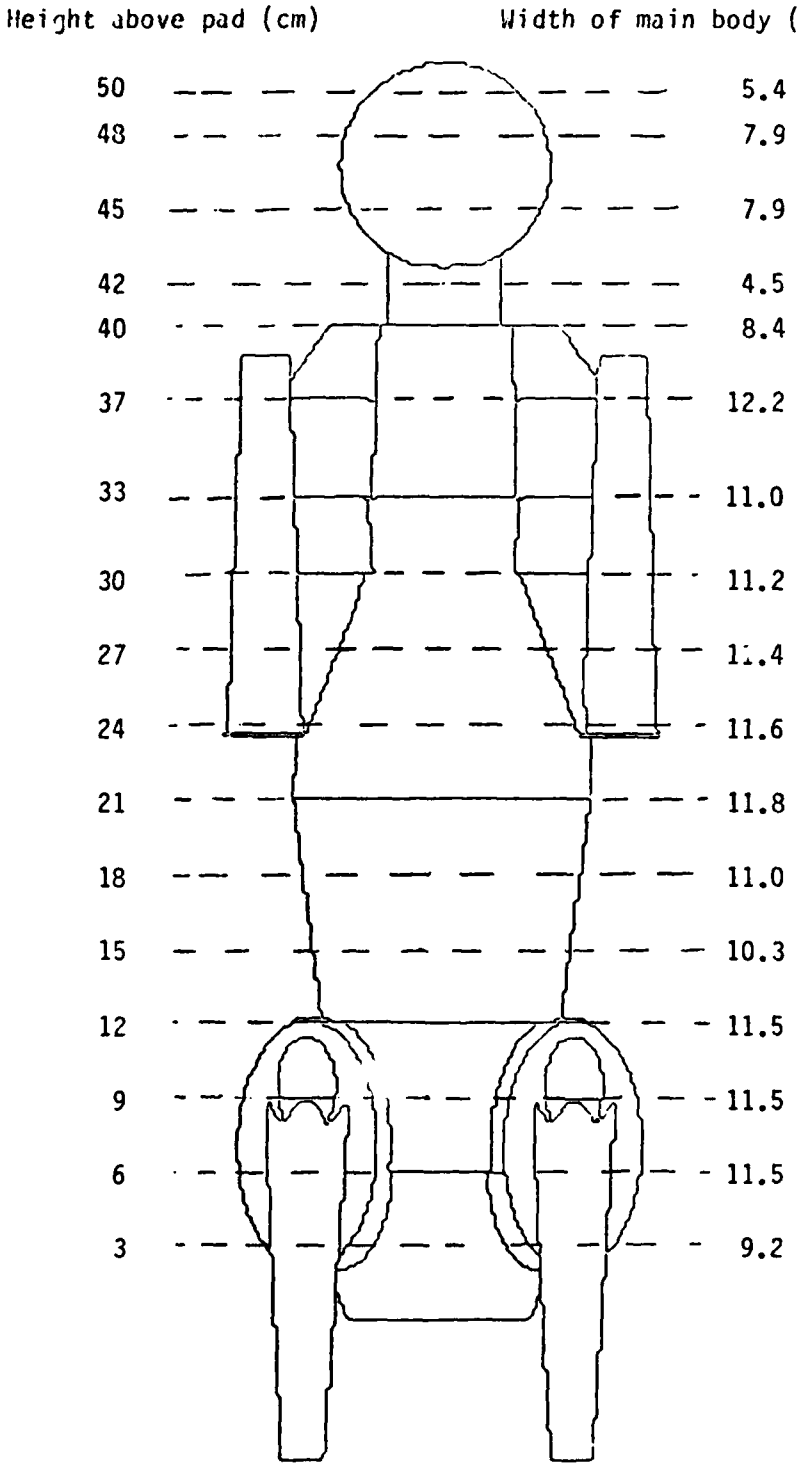

Figure 1. Locations of cross sections, frontal view
azimuth 0.0^{o} elevation 0.0^{o}

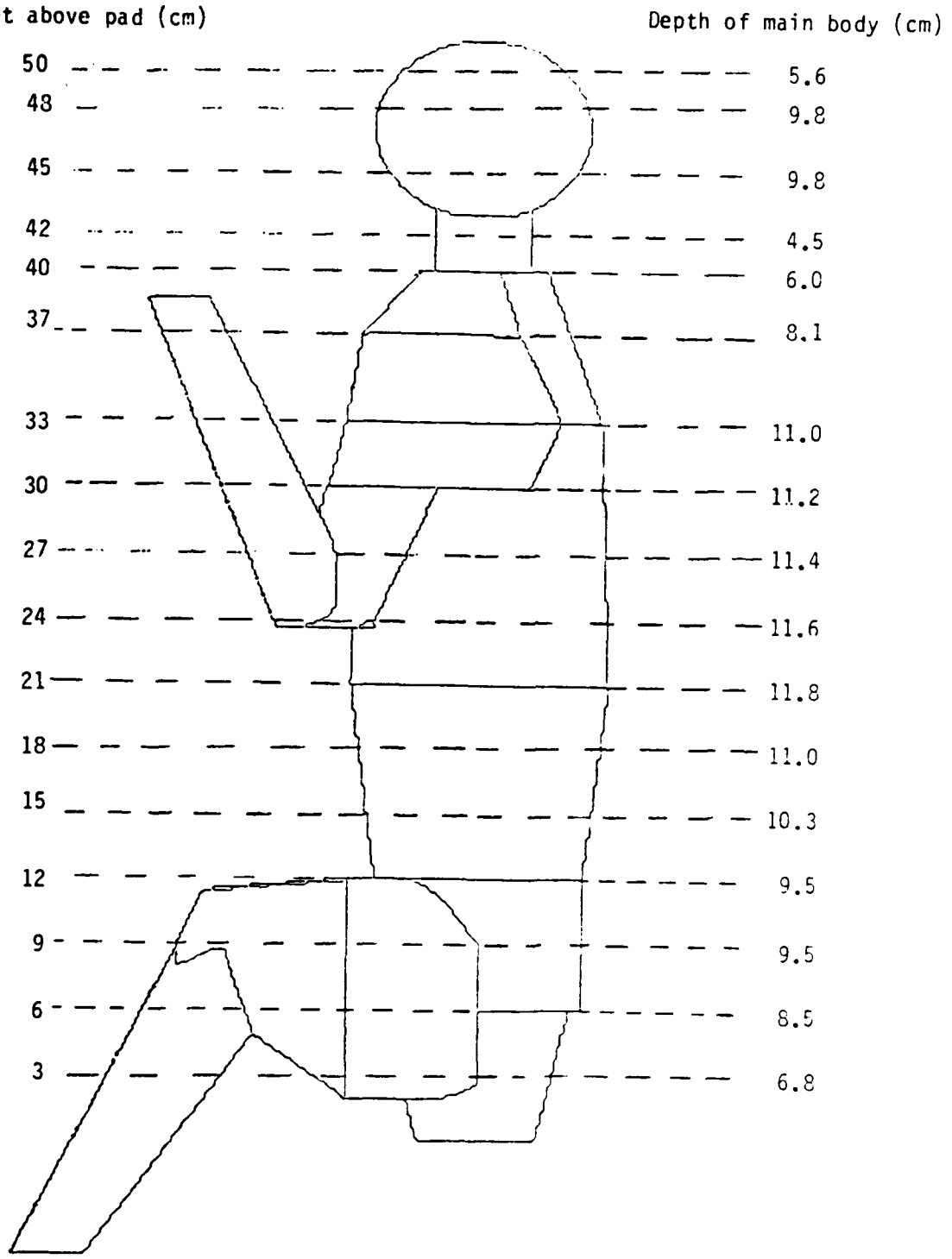

Figure 2. Location of cross sections, side view
azimuth 90.0^{o} elevation 0.0^{o}

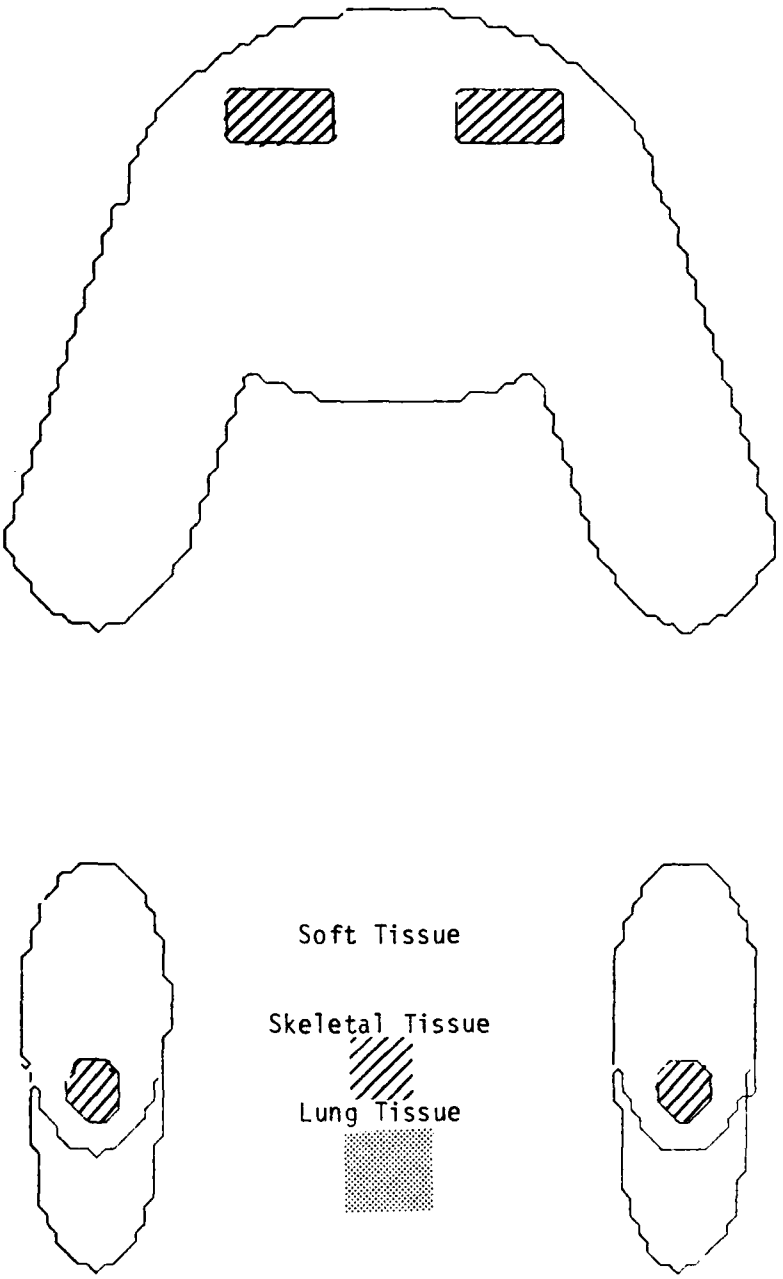

Figure 3. Monkey phantom cross section, Z = 3.0 cm
azimuth 0.0^{o} elevation 90.0^{o}

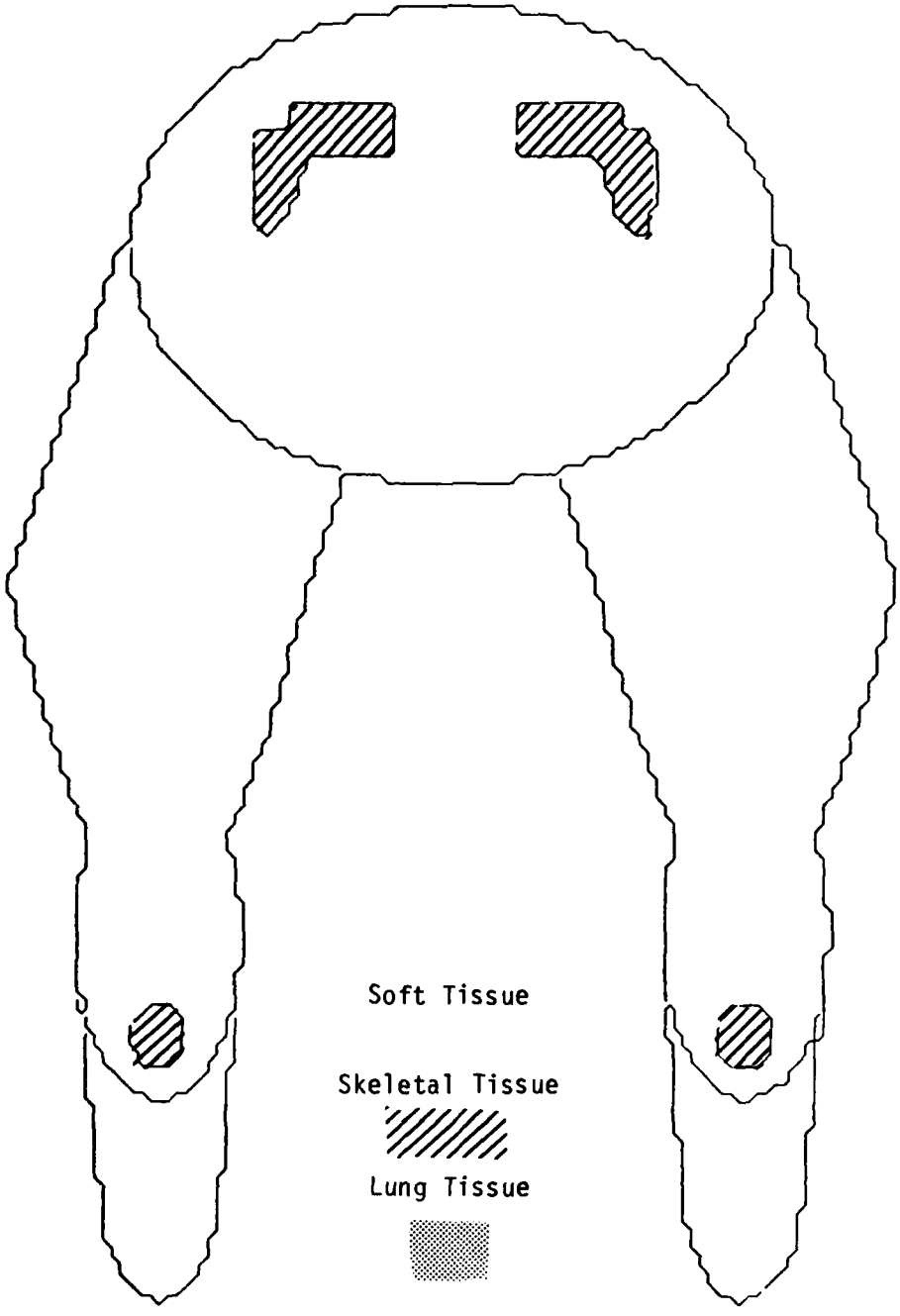

Figure 4. Monkey phantom cross section, Z = 6.0 cm
azimuth 0.0^{o} elevation 90.0^{o}

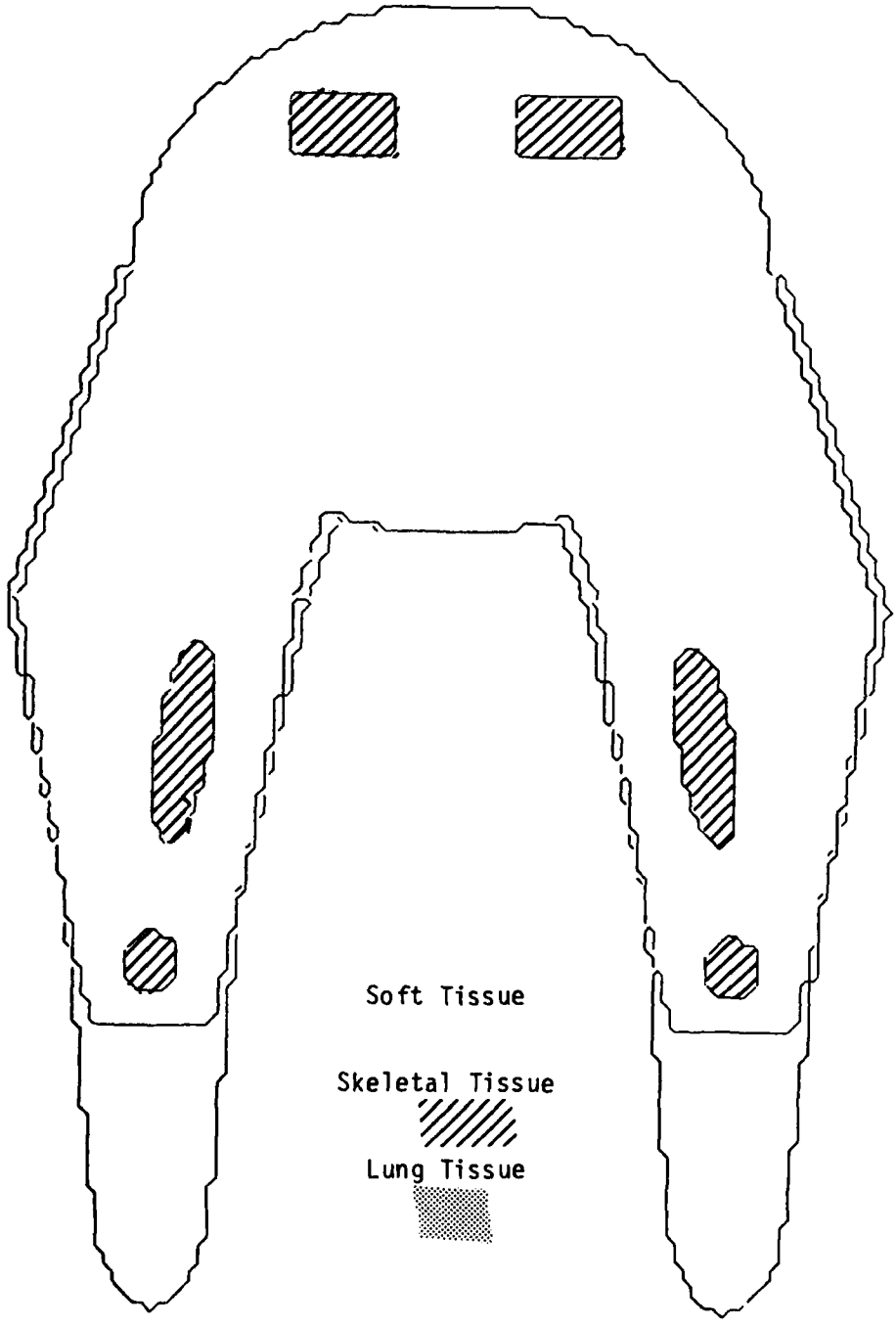

Figure 5. Monkey phantom cross section, Z = 9.0 cm
azimuth 0.0^{o} elevation 90.0^{o}

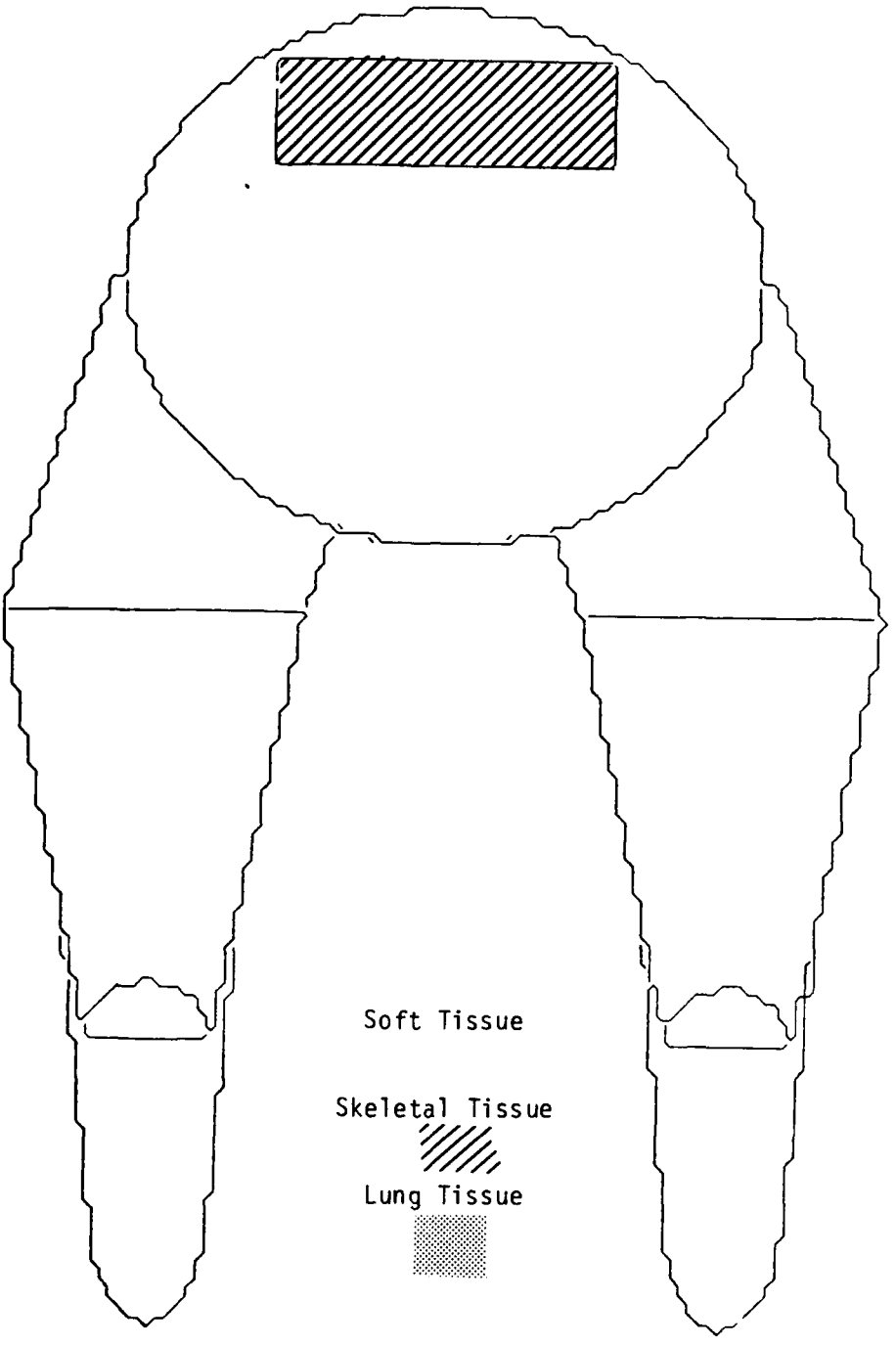

Figure 6. Monkey phantom cross section, Z = 12.0 cm
azimuth 0.0^{o} elevation 90.0^{o}

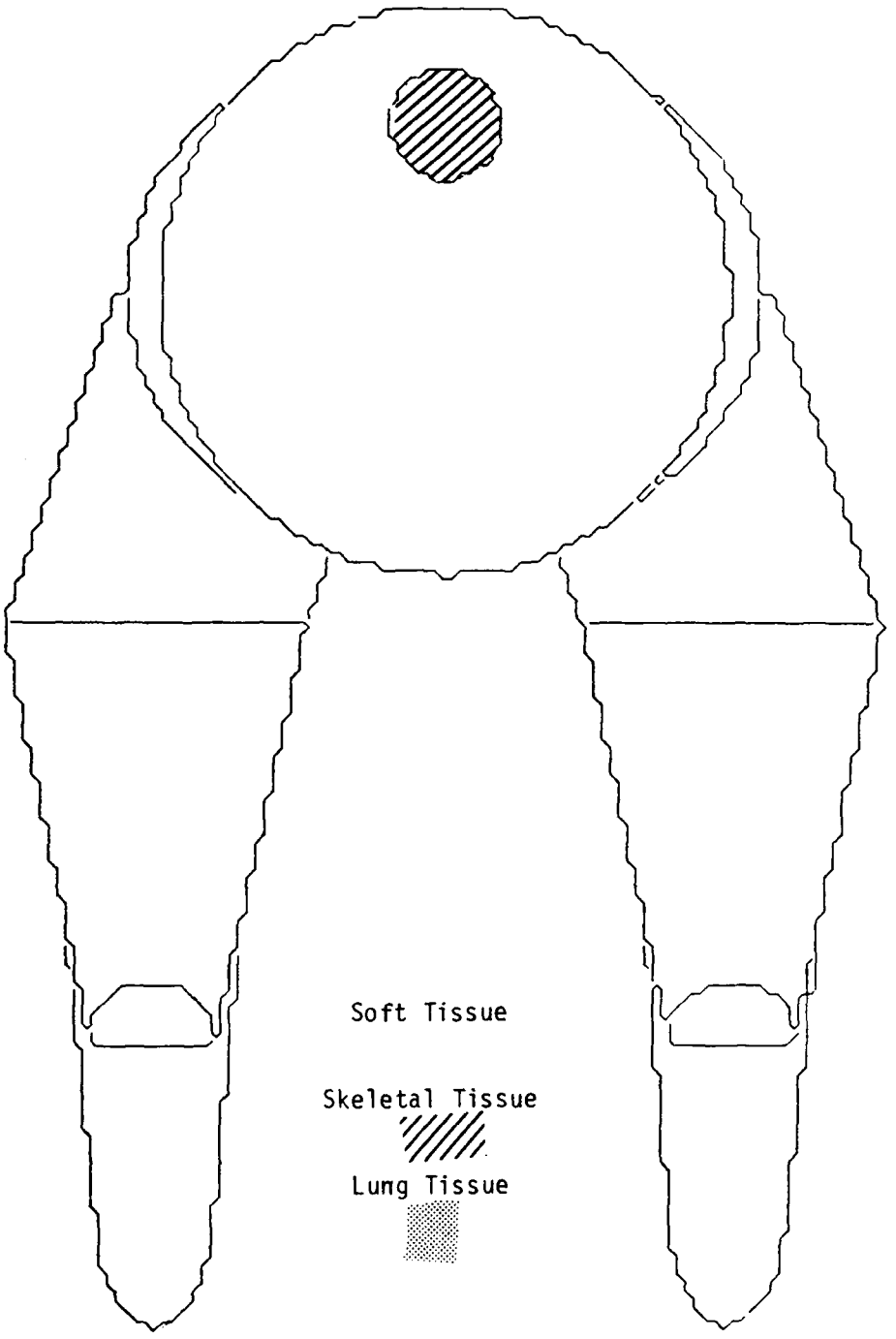

Figure 7. Monkey phantom cross section, Z = 15.0 cm
azimuth 0.0^{o} elevation 90.0^{o}

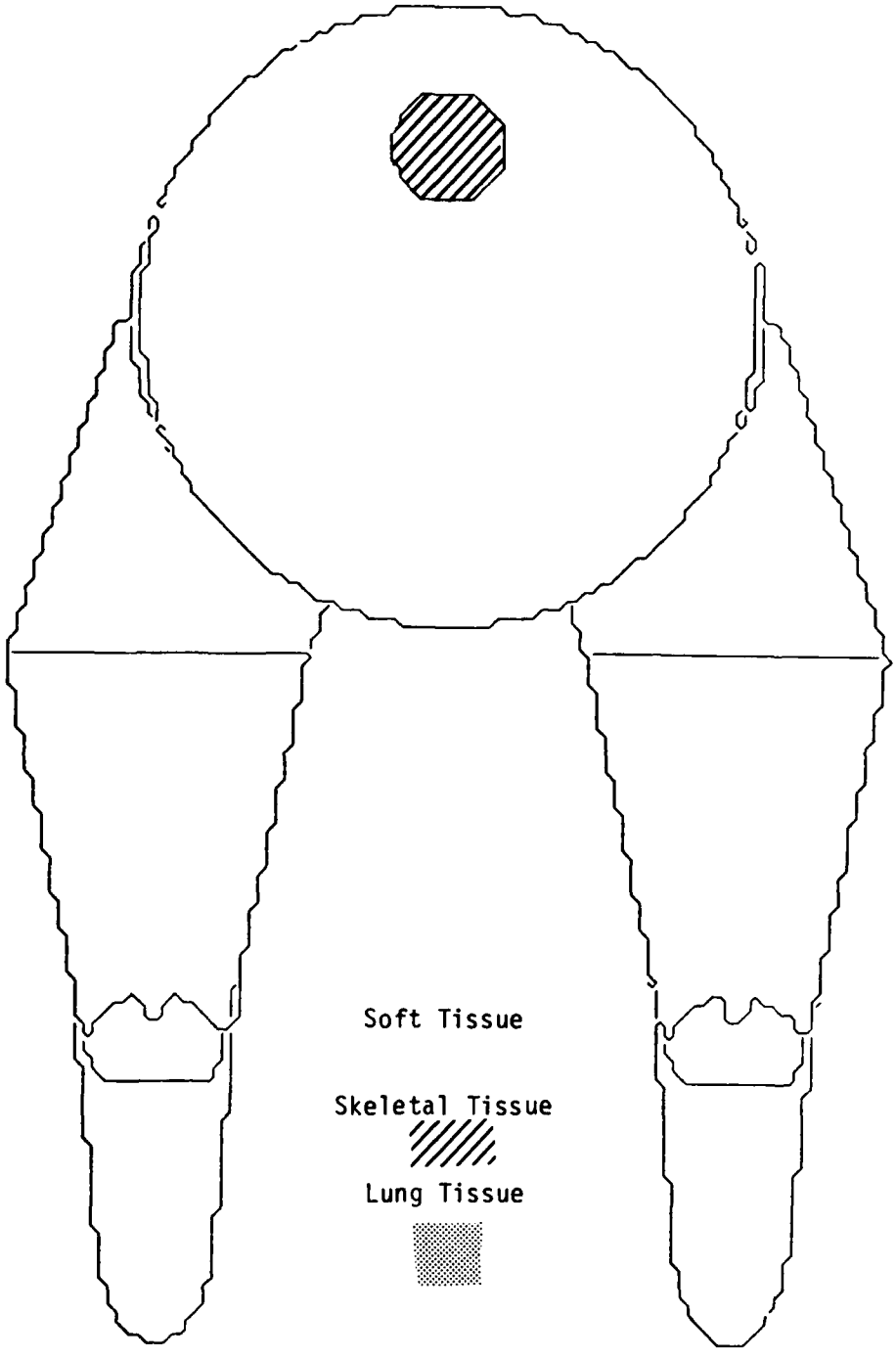

Figure 8. Monkey phantom cross section, Z = 18.0 cm
azimuth 0.0^{o} elevation 90.0^{o}

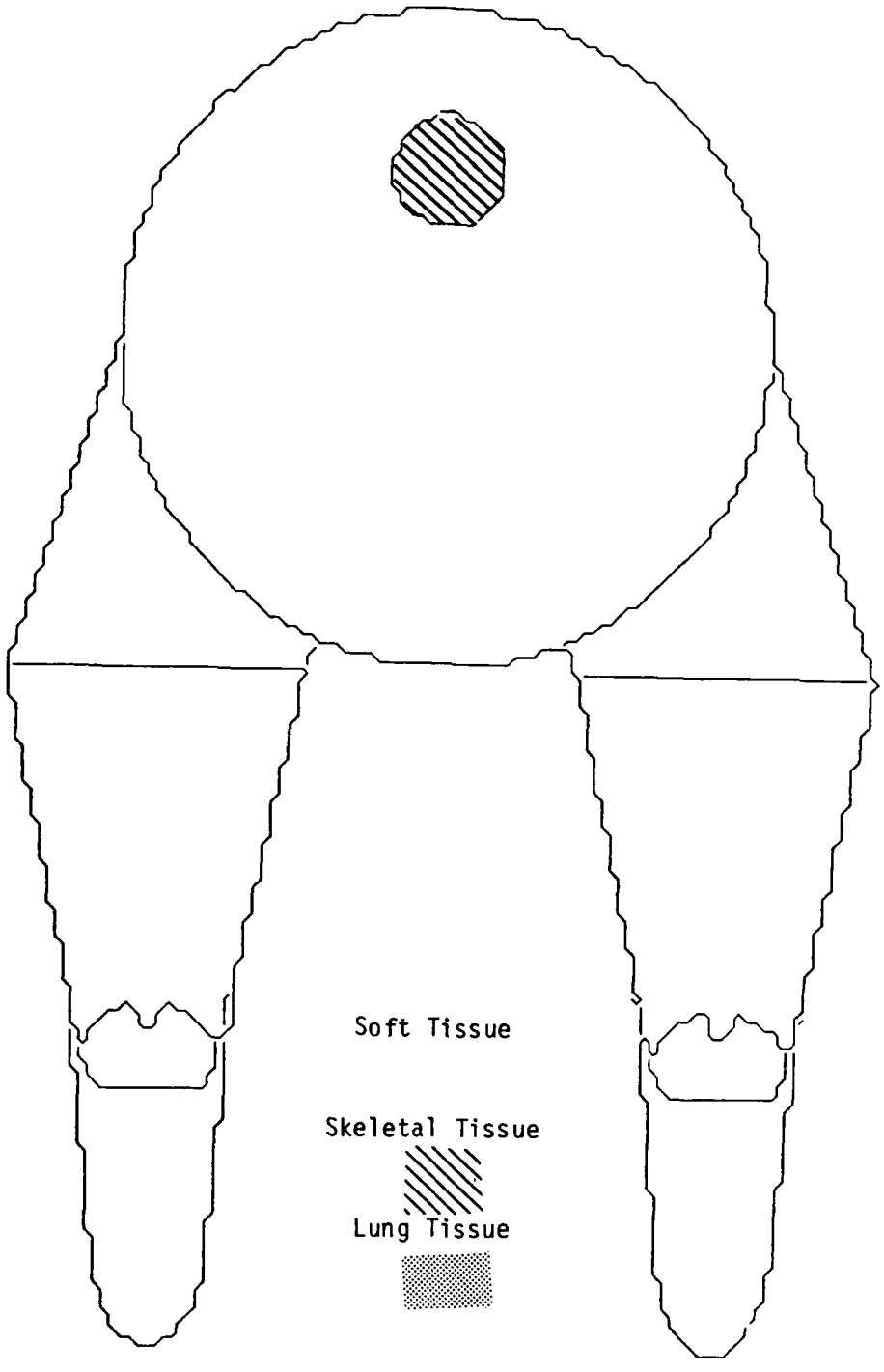

Figure 9. Monkey phantom cross section, Z = 21.0 cm
azimuth 0.0^{o} elevation 90.0^{o}

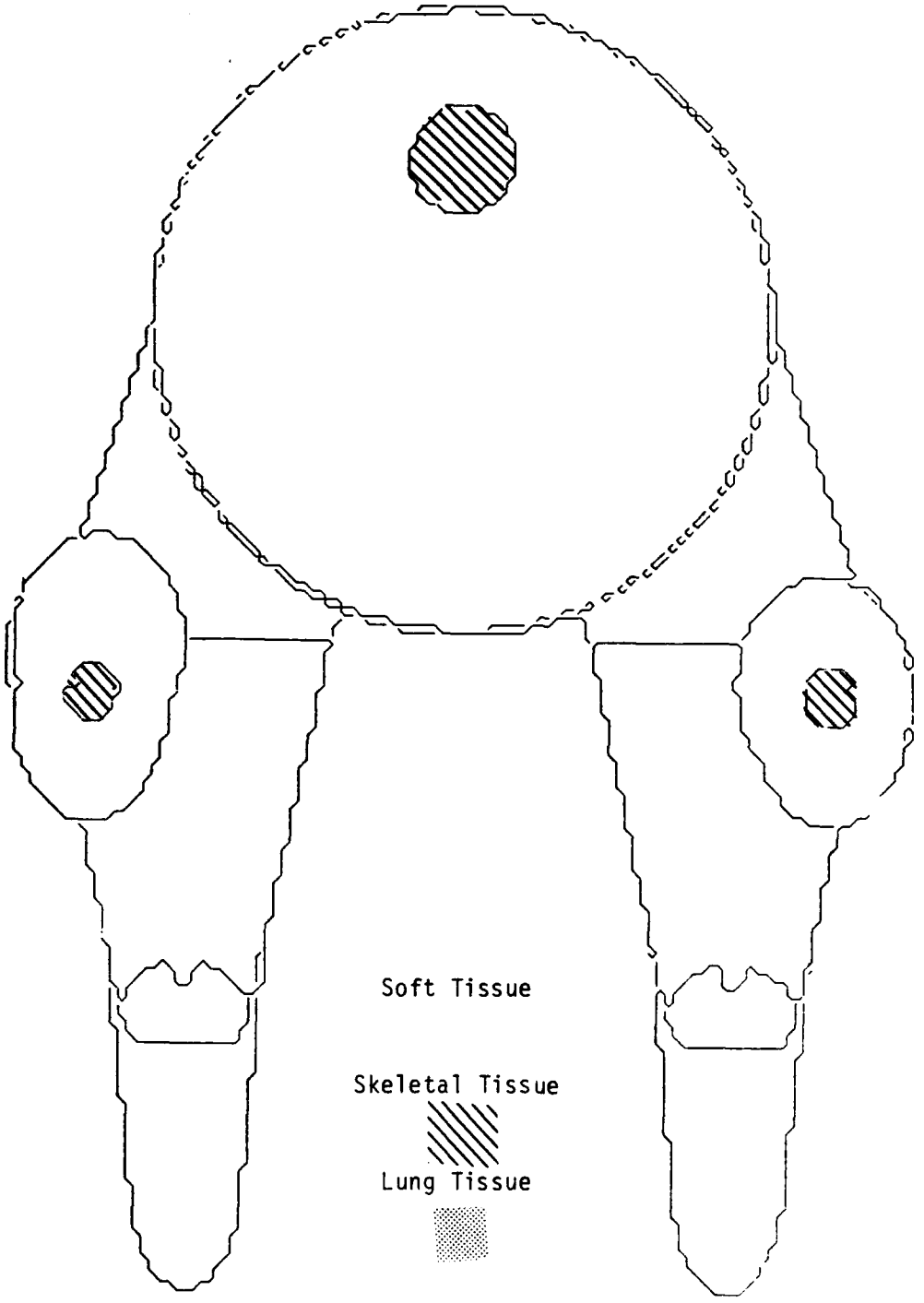

Figure 10. Monkey phantom cross section, Z = 24.0 cm
azimuth 0.0^{o} elevation 90.0^{o}

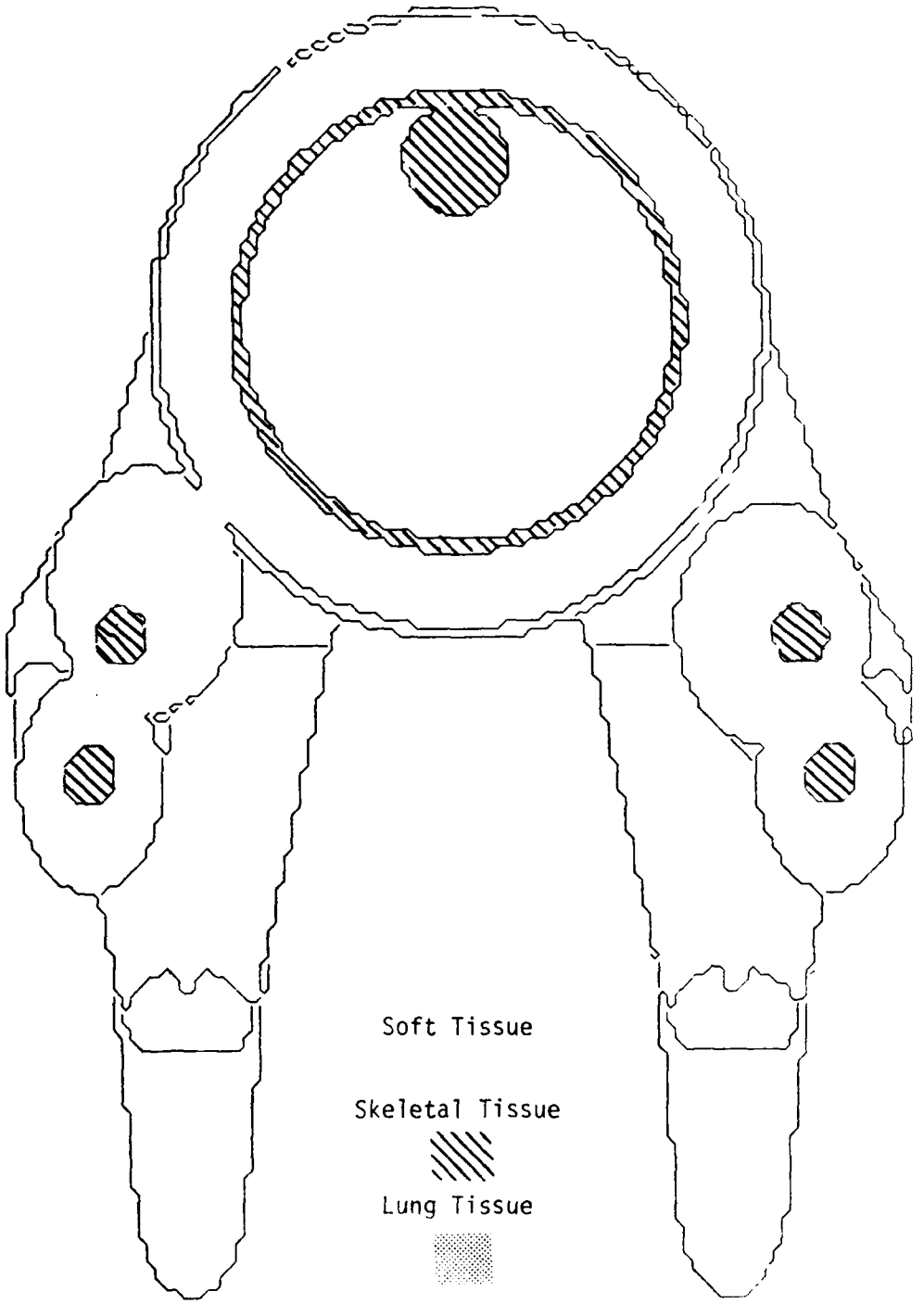

Figure 11. Monkey phantom cross section, Z = 27.0 cm azimuth 0.0^{o} elevation 90.0^{o}

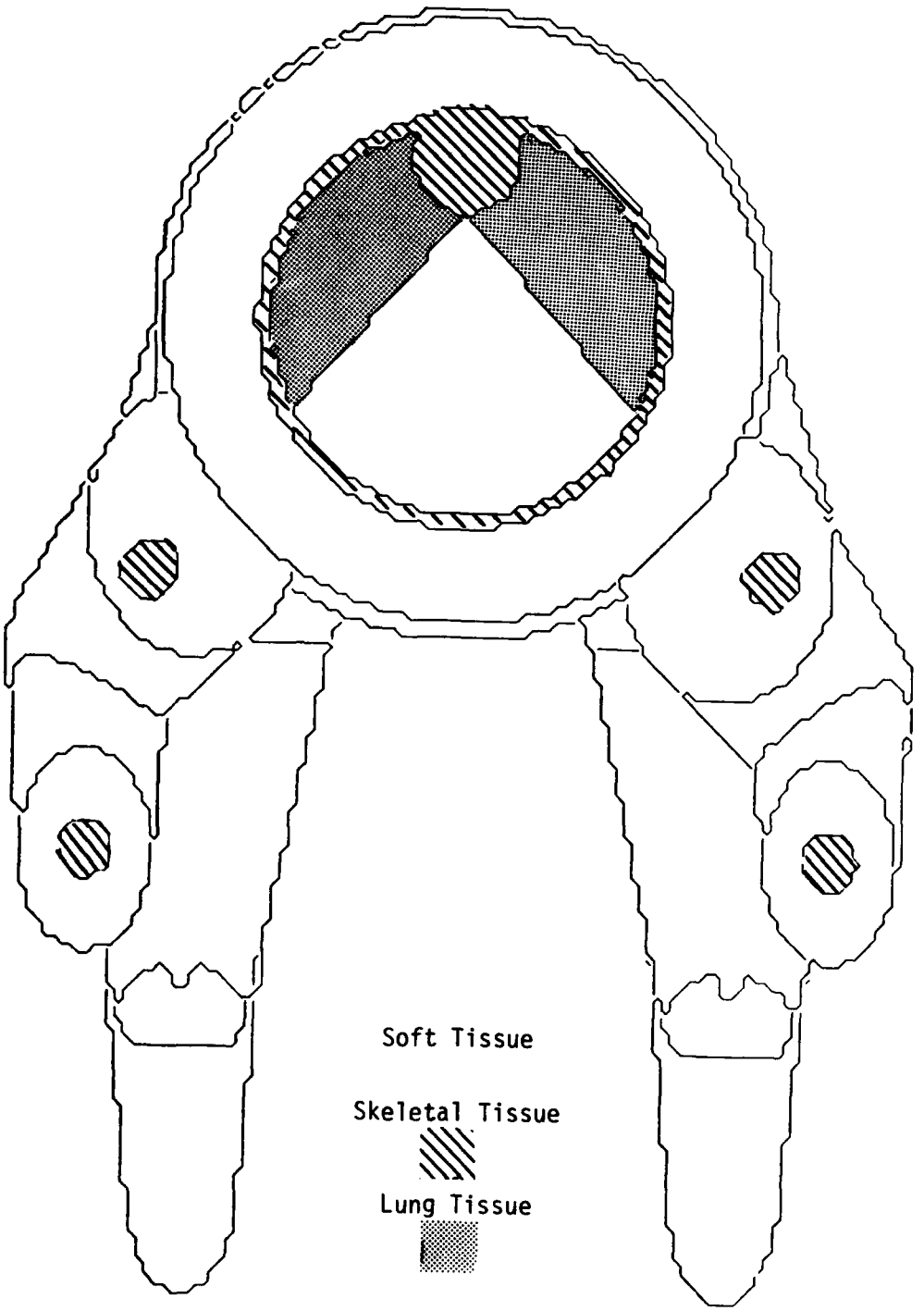

Figure 12. Monkey phantom cross section, Z = 30.0 cm
azimuth 0.0^{o} elevation 90.0^{o}

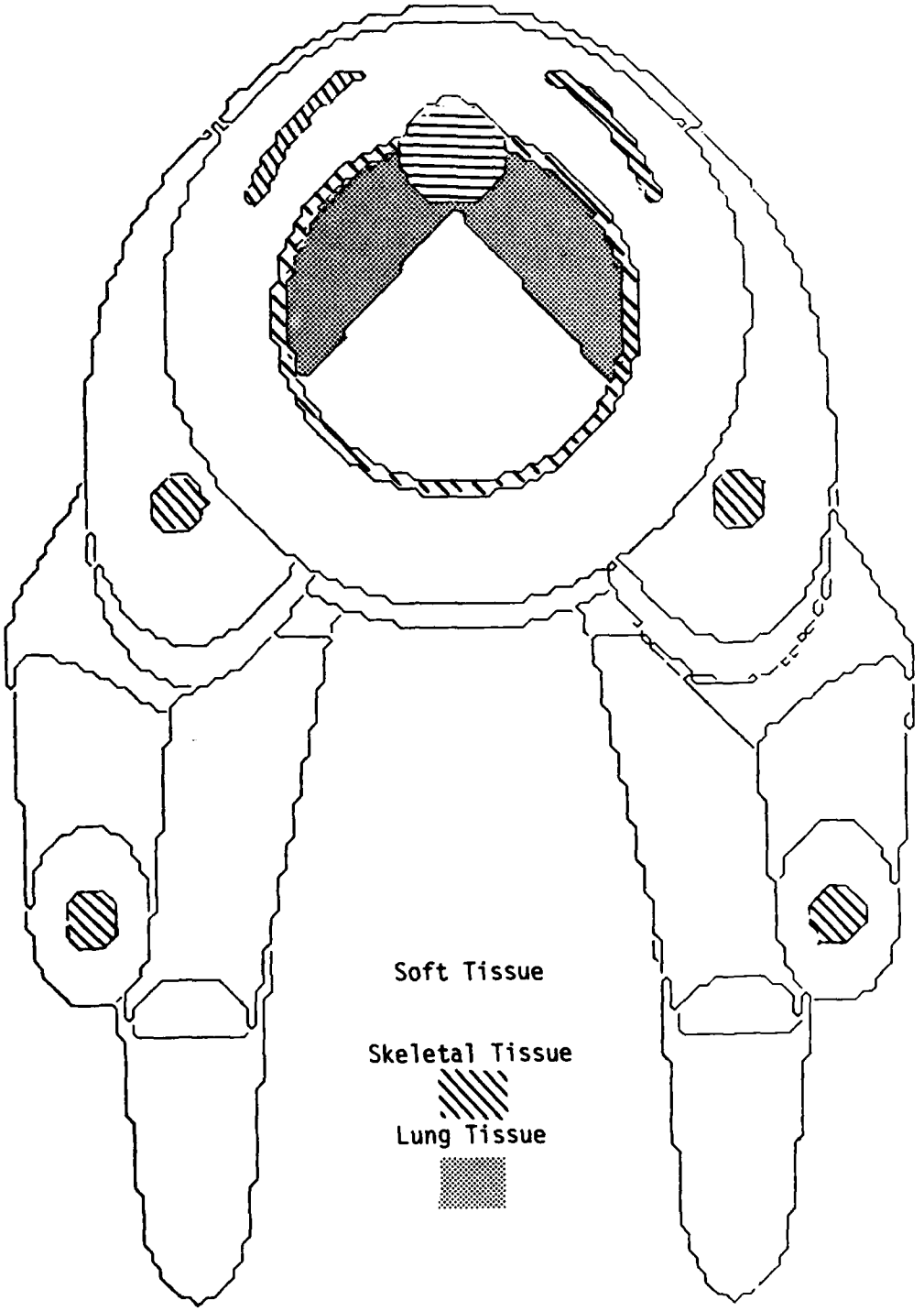

Figure 13. Monkey phantom cross section, Z = 33.0 cm azimuth 0.0^{o} elevation 90.0^{o}

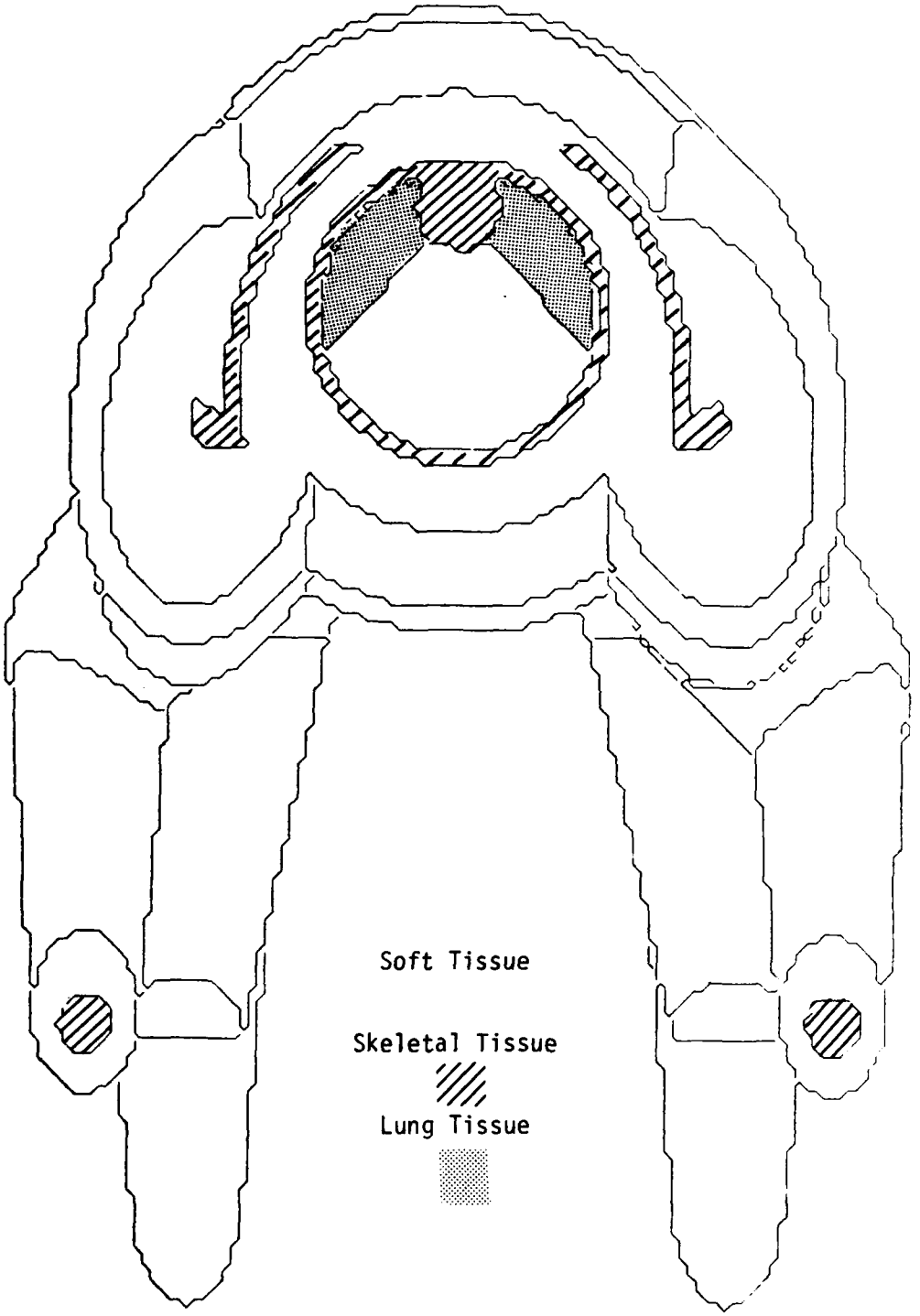

Figure 14. Monkey phantom cross section, Z = 37.0 cm
azimuth 0.0^{o} elevation 90.0^{o}

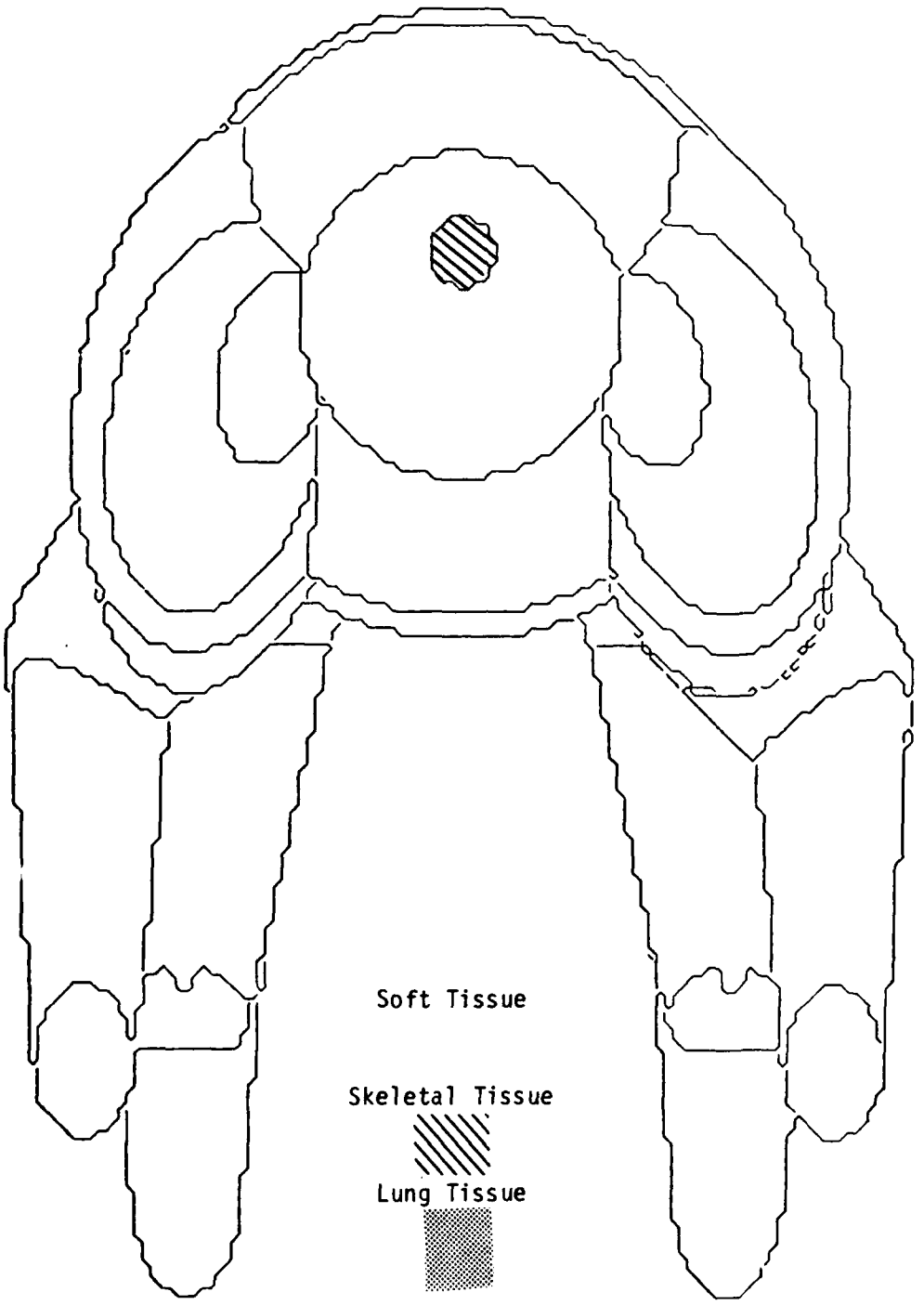

Figure 15. Monkey phantom cross section, Z = 40.0 cm
azimuth 0.0^{o} elevation 90.0^{o}

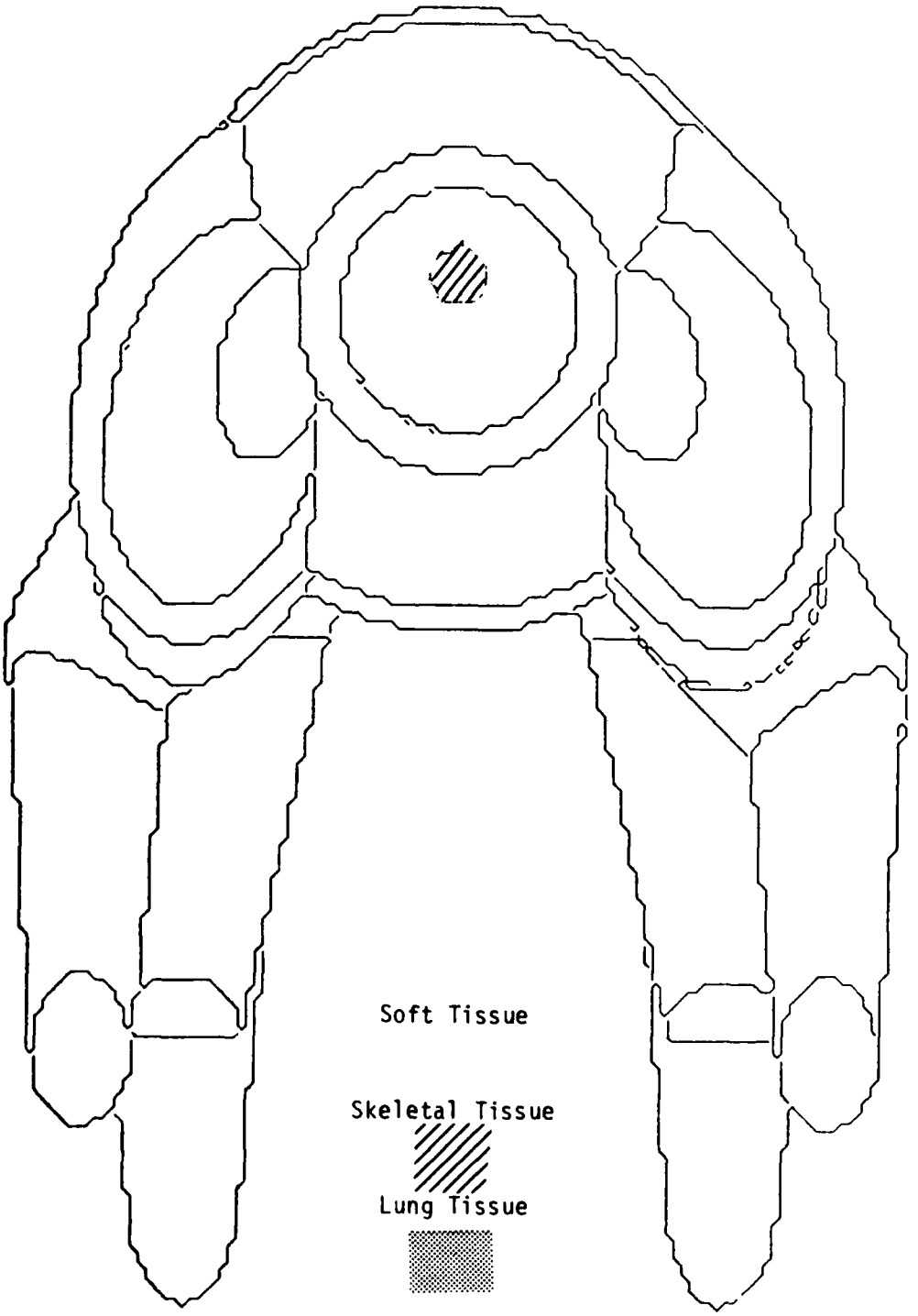

Figure 16. Monkey phantom cross section, ℓ = 42.0 cm azimuth 0.0^{o} elevation 90.0^{o}

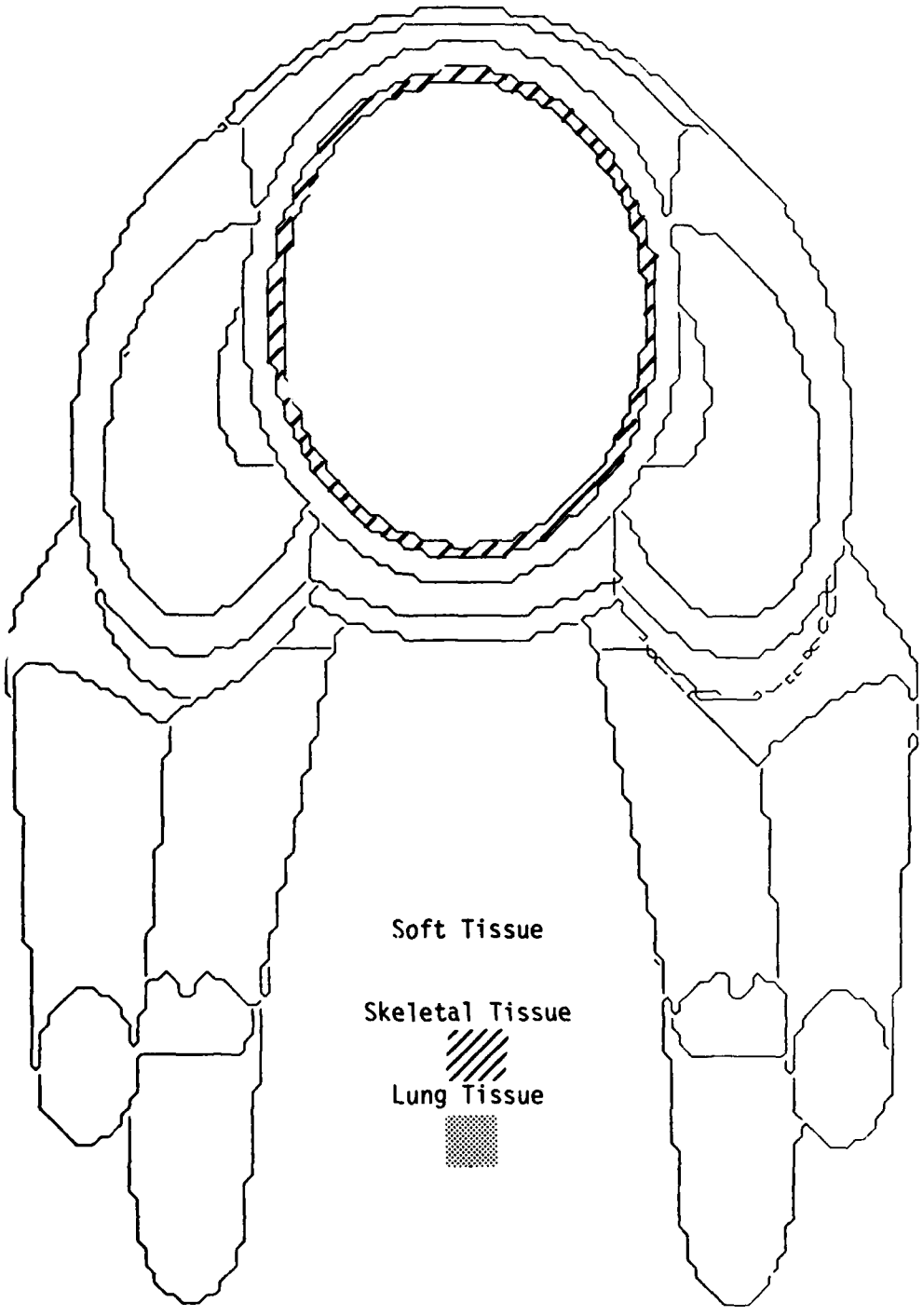

Figure 17. Monkey phantom cross section, Z = 45.0 cm
azimuth 0.0^{o} elevation 90.0^{o}

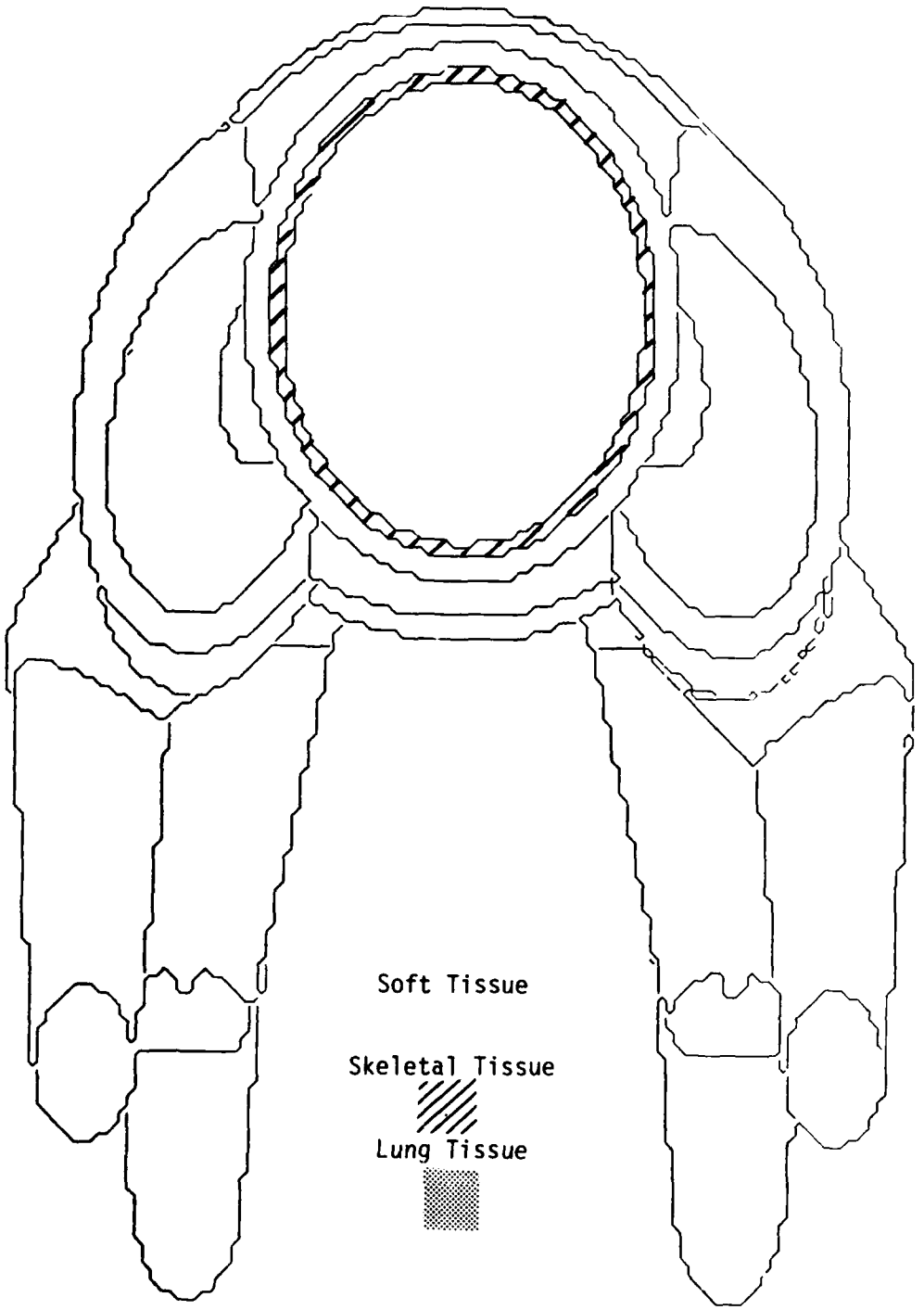

Figure 18. Monkey phantom cross section, Z = 48.0 cm
azimuth 0.0^{o} elevation 90.0^{o}

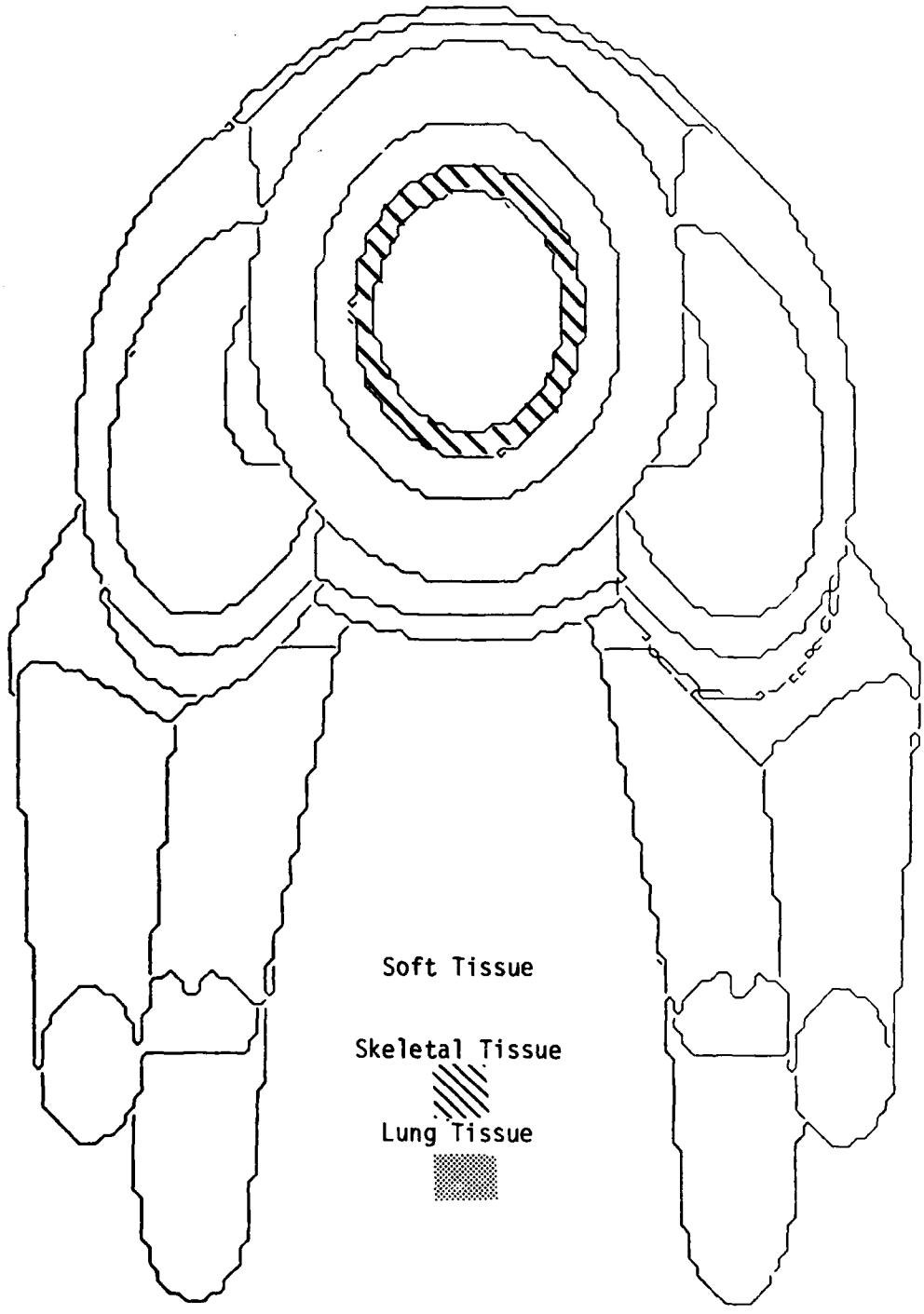

Figure 19. Monkey phantom cross section, Z = 50.0 cm
azimuth 0.0^{o} elevation 90.0^{o}

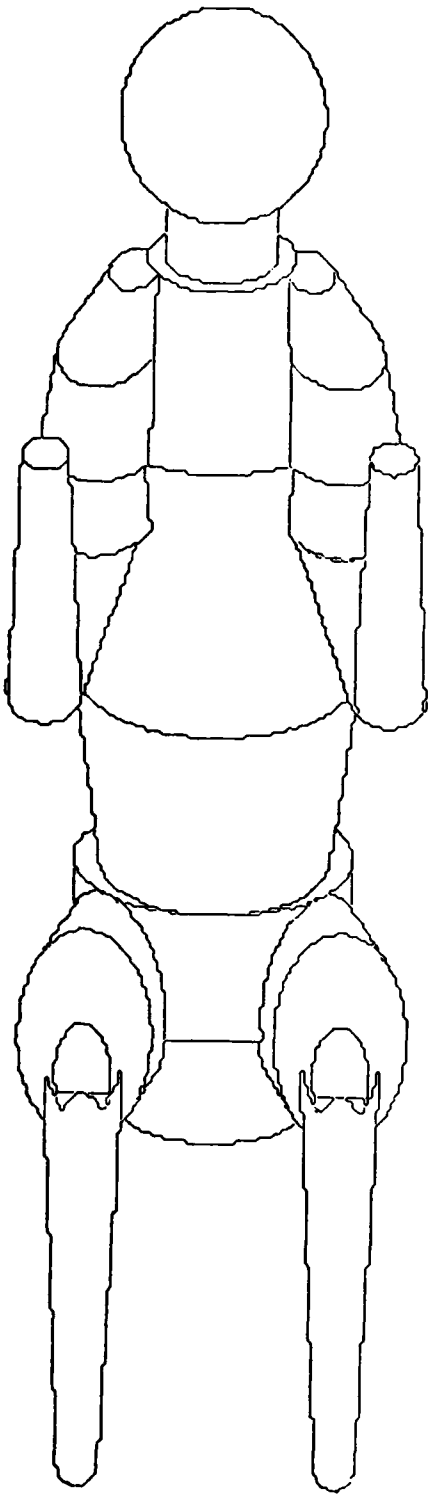

Figure 20. Monkey phantom, front view
azimuth 0.0^{o} elevation 30.0^{o}

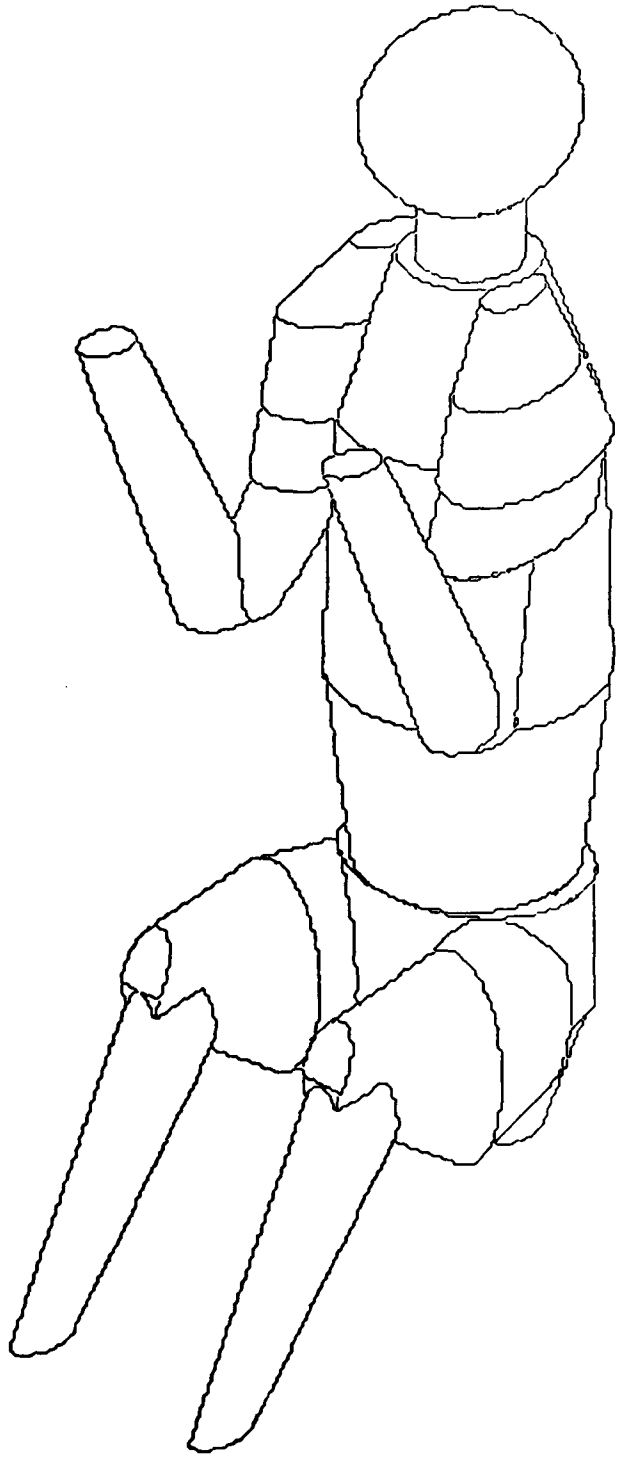

Figure 21. Monkey phantom, 45^{o} view
azimuth 45.0^{o} elevation 30.0^{o}

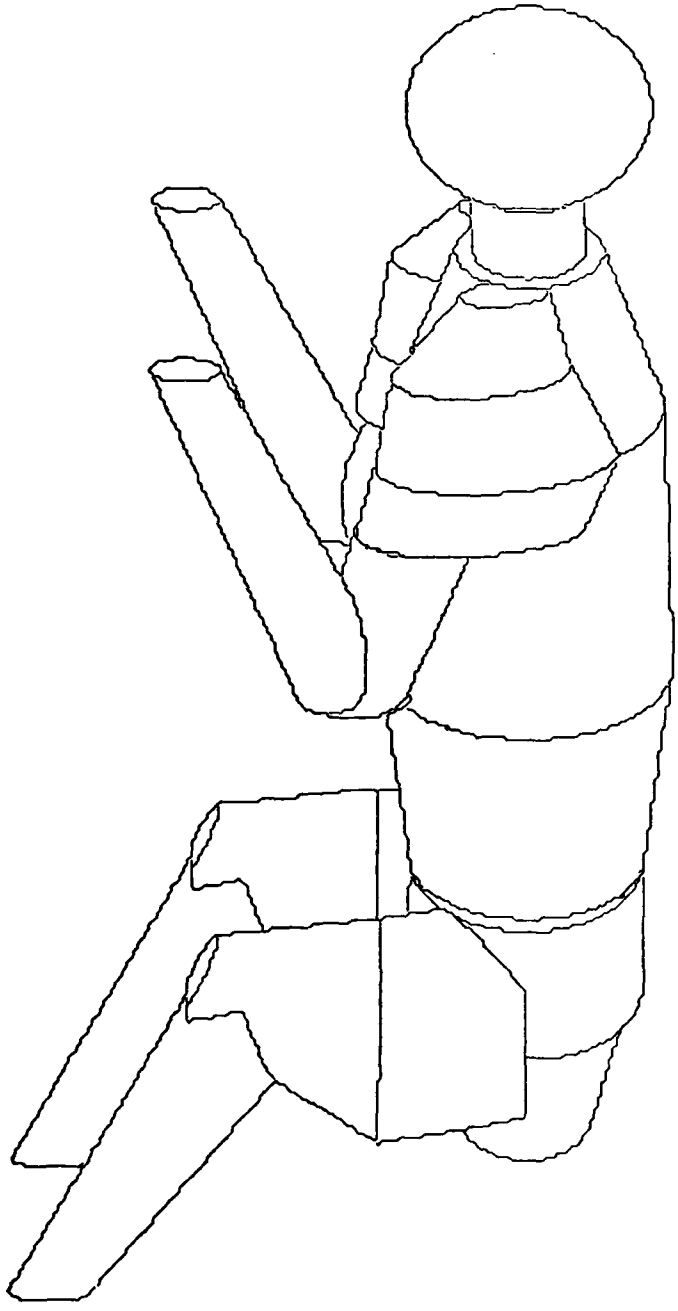

Figure 22. Monkey phantom, side view
azimuth 90.0^{o} elevation 30.0^{o}

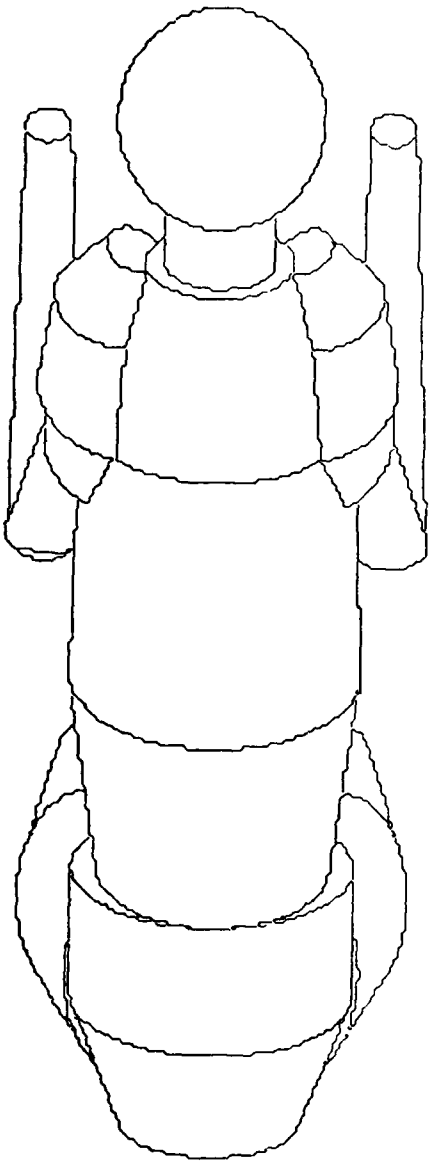

Figure 23. Monkey phantom, back view
azimuth 180.0^{o} elevation 30.0^{o}

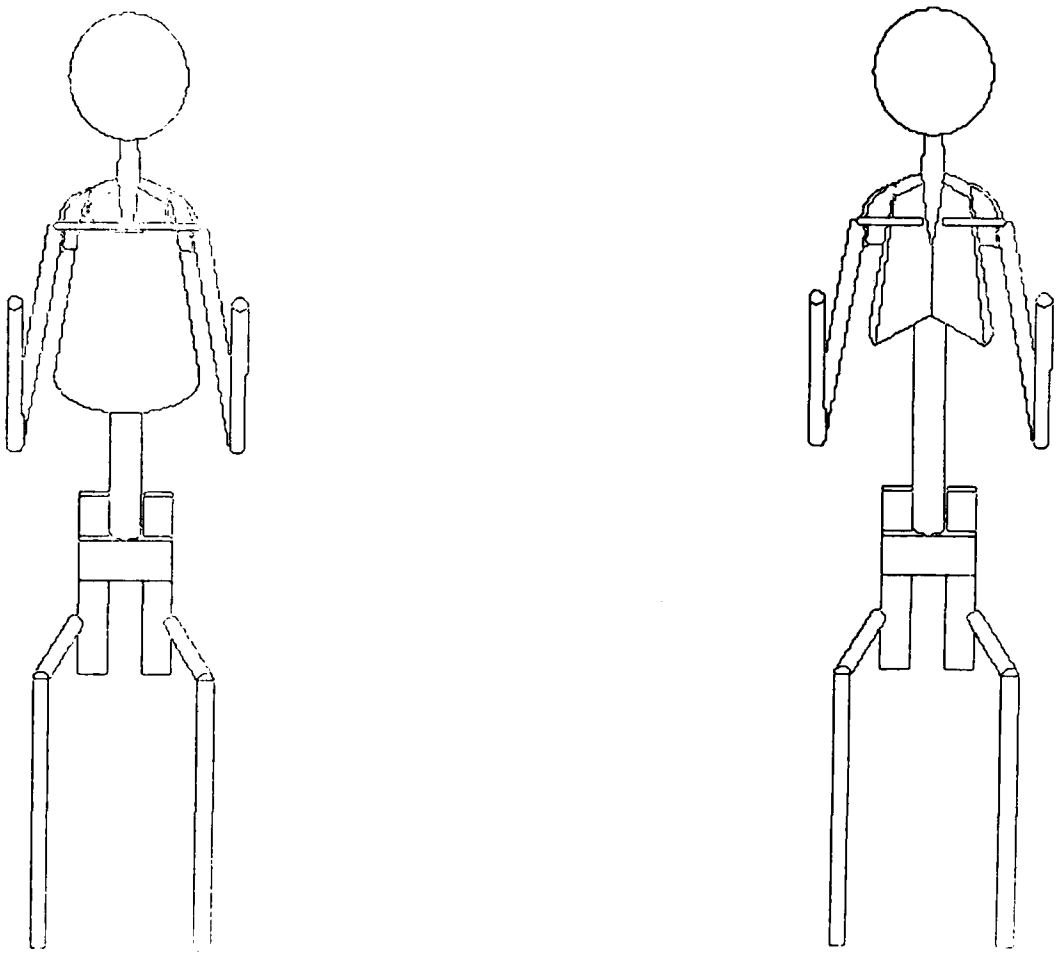

Figure 24. Monkey skeleton with lungs, front view, with and without ribs, azimuth 0.0^{o} elevation 30.0^{o}

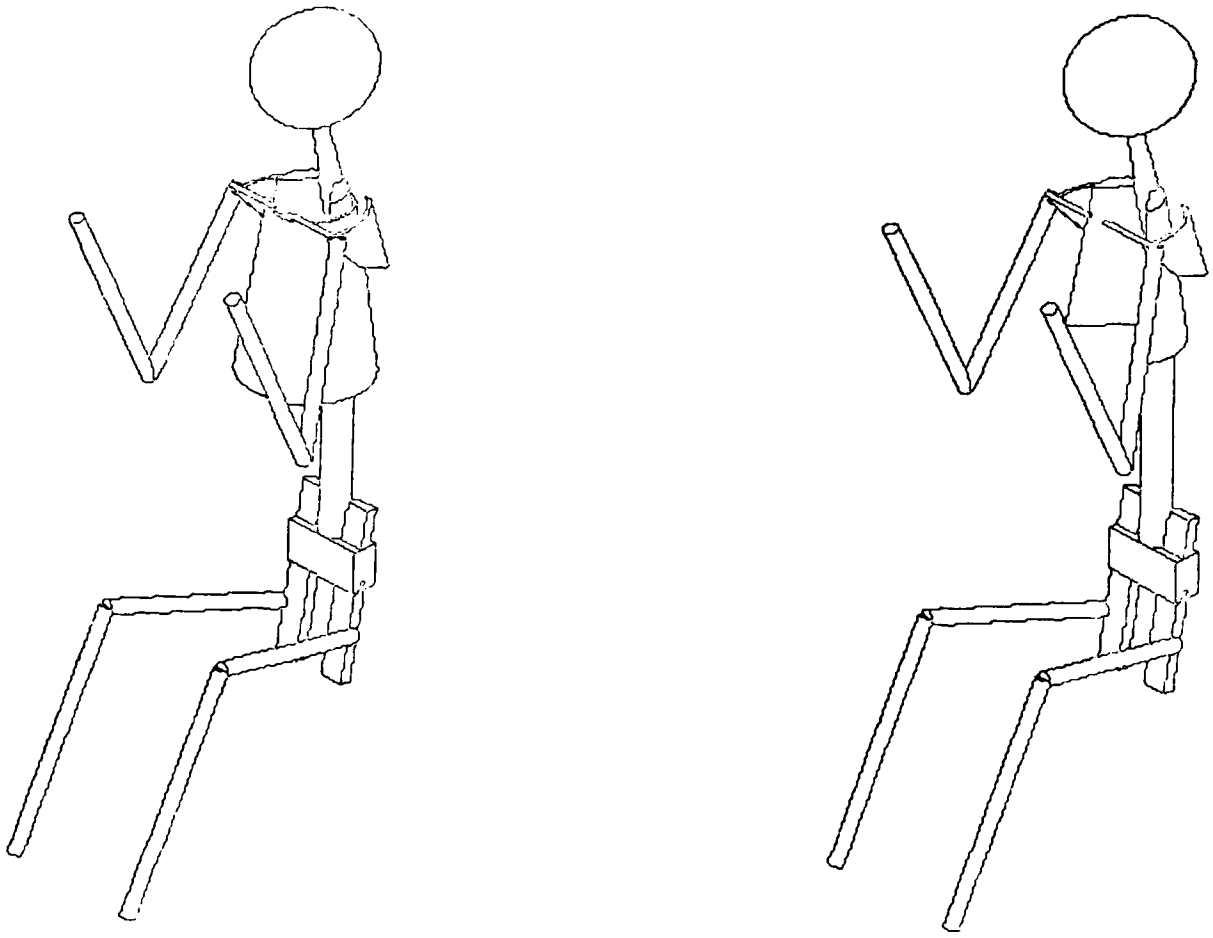

Figure 25. Monkey skeleton with lungs, 45^{o} view, with and without ribs, azimuth 45.0^{o} elevation 30.0^{o}

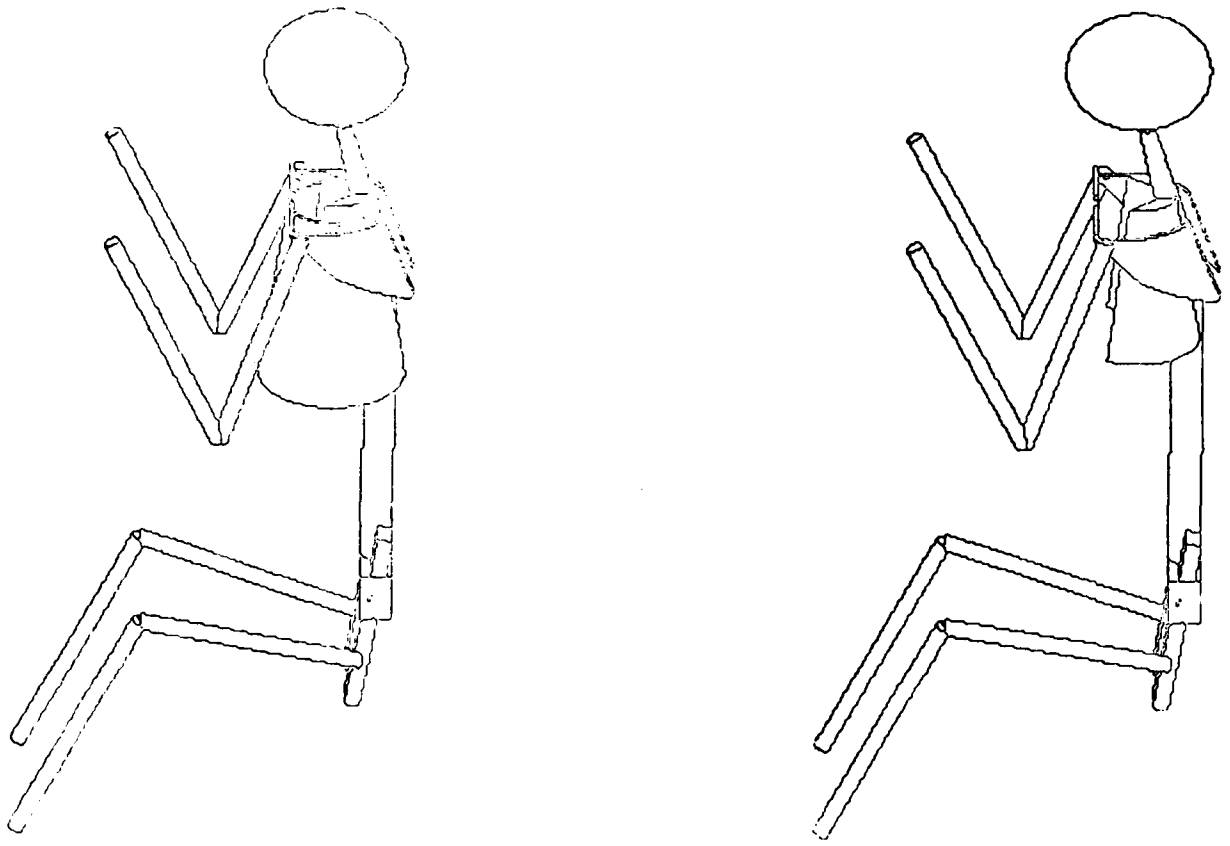

Figure 26. Monkey skeleton with lungs, side view with and without ribs
azimuth 90.0° elevation 30.0°

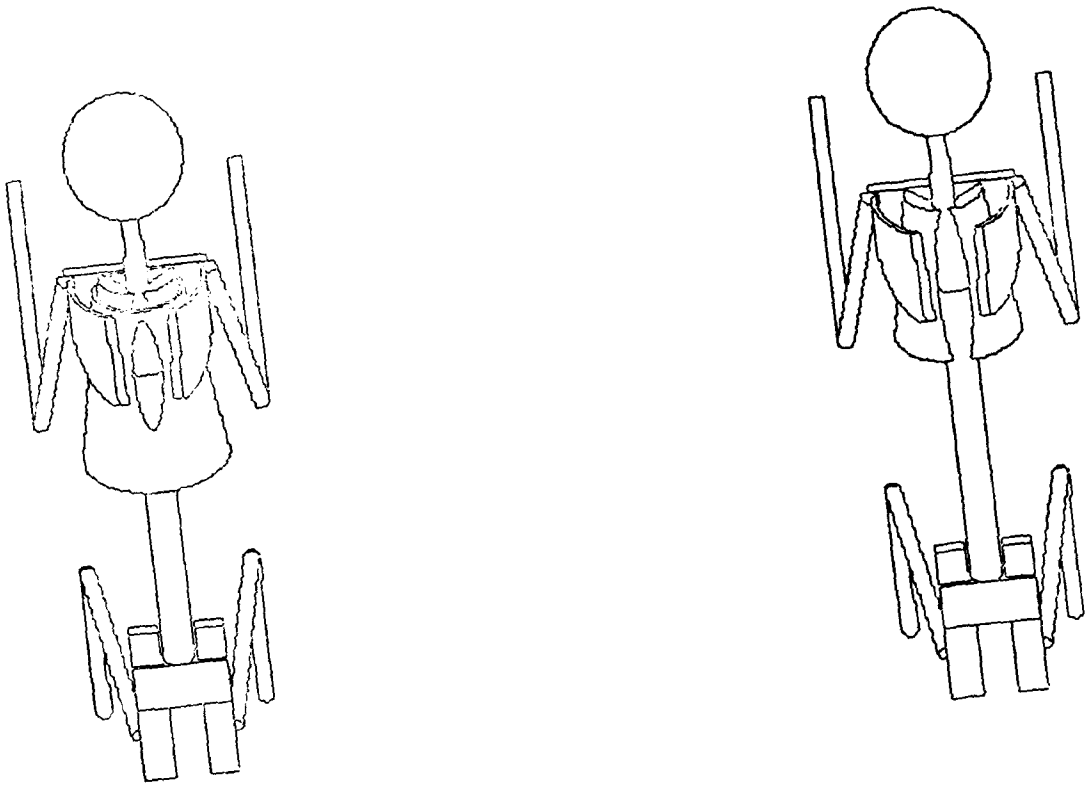

Figure 27. Monkey skeleton with lungs, back view, with and without ribs, azimuth 180.0° elevation 30.0°

sizes discussed in the reference, 3.5 and 5.2 kg,[6] and used to scale the 5.5 kg phantom to the smaller size. The ratios of new to old phantom masses were 0.76 and 0.61 for the head and for the remainder of the phantom, respectively. Likewise, the location of the head midpoint relative to the base of the trunk was adjusted from 46.5 cm to 39.7 cm to remove any gap resulting from the scaling procedure. In its final adjusted form the monkey phantom has a mass of 3.43 kg and has a head which is slightly larger, relative to the trunk or torso, than that of the original phantom.

2.1.2 Elemental Composition

A specification of elemental constituents of monkey tissues is not available. Therefore, the latest constituents determined by Kerr[7] to apply to human lung, skeletal and soft tissues have been used to represent the equivalent monkey tissues until such time as alternative values become available. These constituents are listed as weight percents in Table 4.

2.1.3 Marrow Distribution

The active marrow distribution in the rhesus monkey was measured by S.T. Taketa, et al., and published in 1970.[8] The results of these measurements along with those for other species are given in Table 5, which is reproduced from that report. Figure 28 shows this distribution pictorially, based on scintillation scanning of ^{99m}Tc in an eviscerated monkey. This marrow distribution has been used in the dosimetry calculations as shown in Figure 29, simplified to correspond to the seven gross marrow regions given in Table 5. Some additional detail has been provided in the clavical-scapular region and in the legs increasing the total individual marrow regions to nine. The division of marrow between the clavical and scapulae are as shown in Table 5. Division of marrow between the upper femur and the remainder of the leg was accomplished by placing approximately half the femur marrow (6.7%) in the region near the pelvis and the remainder of the lower limb marrow (13.3%) in the area of the knee joint as supported by the Taketa reference.

Table 4. Elemental composition for various components of reference man to be used as Rhesus monkey analogues

Element	Percent by Weight		
	Lung	Skeleton	Soft Tissue
H	10.21	7.28	10.51
C	10.24	24.64	22.63
N	2.91	3.06	2.34
O	75.63	46.88	63.69
Na	0.19	0.32	0.11
Mg	0.007	0.11	0.013
P	0.080	5.03	0.13
S	0.23	0.31	0.20
Cl	0.27	0.14	0.14
K	0.20	0.15	0.20
Ca	0.009	12.07	0.024
Fe	0.037	0.008	0.006

Table 5. Comparative active erythropoietic bone distribution in several mammalian species

Grouping Skeletal Structure	Man(3) at Age 10	15	40	Monkey	Dog(1)	Rat(4)	Mouse(5)
1 Skull	7.5[a]	9.7	13.0	8.7	1.0	6	
Mandible	0.7	0.9	1.2	2.2	0.1	4	19.1
2 2 Clavicles	0.9	1.1	1.6	0.7	-	-	-
2 Scapulae	2.9	3.6	4.9	3.9	5.1	-	-
3 Upper Limbs (total)	(9.5)	(6.5)	(2.2)	(12.2)	(11.1)	(11)	(5.7)
2 Humeri	6.1	5.2	2.2	9.2	10.8	-	4.1[b]
2 Radii	0.8	0.3	0.0	1.5	0.1	-	-
2 Ulnae	0.9	0.3	0.0	1.3	0.1	-	-
2 Wrists-hands	1.7	0.7	0.0	0.2	0.1	-	1.6
4 Ribs	8.3	9.5	7.1	4.8	20.5	-	16.1
Sternum	1.6	2.0	2.5	1.5	2.8	-	
5 Vertebrae (total)	(25.0)	(32.0)	(42.9)	(33.1)	(42.6)	(24)	(38.1)
Cervical	2.1	2.7	3.6	2.2	6.7	-	-
Thoracic	8.7	11.1	15.0	12.3	17.6	-	-
Lumbar	6.7	8.6	11.5	17.0	15.0	-	-
Sacroccocygeal	7.5	9.6	12.8	1.6	3.3	9	8.2[c]
6 Pelvis	12.0	15.3	20.5	12.9	8.9		
7 Lower limbs (total)	(31.2)	(19.4)	(3.9)	(20.0)	(7.9)	(35)	(12.8)
2 Femurs	17.5	14.0	3.9	13.3	7.2	19	6.0
2 Patellae	0.5	0.2	0.0	0.1	0.0	-	-
2 Tibiae	6.9	2.7	0.0	5.9	0.6	16	4.2
2 Fibulae	1.0	0.4	0.0	0.5	0.0		
2 Ankles-feet	5.3	2.1	0.0	0.2	0.1	-	2.6
TOTAL	99.6	100.0	99.0	100.0	100.0	89	100.0

a Percent of total active bone marrow
b Includes clavicles and scapulae
c Pelvis

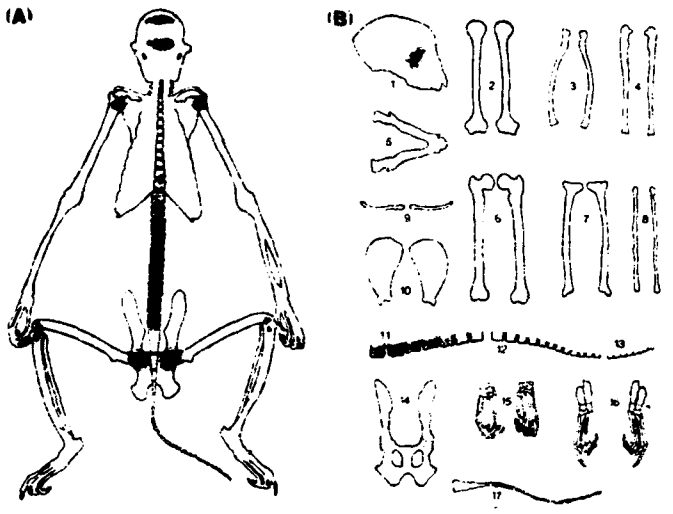

Figure 28. Scintillation scanning of ^{99m}Tc in an eviscerated monkey

Scintillation scanning of ^{99m}Tc in an "eviscerated" monkey (A) and of disarticulated bones (B) from the same animal. Radioactivity was of sufficient intensity to darken film in 1, skull and maximilla (positioned on left side with the anterior portion facing bottom of page); 2, humeri; 6, femora; 7, tibiae; 10, scapule; 11, lumbar and 12, thoracic vertebrae; and 14, hip bones; but not in 3, radii; 4, ulnae; 5, mandible; 8 fibulae; 9, clavicles; 13, cervical vertebrae; 15, feet and ankles; 16, hands and wrists; and 17, sacrococcygeal vertebrae. (Drawings were reconstructed from the ^{99m}TC scans and radiographs of the skeleton.)

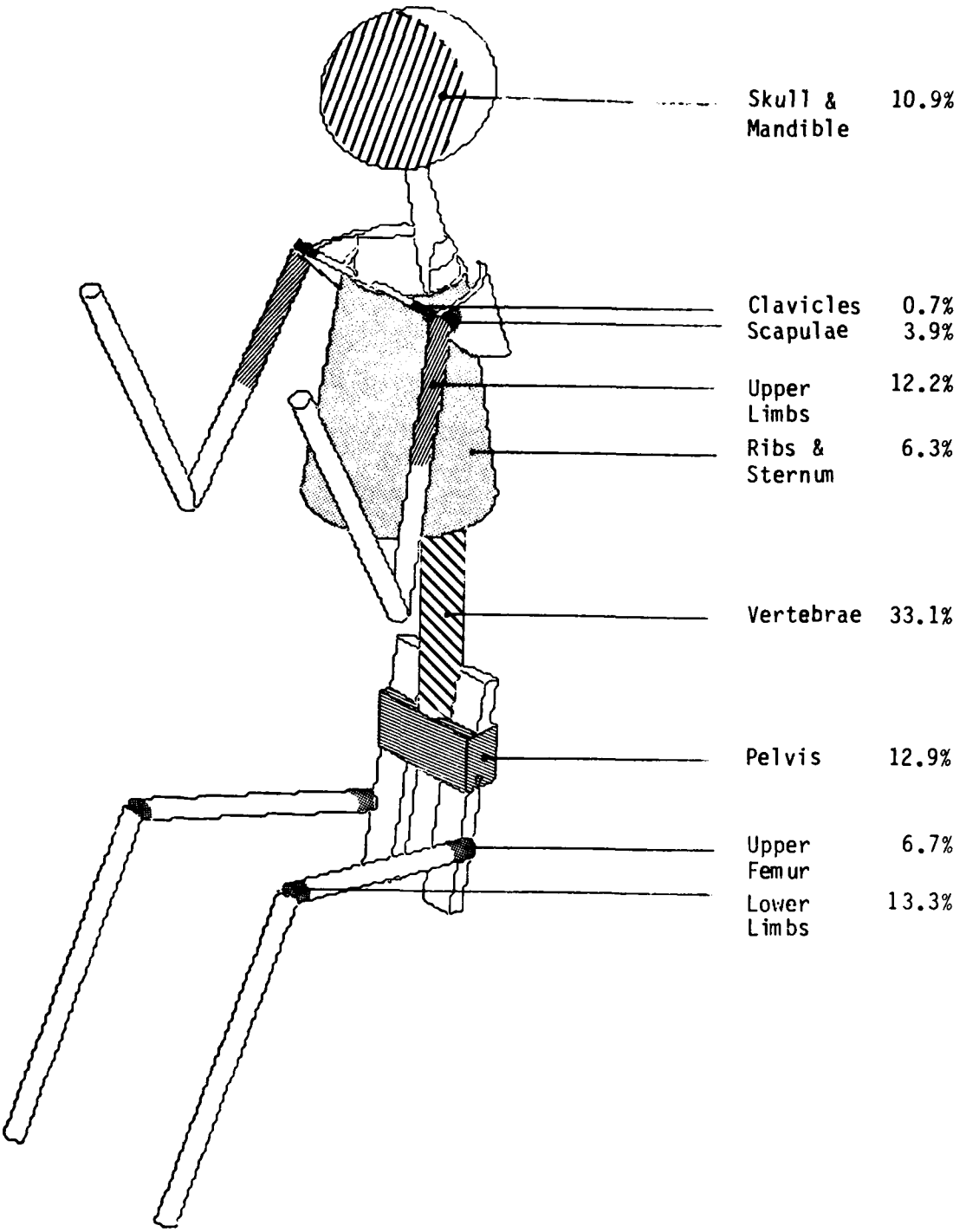

Figure 29. Active marrow distribution used in KERMA calculations

2.1.4 Monkey in Experimental Configuration

A primary mode of exposure for the monkey is more or less centrally located within a plywood box, restrained in a chair made predominately of lucite plastic, with its back to the reactor. This disposition of the monkey is shown in Figure 30. The general dimensions of the chair and box are given Figures 31 and 32, respectively. The elemental constituents and densities of these materials are given in Table 6.[2] The density of the box was determined by dividing the measured mass of the box (44.7 kg)[9] by the volume of its sides, as determined by external measurements.

The box and chair sit on a platform (not modeled) on the floor of the exposure room. The monkey position in the chair is adjusted to place the mid-thorax location at the same height as the reactor core center. The mid-thorax location is generally taken to be 3 cm below the end of the sternum. However, in the case of the phantom the sternum is not modeled separately. Therefore, the location chosen was alternatively defined as being below both lungs and ribs and between 19 and 20 cm below the mid-head in a 3.4 kg monkey. In the scaled 3.4 kg phantom the location of the mid-thorax was taken to be 20 cm above the base, which is 19.66 cm below the mid-head point. This location satisfies the conditions of being below both lungs and ribs.

For irradiations in exposure room one, the box and chair are positioned atop a wood stand to bring the mid-thorax to 120 cm above the floor. Thus, in both exposure rooms the mid-thorax is aligned with the height of the center of the reactor core. Depending on the exposure room in which the experiment is to be performed, the mid-thorax may be either 86 or 92 cm above the platform. The exact location chosen affects the relative location of the monkey within the box. For the purposes of this study the mid-thorax was taken to be located at 86 cm above the bottom of the box, as shown in Figure 33.

2.2 Simple Geometry Phantom

An exact physical mockup of the rhesus monkey phantom would be difficult if not impossible to construct for the purpose of experimentally validating the

Table 6. Elemental constituents of the lucite chair and plywood enclosure

	Constituent wt %	
Element	Lucite	Plywood
H	8.1	6.2
C	60.0	44.5
O	31.9	49.3

Lucite Density: 1.2 g/cm^3

Plywood Density: 0.51 g/cm^3

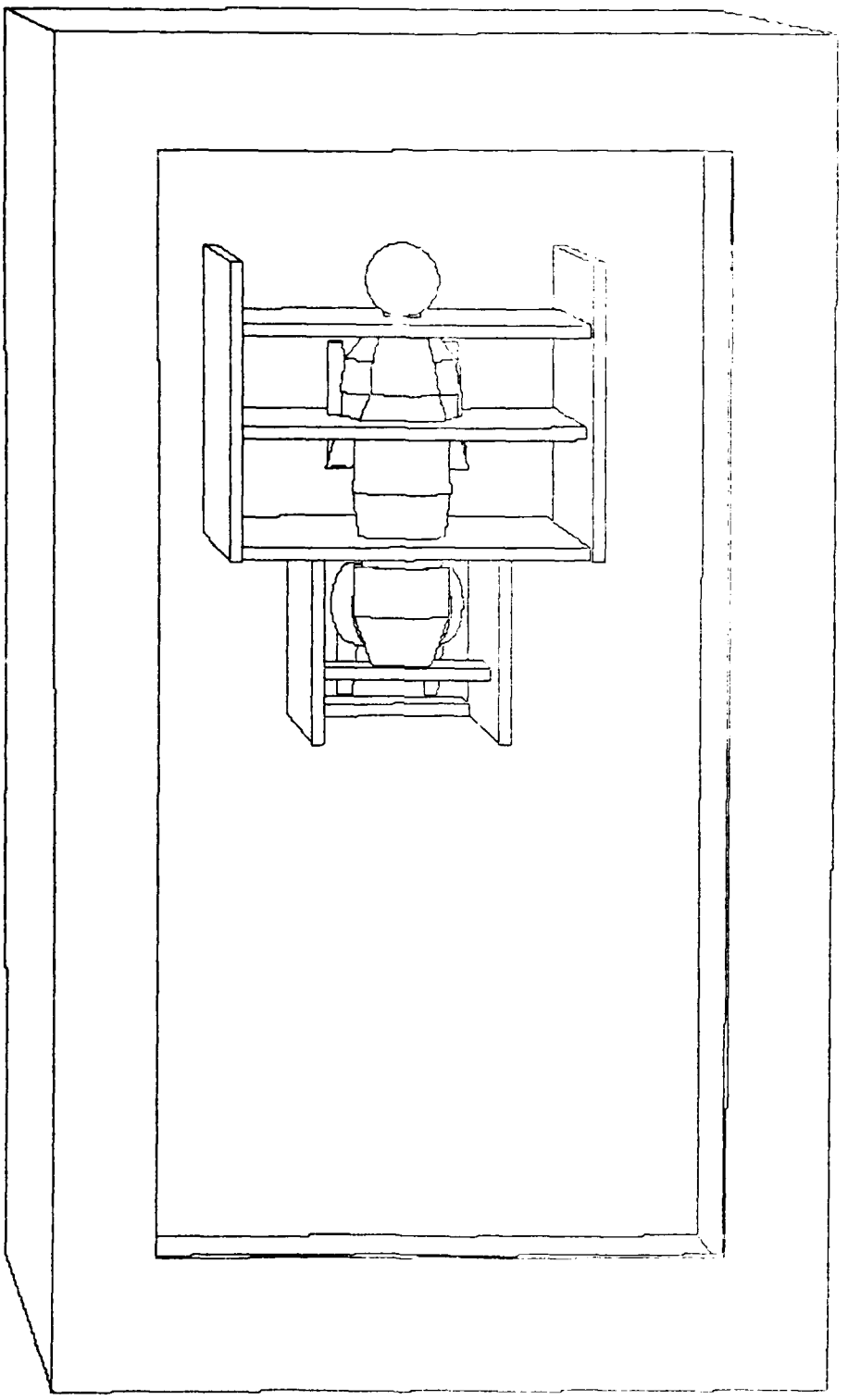

Figure 30. Chair and box with complex phantom
azimuth 175.0° elevation 5.0°

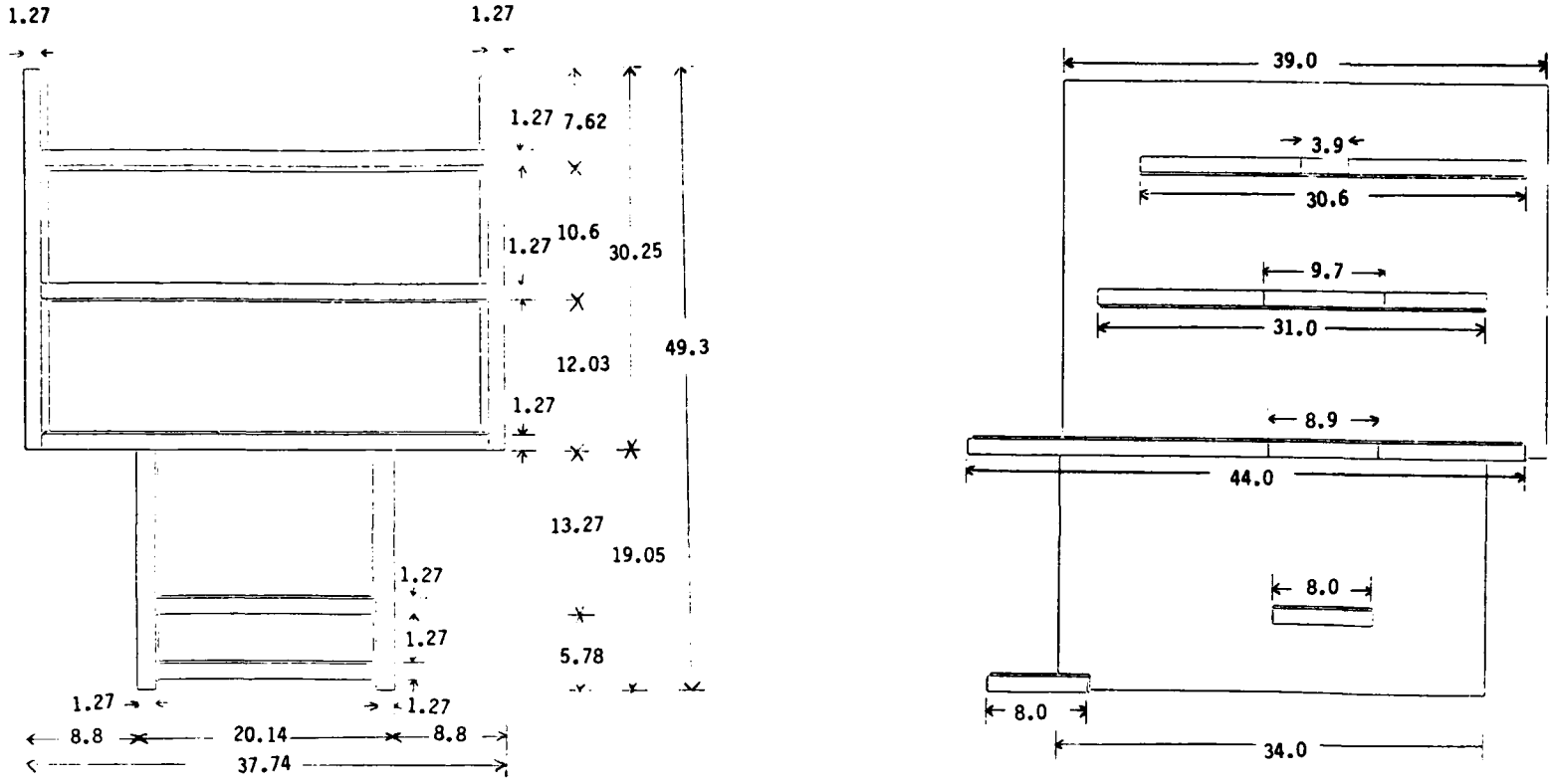

Figure 31. Dimensions of the lucite restraining chair (cm)

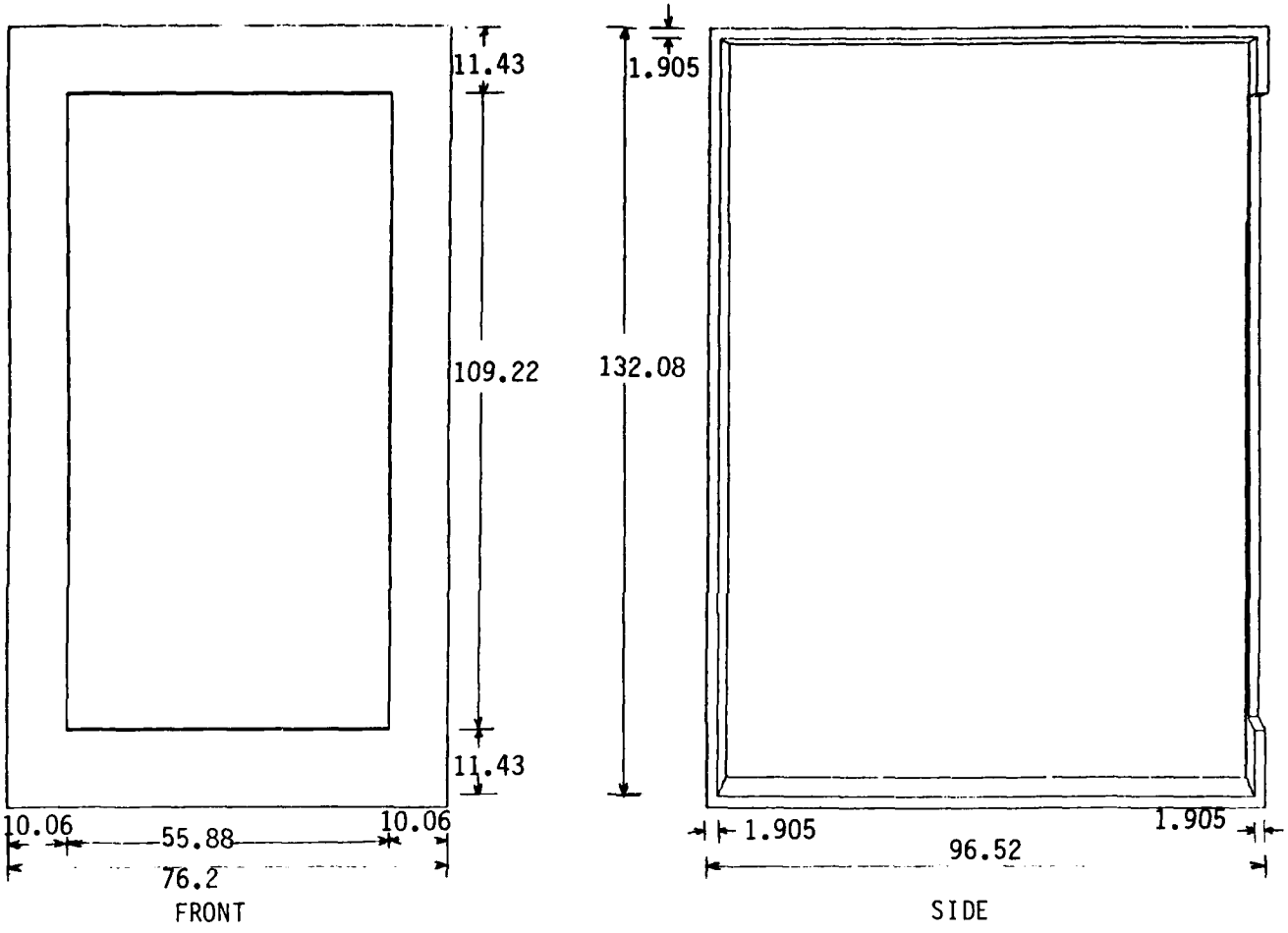

Figure 32. Dimensions of the plywood exposure enclosure

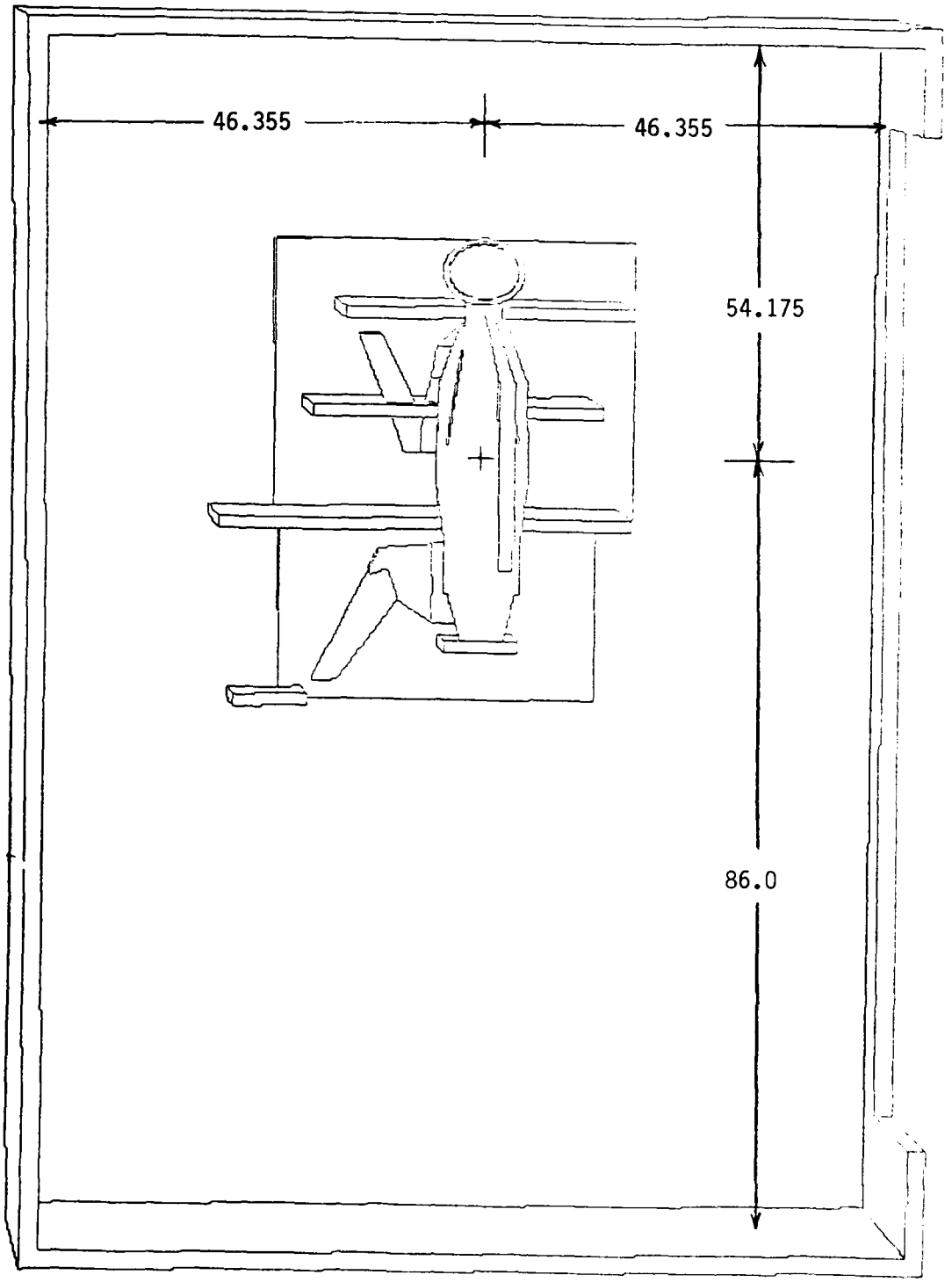

Figure 33. Orientation of complex phantom and chain within the plywood enclosure

radiation transport calculations described in this report. Therefore, a simple geometry phantom was developed, which could easily be replicated with a physical model for use in experimental studies. The dimensions of the simple phantom were chosen to generally correspond to those of the unscaled phantom head, neck and trunk, minus the shoulders. The specifications arrived at in cooperation with the sponsor (who will actually build the phantom) are as follows:

Trunk: cylinder
height: 33.0 cm
diameter: 10.2 cm
composition: TE liquid in a lucite cylinder with 0.125" thick walls

Neck: cylinder
height: 4.5 cm
diameter: 4.5 cm
composition: A-150 plastic

Head: sphere
diameter: 9.5 cm, truncated to a height of 8.0 cm, with the flat side sitting on neck
composition: A-150 plastic

The constituents of lucite were given previously in Table 6. The constituents of TE (Tissue Equivalent) liquid and A-150 plastic are given in Table 7.[10]

The simplified phantom was located within the restraining chair and exposure box as shown in Figure 34. The mid-head location of the simple phantom within the box was taken to be the same as that of the complex, with the mid-thorax specified to be 22.5 cm below. The exposure configuration thus obtained is shown in Figure 35.

Table 7. Elemental constituents of the simplified phantom

	Constituent Wt%	
Element	Tis. Equiv. Liquid	A-150 Plastic
H	10.2	10.1
C	12.0	77.6
N	3.6	3.5
O	74.2	5.2
Ca		1.8
F		1.7

Tissue Equivalent Liquid Density: 1.08 g/cm^3

A-150 Plastic Density: 1.11 g/cm^3

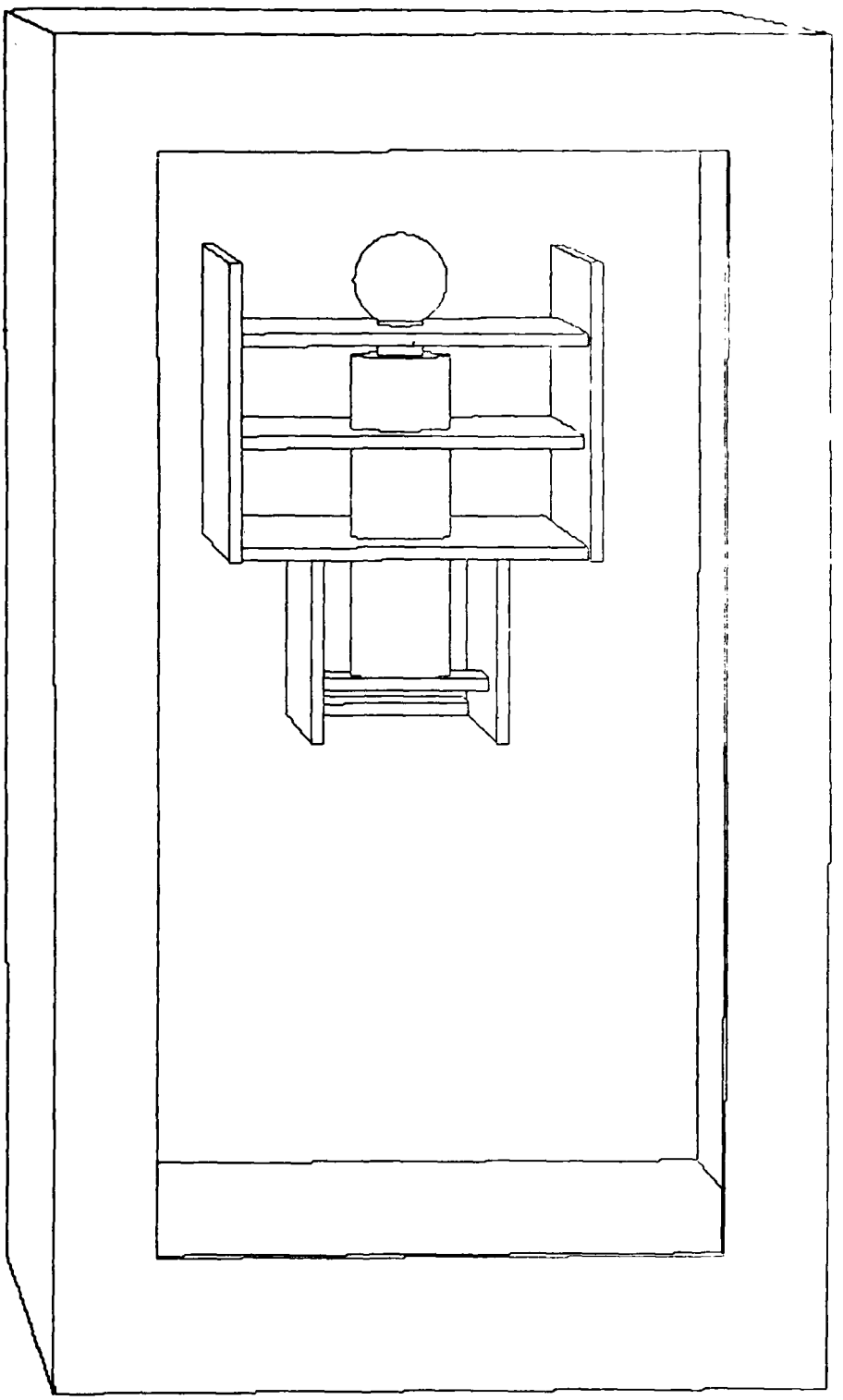

Figure 34. Chair and box with simple phantom, azimuth 175.0° elevation 5.0°

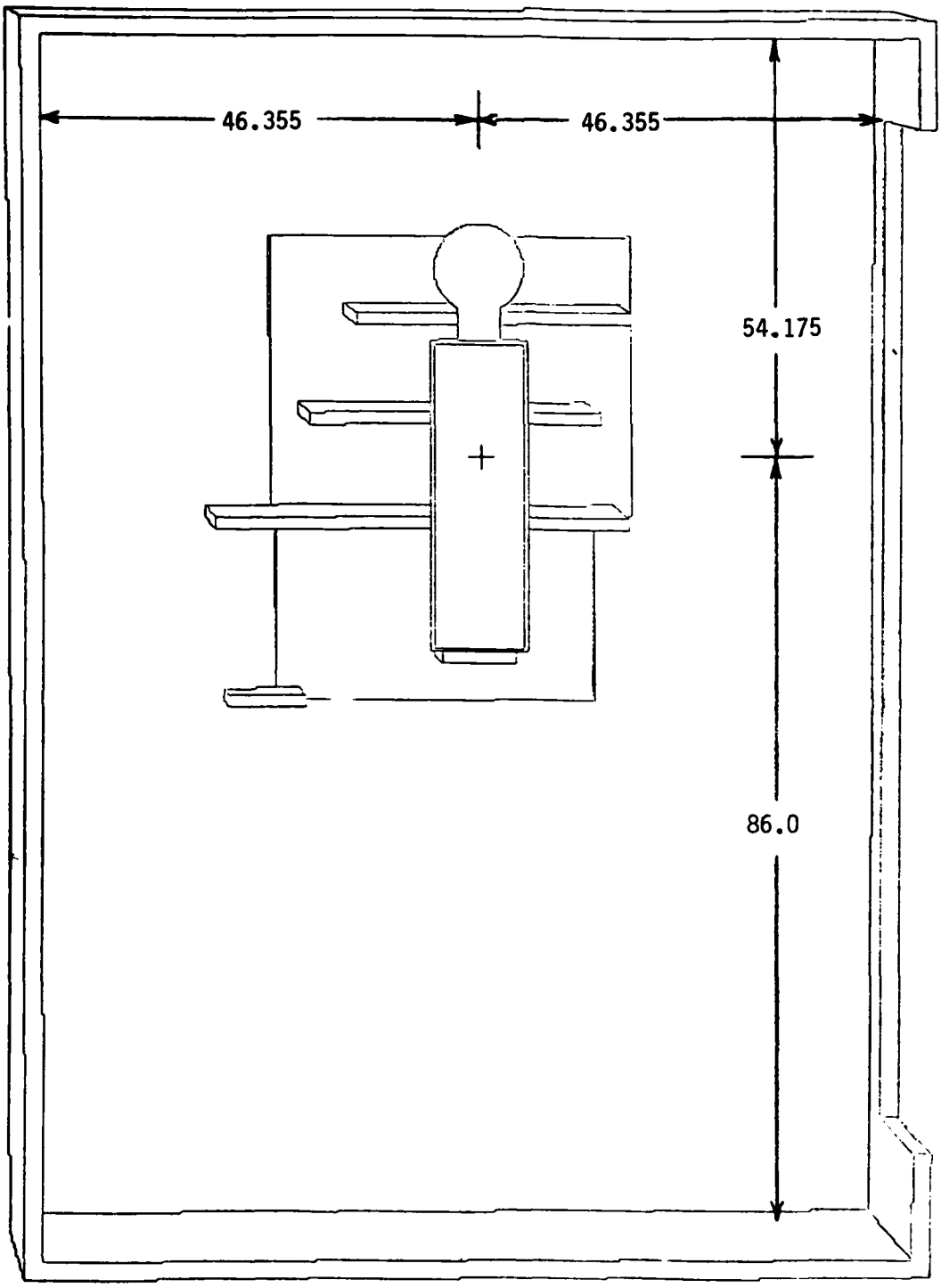

Figure 35. Orientation of simple phantom and chair within the plywood enclosure

SECTION 3

FLUENCE AND KERMA CALCULATIONS

Calculations of neutron and gamma radiation transport within the phantom-chair-box system were performed using the MORSE Monte Carlo code in the adjoint mode. In that mode particles are started at the detector position within the phantom and are followed through an inverse of the applicable physical processes until they leak from the system and are tallied by energy and direction. This process is achieved by inverting the transport cross section matrix and then performing the transport calculation much as if it were in the normal forward mode.

The value of the adjoint approach is that the results of the calculation are the equivalent of the detector response as perturbed in energy and angle by the surrounding media. Thus, if one can make the assumption that those media do not perturb a radiation field beyond their own confines, the results of the calculation may be used to determine fluence values $\Phi(E',\Omega')$ internal to the system placed in any arbitrary location or orientation within the radiation field, according to the expression:

$$\Phi(E',\Omega') = \int_S \int_E \int_\Omega \Phi(S,E,\Omega)\,\Phi^*(S,E\rightarrow E',\Omega\rightarrow\Omega')\; N\cdot\Omega\, d\Omega\, dE\, dS$$

where $\Phi(S,E,\Omega)$ is the free-field radiation fluence impinging on the surface at S, differential in energy (E) and angle (Ω), Φ^* is the adjoint fluence, born at the detector with energy E' and angle Ω', and leaking from the surface at S with energy E and angle Ω. Finally, N is a unit vector normal to the surface at S.

The above integral process is often referred to as forward-adjoint coupling and is accomplished using the VCS code system.[11] This code system is capable of associating each individual Monte Carlo adjoint leakage history with the appropriate free-field angular fluence obtained by one-, two or three-dimensional calculation methods. Because these leakage histories are fully correlated with

the description of each individual particle started at the detector site, the code system is capable of calculating either the energy-differential fluence at the detector, which results from the incident fluence, or the associated KERMA or any other appropriate quantity.

Calculations of neutron and gamma ray transport were performed for detector locations at mid-head and mid-thorax for both the complex monkey phantom and its simplified analogue. Calculations were also performed for detectors corresponding to the marrow distribution in the complex phantom, as previously described. These calculations were performed in two parts, the first starting approximately 100,000 neutrons and the second starting 100,000 gamma rays, each, for the mid-head and mid-thorax locations. This number of starting particles has been found to produce statistically reliable results (fractional standard deviations of 0.10 or lower in each of the three fluence components: neutrons, neutron-induced gamma rays and gamma rays, when each is KERMA-weighted and summed over energy and angle). For each of nine marrow regions 20,000 of each radiation type were started, giving a total of 180,000 starting particles of each type for the marrow as a whole.

Cross sections were obtained from the DNA Few Group Cross Section Library (DLC-31).[12] This library contains coupled sets of multigroup transfer cross sections in 37 neutron and 21 gamma energy intervals as shown in Table 8. The neutron cross sections were collapsed into the few group format using an assumption of in-group fluence proportional to the inverse of the energy. The thermal group was Maxwellian (300^{o} K) weighted. The gamma ray cross sections were collapsed using uniform in-group weighting. The angle of scattering was treated using a P_3 Legendre polynomial expansion.

The results of the calculations have been retained in their fully detailed form as previously described and are available for reuse at anytime. They are depicted here as adjoint leakage scalar fluence from a soft tissue KERMA detector. The KERMA values are provided in Table 9 and correspond to the components of ICRU muscle[10]. Neutron KERMA were calculated using the MACK Code[13], while those

for gamma rays were obtained from DLC-31. The adjoint KERMA-weighted leakage scalar fluence K*(E) is actually nothing more than the detector KERMA values perturbed by transport through the system and may be defined as:

$$K^*(E) = \int_S \int_{E'} \int_{\Omega'} \int_{\Omega} K(E')\, \Phi^*(S, E \rightarrow E', \Omega \rightarrow \Omega') N \cdot \Omega \, d\Omega \, d\Omega' \, dE' \, dS$$

where K(E') is the KERMA value at detector energy E'. Φ^* represents the adjoint leakage fluence from an unweighted or uniform detector response used as the adjoint source, which is in turn weighted by K(E').

The six figures beginning with Figure 36 depict the adjoint neutron scalar fluence for neutron and neutron-induced gamma ray KERMA and the adjoint gamma ray scalar fluence for gamma ray KERMA, applicable to each phantom type and dosimeter location. These data are presented as group fluences and are similarly tabulated in the Appendix. This format is used to present the adjoint scalar fluence in a form equivalent to the KERMA, which are used as the adjoint source. This format is also used later in the report to present the transmitted fluence spectra, because it allows for simple convolution with group KERMA to obtain total KERMA values. The horizontal scale is linear above 1 MeV to provide better resolution for the reader in this dosimetrically important range. For the complex phantom the results for mid-head, mid-thorax and marrow locations are plotted together for each radiation component. The KERMA values are coplotted for comparison purposes, since, as mentioned previously, the adjoint fluences may be regarded as transport-weighted KERMA. For the neutron and gamma components the adjoint leakage fluences are larger for the mid-head than for the mid-thorax location, reflecting the relative masses of material surrounding the two sites. Because the marrow is distributed among shallow and deep sites the aggregate marrow response shows an irregular relationship with but is generally between those of the other two locations. The behavior of gamma ray production by neutrons as a function of neutron energy in the complex phantom is dominated by a minimum caused by a decrease in the likelihood that neutrons of increasing energy, but still below the inelastic threshold, will undergo the series of scattering events required for thermalization and capture without leaking from the system. Likewise, geometry plays a part in the production of gamma ray KERMA by incident neutrons. The

mid-thorax presents the most favorable geometry by surrounding the dosimetry point with production media in a nearly uniform manner. The mid-head location is a bit more toward an extremity and so receives fewer of the volume-generated gamma rays. That marrow component which is located at shallow locations receives even less, since the gamma rays can reach such marrow only from half-space. Hence, the aggregate marrow neutron-gamma response resembles that of the mid-head rather than the mid-thorax.

The adjoint fluences from the simple phantom show characteristics similar to those of the complex phantom, although the neutron adjoint fluences are slightly lower for the simple phantom. The neutron-induced gamma ray responses are also similar. However, the minimum, which was so evident in the complex phantom response, is considerably less pronounced in the case of the simple phantom. The simple phantom is not more massive overall than the complex phantom. However, it is more compact, particularly in the trunk, i.e., it is larger in diameter and shorter, which results in less leakage of neutrons subsequent to their penetration of the system.

It is recognized that, while of some academic interest, the adjoint leakage scalar fluence may in fact be of little relevance to the understanding of the dosimetry characteristics of a complex system, such as the monkey-chair-box. This is particularly true when the dosimeter location within such a system favors a particular exposure direction and the experimental radiation field is itself highly directional. As a first order attempt to understand the non-isotropic nature of the system, it is useful to examine the adjoint fluence integrated over less than 4π steradians. To this end, the three figures beginning with Figure 42 depict the adjoint leakage fluence from the mid-thorax location in the realistic (complex) phantom, integrated separately over 4π steradians and over the hemisphere facing the reactor (front 2π) and that facing away from the reactor (back 2π). This case is considered to be qualitatively representative of all cases studied here. However, these data are tabulated for all calculated configurations in the Appendix.

Table 8. Neutron and gamma-ray energy boundaries for the 37-21 coupled neutron-gamma library

Group #	Neutron Group (eV) Energy	Lethargy	Gamma Group (eV) Energy	Eff. Avg.
1	1.96+7	-0.675	1.40+7	1.20+7
2	1.69+7	-0.525	1.00+7	9.00+6
3	1.49+7	-0.400	8.00+6	7.50+6
4	1.42+7	-0.350	7.00+6	6.50+6
5	1.38+7	-0.325	6.00+6	5.50+6
6	1.28+7	-0.250	5.00+6	4.50+6
7	1.22+7	-0.200	4.00+6	3.50+6
8	1.11+7	-0.100	3.00+6	2.75+6
9	1.00+7	0.000	2.50+6	2.25+6
10	9.05+6	0.100	2.00+6	1.75+6
11	8.19+6	0.200	1.50+6	1.25+6
12	7.41+6	0.300	1.00+6	8.50+5
13	6.38+6	0.450	7.00+5	5.75+5
14	4.97+6	0.700	4.50+5	3.75+5
15	4.72+6	0.750	3.00+5	2.25+5
16	4.07+6	0.900	1.50+5	1.25+5
17	3.01+6	1.200	1.00+5	8.50+4
18	2.39+6	1.433	7.00+4	5.57+4
19	2.31+6	1.467	4.50+4	3.75+4
20	1.83+6	1.700	3.00+4	2.50+4
21	1.11+6	2.200	2.00+4	1.50+4
22	5.50+5	2.900	1.00+4	
23	1.58+5	4.150		
24	1.11+5	4.500		
25	5.25+4	5.250		
26	2.48+4	6.00		
27	2.19+4	6.125		
28	1.03+4	6.875		
29	3.35+3	8.000		
30	1.23+3	9.000		
31	5.83+2	9.750		
32	1.01+2	11.500		
33	2.90+1	12.750		
34	1.07+1	13.750		
35	3.06+0	15.000		
36	1.13+0	16.000		
37	4.14-1	17.000		
Lower Bound	1.00-5	27.631		

*Read as 1.96×10^{7}.

Table 9. Soft tissue KERMA
(rads per unit fluence)

Group #	UPPER E(MeV)	Neutron KERMA	Group #	UPPER E(MeV)	Neutron KERMA
1	19.6	7.37-9	31	5.83-4	3.83-12
2	16.9	7.12-9	32	1.01-4	1.10-12
3	14.9	6.88-9	33	2.90-5	9.29-13
4	14.2	6.74-9	34	1.07-5	1.31-12
5	13.8	6.55-9	35	3.06-6	2.24-12
6	12.8	6.43-9	36	1.13-6	3.64-12
7	12.2	6.31-9	37	4.14-7	1.77-11
8	11.1	6.01-9	Lower Bound	1.00-11	
9	10.0	5.77-9			
10	9.05	5.53-9			
11	8.19	5.45-9	1	14.0	2.98-9
12	7.41	5.16-9	2	10.0	2.35-9
13	6.38	4.74-9	3	8.0	2.03-9
14	4.97	4.56-9	4	7.0	1.87-9
15	4.72	4.44-9	5	6.0	1.65-9
16	4.07	4.23-9	6	5.0	1.44-9
17	3.01	3.59-9	7	4.0	1.22-9
18	2.39	3.34-9	8	3.0	1.03-9
19	2.31	3.22-9	9	2.5	9.05-10
20	1.83	2.80-9	10	2.0	7.57-10
21	1.11	2.16-9	11	1.5	5.88-10
22	5.50-1	1.40-9	12	1.0	4.28-10
23	1.58-1	8.12-10	13	0.7	3.02-10
24	1.11-1	5.80-10	14	0.45	1.95-10
25	5.25-2	3.26-10	15	0.30	1.09-10
26	2.48-2	2.11-10	16	0.15	5.32-11
27	2.19-2	1.53-10	17	0.10	3.47-11
28	1.03-2	6.93-11	18	0.07	3.17-11
29	3.35-3	2.42-11	19	0.045	4.96-11
30	1.23-3	9.57-12	20	0.030	1.14-10
			21	0.020	3.66-10
			Lower Bound	0.010	

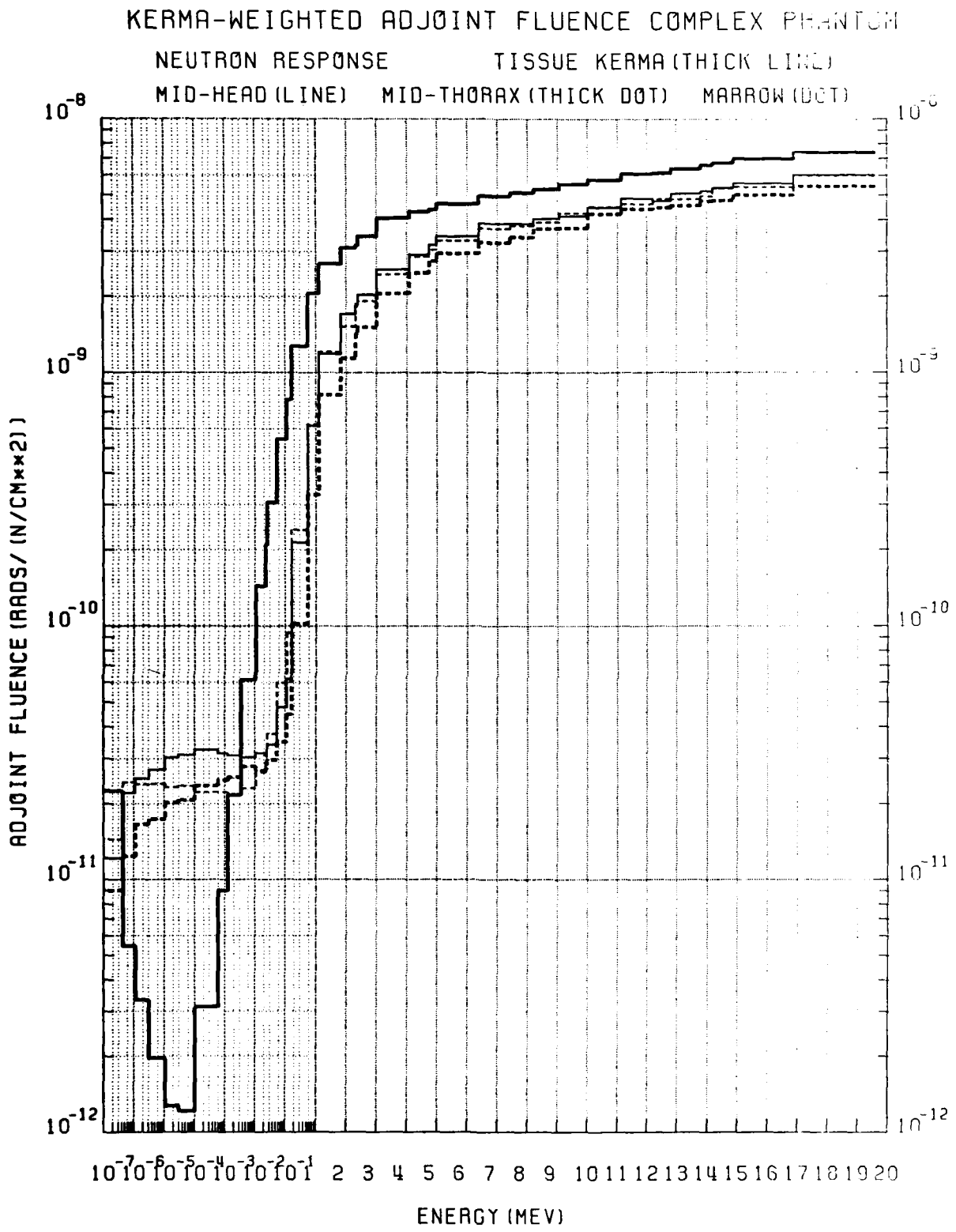

Figure 36. KERMA-weighted adjoint fluence complex phantom (n)

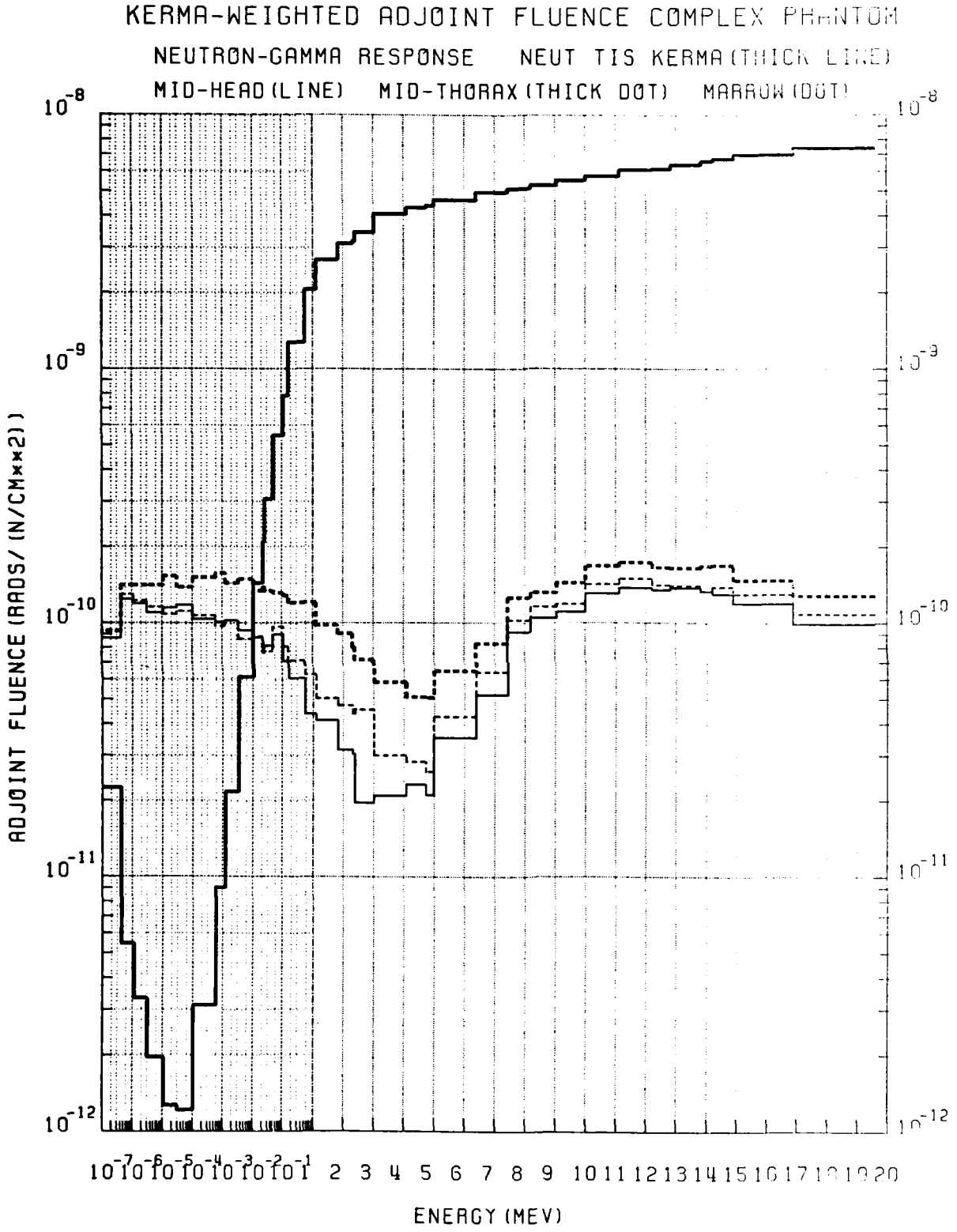

Figure 37. KERMA-weighted adjoint fluence complex phantom (n-g)

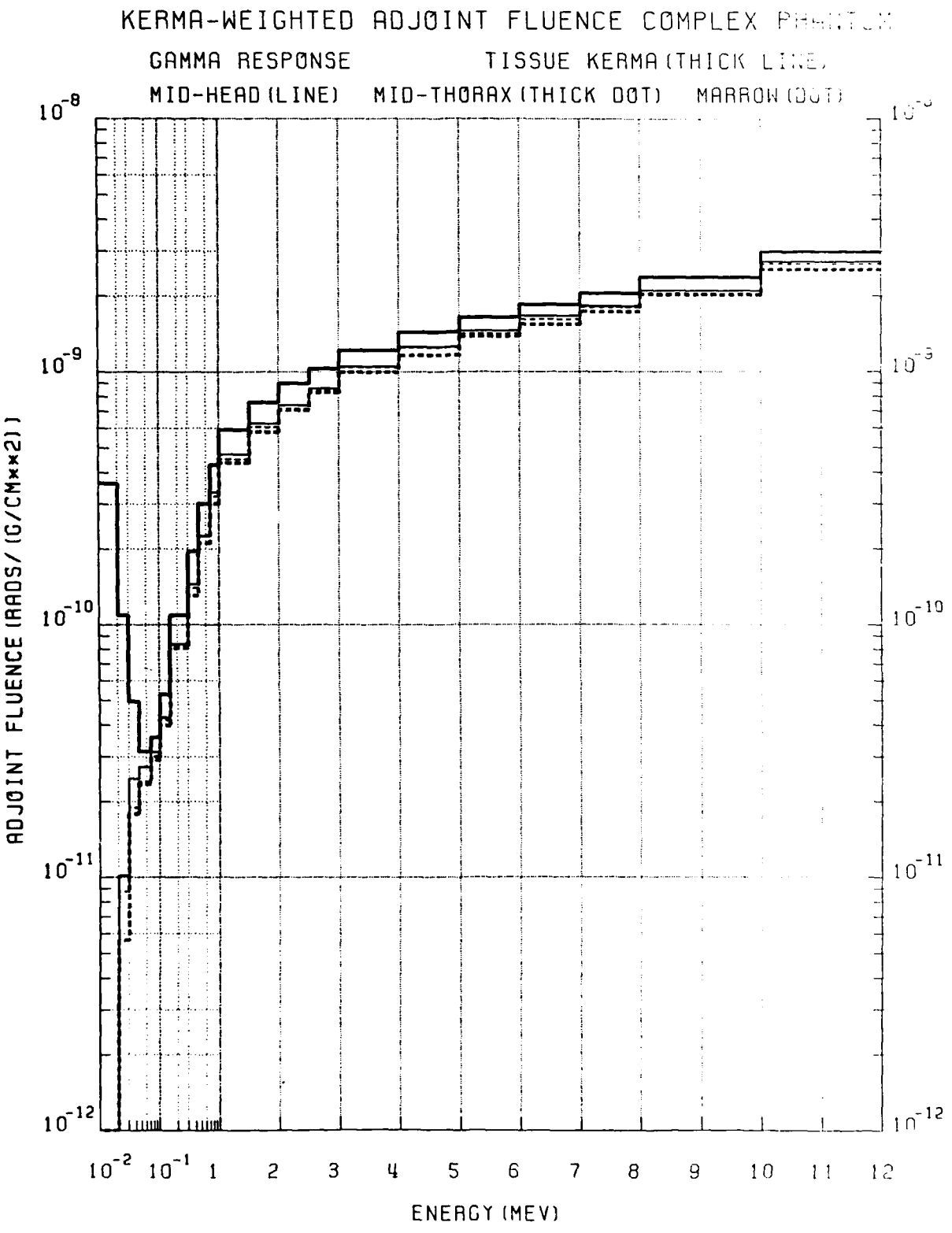

Figure 38. KERMA-weighted adjoint fluence complex phantom (g)

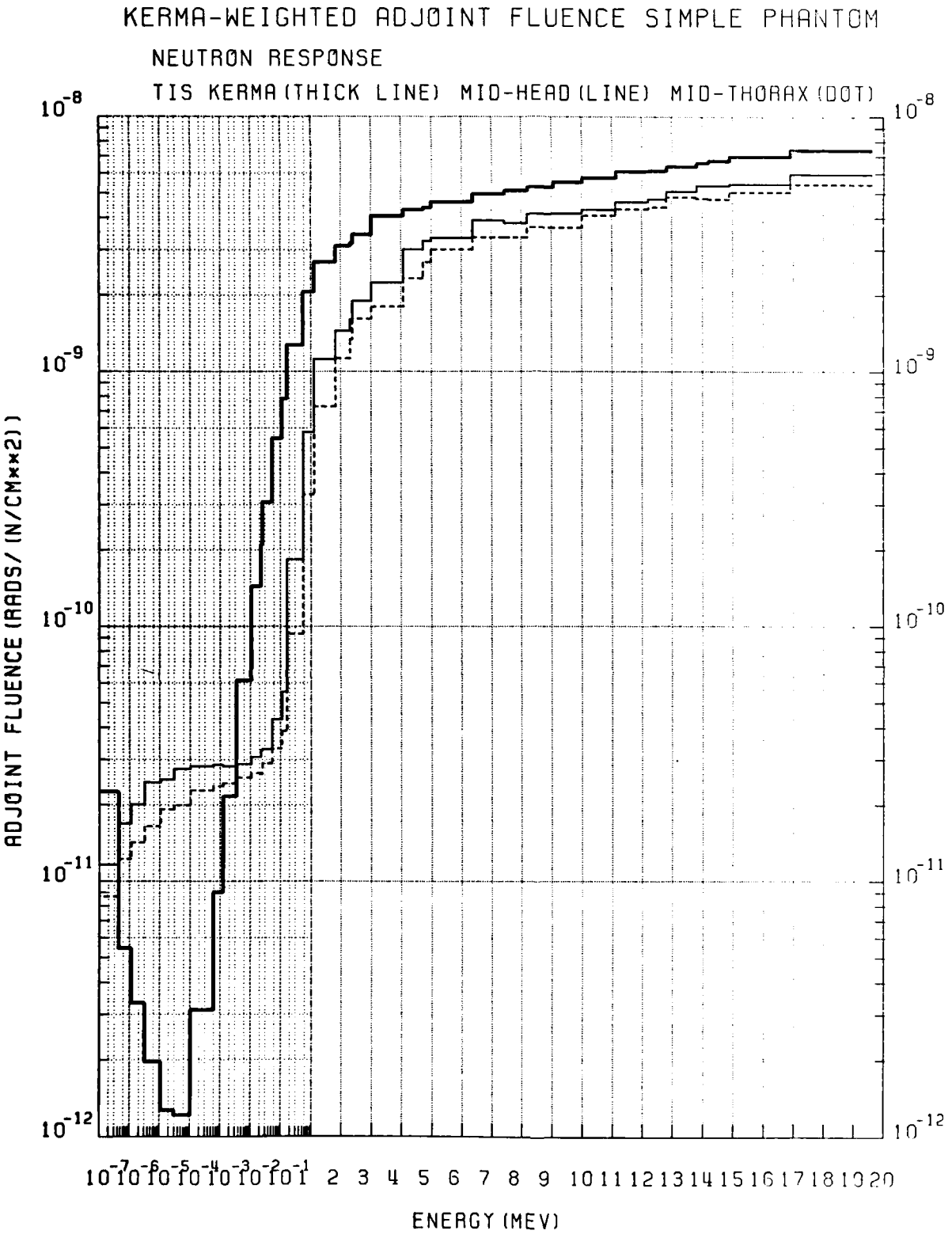

Figure 39. KERMA-weighted adjoint fluence simple phantom (n)

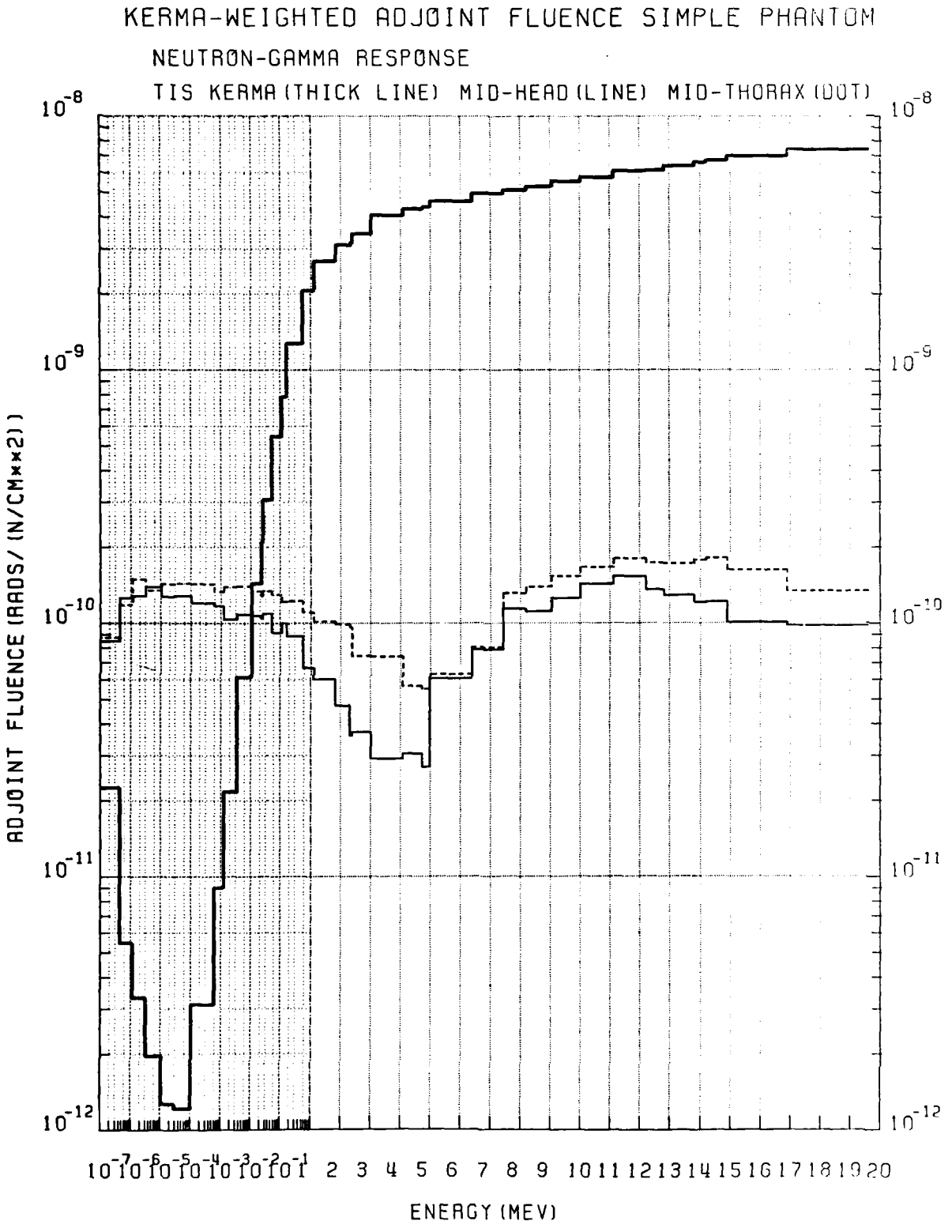

Figure 40. KERMA-weighted adjoint fluence simple phantom (n-g)

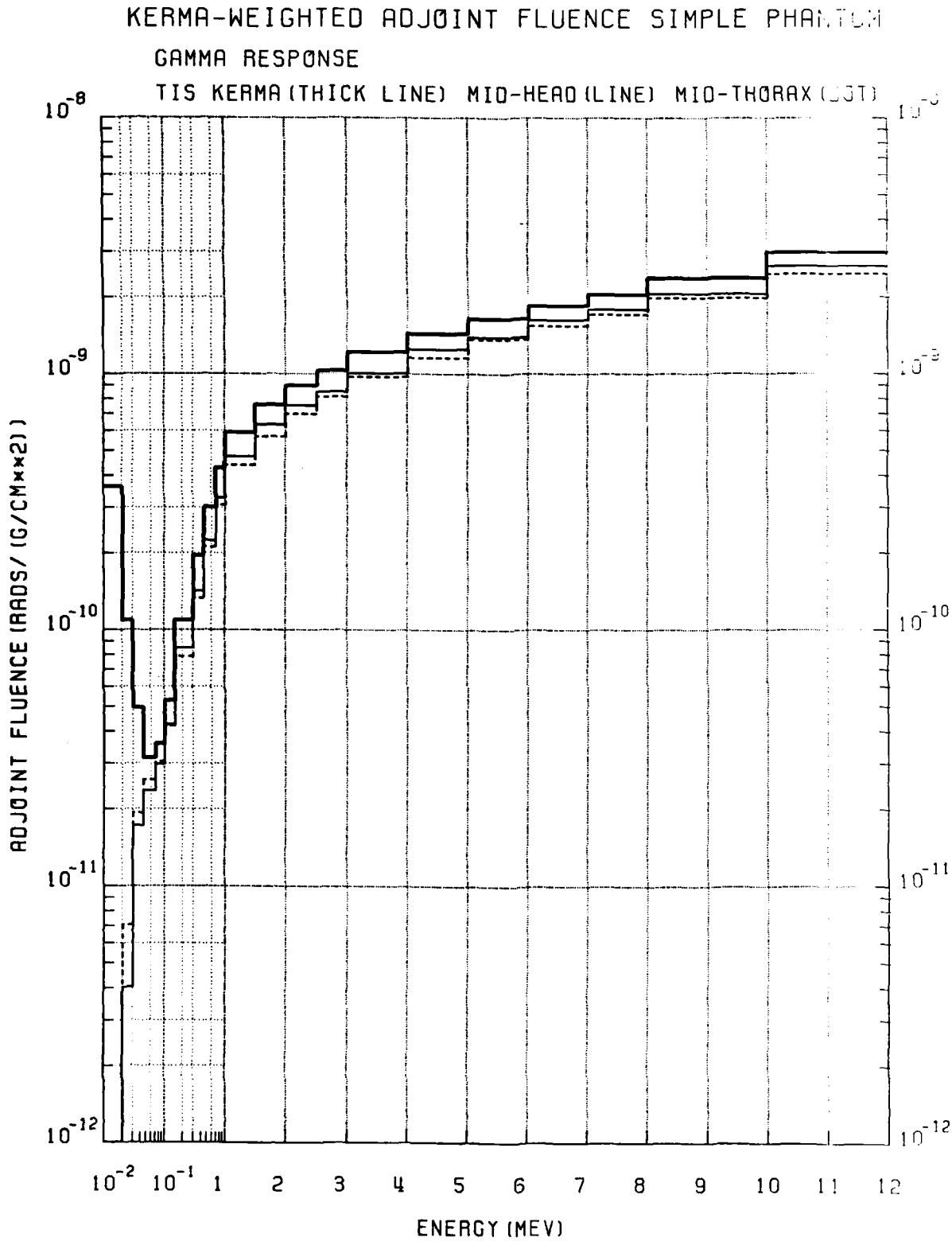

Figure 41. KERMA-weighted adjoint fluence simple phantom (g)

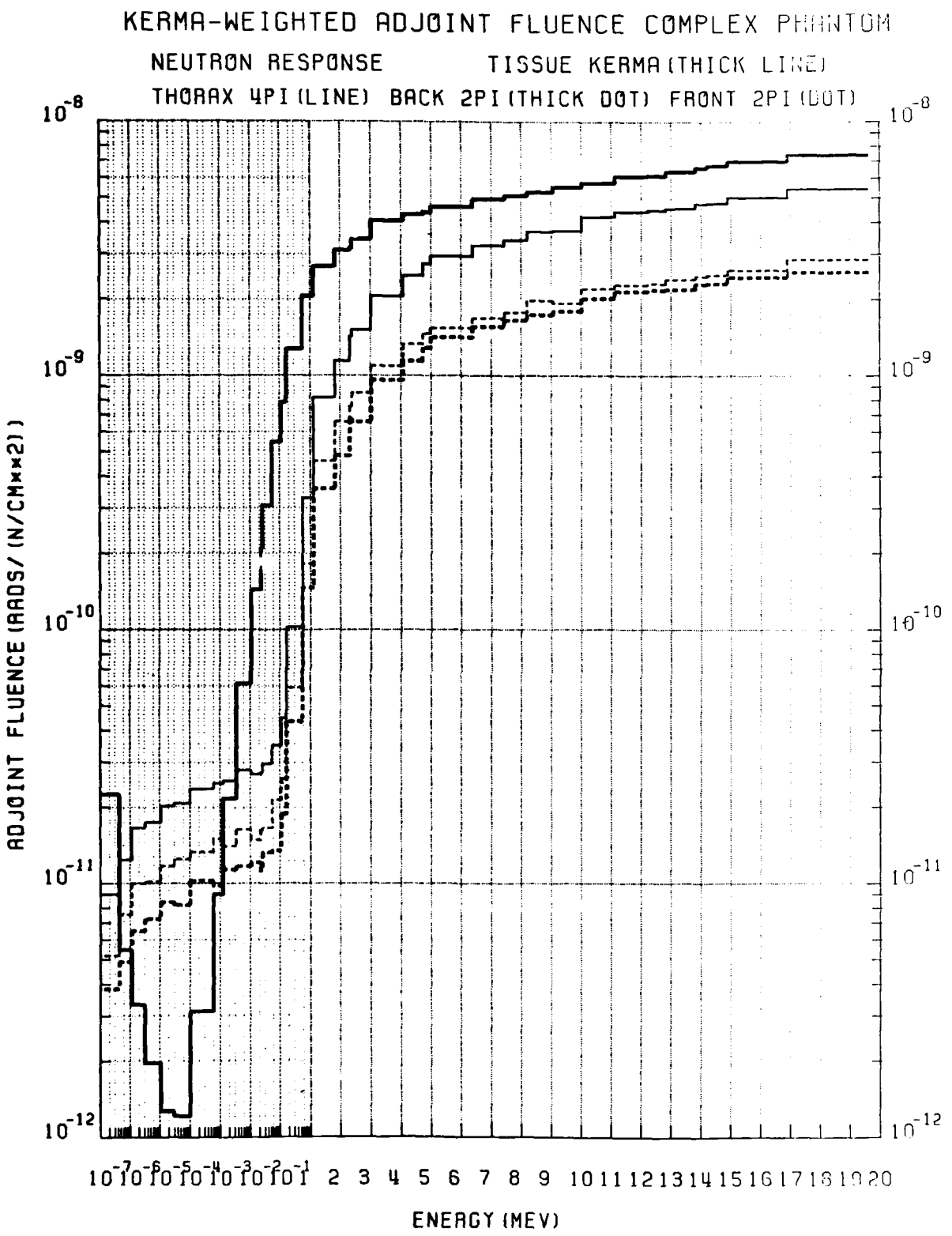

Figure 42. KERMA-weighted adjoint fluence simple phantom (n)

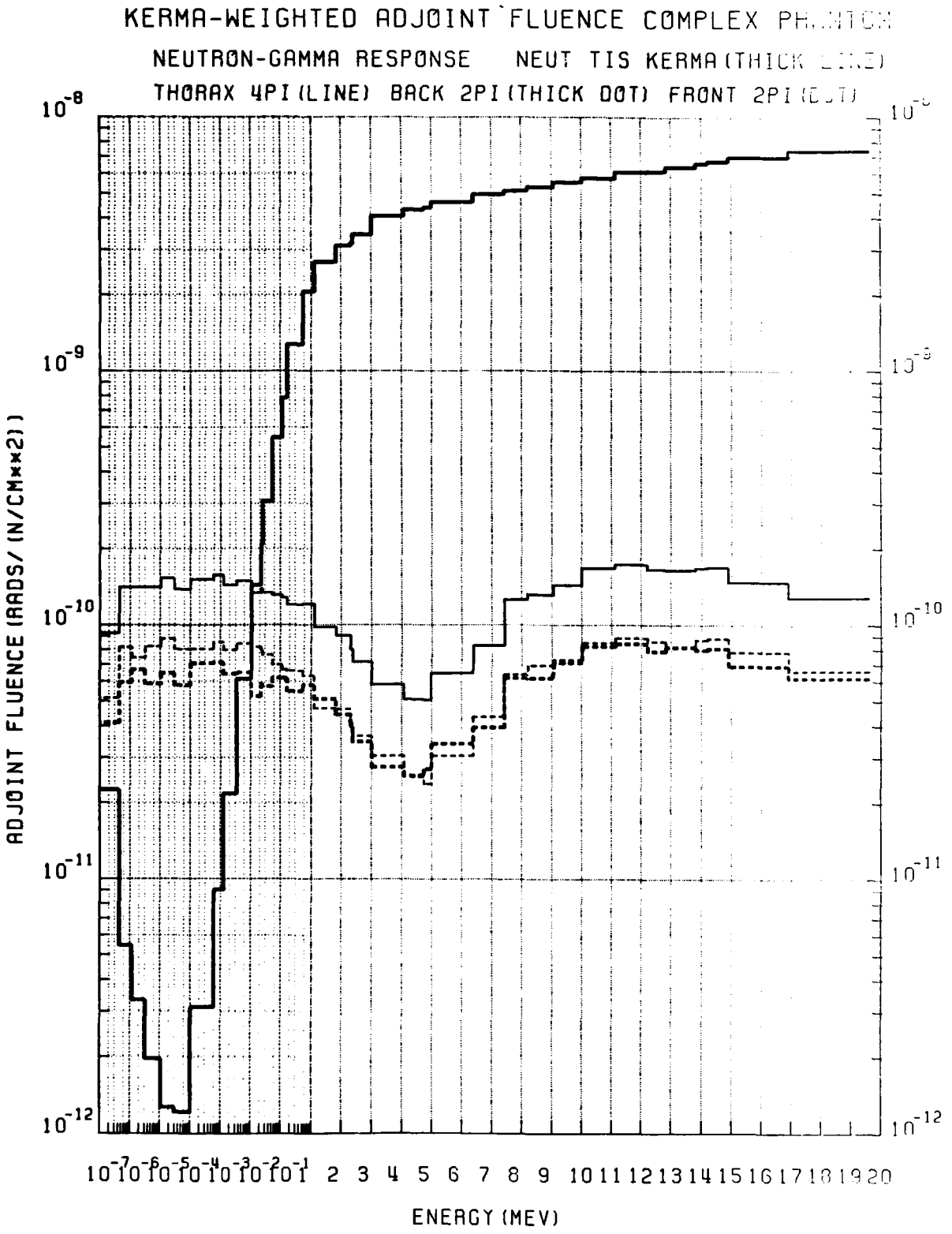

Figure 43. KERMA-weighted adjoint fluence complex phantom (n-g)

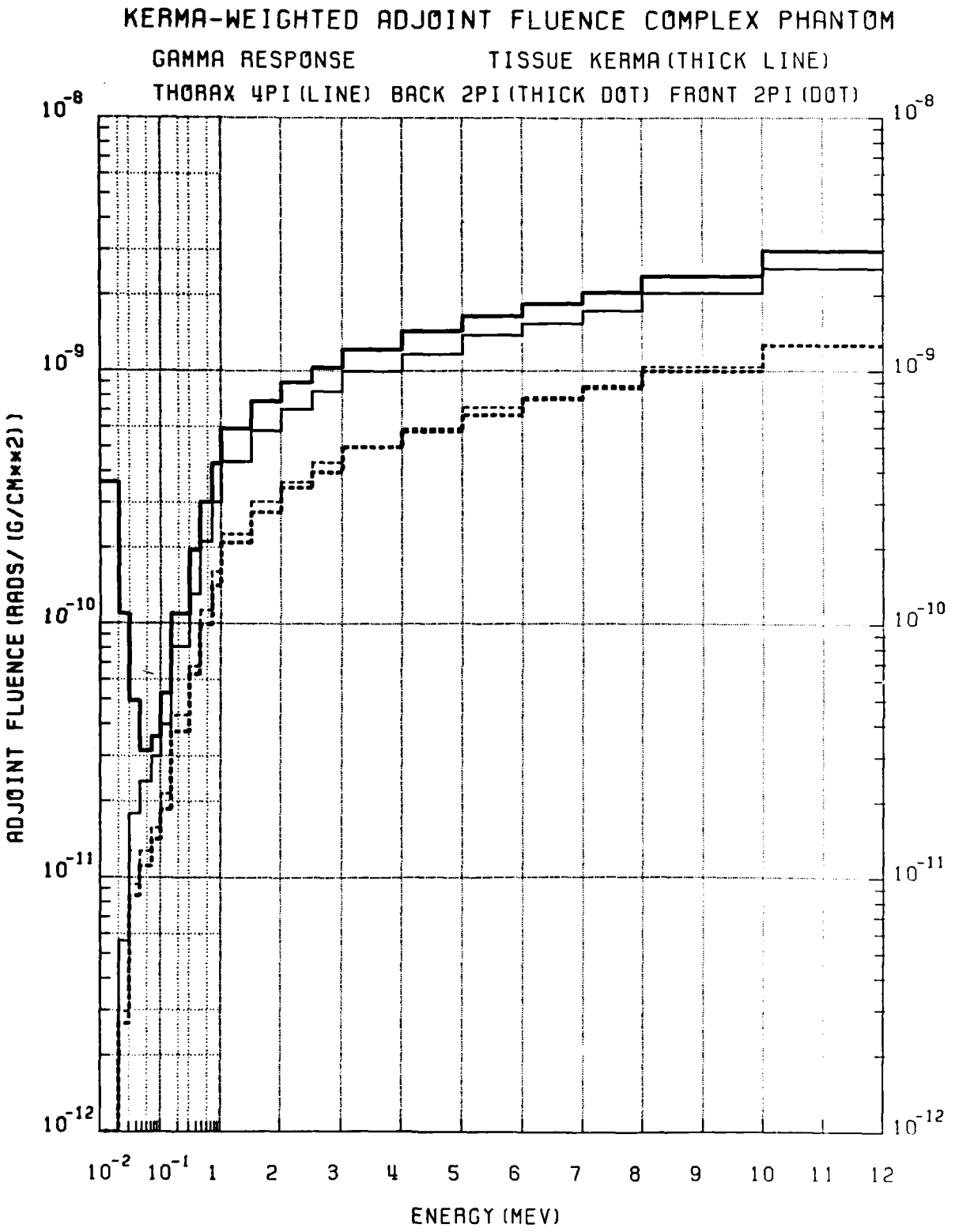

Figure 44. KERMA-weighted adjoint fluence complex phantom (g)

The neutron and gamma ray adjoint fluences of the system, which includes the complex phantom, chair and box, have slightly larger values in the direction facing the reactor, particularly at lower incident energies. This corresponds to exposure of the back of the monkey phantom itself. The bias in favor of this direction is not large and, since the mid-thorax is centrally located front to back, is probably due to the shielding contribution of the box. The effect is likely to be enhanced somewhat for the marrow, which is somewhat biased toward the posterior of the phantom.

The neutron-induced gamma ray adjoint fluence, shown in Figure 43, shows less preference for the frontal exposure except at very low neutron energies. It is expected that these are the most affected by the box surrounding the monkey.

It should be noted that the adjoint fluence integrated over 4π or even 2π does not reflect any variation with polar angle, which is significant, as will be described later in this report.

3.1 Free-Field Coupling

It is the ultimate goal of these calculations to be able to predict fluence and KERMA values in instances which are not practical for experimental dosimetry. To do this using the forward-adjoint coupling technique, described previously, requires that an applicable free-field fluence be defined. This has been done in a previous program using one and three-dimensional calculational techniques.[2] The one-dimension results were found to give good representations of the free-field scalar fluence spectra, although the absolute normalization and, perhaps, the angular distribution were not correct due to simplifications in source geometry. Because monitor data are available for these experimental exposures, the absolute normalization is not a critical issue. On the other hand no confirmation of radiation fluence angular distribution calculated by one dimensional techniques has been accomplished using experimental or multi-dimensional calculations. However, such multi-dimensional calculations are beyond the scope of this study. Thus, one dimensional energy and angle-differential fields have been chosen to represent the AFRRI exposure room radiation environments.

AFRRI has two exposure rooms, characterized as ER1 and ER2 in the previous study. Forward-adjoint coupling has been performed for each of these rooms in separate configurations. The ER2 configuration is that of the bare room, with the dosimetry point 100 centimeters from the reactor core centerline, 92 centimeters from the floor. This corresponds to case 5 in the previous study. The ER1 configuration includes a two inch thick lead slab between the reactor and the dosimetry point, which is 100 centimeters from the core centerline and 120 centimeters above the floor. This corresponds to case 7 in the previous study. The neutron and gamma spectra ray spectra calculated for these two locations are depicted in Figures 45 and 46, respectively. These have been normalized to produce the following measured soft tissue free-in-air (FIA) KERMA rates (rad-FIA per Kw-min):[9]

ER1 with 2" Pb @ 100 cm
    neutron 7.80
    gamma ray 2.22
ER2 bare @ 100 cm
    neutron 10.8
    gamma ray 19.8

Beside the obvious reduction in gamma rays caused by the lead it should be noted that the lead also causes a substantial shift in the neutron spectrum toward lower energies in the region of 1 MeV and above. It also results in substantial depletion of thermal and epithermal neutrons. It should be noted that measurements made at other distances from the reactor[14] show a reduction of free-field intensity of ten percent or more at locations offset from the reactor centerline, corresponding to the mid-head location. However, no free-field values for the mid-head location are available at the 100 cm distance. Therefore, for the purposes of this report all data are normalized to the intensity measured 100 cm from the reactor midline.

The VCS system calculates the transmitted fluence at the detector from an externally incident fluence, taking into account its full energy-angle detail. However, before examining the calculated transmitted fluences it is useful to examine the character of such transmission on the basis of transmission factors

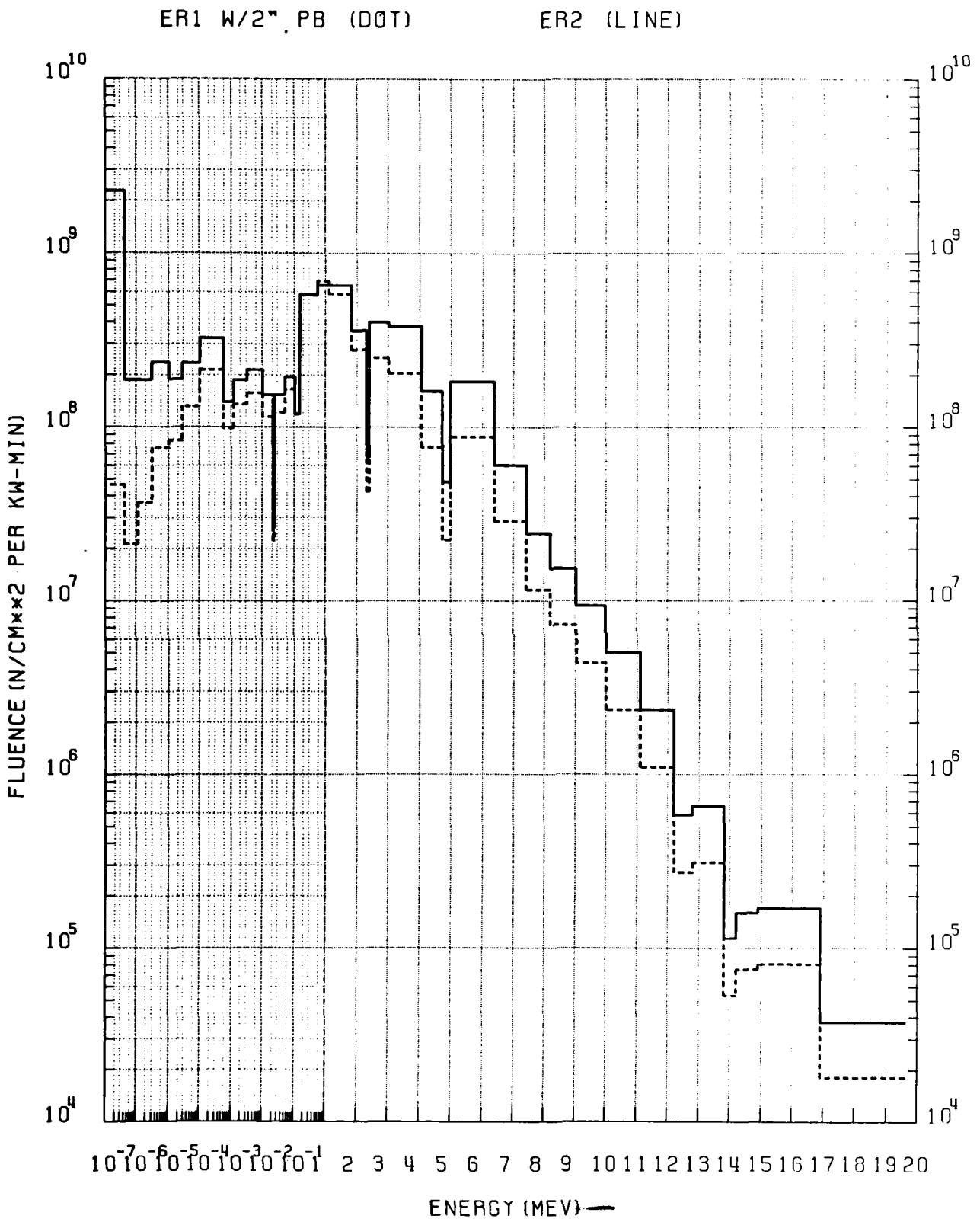

Figure 45. Neutron fluence for ER1 and ER2

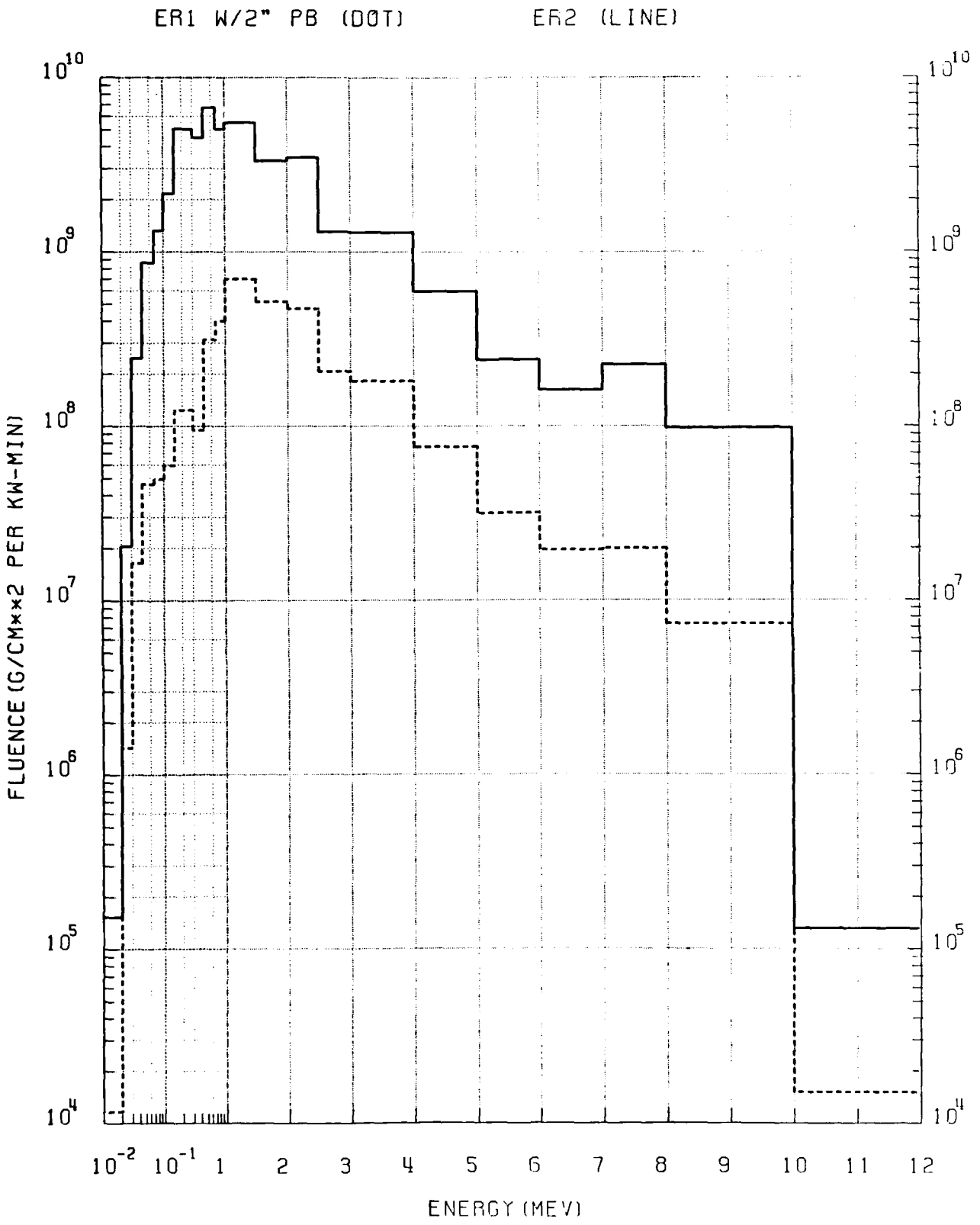

Figure 46. Gamma fluence for ER1 and ER2

calculated by dividing the KERMA-weighted transmitted fluence by that of the free-field. These transmission factors are presented in Table 10 for the complex and simple phantoms in each exposure room, along with their corresponding fractional standard deviation (FSD).

Looking first at the simple phantom, there appears to be little difference in either room between transmission to the mid-head and to the mid-thorax, at least for neutrons and gamma rays and within the statistical uncertainties in the calculations. In the case of the neutron-induced gamma ray transmission, obtained by dividing the gamma ray KERMA produced by the neutron interactions in the phantom by the neutron free-field KERMA, the transmission to the mid-thorax is considerably greater than that to the mid-head. This is due to geometry considerations, as previously discussed.

Looking further at the differences in transmission between the two rooms it can be seen that the incident gamma ray spectra do not differ sufficiently to produce significantly different transmission factors in the two rooms. On the other hand, the neutron spectra are sufficiently different to produce something of a paradox between the neutron and neutron-gamma ray transmission factors for the two rooms. The absence of the lead shield in room 2 allows a large number of epithermal and thermal neutrons to be incident on the phantom in that room. These count for very little in so far as neutron KERMA is concerned but are very efficient in producing gamma rays in the phantom. Thus, the neutron-gamma KERMA per unit free-field neutron KERMA are largest in room 2. However, even through this is evidence of a softer neutron spectrum in room 2, the neutron transmission in that room is higher than in room 1. This seeming paradox is explained by the fact that, in the energy region most heavily weighted by the KERMA, it is the neutron spectrum in room 2 which is the hardest or most energetic and, hence, the most penetrating. The lead in room 1 softens the spectrum in the KERMA-weighted region by repeated scatterings, while absorbing the low energy neutrons which have little KERMA value.

There is little qualitative difference between the behavior of transmission for the simple and complex phantoms, though there seems to be some evidence for consistently less gamma ray transmission to the complex mid-head. This may be due

Table 10. Calculated transmission factors for the complex and simple monkey phantoms

Exposure Room 1, @ 100 cm from core centerline, with 2 inches of lead intervening.

Location	Component	Transmission Factor (FSD) Complex	Simple
Mid Head	n	0.635 (.03)	0.572 (.03)
	n-γ	0.040 (.07)	0.058 (.06)
		0.909 (.03)	0.971 (.03)
Mid Thorax	n	0.593 (.03)	0.572 (.03)
	n-γ	0.088 (.05)	0.089 (.05)
		0.952 (.03)	0.925 (.03)
Active Marrow	n	0.685 (.03)	
	n-γ	0.048 (.05)	
	γ	0.919 (.03)	

Complex Phantom Marrow Region/Component	n	n-γ	γ
Skull	0.493 (.07)	0.025 (.18)	0.756 (.06)
Clavicles	0.705 (.07)	0.036 (.13)	0.851 (.06)
Scapulae	0.635 (.07)	0.042 (.13)	0.967 (.06)
Upper Limbs	0.620 (.07)	0.038 (.14)	0.916 (.06)
Ribs	0.701 (.07)	0.049 (.12)	0.903 (.06)
Vertebrae	0.749 (.06)	0.063 (.11)	1.036 (.06)
Pelvis	1.037 (.06)	0.057 (.14)	0.953 (.05)
Upper Femur	0.987 (.06)	0.059 (.15)	0.961 (.06)
Lower Limbs	0.299 (.09)	0.027 (.15)	0.711 (.06)

Table 10. Calculated transmission factors for the complex and simple monkey phantoms (continued)

Exposure Room 2, @ 100 cm from core centerline, bare room.

Location	Component	Transmission Factor (FSD) Complex	Simple
Mid Head	n	0.738 (.04)	0.661 (.04)
	n-γ	0.069 (.06)	0.090 (.05)
		0.920 (.03)	0.968 (.03)
Mid Thorax	n	0.718 (.04)	0.695 (.04)
	n-γ	0.136 (.05)	0.131 (.05)
		0.972 (.03)	0.957 (.03)
Active Marrow	n	0.722 (.03	
	n-γ	0.087 (.05)	
	γ	0.935	

Complex Phantom Marrow Region/Component	n	n-γ	γ
Skull	0.541 (.09)	0.047 (.14)	0.728 (.06)
Clavicles	0.859 (.08)	0.074 (.10)	0.887 (.06)
Scapulae	0.749 (.08)	0.093 (.12)	0.971 (.06)
Upper Limbs	0.735 (.08)	0.074 (.12)	0.925 (.06)
Ribs	0.793 (.08)	0.093 (.10	0.916 (.05)
Vertebrae	0.836 (.07)	0.107 (.10)	1.058 (.05)
Pelvis	1.164 (.07)	0.106 (.11)	1.006 (.05)
Upper Femur	0.994 (.07)	0.104 (.13)	1.020 (.05)
Lower Limbs	0.337 (.11)	0.050 (.14)	0.696 (.06)

to the skeletal material of the skull, which has a higher density than soft tissue, thus affecting gamma ray transport, but little difference with soft tissue in hydrogen density, thus leaving neutron transport relatively unaffected. In fact the elliptical geometry of the complex head appears to provide for increased transmission of neutron KERMA with an attendant decrease in neutron-induced gamma ray production, compared to the simple phantom.

The mean value of the transmission of KERMA to marrow locations in the complex phantom is similar to that for the mid-head, though the neutron transmission is consistently larger. However, transmission values for the various marrow regions show that the mean value is made up of widely differing components. Those range from the low transmission factors for the best shielded components, such as the lower limbs and the skull, to transmission factors of the order of unity for the least well shielded locations, i.e., the vertebrae, pelvis and upper femur. Buildup in the phantom and scatter from the surrounding chair and box play a role in producing such large transmission factors for marrow locations closest to the reactor. The low transmission to the lower limbs is also understandable. However, the low transmission to the skull, particularly as compared to another location similar in depth and distribution, the ribs, is subject to question. It is possible that the box is responsible. However, if this is so then a premium is placed on the correct angular distribution incident on this location. As noted previously, the free-field angular distribution used in these calculations has not been verified.

Figures 47 through 62 depict the transmitted neutron and gamma ray spectra at the various dosimetry points in the complex and simple phantoms in each exposure room. Data appearing in these figures are tabulated in the Appendix along with that for all detailed marrow locations. In each figure the free-field (FF) scalar fluence is depicted as a thick line. The mid-head fluence is represented by a thin solid line, the mid-thorax fluence by a thin dotted line and, in the case of the complex phantom, the marrow fluence is represented by a thick dotted line.

Figures 47 through 50 depict the fluences in the complex phantom in exposure room one. The transmitted neutron fluences in Figure 47 show substantial reduction below the free-field above one MeV. Below that energy the phantom tends

to increase the transmitted fluence relative to the free-field, particularly in the thermal region. The neutron-induced gamma fluence shown in Figure 48 is noteworthy mainly for the large peak between 2 and 2.5 MeV, which is the energy range of the hydrogen capture gamma ray. In this one group the fluence from the neutron-induced gamma rays approches and even exceeds that of the room free-field gamma rays as shown by the thick solid line. The gamma ray transmission shown in Figure 49 is noteworthy for the large buildup of gamma ray fluence below one MeV. This buildup is particularly noticeable for the mid-thorax location, which is probably due to the fact that, while the torso and head of the complex phantom are of similar diameter, the skull material tends to screen out low energy gamma rays, as does the nearby box.

Figure 50 shows the total gamma ray fluence in the complex phantom co-plotted with the free-field. The large enhancement of the gamma ray fluence in the range about 100 keV and 1 MeV are very noticeable. At higher energies there is some enhancement due to the lack of attenuation by the phantom for incident gamma rays and some production of high energy gamma rays by incident neutrons, particularly in hydrogen and nitrogen. The marrow fluence appears to be more in line with that of the mid-head than the mid-thorax, though there is considerable statistical uncertainty in the fluence in individual energy groups.

Figures 51 through 54 provide information for the complex phantom in exposure room two similar to that described above for room one. The general characteristics of the transmitted fluences in the two rooms are similar even though differences exist in the free-field spectra. Thus, the build up of the low energy neutrons and gamma rays in the phantom is less noticeable, since the free-field contains more to begin with. Further, the effect of the neutron-induced gamma rays in the phantom is less pronounced because of the low free-field neutron-gamma ray ratio.

Figures 55 through 58 depict the transmitted fluence calculated via VCS for the simple phantom in exposure room one. In Figures 55 and 57 it can be seen that for the high energy (E > 1 MeV) portions of the transmitted neutron and gamma ray spectra there is no consistent difference between those for the mid-head and those for the mid-thorax from group to group. Instead, fluences for the two locations

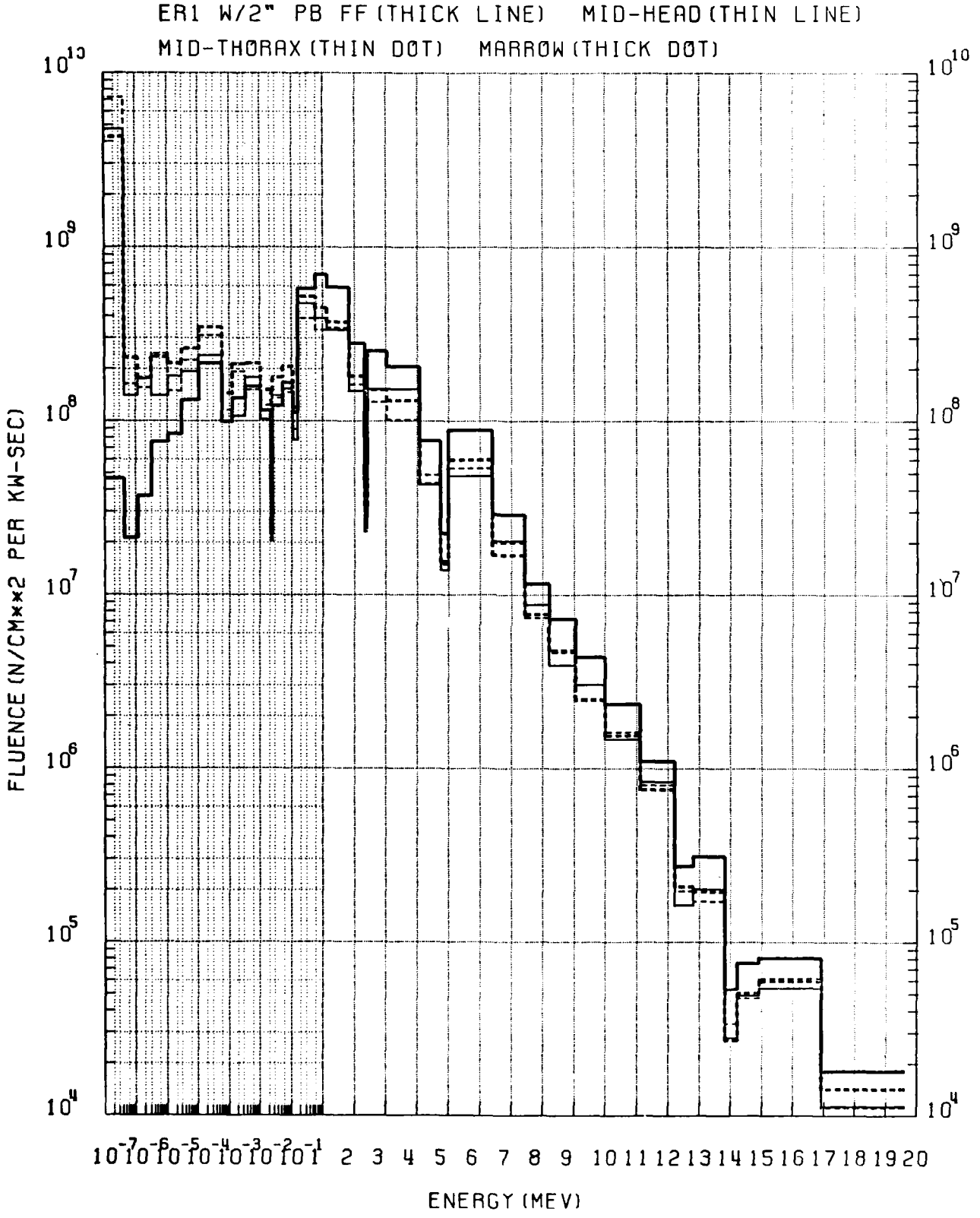

Figure 47. Neutron fluence for ER1 and complex phantom

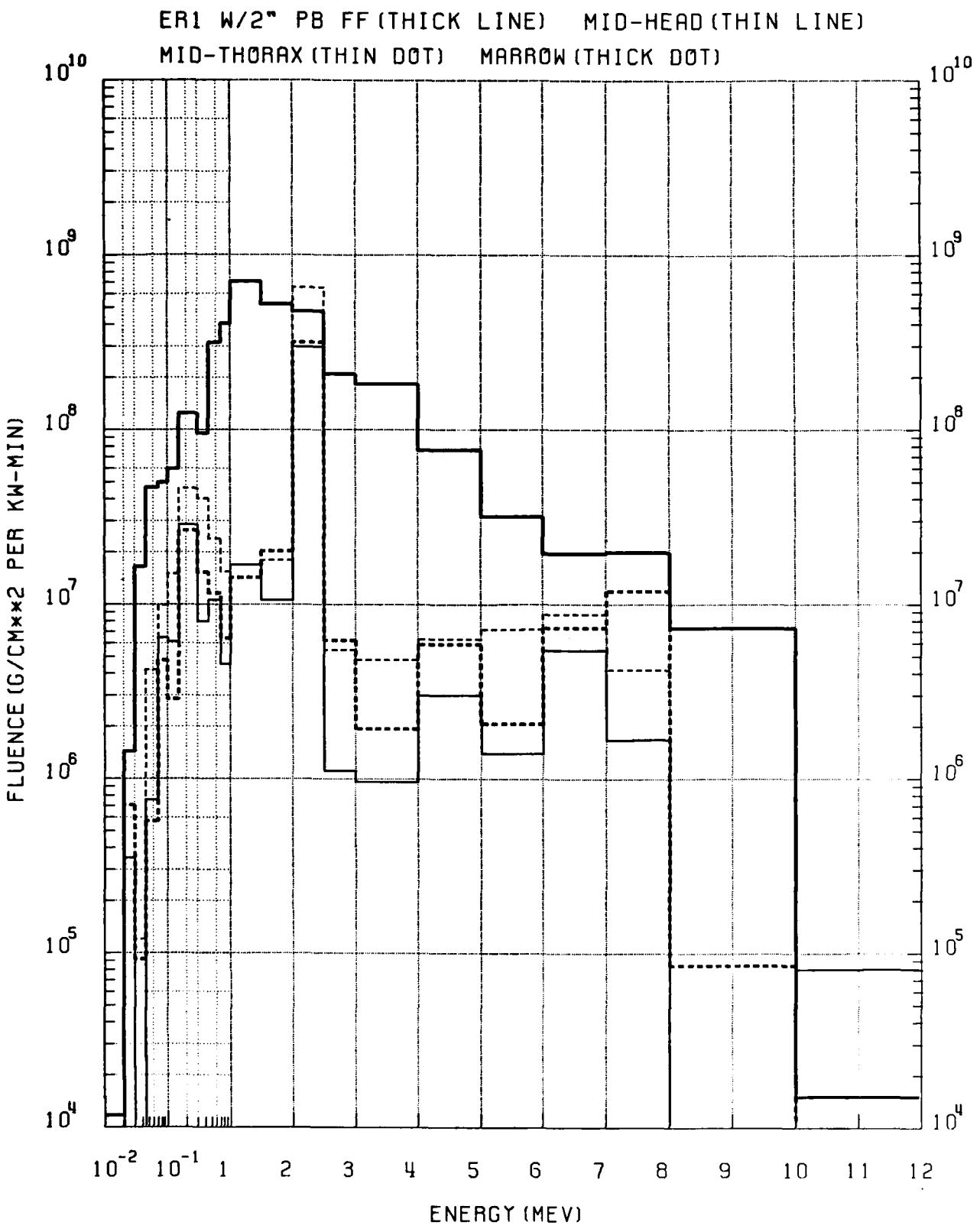

Figure 48. N-G fluence for ER1 and complex phantom

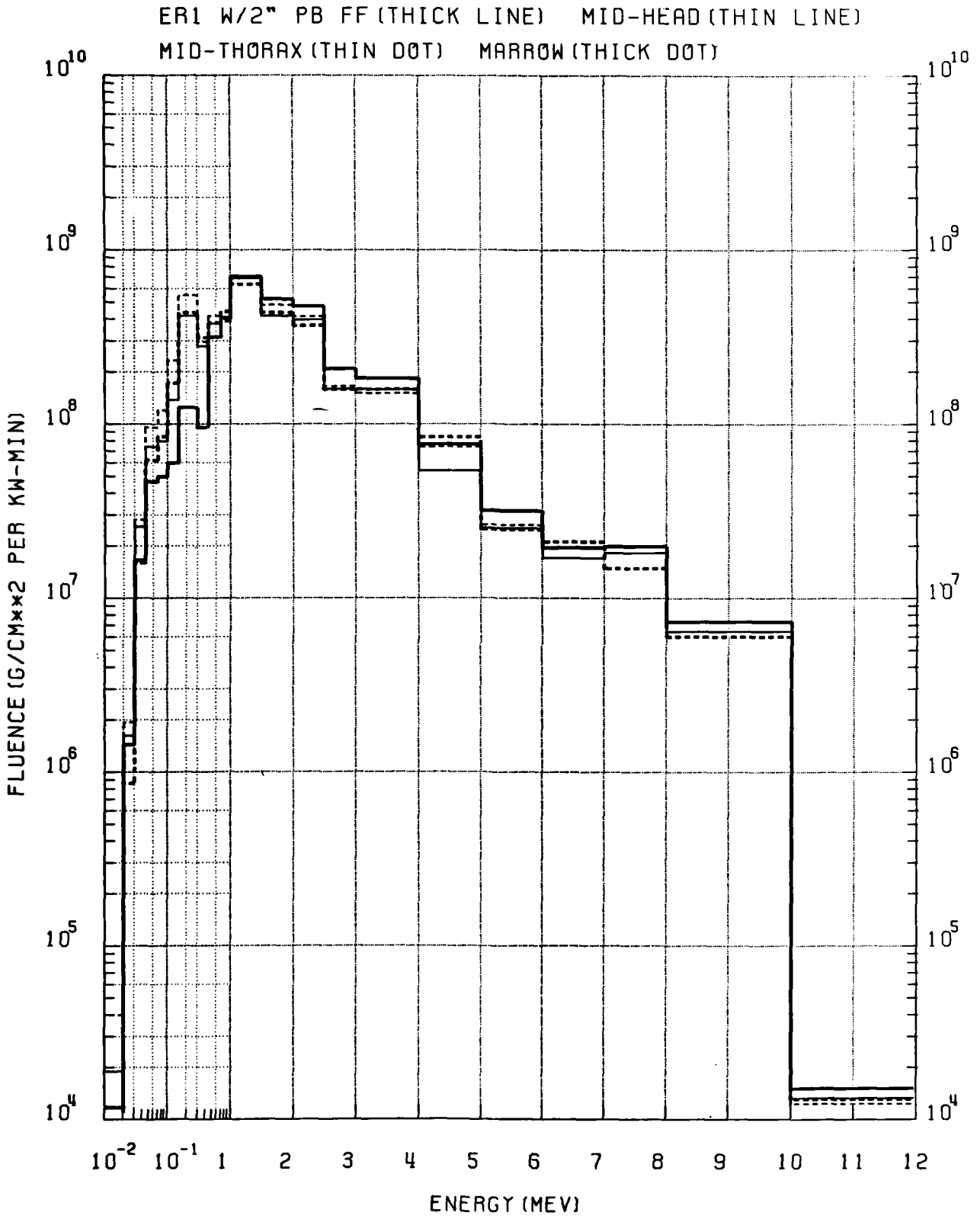

Figure 49. G-G fluence for ER1 and complex phantom

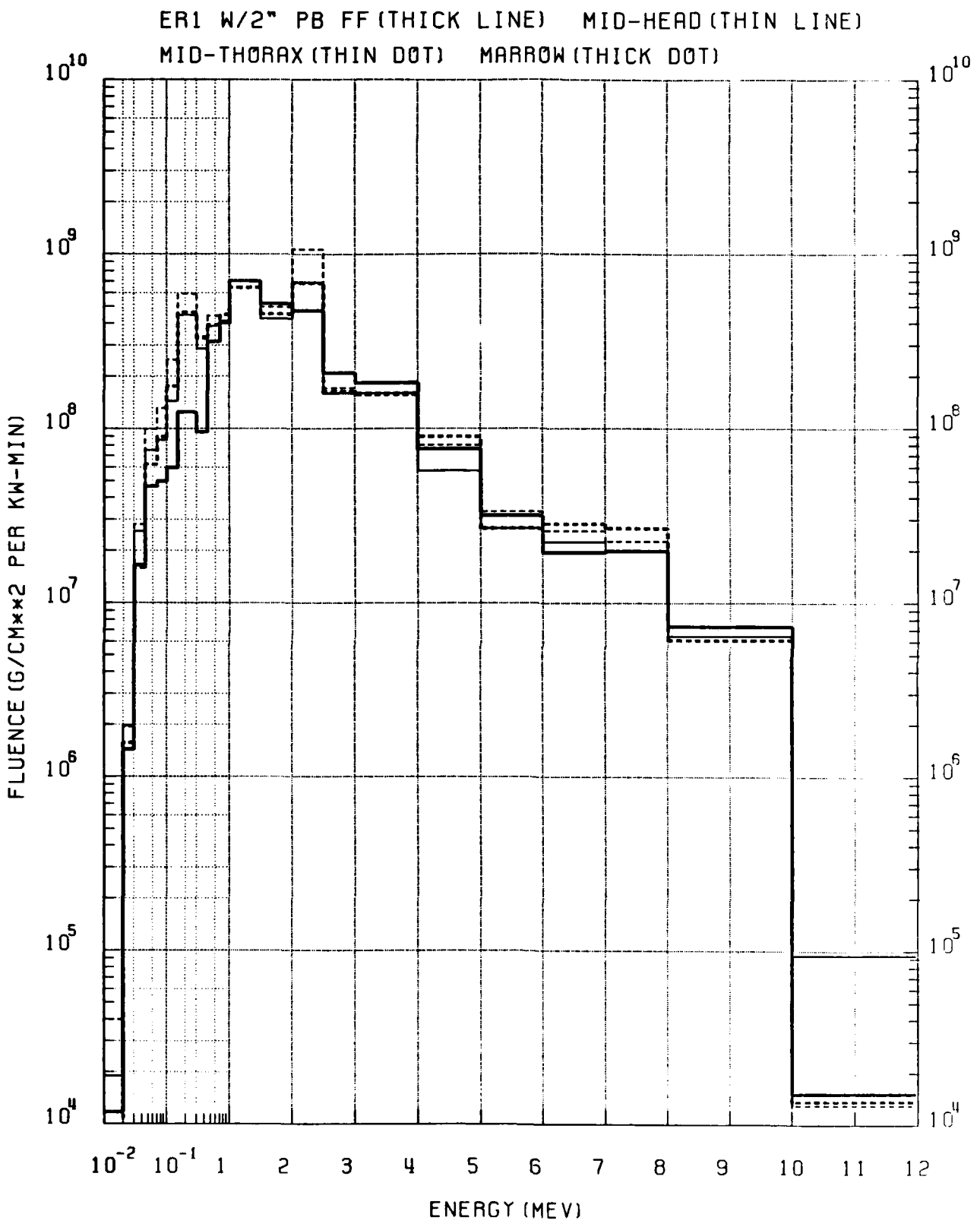

Figure 50. Total gamma fluence for ER1 and complex phantom

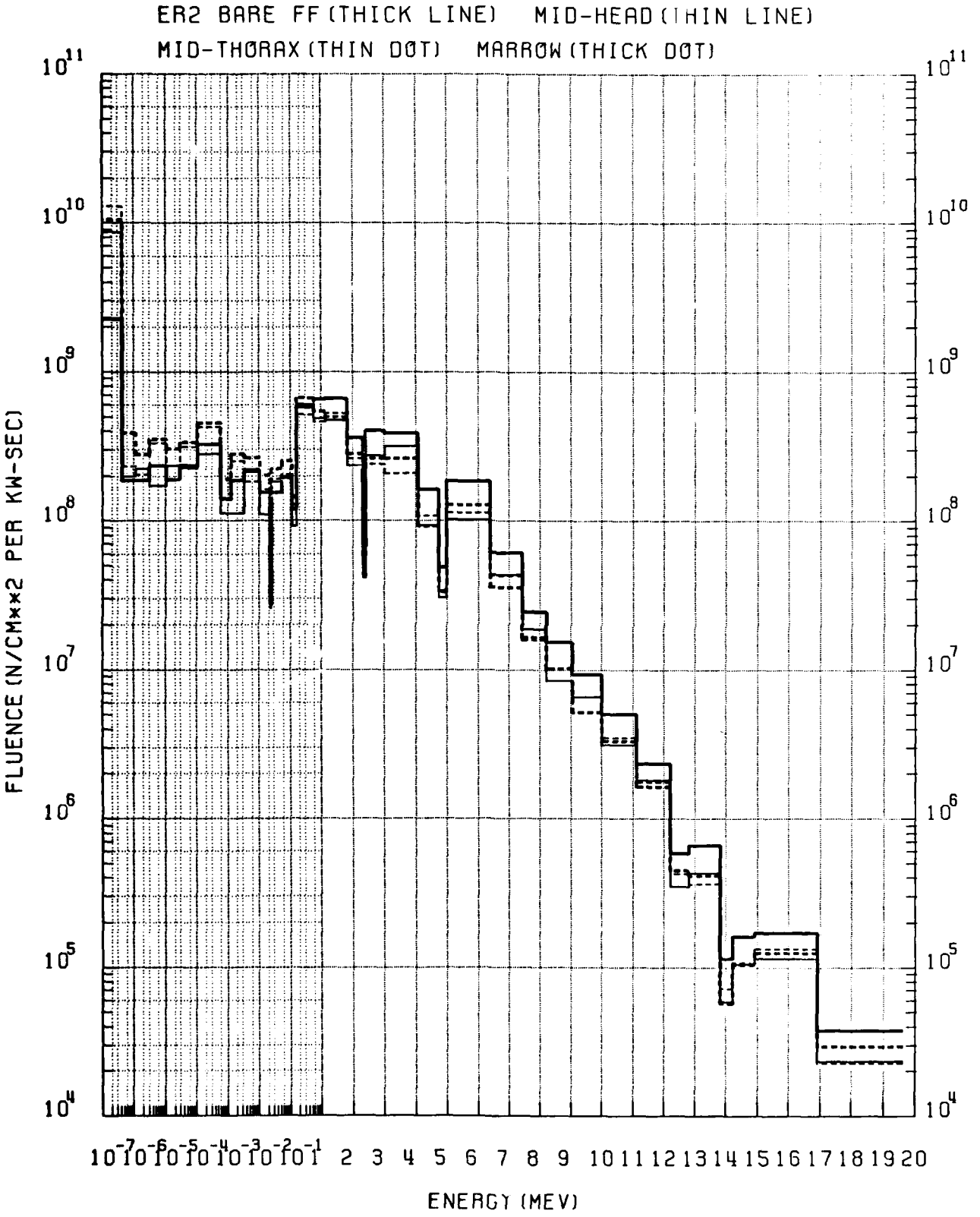

Figure 51. Neutron fluence for ER2 and complex phantom

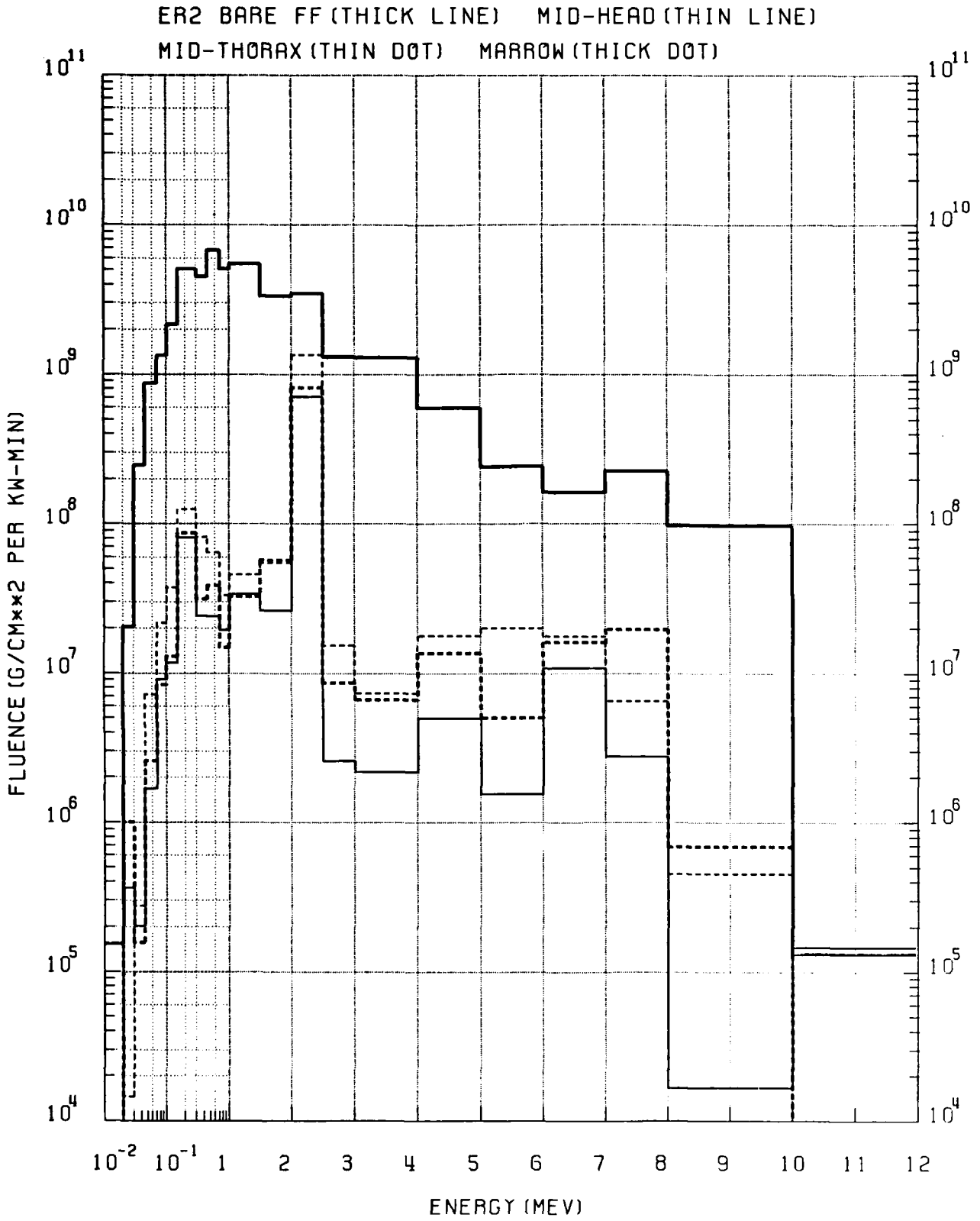

Figure 52. N-G fluence for ER2 and complex phantom

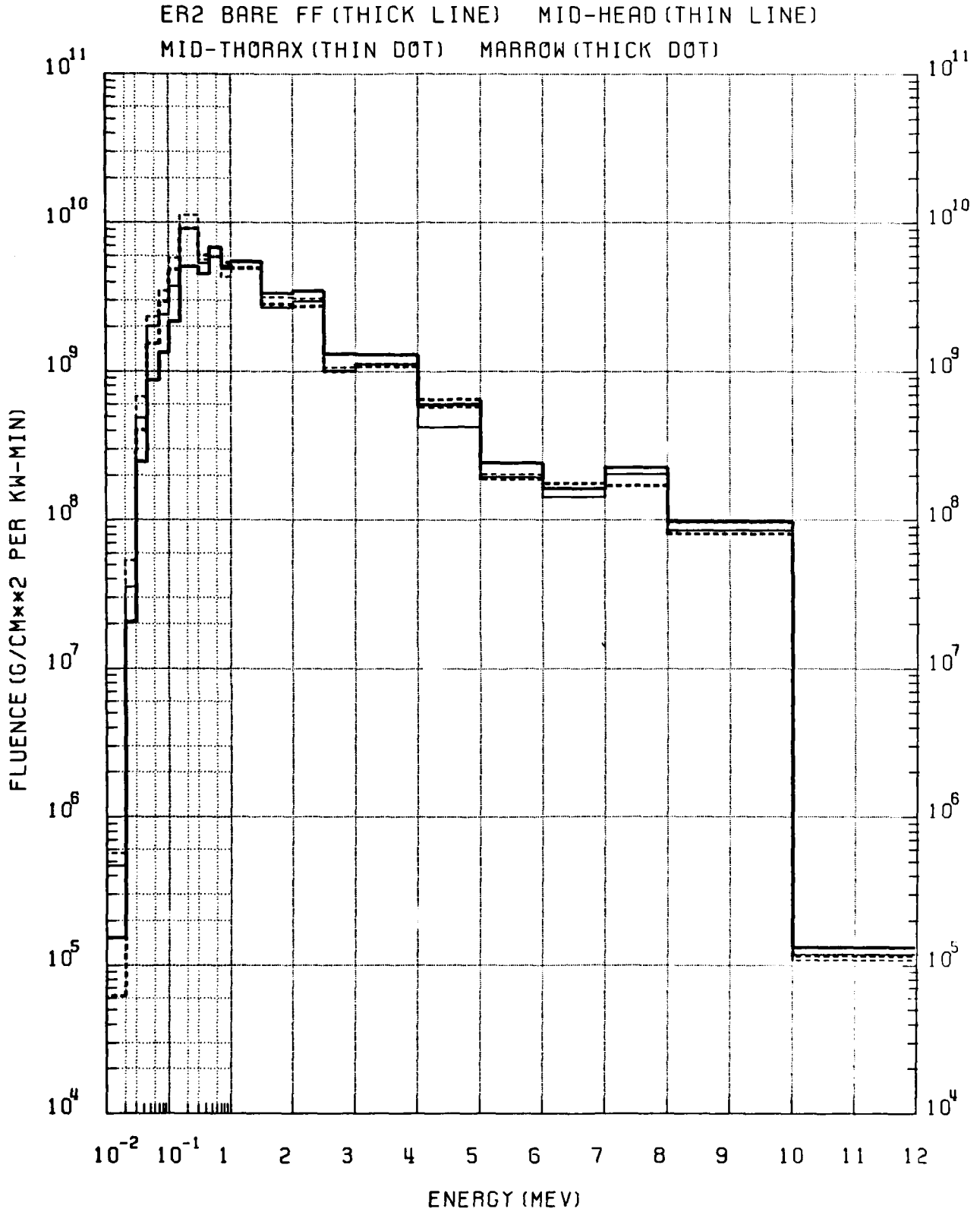

Figure 53. G-G fluence for ER2 and complex phantom

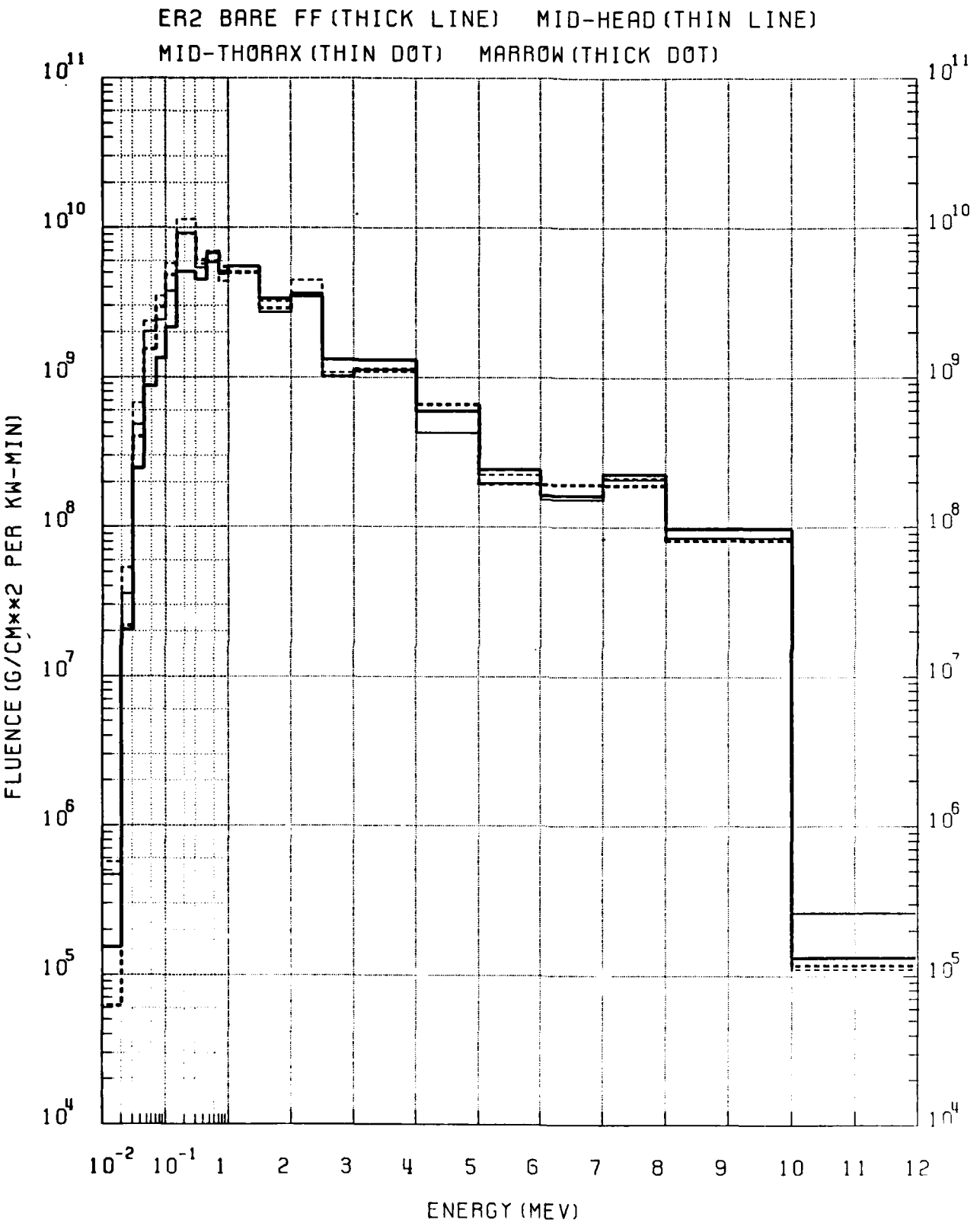

Figure 54. Total gamma fluence for ER2 and complex phantom

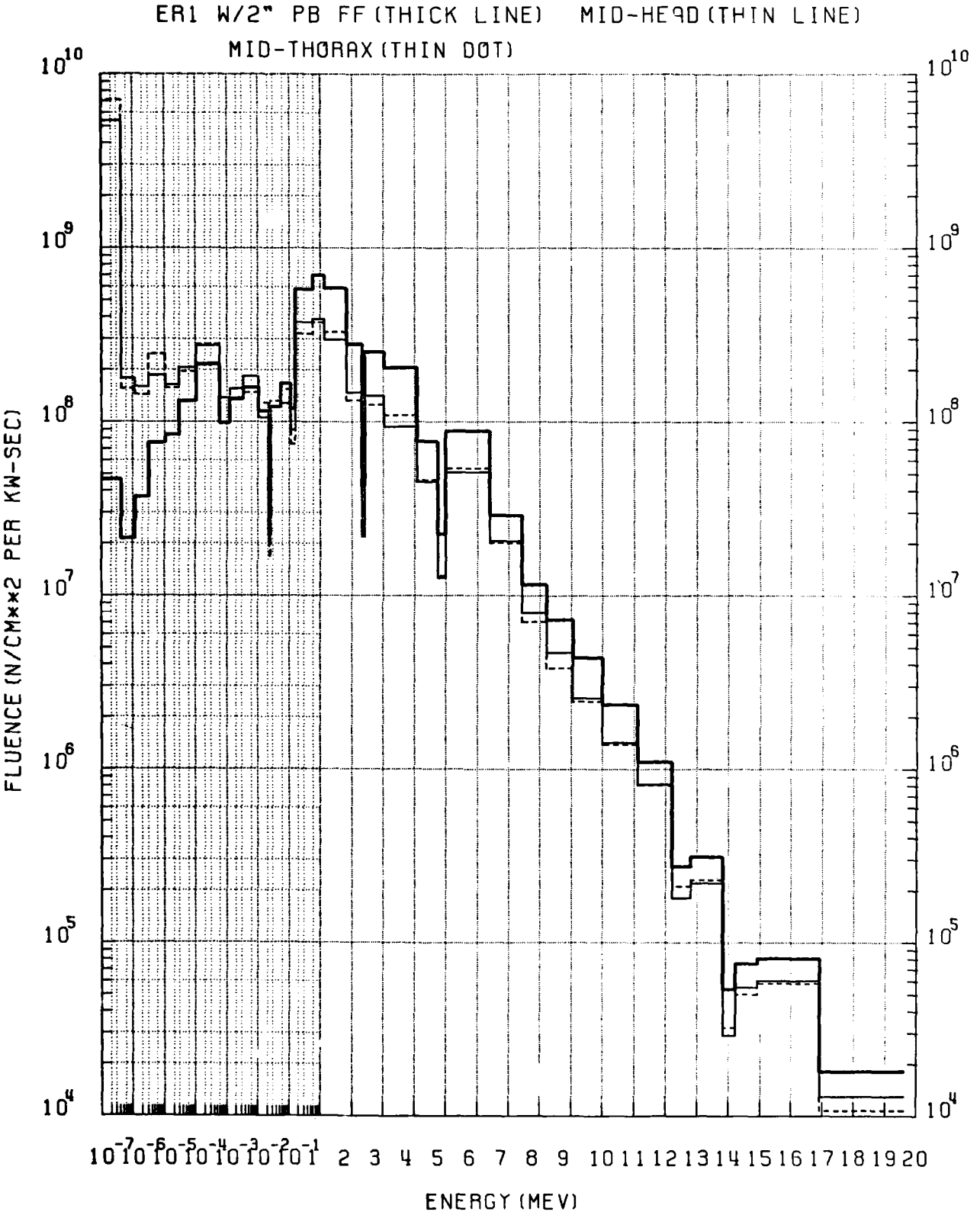

Figure 55. Neutron fluence for EK1 and simple phantom

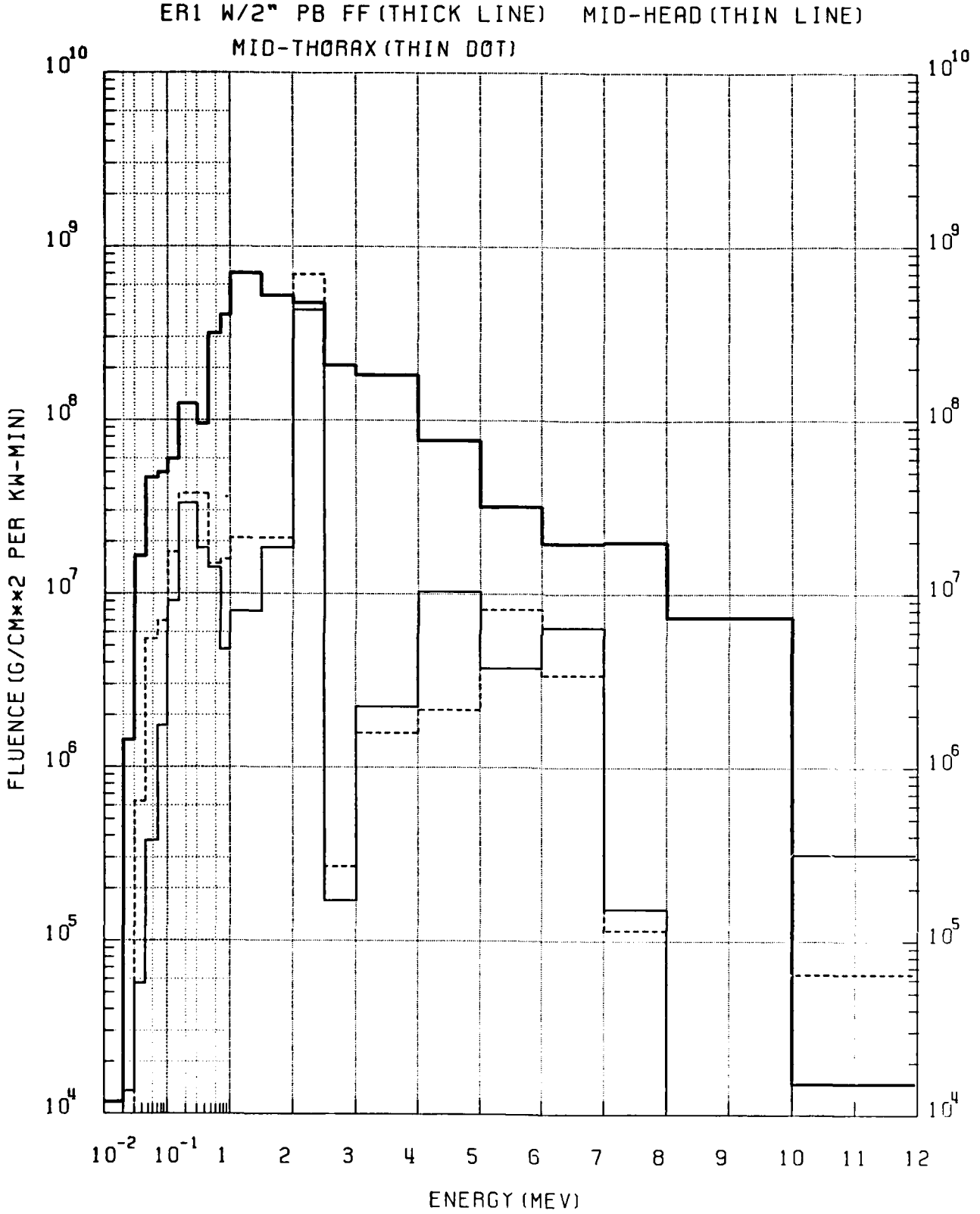

Figure 56. N-G fluence for ER1 and simple phantom

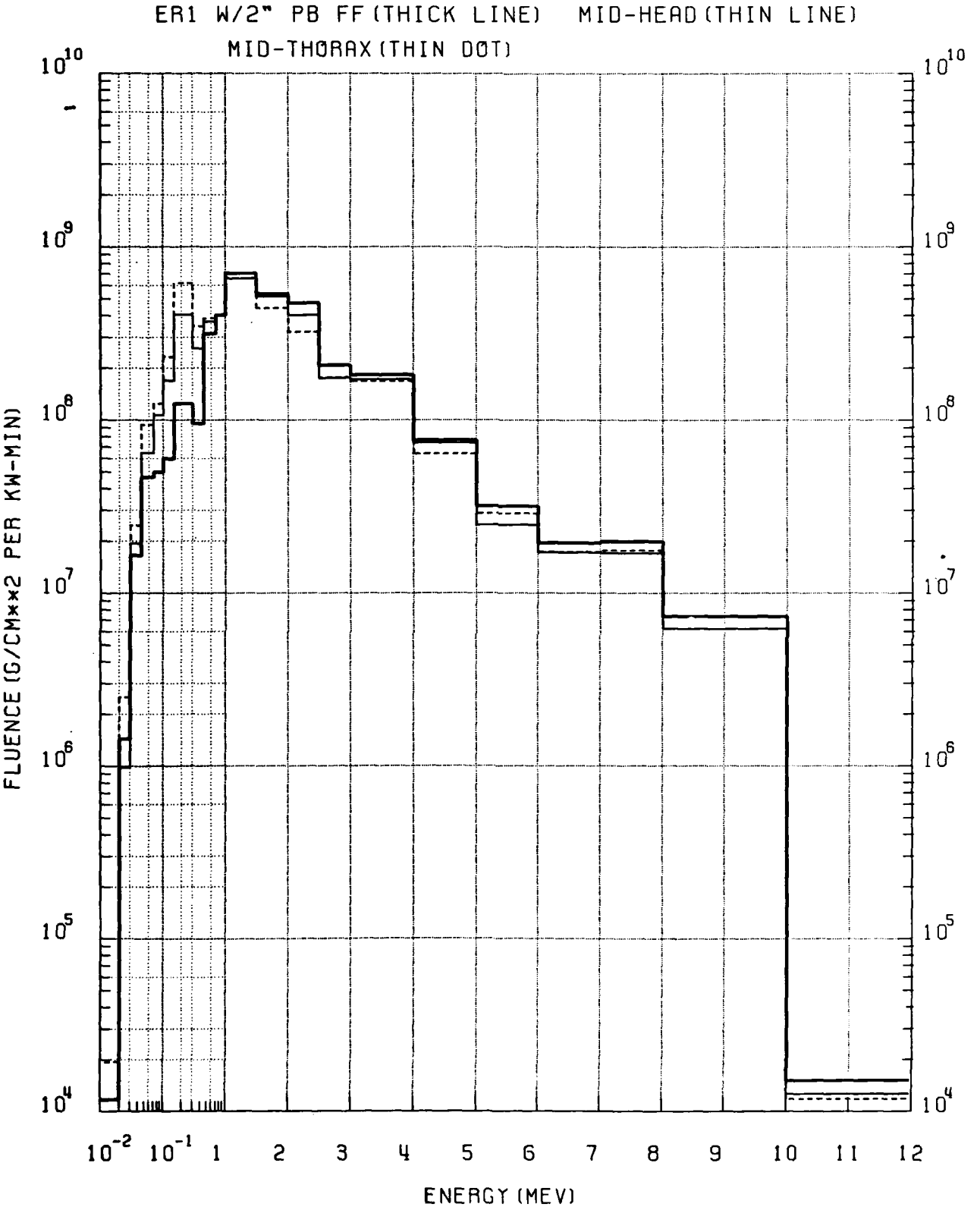

Figure 57. G-G fluence for ER1 and simple phantom

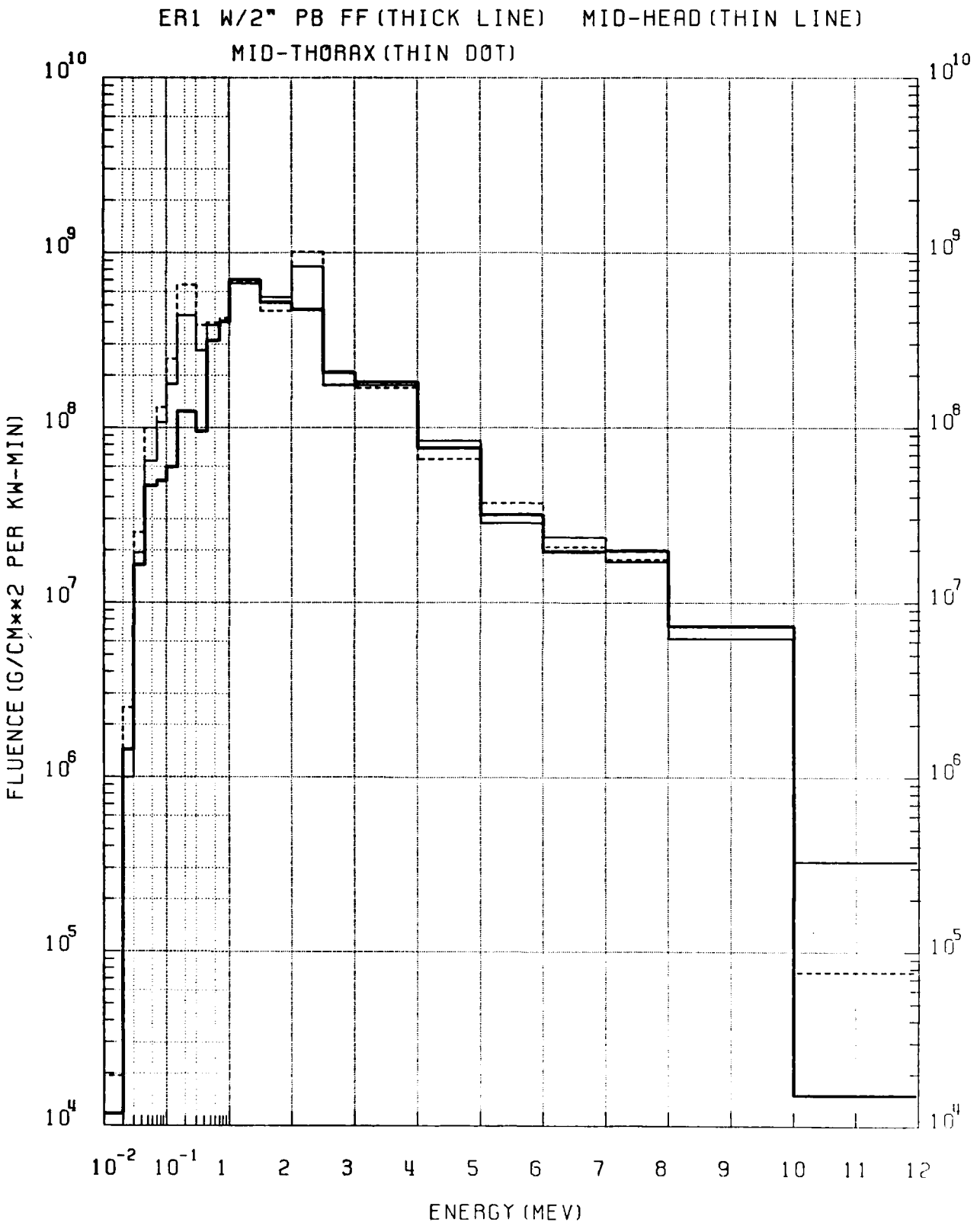

Figure 58. Total gamma fluence for ER1 and simple phantom

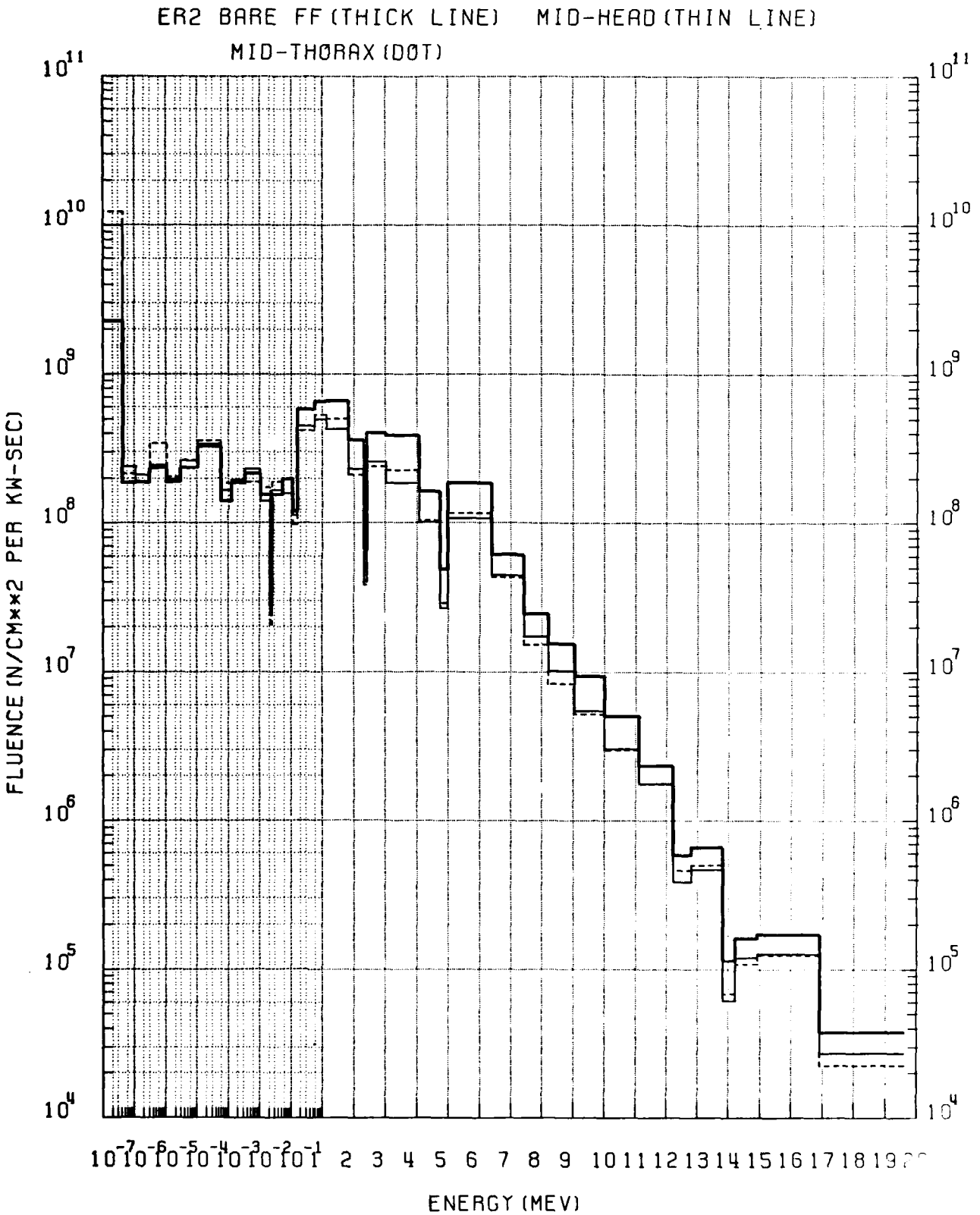

Figure 59. Neutron fluence for ER2 and simple phantom

AD-A162 706 PHANTOM DOSIMETRY CALCULATIONS FOR USE IN RADIATION EFFECTS CORRELATIONS(U) SCIENCE APPLICATIONS INC SCHAUMBURG IL D C KAUL ET AL. 30 JUL 84 SAI-84-1706 2/2

UNCLASSIFIED DNA-TR-83-51 DNA001-83-C-0187 F/G 6/18 NL

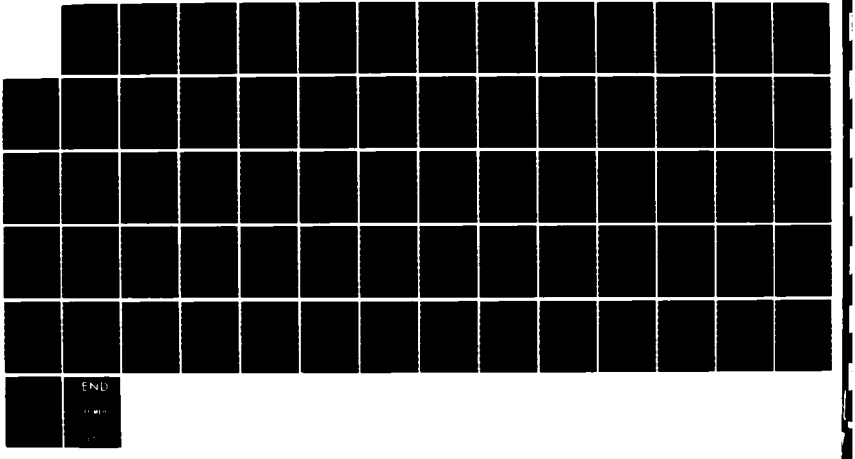

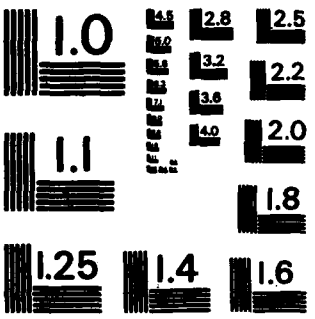

MICROCOPY RESOLUTION TEST CHART
NATIONAL BUREAU OF STANDARDS - 1963 - A

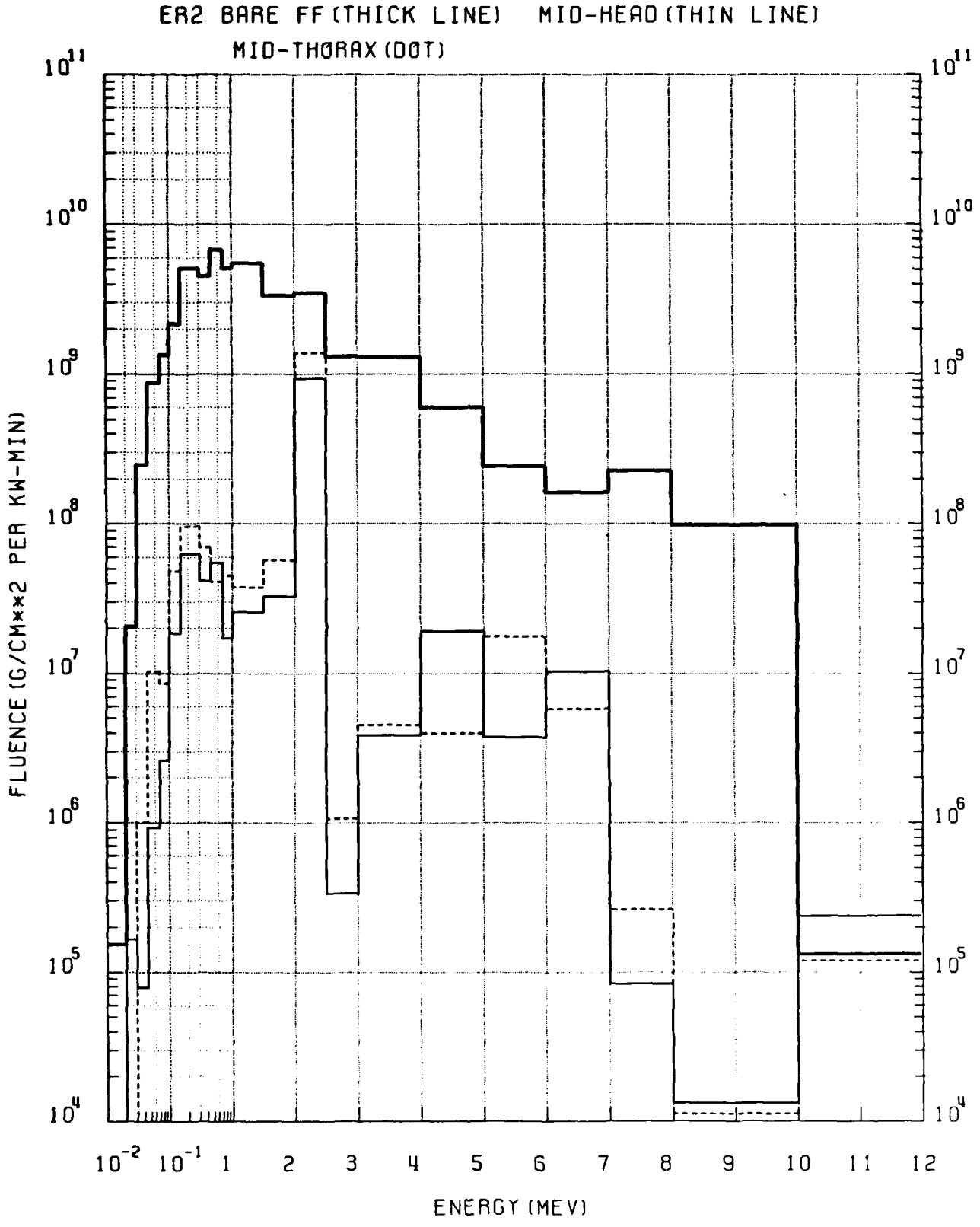

Figure 60. N-G fluence for ER2 and simple phantom

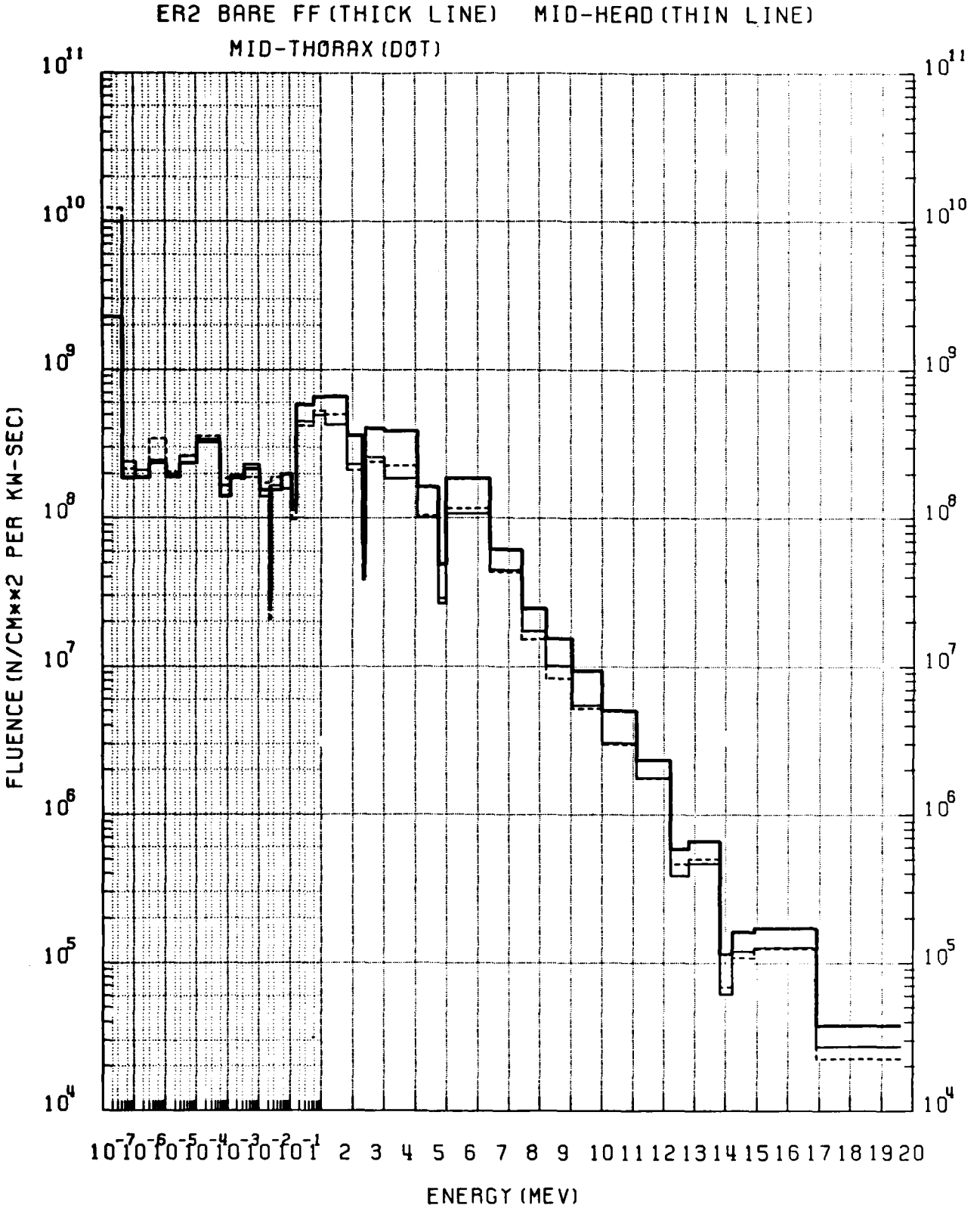

Figure 59. Neutron fluence for ER2 and simple phantom

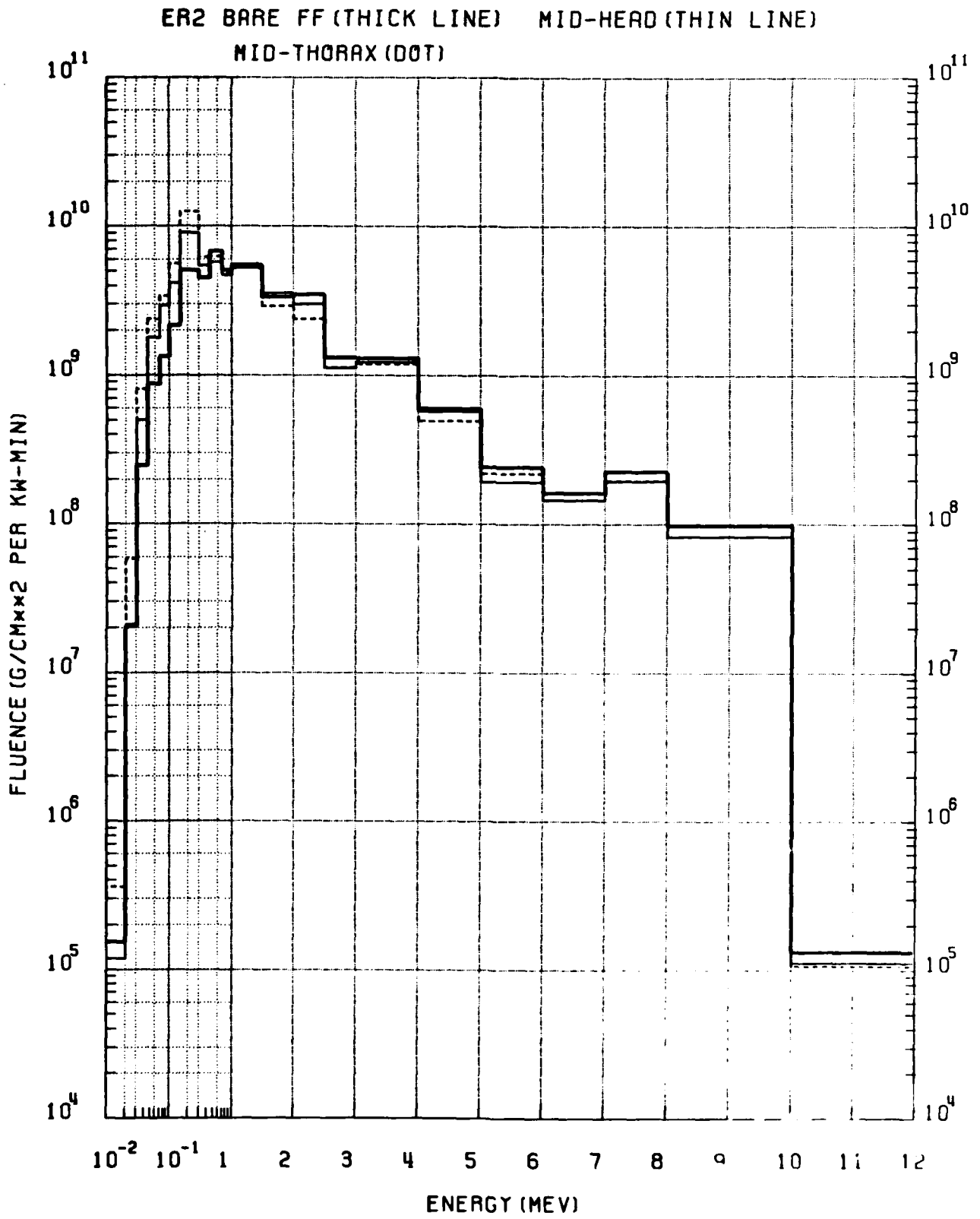

Figure 61. G-G fluence for ER2 and simple phantom

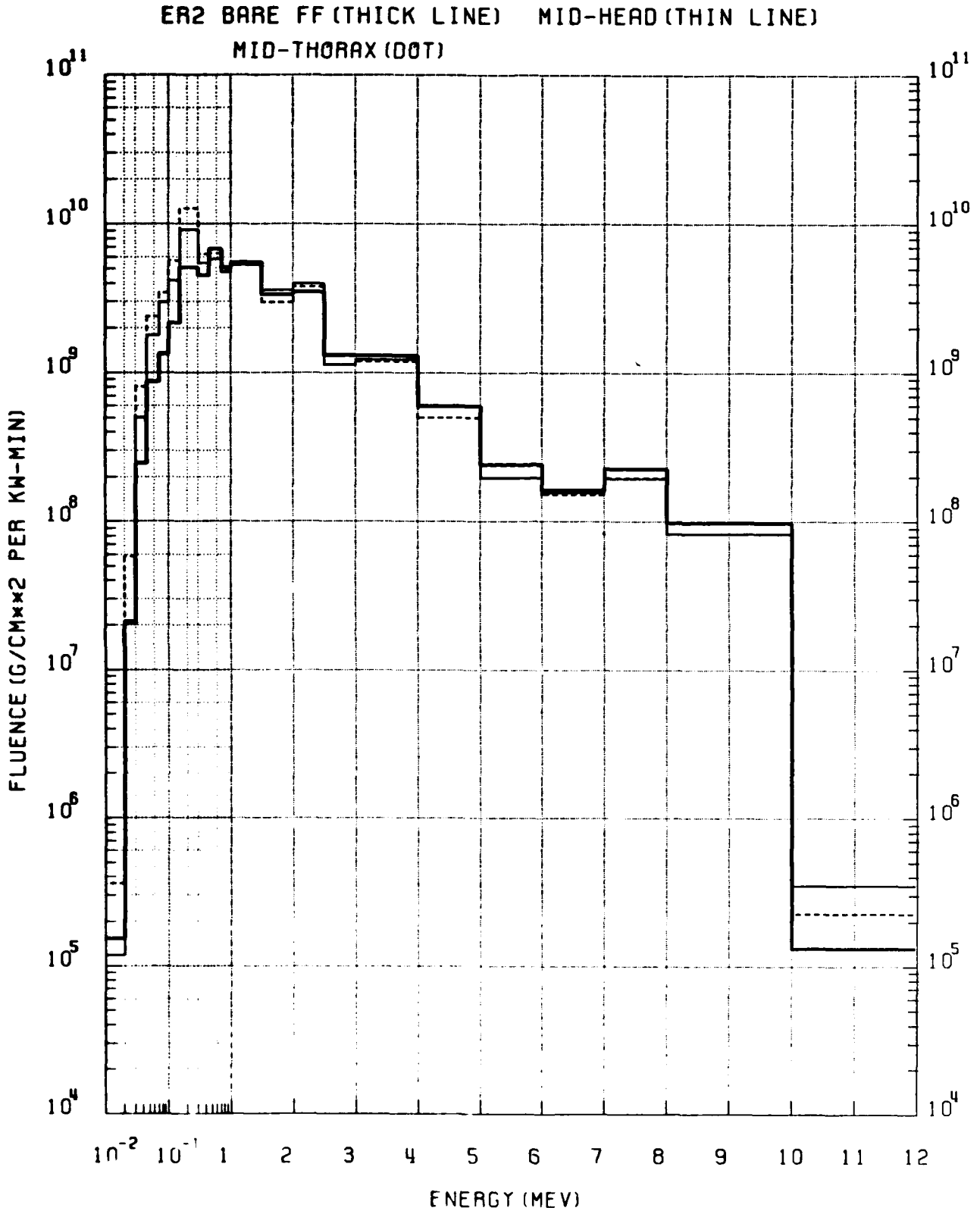

Figure 62. Total gamma fluence for ER2 and simple phantom

oscillate around each other within the limits of their statistical uncertainty, which is of the order of 10 to 18 percent. At low energies there is little consistent difference between mid-head and mid-thorax for neutrons except at thermal, which translates into a similar difference in neutron-gammas (Figure 56) with the mid-thorax having the larger value. On the other hand the low energy gamma rays at the mid-thorax location are consistently higher than those for the mid-head for all energy groups less than an MeV. Since the simple phantom has no skull, skeletal shielding cannot be blamed for this phenomenon. It may be that it is due to the shielding of low energy photons by the wood box, which again puts a premium on the correct incident angular fluence description to calculate the correct transmission.

The general trends for the simple phantom in room two (Figures 59 through 62) are similar to those described for room one. An exception to this is that, in the absence of the lead shield, the free-field gamma ray fluence is generally greater than that in the phantom at energies above one MeV. However, below that energy the build up from scattering of externally-incident gamma rays causes the transmitted fluence to exceed the free-field.

In summary the detailed results of the calculations indicate that the dosimetric behavior of the simple and complex phantoms is qualitatively similar, though transmission magnitudes may differ between the two. Further, the results show that transmission into a subject even as small as a rhesus monkey is affected by variations in incident spectra, particularly in the case of neutrons. Finally, the results show that both the neutron and the gamma ray spectra at locations within a phantom, are remarkably consistent, regardless of the incident spectra, and are different than those of the free-field, with the biggest differences arising in the low energy regions as a result of down-scatter buildup.

3.2 Scalar Coupling

Thus far this report has described the results for forward-adjoint fluence coupling via the VCS code, which is a complex process requiring a large computer. It would be convenient if it were possible to approximate this process using a

scalar fluence coupling approach which is either not dependent on incident angle or marginally so. The mathematical expression for such a procedure is:

$$\text{Detector Response} = \int_E \int_\Omega \Phi(E,\Omega)\ K^*(E)\, d\Omega\, dE$$

in multigroup form this reduces to:

$$\text{Detector Response} = \sum_i^n \sum_j^{4\pi} \Phi(E_i, \Omega_j) K^*(E_i)$$

where $K^*(E_i)$ is the KERMA-weighted adjoint fluence from an isotropic detector integrated over all angles at the leakage surface for leakage energy group i as described previously. In the DNA group structure, n = 58, which results in a convolution process manageable on a small computer or even a hand calculator. A better approximation might be to couple by hemispheres, as in:

$$\text{Detector Response}_{2\pi} = \sum_i^n \sum_j^{2\pi} \Phi(E_i, \Omega_j) \sum_k^{2\pi} K^*(E_i, \Omega_k)$$

where Φ and K^* are the forward and adjoint fluence, respectively, integrated individually over the leakage surfaces which constitute those in the direction of the source (forward) or away from the source (backward).

Both of the above scalar processes have been tried. The results are presented in Tables 11 through 15 in terms of transmission factors, along with those obtained from the VCS computation, which is considered to be the standard for comparison. The most obvious conclusion which can be drawn from a comparison of the results of the various coupling modes is that the scalar processes are not good approximations of the full VCS coupling scheme. This is true of both the full scalar (4π) coupling and the hemispherical (2π) coupling. The hemispherical coupling indicates the great importance of the fluence coming from the direction of the reactor. However, even that more complex approximation is unable to properly account for what is clearly a match between the direction of the forward fluence and the angular sensitivity of the monkey system, either simple or complex. This means that there is a significant decrease in both fluence and angular sensitivity to that fluence for directions other than a direct line

between the center of the reactor and the detector. If this is so, then the effect should be greater for the mid-thorax location than the mid-head or marrow since the mid-thorax angular sensitivity is likely to vary more with polar angle than those for the mid-head or for the marrow, which has components near the surface of the monkey. Tables 11 through 15 indicate that this is indeed the case. Further, it is indicated that neutrons are more affected by this phenomenon than gamma rays. This is to be expected since the gamma rays are more penetrating, thereby giving a more uniform sensitivity as a function of angle.

Finally, it can be seen from the tables that even the neutron-induced gamma ray component exhibits an angular sensitivity, which is between those of the other two components in severity. Normally, the neutron-induced gamma ray component is not so angle sensitive, because it depends on the incident total neutron fluence rather than fluence energy. However, in this case it is possible that the wood box is stopping the lower energy neutrons from reaching the phantom; thus preventing the production of gamma rays in a geometrically advantageous position. As a result of this, the window in the box may play some part in defining the angular sensitivity of neutron-induced gamma ray response.

In summary, it would seem that simple scalar coupling methods should be avoided in estimating transmitted dose in the AFRRI experimental configuration. It is also probable that attempting to find some other scalar coupling scheme sufficiently flexible to cover all situations would require more time than implementing a version of VCS optimized for small computer use.

Table 11. Results of forward-adjoint scalar fluence coupling (rads per KW-min) mid-head complex phantom

		Scalar Coupling Mode					Scalar/VCS	
Location	Component	4π	2πBack	2πForward	2πTotal	VCS (FSD)	4π	2π
Mid-head, Complex Phantom, Room 1, 100 cm from core-centerline, 2" Pb intervening.								
	n	3.70	0.03	3.76	3.78	4.96 (.03)	0.75	0.76
	n-γ	0.27	0.01	0.26	0.27	0.32 (.07)	0.84	0.84
	γ	1.83	0.03	1.81	1.85	2.02 (.03)	0.91	0.92
Mid-head, Complex Phantom, Room 2, 100 cm from core-centerline, bare room.								
	n	5.65	0.06	5.73	5.79	7.97 (.04)	0.71	0.73
	n-γ	0.60	0.03	0.58	0.61	0.74 (.06)	0.81	0.82
	γ	16.08	0.10	16.18	16.27	18.21 (.03)	0.88	0.89

Table 12. Results of forward-adjoint scalar fluence coupling (rads per kw-min) mid-thorax, complex phantom

		Scalar Coupling Mode					Scalar/VCS	
Location	Component	4π	2πBack	2πForward	2πTotal	VCS (FSD)	4π	2π
Mid-thorax, Complex Phantom, Room 1, 100 cm from core-centerline, 2" Pb.								
	n	2.68	0.02	2.92	2.94	4.62 (.03)	0.58	0.64
	n-γ	0.50	0.02	0.51	0.53	0.69 (.05)	0.72	0.77
	γ	1.71	0.03	1.74	1.77	2.11 (.03)	0.81	0.84
Mid-thorax, Complex Phantom, Room 2, 100 cm from core-centerline, bare room.								
	n	4.26	0.04	4.59	4.63	7.76 (.04)	0.55	0.60
	n-γ	0.91	0.04	0.93	0.97	1.47 (.05)	0.62	0.66
	γ	15.06	0.09	15.52	15.61	19.24 (.03)	0.78	0.81

Table 13. Results of forward adjoint scalar fluence coupling (rads per kw-min) active marrow, complex phantom

		Scalar Coupling Mode					Scalar/VCS	
Location	Component	4π	2πBack	2πForward	2πTotal	VCS (FSD)	4π	2π
Active marrow, Complex Phantom, Room 1, 100 cm from core-centerline, 2" Pb intervening.								
	n	3.60	0.02	3.93	3.95	5.34 (.03)	0.67	0.74
	n-γ	0.31	0.01	0.32	0.33	0.37 (.05)	0.84	0.89
	γ	1.78	0.03	1.81	1.84	2.04 (.02)	0.87	0.89
Active marrow, Complex Phantom, Room 2, 100 cm from core-centerline, bare room.								
	n	5.47	0.05	5.94	5.99	8.34 (.03)	0.66	0.72
	n-γ	0.65	0.03	0.67	0.70	0.94 (.05)	0.69	0.74
	γ	15.68	0.09	16.18	16.27	18.51 (.02)	0.85	0.88

Table 14. Results of forward-adjoint scalar fluence coupling (rads per kw-min) mid-head simple phantom

		Scalar Coupling Mode					Scalar/VCS	
Location	Component	4π	2πBack	2πForward	2πTotal	VCS (FSD)	4π	2π
Mid-head, Simple Phantom, Room, 1 100 cm from core-centerline, 2" Pb intervening.								
	n	3.42	0.02	3.44	3.46	4.46 (.03)	0.77	0.78
	n-γ	0.35	0.01	0.35	0.36	0.45 (.06)	0.78	0.80
	γ	1.82	0.03	1.79	1.83	2.15 (.03)	0.85	0.85
Mid-head, Simple Phantom, Room 2, 100 cm from core-centerline, bare room.								
	n	5.27	0.06	5.25	5.31	7.13 (.04)	0.74	0.74
	n-γ	0.70	0.04	0.70	0.74	0.98 (.05)	0.71	0.76
	γ	16.00	0.10	15.96	16.05	19.17 (.03)	0.83	0.84

Table 15. Results of forward-adjoint scalar fluence coupling (rads per kw-min) mid-thorax, simple phantom

		Scalar Coupling Mode					Scalar/VCS	
Location	Component	4π	2πBack	2πForward	2πTotal	VCS (FSD)	4π	2π
Mid-thorax, Simple Phantom, Room 1, 100 cm from core-centerline, 2" Pb intervening.								
	n	2.58	0.02	2.72	2.73	4.46 (.03)	0.58	0.61
	n-γ	0.50	0.02	0.50	0.52	0.69 (.05)	0.72	0.75
	γ	1.70	0.03	1.69	1.72	2.05 (.03)	0.83	0.84
Mid-thorax, Simple Phantom, Room 2, 100 cm from core-centerline, bare room.								
	n	4.11	0.04	4.30	4.34	7.51 (.04)	0.55	0.58
	n-γ	0.89	0.04	0.90	0.94	1.41 (.05)	0.63	0.67
	γ	14.97	0.09	15.03	15.12	18.95 (.03)	0.79	0.80

SECTION 4

VERIFICATION AND VALIDATION

It is intended that, at some future time, KERMA and scalar fluence measurements be made by AFRRI in the simplified phantom at the locations calculated and presented in the previous section. In lieu of these it is still possible to make some comparisons with previously obtained experimental data as reported by AFRRI[14] for the purposes of verifying and validating the calculational procedures described herein.

AFRRI has made several measurements of the free-field gamma ray and total KERMA levels at several locations in the two exposure rooms with and without simple phantoms and other experimental apparatus. In particular, measurements were made using a small simple phantom of the same trunk height and diameter as the calculated simple phantom. The configuration of that phantom is shown in Figure 63, along with the outline of the calculational model. The two are very similar and are made of identical materials.

The small phantom was irradiated in its configuration with chair and box in exposure room one, behind the two inches of lead, at a distance of 90 cm from core centerline. The small phantom was similarly exposed in the otherwise bare exposure room two at a distance of 125 cm from core centerline. The free field was measured at the mid-head and mid-thorax locations in the absence of the phantom but with the chair and box in place. The results of these measurements, along with the equivalent calculations are provided in Tables 16 and 17 for exposure rooms one and two, respectively.

The calculations were performed by first computing the transmission to each location in the chair and box in each room, but in the absence of the phantom. This transmission was normalized to the reported free field values, as measured. This normalization was then carried over to the calculation of KERMA within the simple phantom. The measured free-field values appear in the first column in each table. The two quantities actually measured are the gamma ray and total KERMA

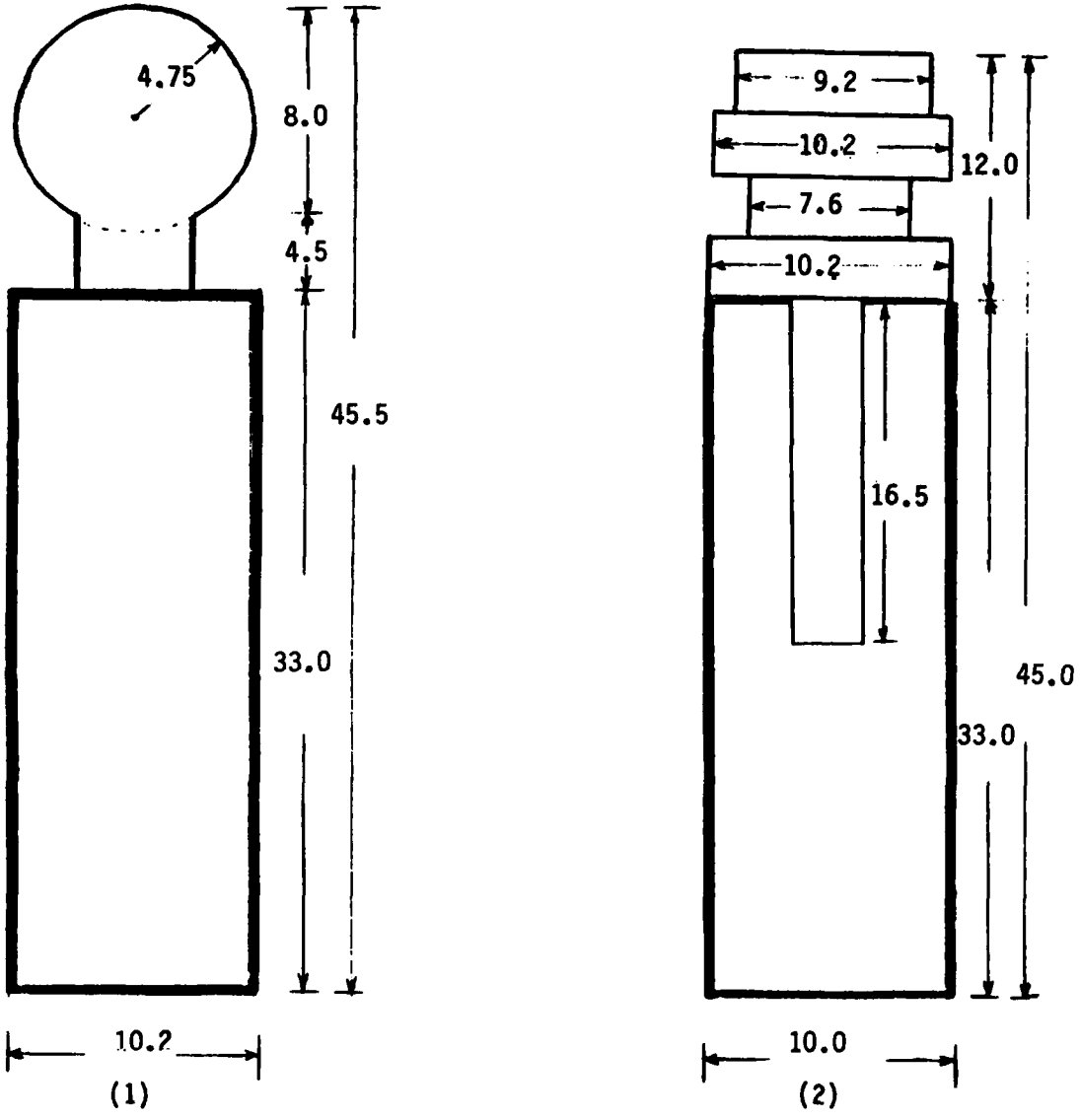

Figure 63. Simple phantoms as calculated (1) and as measured (2)

Table 16. Experimental and calculated KERMA-Exposure Room 1

Configuration: 90 cm from core midline, 2" pb intervening

Location	Component	EXP. Free Field KERMA (Rads per Kw-min)	PHANTOM KERMA (Rads per Kw-min) EXP.(FSD)	Calc.(FSD)	Δ (1)	TRANSMISSION EXP	Calc.	N/γ Ratio EXP	Calc.
Mid-Head	n	10.1 (.03)	5.69 (.04)	5.49 (.05)	-.04	0.56	0.54		
	n-γ			0.56 (.07)			0.06 (2)		
	γ			2.46 (.04)			0.95		
	TOT γ	2.6 (.03)	3.35 (.03)	3.02 (.04)	-.10	1.29 (3)	1.16		
	TOT	12.7 (.03)	9.04 (.03)	8.51 (.03)	-.06	0.71 (4)	0.67	1.70	1.82
Mid-Thorax	n	11.8 (.03)	7.1 (.04)	6.33 (.05)	-.11	0.60	0.54		
	n-γ			.98 (.05)			0.08		
	γ			2.83 (.04)			0.91		
	TOT γ	3.1 (.03)	4.1 (.03)	3.81 (.04)	-.07	1.32	1.23		
	TOT	14.9 (.03)	11.2 (.03)	10.14 (.03)	-.09	0.75	0.68	1.73	1.66

(1) $\frac{\text{CAL} - \text{EXP}}{\text{EXP}}$

(2) $\frac{\text{n-}\gamma \text{ Phantom KERMA}}{\text{n Free Field KERMA}}$

(3) $\frac{\text{Total } \gamma \text{ Phantom KERMA}}{\text{Total } \gamma \text{ Free Field KERMA}}$

(4) $\frac{\text{Total Phantom KERMA}}{\text{Total Free Field KERMA}}$

Table 17. Experimental and calculated KERMA-Exposure Room 2

Configuration: 125 cm from core midline, bare room

Location	Component	EXP. Free Field KERMA (Rads per Kw-min)	PHANTOM KERMA (Rads per Kw-min) EXP.(FSD)	Calc.(FSD)	Δ (1)	TRANSMISSION EXP	Calc.	N/γ Ratio EXP	Calc.
Mid-Head	n	6.9 (.10)	3.7 (.16)	3.9 (.11)	+.05	0.54	0.57		
	n-γ			.5 (.12)			0.07(2)		
	γ			15.2 (.05)			0.92		
	TOT γ	16.5 (.03)	14.7 (.03)	15.7 (.05)	+.07	0.89(3)	0.95		
	TOT	23.4 (.03)	18.4 (.03)	19.6 (.04)	+.07	0.79(4)	0.84	0.25	.25
Mid-Thorax	n	9.8 (.08)	4.5 (.15)	5.7 (.09)	+.27	0.46	0.58		
	n-γ			1.1 (.10)			0.11		
	γ			16.0 (.05)			0.93		
	TOT γ	17.2 (.03)	16.0 (.03)	17.1 (.05)	+.07	0.93	0.99		
	TOT	27.0 (.03)	20.5 (.03)	22.8 (.04)	+.11	0.76	0.84	0.28	.33

(1) $\frac{\text{CALC.-EXP}}{\text{EXP}}$

(2) $\frac{\text{n-}\gamma\text{ Phantom KERMA}}{\text{n Free Field KERMA}}$

(3) $\frac{\text{Total }\gamma\text{ Phantom KERMA}}{\text{Total }\gamma\text{ Free Field KERMA}}$

(4) $\frac{\text{Total Phantom KERMA}}{\text{Total Free Field KERMA}}$

values, each with a reported precision represented by a fractional standard deviation of 0.025. The neutron KERMA is a derived quantity, obtained by taking the difference of the other two quantities. Assuming that the reported KERMA are the means of well-behaved normal distributions the variance of the neutron KERMA may be obtained according to the expression: [15]

$$\sigma^2_{neutron} = \sigma^2_{total} + \sigma^2_{gamma}$$

where σ = MEAN*FSD.

For exposure room one the measured and derived neutron free-field KERMA all have approximately the same precision. However, in the case of room two the neutron KERMA exhibit a significant decline in precision. This is due to the fact that the gamma ray and total KERMA in room two are of the same order, whereas in room one the neutron and total KERMA were of the same order.

The calculated phantom KERMA values appear in the third column of data in Table 16 and 17. The FSD values corresponding to each transmitted KERMA were obtained by again assuming a well behaved normal distribution of mean values as represented by the measured free-field and the calculated transmission factor given in column 6 and calculating their values using the expression:[15]

$$\sigma_p^2 = \sigma_1^2 \sigma_2^2 + m_1^2 \sigma_2^2 + m_2^2 \sigma^2$$

where σ_p^2 is the variance of the product of the means, m_1 and m_2 which have respective variances, σ_1^2, and σ_2^2 . As a result of these calculations, it can be seen that the calculated phantom KERMA for room one have a high level of precision, as do the phantom gamma ray and total KERMA in room two. However, the precision of the calculated neutron KERMA in room two can be no better than that of the free-field to which it is normalized, and, thus, it is considerably worse than for the other components.

The calculated phantom KERMA may be compared with the measured values shown in column two of Tables 16 and 17. The agreement between all the measured and calculated KERMA values, neutron and gamma ray, are very good for room one. This is gratifying because of the high precision attributed to all the measured

quantities. For room two the agreement between calculated and measured gamma ray and total KERMA is similar to that achieved for room one. However, the measured and calculated mid-thorax neutron KERMA are considerably at odds. In spite of this apparent discrepancy a simple students t-test indicates that the two values are statistically indistinguishable to 95% certainty, due to their large associated FSD values. Therefore, it is possible to say that the only really large difference between the calculated and measured phantom KERMA may be attributed to the inherent uncertainties in measured quantities, possibly compounded by the statiscal uncertainty of the calculations.

In fact, as long as the measured gamma ray KERMA is a small fraction of the total, the uncertainty of the neutron KERMA will be of the same order as that of the total, which is likely to be very good. This is typified by the results for exposure room one, where the lead shield substantially reduces the gamma ray KERMA in favor of the neutron KERMA. On the other hand, the neutron KERMA in room two is small compared to the total and gamma ray KERMA values; in this case the variance of the neutron KERMA, being the sum of the variances of the two larger components, results in a standard deviation which is at least a large fraction of the neutron KERMA value.

This discrepancy involving phantom neutron KERMA may be too large to be tolerated if calculated and measured quantities are to be used side by side for correlation with biological effects. Fortunately, other information is available which helps to shed some light on the origin of this discrepancy. If one looks at the free-field spectra for the two rooms as shown previously in Figure 45, which have been validated by experimental means, one can see that the neutron spectrum above 100 KeV, i.e., that which contributes most to KERMA, is harder in room two than in room one. It should therefore be expected that the neutron transmission factor for identical locations within the phantom should increase going from room one to room two. The calculated values show such an increase, going from .54 in room one to .58 in room two for the mid-thorax location. However, for that same location the neutron transmission derived from the measurements shows a significant decrease going from room one to room two. Thus, a physical argument favors the calculated value.

The results of this effort to verify and validate the calculations described in this report are mixed due to the statistical uncertainties of both the experimentally measured and the calculated results but do seem to indicate a satisfactory reliability overall. This is particularly true under those circumstances which are most advantageous to the experimental methods. On the other hand, the results also suggest that, although extreme care was taken to obtain high precision in these experiments, the level of precision achieved was probably not sufficient to work reliably with room two in its bare configuration. Under such circumstances, the calculational approach may be found to be a particularly useful compliment to experimental methods.

LIST OF REFERENCES

1. Bond, V.P. and Robinson, C.V., A Mortality Determination in Nonuniform Exposures of the Mammal, Radiation Research Supplement 7, 265-275, 1967.

2. Verbinski, V.V., et al., Radiation Field Characterization for the AFRRI TRIGA Reactor, Vol. 1 and 2,, DNA5793F-1,-2, Science Applications, Inc., La Jolla, CA, 1981.

3. Straker E.A., Scott W.H., and Byrn N.R., The MORSE Code with Combinatorial Geometry, Topical Report to the Defense Nuclear Agency, DNA2860T, SAI-72-511-LJ, Science Applications, Incorporated, La Jolla, CA, 1972.

4. Bain L.W. and Reisinger M.J., The GIFT User Manual: Volume 1. Introduction and Input Requirements, BRL Report No. 1802, USA Ballistic Research Laboratories, Aberdeen Proving Groupd, MD, 1975.

5. Cristy M. and Eckerman K.F., Specific Absorbed Fractions of Energy at Various Ages from Internal Photon Sources. I-Methods, ORNL/TM-8381; Volume 1, Oak Ridge National Laboratory, Oak Ridge, TN, 1983.

6. Bourne G.H. (Editor), The Rhesus Monkey, Vol. 1, Anatomy and Physiology, and Vol. 2, Management, Reproduction, and Pathology. Academic Press, New York, 1975.

7. KERR G.D., Photon and Neutron Fluence-to-KERMA Conversion Factors for ICRP-1975 Reference Man Using Improved Elemental Compositions for Bone and Marrow of the Skeleton, ORNL/TM-8318, Oak Ridge National Laboratory, Oak Ridge, TN, 1982.

8. Taketa, S.T., Carsten A.L., Cohn S.H., Atkins H.L., and Bond V.P., "Active Bone Marrow Distribution in the Monkey," In Life Sciences Part II, Vol. 9, No. 3., pp.169-174, Pergamon Press, 1970.

9. Zeman, G., CDR,USN, Armed Forces Radiobiological Research Institute DF to Defense Nuclear Agency (Major Campbell) 3 November 1983.

10. ICRU Report 26, Neutron Dosimetry for Biology and Medicine, International Commission on Radiation Units and Measures, Washington, D.C., 15 January 1977.

11. Rhoades, W.A., Development of A Code System for Determining Radiation Protection of Armored Vehicles (The VCS Code), ORNL-TM-4664, Oak Ridge National Laboratory, Oak Ridge, TN, 1974.

12. Bartine, D.E., et al., Production and Testing of the DNA Few-Group Coupled Neutron-Gamma Cross Section Library, ORNL/TM-4840, Oak Ridge National Laboratory, Oak Ridge, TN, 1977.

13. Abdou, M.A., et al., MACK: A Computer Program to Calculate Neutron Energy Release Parameters (Fluence-to-KERMA Factors) and Multigroup Neutron Reaction Cross Sections From Nuclear Data in ENDF Format, ORNL-TM-3994, Oak Ridge National Laboratory, July 1973.

14. Zeman, G.H., Phantom Dosimetry for TRIGA Reactor Irradiations in Chair and Wheel Arrays, Draft report, Armed Forces Radiobiological Research Institute, Bethesda, MD, September 1983.

15. Hogg, R.V., and Craig, A.T., Introduction to Mathematical Statistics, Macmillan Publishing Company, Inc., New York, 1970.

APPENDIX

This appendix contains tabulated values for adjoint leakage, free-field and transmitted fluence corresponding to those presented in graphical form in the body of the report. These fluence values are tabulated in the 37 neutron - 21 gamma ray energy group format of the DNA Few Group Cross Section Library (DLC-31). The adjoint leakage fluence is tabulated in units analogous to KERMA factors, i.e., rads per unit fluence. Free-field and transmitted fluence values are tabulated as group fluence, i.e., total fluence per group, and may be convoluted with any set of KERMA by simple matrix multiplication to obtain total transmitted KERMA values.

GUIDE TO APPENDIX TABLES

Subject	Table Number — Radiation Component			
	Neutron	Neutron-gamma	Gamma	Total Gamma
o 2PI (front) integrated leakage fluence	A-1	A-5	A-9	-
o 2PI (back) integrated leakage fluence	A-2	A-6	A-10	-
o 4PI integrated leakage fluence				
Mid-head, mid-thorax, average marrow	A-3	A-7	A-11	-
Marrow region, average marrow	A-4	A-8	A-12	-
o ER1 scalar fluence				
Free-field, mid-head, mid-thorax, average marrow	A-13	A-15	A-17	A-19
Free-field, marrow region, average marrow	A-14	A-16	A-18	A-20
o ER2 scalar fluence				
Free-field, mid-head, mid-thorax, average marrow	A-21	A-23	A-25	A-27
Free-field, marrow region, average marrow	A-22	A-24	A-26	A-28

Table A-1. 2 PI (front) integrated adjoint leakage neutron fluence (rads / N/cm**2) (FSD)

Energy Group	Upper Energy (MeV)	Complex Mid-Head	Complex Mid-Thorax	Complex Marrow	Simple Mid-Head	Simple Mid-Thorax
1	1.960E+01	3.012E-09 .026	2.861E-09 .025	3.261E-09 .023	3.045E-09 .023	2.774E-09 .025
2	1.690E+01	2.769E-09 .026	2.586E-09 .029	2.783E-09 .027	2.719E-09 .028	2.532E-09 .029
3	1.490E+01	2.620E-09 .029	2.475E-09 .028	2.704E-09 .026	2.700E-09 .027	2.420E-09 .029
4	1.420E+01	2.679E-09 .027	2.446E-09 .027	2.535E-09 .026	2.678E-09 .027	2.470E-09 .028
5	1.380E+01	2.531E-09 .028	2.384E-09 .030	2.483E-09 .027	2.638E-09 .028	2.484E-09 .026
6	1.280E+01	2.440E-09 .027	2.292E-09 .027	2.539E-09 .026	2.351E-09 .029	2.318E-09 .031
7	1.220E+01	2.523E-09 .028	2.261E-09 .026	2.327E-09 .028	2.328E-09 .029	2.258E-09 .027
8	1.110E+01	2.316E-09 .028	2.198E-09 .030	2.308E-09 .028	2.249E-09 .031	2.066E-09 .029
9	1.000E+01	2.106E-09 .029	1.920E-09 .030	2.193E-09 .028	2.068E-09 .029	1.811E-09 .030
10	9.050E+00	2.022E-09 .026	1.965E-09 .031	2.054E-09 .029	2.121E-09 .029	1.810E-09 .030
11	8.190E+00	2.043E-09 .028	1.762E-09 .032	2.022E-09 .028	1.951E-09 .029	1.754E-09 .032
12	7.410E+00	1.965E-09 .029	1.683E-09 .032	1.958E-09 .030	1.968E-09 .031	1.651E-09 .036
13	6.380E+00	1.730E-09 .026	1.533E-09 .030	1.790E-09 .030	1.651E-09 .031	1.538E-09 .032
14	4.970E+00	1.620E-09 .031	1.456E-09 .033	1.620E-09 .030	1.621E-09 .027	1.426E-09 .035
15	4.720E+00	1.441E-09 .031	1.323E-09 .035	1.517E-09 .031	1.545E-09 .035	1.230E-09 .035
16	4.070E+00	1.326E-09 .034	1.086E-09 .032	1.371E-09 .031	1.105E-09 .034	9.611E-10 .036
17	3.010E+00	1.098E-09 .034	8.516E-10 .037	1.027E-09 .032	9.408E-10 .037	8.508E-10 .038
18	2.390E+00	9.174E-10 .036	7.509E-10 .042	9.915E-10 .035	7.503E-10 .041	7.190E-10 .039
19	2.310E+00	8.496E-10 .033	6.543E-10 .046	8.209E-10 .037	7.281E-10 .042	6.088E-10 .046
20	1.830E+00	6.000E-10 .040	4.570E-10 .040	6.628E-10 .034	5.561E-10 .040	3.805E-10 .047
21	1.110E+00	3.110E-10 .045	1.815E-10 .055	3.524E-10 .039	3.055E-10 .043	1.751E-10 .056
22	5.500E-01	1.070E-10 .052	5.881E-11 .064	1.354E-10 .047	1.007E-10 .058	5.437E-11 .066
23	1.580E-01	3.282E-11 .052	2.585E-11 .053	5.554E-11 .051	2.869E-11 .055	2.157E-11 .055
24	1.110E-01	2.384E-11 .055	2.129E-11 .052	3.528E-11 .056	2.251E-11 .050	1.899E-11 .047
25	5.250E-02	1.834E-11 .050	1.642E-11 .044	2.107E-11 .046	1.729E-11 .051	1.630E-11 .046
26	2.480E-02	1.693E-11 .045	1.617E-11 .048	1.626E-11 .051	1.716E-11 .047	1.467E-11 .047
27	2.190E-02	1.696E-11 .043	1.479E-11 .044	1.545E-11 .047	1.661E-11 .047	1.423E-11 .051
28	1.030E-02	1.590E-11 .046	1.622E-11 .044	1.374E-11 .047	1.474E-11 .047	1.421E-11 .045
29	3.350E-03	1.592E-11 .048	1.397E-11 .049	1.223E-11 .046	1.446E-11 .049	1.409E-11 .046
30	1.230E-03	1.608E-11 .047	1.486E-11 .048	1.290E-11 .055	1.455E-11 .050	1.319E-11 .045
31	5.830E-04	1.732E-11 .043	1.327E-11 .045	1.282E-11 .049	1.449E-11 .049	1.280E-11 .046
32	1.010E-04	1.668E-11 .048	1.242E-11 .049	1.340E-11 .052	1.468E-11 .049	1.167E-11 .048
33	2.900E-05	1.547E-11 .051	1.169E-11 .057	1.357E-11 .058	1.337E-11 .056	1.083E-11 .061
34	1.070E-05	1.411E-11 .056	1.010E-11 .062	1.308E-11 .061	1.311E-11 .054	9.933E-12 .068
35	3.060E-06	1.250E-11 .068	9.946E-12 .067	1.412E-11 .064	1.042E-11 .073	8.160E-12 .079
36	1.130E-06	1.162E-11 .085	7.481E-12 .094	1.413E-11 .073	8.682E-12 .099	7.128E-12 .105
37	4.140E-07	6.564E-12 .034	5.181E-12 .038	8.599E-12 .030	5.935E-12 .039	5.198E-12 .038

Table A-2. 2 PI (back) integrated adjoint leakage neutron fluence (rads / n/cm**2) (FSD)

Energy Group	Upper Energy (MeV)	Complex Mid-Head		Complex Mid-Thorax		Complex Marrow		Simple Mid-Head		Simple Mid-Thorax	
1	1.960E+01	2.975E-09	.025	2.545E-09	.027	2.708E-09	.023	2.873E-09	.027	2.652E-09	.025
2	1.690E+01	2.795E-09	.029	2.435E-09	.028	2.598E-09	.026	2.690E-09	.028	2.522E-09	.029
3	1.490E+01	2.734E-09	.027	2.293E-09	.028	2.599E-09	.025	2.652E-09	.029	2.299E-09	.029
4	1.420E+01	2.499E-09	.027	2.279E-09	.027	2.408E-09	.024	2.658E-09	.028	2.277E-09	.030
5	1.380E+01	2.554E-09	.027	2.178E-09	.028	2.353E-09	.025	2.437E-09	.028	2.337E-09	.028
6	1.280E+01	2.306E-09	.027	2.171E-09	.028	2.278E-09	.025	2.391E-09	.030	2.094E-09	.031
7	1.220E+01	2.317E-09	.029	2.147E-09	.030	2.275E-09	.027	2.294E-09	.029	2.061E-09	.030
8	1.110E+01	2.164E-09	.030	2.013E-09	.028	2.180E-09	.026	2.037E-09	.027	2.021E-09	.029
9	1.000E+01	2.028E-09	.028	1.791E-09	.031	2.065E-09	.028	2.092E-09	.031	1.853E-09	.031
10	9.050E+00	1.998E-09	.029	1.734E-09	.031	1.843E-09	.028	2.007E-09	.030	1.847E-09	.032
11	8.190E+00	1.816E-09	.032	1.652E-09	.033	1.772E-09	.030	1.852E-09	.030	1.596E-09	.031
12	7.410E+00	1.900E-09	.033	1.552E-09	.036	1.737E-09	.030	1.946E-09	.030	1.701E-09	.029
13	6.380E+00	1.709E-09	.030	1.410E-09	.034	1.511E-09	.028	1.674E-09	.030	1.457E-09	.034
14	4.970E+00	1.570E-09	.033	1.283E-09	.035	1.426E-09	.031	1.617E-09	.029	1.245E-09	.034
15	4.720E+00	1.478E-09	.034	1.135E-09	.039	1.330E-09	.031	1.453E-09	.034	1.086E-09	.038
16	4.070E+00	1.220E-09	.034	9.574E-10	.034	1.066E-09	.033	1.113E-09	.037	8.320E-10	.040
17	3.010E+00	9.295E-10	.040	6.566E-10	.042	8.836E-10	.035	9.483E-10	.036	7.509E-10	.037
18	2.390E+00	9.432E-10	.035	6.720E-10	.042	8.255E-10	.034	8.485E-10	.039	6.119E-10	.046
19	2.310E+00	8.500E-10	.041	4.825E-10	.045	7.019E-10	.041	7.080E-10	.042	5.103E-10	.046
20	1.830E+00	5.788E-10	.040	3.566E-10	.050	5.374E-10	.038	5.604E-10	.039	3.444E-10	.050
21	1.110E+00	3.034E-10	.043	1.463E-10	.059	2.720E-10	.041	2.706E-10	.048	1.533E-10	.065
22	5.500E-01	1.051E-10	.049	4.320E-11	.070	1.044E-10	.047	8.182E-11	.061	3.882E-11	.069
23	1.580E-01	2.883E-11	.054	1.868E-11	.050	3.836E-11	.050	2.654E-11	.058	1.731E-11	.058
24	1.110E-01	2.372E-11	.056	1.346E-11	.046	2.427E-11	.053	2.054E-11	.046	1.408E-11	.046
25	5.250E-02	1.556E-11	.050	1.314E-11	.049	1.637E-11	.046	1.566E-11	.047	1.262E-11	.051
26	2.480E-02	1.392E-11	.052	1.118E-11	.053	1.235E-11	.055	1.530E-11	.046	1.158E-11	.059
27	2.190E-02	1.442E-11	.050	1.200E-11	.050	1.106E-11	.050	1.405E-11	.045	1.220E-11	.051
28	1.030E-02	1.426E-11	.047	1.165E-11	.050	9.019E-12	.050	1.399E-11	.048	1.130E-11	.051
29	3.350E-03	1.482E-11	.051	1.130E-11	.050	9.345E-12	.053	1.378E-11	.050	1.013E-11	.051
30	1.230E-03	1.534E-11	.050	9.767E-12	.059	9.261E-12	.060	1.401E-11	.053	1.043E-11	.058
31	5.830E-04	1.504E-11	.047	1.017E-11	.052	9.365E-12	.050	1.370E-11	.045	9.905E-12	.052
32	1.010E-04	1.439E-11	.052	8.193E-12	.061	1.008E-11	.054	1.283E-11	.058	8.166E-12	.057
33	2.900E-05	1.470E-11	.054	8.420E-12	.066	9.506E-12	.057	1.165E-11	.055	8.280E-12	.068
34	1.070E-05	1.306E-11	.056	7.228E-12	.069	1.079E-11	.065	1.121E-11	.065	6.394E-12	.074
35	3.060E-06	1.244E-11	.069	6.474E-12	.101	9.669E-12	.069	9.548E-12	.088	6.010E-12	.107
36	1.130E-06	1.034E-11	.091	4.883E-12	.140	1.016E-11	.085	8.107E-12	.101	5.040E-12	.132
37	4.140E-07	5.562E-12	.042	3.832E-12	.043	5.813E-12	.034	5.612E-12	.036	3.485E-12	.043

Table A-3. 4 PI integrated adjoint leakage neutron fluence (rads / n/cm**2) (FSD)

Energy Group	Upper Energy (MeV)	Complex Mid-Head	Complex Mid-Thorax	Complex Marroq	Simple Mid-Head	Simple Mid-Thorax
1	1.960E+01	5.988E-09 .018	5.406E-09 .019	5.969E-09 .016	5.918E-09 .018	5.426E-09 .018
2	1.690E+01	5.564E-09 .019	5.020E-09 .020	5.381E-09 .018	5.409E-09 .020	5.055E-09 .020
3	1.490E+01	5.354E-09 .021	4.768E-09 .020	5.303E-09 .018	5.352E-09 .020	4.719E-09 .019
4	1.420E+01	5.178E-09 .019	4.725E-09 .019	4.942E-09 .018	5.337E-09 .018	4.747E-09 .018
5	1.380E+01	5.085E-09 .019	4.561E-09 .020	4.836E-09 .019	5.075E-09 .020	4.821E-09 .019
6	1.280E+01	4.746E-09 .019	4.463E-09 .019	4.816E-09 .018	4.742E-09 .020	4.412E-09 .022
7	1.220E+01	4.840E-09 .019	4.408E-09 .020	4.602E-09 .019	4.622E-09 .021	4.320E-09 .019
8	1.110E+01	4.480E-09 .020	4.210E-09 .021	4.487E-09 .019	4.286E-09 .021	4.087E-09 .020
9	1.000E+01	4.134E-09 .019	3.711E-09 .022	4.258E-09 .019	4.160E-09 .019	3.663E-09 .021
10	9.050E+00	4.020E-09 .020	3.698E-09 .021	3.897E-09 .020	4.127E-09 .020	3.658E-09 .023
11	8.190E+00	3.859E-09 .022	3.414E-09 .023	3.795E-09 .021	3.803E-09 .020	3.349E-09 .021
12	7.410E+00	3.865E-09 .021	3.235E-09 .024	3.696E-09 .021	3.914E-09 .022	3.352E-09 .023
13	6.380E+00	3.439E-09 .019	2.943E-09 .022	3.301E-09 .020	3.326E-09 .022	2.995E-09 .025
14	4.970E+00	3.190E-09 .022	2.739E-09 .025	3.047E-09 .022	3.238E-09 .019	2.671E-09 .025
15	4.720E+00	2.919E-09 .023	2.458E-09 .027	2.847E-09 .021	2.998E-09 .025	2.316E-09 .026
16	4.070E+00	2.546E-09 .023	2.043E-09 .023	2.437E-09 .022	2.219E-09 .026	1.793E-09 .027
17	3.010E+00	2.027E-09 .026	1.508E-09 .028	1.911E-09 .024	1.889E-09 .025	1.602E-09 .027
18	2.390E+00	1.861E-09 .024	1.423E-09 .028	1.817E-09 .024	1.599E-09 .029	1.331E-09 .031
19	2.310E+00	1.700E-09 .027	1.137E-09 .034	1.523E-09 .028	1.436E-09 .029	1.119E-09 .031
20	1.830E+00	1.179E-09 .030	8.136E-10 .031	1.200E-09 .025	1.117E-09 .029	7.248E-10 .035
21	1.110E+00	6.145E-10 .031	3.279E-10 .039	6.244E-10 .028	5.761E-10 .033	3.284E-10 .042
22	5.500E-01	2.121E-10 .036	1.020E-10 .046	2.397E-10 .033	1.825E-10 .040	9.318E-11 .049
23	1.580E-01	6.165E-11 .038	4.454E-11 .038	9.389E-11 .036	5.524E-11 .041	3.887E-11 .044
24	1.110E-01	4.756E-11 .040	3.475E-11 .038	5.954E-11 .040	4.305E-11 .036	3.307E-11 .035
25	5.250E-02	3.390E-11 .040	2.956E-11 .036	3.744E-11 .034	3.294E-11 .040	2.892E-11 .040
26	2.480E-02	3.085E-11 .036	2.735E-11 .041	2.861E-11 .041	3.246E-11 .036	2.626E-11 .041
27	2.190E-02	3.138E-11 .038	2.678E-11 .036	2.650E-11 .038	3.066E-11 .037	2.644E-11 .038
28	1.030E-02	3.016E-11 .039	2.787E-11 .036	2.276E-11 .038	2.873E-11 .038	2.551E-11 .040
29	3.350E-03	3.074E-11 .041	2.527E-11 .039	2.157E-11 .040	2.824E-11 .041	2.422E-11 .039
30	1.230E-03	3.142E-11 .040	2.462E-11 .043	2.216E-11 .046	2.857E-11 .039	2.362E-11 .040
31	5.830E-04	3.236E-11 .038	2.344E-11 .040	2.219E-11 .042	2.819E-11 .040	2.270E-11 .038
32	1.010E-04	3.107E-11 .041	2.061E-11 .041	2.348E-11 .045	2.750E-11 .043	1.983E-11 .040
33	2.900E-05	3.017E-11 .042	2.011E-11 .048	2.308E-11 .049	2.502E-11 .045	1.911E-11 .053
34	1.070E-05	2.717E-11 .045	1.733E-11 .053	2.387E-11 .053	2.432E-11 .047	1.633E-11 .057
35	3.060E-06	2.494E-11 .057	1.642E-11 .065	2.379E-11 .055	1.997E-11 .067	1.417E-11 .072
36	1.130E-06	2.196E-11 .071	1.236E-11 .092	2.429E-11 .067	1.679E-11 .084	1.217E-11 .096
37	4.140E-07	1.213E-11 .027	9.014E-12 .028	1.441E-11 .022	1.155E-11 .025	8.682E-12 .029

Table A-4. 4 PI integrated adjoint leakage neutron fluence by marrow region (rads / n/cm**2) (FSD)

Energy Group	Upper Energy (MeV)	Skull	Clavicles	Scapulae	Upper Limbs	Ribs
1	1.960E+01	6.149E-09 .041	5.818E-09 .036	5.994E-09 .038	6.140E-09 .041	5.601E-09 .037
2	1.690E+01	5.530E-09 .043	5.837E-09 .042	5.700E-09 .043	5.242E-09 .046	5.107E-09 .046
3	1.490E+01	6.012E-09 .041	5.262E-09 .041	5.156E-09 .043	5.464E-09 .041	5.836E-09 .041
4	1.420E+01	5.322E-09 .046	5.259E-09 .044	5.038E-09 .046	5.250E-09 .041	5.091E-09 .039
5	1.380E+01	5.210E-09 .043	4.891E-09 .041	4.752E-09 .044	5.231E-09 .042	5.045E-09 .044
6	1.280E+01	5.104E-09 .048	4.973E-09 .045	5.065E-09 .042	5.025E-09 .044	4.607E-09 .043
7	1.220E+01	4.919E-09 .043	5.112E-09 .040	4.713E-09 .049	4.904E-09 .046	4.706E-09 .043
8	1.110E+01	4.957E-09 .042	4.576E-09 .043	4.421E-09 .045	4.565E-09 .045	4.267E-09 .044
9	1.000E+01	4.673E-09 .041	4.253E-09 .043	4.115E-09 .045	4.414E-09 .046	4.119E-09 .050
10	9.050E+00	4.423E-09 .040	4.172E-09 .052	3.981E-09 .046	3.887E-09 .048	3.739E-09 .050
11	8.190E+00	4.262E-09 .048	3.544E-09 .054	3.794E-09 .044	3.559E-09 .047	3.845E-09 .047
12	7.410E+00	4.447E-09 .045	3.810E-09 .053	3.475E-09 .052	3.546E-09 .056	3.386E-09 .046
13	6.380E+00	3.355E-09 .047	3.339E-09 .051	3.298E-09 .050	3.292E-09 .050	3.118E-09 .048
14	4.970E+00	3.506E-09 .051	2.888E-09 .055	2.825E-09 .050	2.998E-09 .044	2.959E-09 .052
15	4.720E+00	3.399E-09 .048	2.965E-09 .050	2.775E-09 .051	3.222E-09 .048	2.706E-09 .053
16	4.070E+00	2.798E-09 .054	2.460E-09 .056	2.363E-09 .050	2.677E-09 .051	2.218E-09 .053
17	3.010E+00	2.083E-09 .049	2.076E-09 .054	1.828E-09 .057	2.085E-09 .055	2.008E-09 .057
18	2.390E+00	2.173E-09 .050	1.874E-09 .052	1.836E-09 .061	1.800E-09 .055	1.549E-09 .062
19	2.310E+00	1.788E-09 .053	1.675E-09 .065	1.468E-09 .064	1.733E-09 .060	1.356E-09 .064
20	1.830E+00	1.464E-09 .056	1.194E-09 .065	1.209E-09 .063	1.154E-09 .060	1.111E-09 .064
21	1.110E+00	8.130E-10 .062	6.289E-10 .070	6.830E-10 .070	7.512E-10 .067	5.493E-10 .077
22	5.500E-01	4.054E-10 .065	2.360E-10 .081	2.135E-10 .089	2.629E-10 .082	1.846E-10 .087
23	1.580E-01	1.568E-10 .073	8.865E-11 .096	7.572E-11 .087	9.685E-11 .094	7.002E-11 .105
24	1.110E-01	9.623E-11 .083	4.875E-11 .094	4.681E-11 .098	5.814E-11 .096	4.758E-11 .096
25	5.250E-02	5.732E-11 .090	3.571E-11 .090	3.417E-11 .083	3.991E-11 .081	3.217E-11 .088
26	2.480E-02	3.219E-11 .094	2.728E-11 .100	2.538E-11 .090	2.524E-11 .095	2.890E-11 .100
27	2.190E-02	2.489E-11 .091	2.285E-11 .090	2.308E-11 .095	2.832E-11 .085	2.861E-11 .087
28	1.030E-02	2.156E-11 .085	2.326E-11 .094	2.516E-11 .090	2.278E-11 .093	2.194E-11 .096
29	3.350E-03	1.452E-11 .112	2.080E-11 .096	2.375E-11 .091	2.201E-11 .097	2.445E-11 .098
30	1.230E-03	1.825E-11 .119	2.072E-11 .114	2.239E-11 .103	2.046E-11 .102	2.309E-11 .090
31	5.830E-04	1.699E-11 .121	2.403E-11 .091	2.534E-11 .091	2.478E-11 .096	2.391E-11 .098
32	1.010E-04	1.657E-11 .128	3.024E-11 .092	2.249E-11 .100	2.552E-11 .101	2.433E-11 .112
33	2.900E-05	1.568E-11 .129	2.752E-11 .104	2.357E-11 .115	2.630E-11 .109	2.575E-11 .112
34	1.070E-05	2.136E-11 .138	3.036E-11 .106	2.447E-11 .115	2.830E-11 .114	2.124E-11 .119
35	3.060E-06	2.703E-11 .160	2.716E-11 .137	1.995E-11 .146	2.612E-11 .132	2.353E-11 .129
36	1.130E-06	2.576E-11 .166	2.569E-11 .170	1.935E-11 .175	3.136E-11 .151	1.809E-11 .175
37	4.140E-07	1.697E-11 .050	1.440E-11 .053	1.552E-11 .051	1.635E-11 .054	1.287E-11 .056

Table A-4. 4 PI integrated adjoint leakage neutron fluence by marrow region (rads / n/cm**2) (FSD)

Energy Group	Upper Energy (MeV)	Vertebrae	Pelvis	Upper Femur	Lower Limbs	Average
1	1.960E+01	5.974E-09 .037	5.800E-09 .038	5.980E-09 .040	5.989E-09 .039	5.969E-09 .016
2	1.690E+01	5.212E-09 .042	5.529E-09 .045	5.349E-09 .041	5.694E-09 .042	5.381E-09 .018
3	1.490E+01	4.796E-09 .045	5.261E-09 .042	5.735E-09 .040	5.453E-09 .045	5.303E-09 .018
4	1.420E+01	4.558E-09 .046	4.632E-09 .042	5.253E-09 .041	5.336E-09 .042	4.942E-09 .018
5	1.380E+01	4.407E-09 .047	4.845E-09 .048	4.717E-09 .044	5.208E-09 .041	4.836E-09 .019
6	1.280E+01	4.598E-09 .040	4.610E-09 .046	4.509E-09 .046	5.305E-09 .041	4.816E-09 .018
7	1.220E+01	4.531E-09 .046	4.388E-09 .048	4.391E-09 .047	4.447E-09 .048	4.602E-09 .019
8	1.110E+01	4.306E-09 .046	4.374E-09 .044	4.353E-09 .045	4.778E-09 .045	4.487E-09 .019
9	1.000E+01	4.109E-09 .046	4.043E-09 .044	4.054E-09 .051	4.563E-09 .042	4.258E-09 .019
10	9.050E+00	3.596E-09 .050	3.924E-09 .045	3.913E-09 .046	4.226E-09 .050	3.897E-09 .020
11	8.190E+00	3.631E-09 .051	3.736E-09 .049	3.742E-09 .047	4.107E-09 .050	3.795E-09 .021
12	7.410E+00	3.671E-09 .051	3.442E-09 .049	3.286E-09 .052	3.936E-09 .045	3.696E-09 .021
13	6.380E+00	3.325E-09 .048	3.271E-09 .043	3.140E-09 .050	3.401E-09 .045	3.301E-09 .020
14	4.970E+00	2.943E-09 .053	3.063E-09 .049	3.148E-09 .048	3.025E-09 .054	3.047E-09 .022
15	4.720E+00	2.623E-09 .051	2.682E-09 .052	2.744E-09 .055	2.905E-09 .054	2.847E-09 .021
16	4.070E+00	2.251E-09 .054	2.320E-09 .056	2.300E-09 .057	2.690E-09 .050	2.437E-09 .022
17	3.010E+00	1.767E-09 .059	1.687E-09 .055	2.070E-09 .057	2.075E-09 .056	1.911E-09 .024
18	2.390E+00	1.681E-09 .058	1.748E-09 .060	1.762E-09 .055	2.093E-09 .056	1.817E-09 .024
19	2.310E+00	1.361E-09 .073	1.409E-09 .071	1.301E-09 .072	1.825E-09 .059	1.523E-09 .028
20	1.830E+00	1.098E-09 .064	1.216E-09 .058	1.216E-09 .058	1.299E-09 .054	1.200E-09 .025
21	1.110E+00	4.815E-10 .073	6.782E-10 .065	6.595E-10 .066	6.571E-10 .076	6.244E-10 .028
22	5.500E-01	1.907E-10 .086	2.561E-10 .076	1.990E-10 .083	2.433E-10 .088	2.397E-10 .033
23	1.580E-01	7.275E-11 .095	1.035E-10 .091	8.658E-11 .096	1.035E-10 .089	9.389E-11 .036
24	1.110E-01	4.908E-11 .108	6.896E-11 .092	6.752E-11 .096	5.362E-11 .098	5.954E-11 .040
25	5.250E-02	3.309E-11 .079	4.123E-11 .085	3.158E-11 .092	3.251E-11 .090	3.744E-11 .034
26	2.480E-02	3.115E-11 .090	3.020E-11 .094	2.871E-11 .086	2.170E-11 .109	2.861E-11 .041
27	2.190E-02	2.727E-11 .086	3.053E-11 .084	2.391E-11 .085	2.185E-11 .104	2.650E-11 .038
28	1.030E-02	2.468E-11 .084	2.464E-11 .092	2.073E-11 .097	1.783E-11 .103	2.276E-11 .038
29	3.350E-03	2.373E-11 .084	2.372E-11 .101	1.925E-11 .089	1.872E-11 .105	2.157E-11 .040
30	1.230E-03	2.615E-11 .097	2.134E-11 .093	1.983E-11 .102	1.853E-11 .123	2.216E-11 .046
31	5.830E-04	2.346E-11 .096	2.157E-11 .097	1.910E-11 .099	2.122E-11 .099	2.219E-11 .042
32	1.010E-04	2.573E-11 .098	2.267E-11 .102	2.208E-11 .101	2.272E-11 .105	2.348E-11 .045
33	2.900E-05	2.292E-11 .119	2.301E-11 .113	2.359E-11 .103	2.476E-11 .107	2.308E-11 .049
34	1.070E-05	2.281E-11 .129	2.279E-11 .123	2.489E-11 .116	2.577E-11 .120	2.387E-11 .053
35	3.060E-06	2.098E-11 .130	2.463E-11 .140	2.187E-11 .136	2.720E-11 .134	2.379E-11 .055
36	1.130E-06	2.146E-11 .164	2.131E-11 .157	2.332E-11 .176	3.131E-11 .157	2.429E-11 .067
37	4.140E-07	1.225E-11 .059	1.436E-11 .054	1.349E-11 .055	1.684E-11 .048	1.441E-11 .022

Table A-5. 2 PI (front) integrated adjoint leakage neutron-gamma ray fluence (rads / n/cm**2) (FSD)

Energy Group	Upper Energy (MeV)	Complex Mid-Head		Complex Mid-Thorax		Complex Marrow		Simple Mid-Head		Simple Mid-Thorax	
1	1.960E+01	5.235E-11	.042	6.568E-11	.040	5.641E-11	.038	4.805E-11	.039	6.897E-11	.035
2	1.690E+01	6.103E-11	.035	7.804E-11	.034	6.677E-11	.035	4.918E-11	.046	8.226E-11	.032
3	1.490E+01	6.551E-11	.035	8.810E-11	.038	6.880E-11	.031	6.002E-11	.041	9.126E-11	.031
4	1.420E+01	6.676E-11	.034	8.688E-11	.035	6.685E-11	.032	5.977E-11	.040	9.115E-11	.031
5	1.380E+01	7.044E-11	.035	8.211E-11	.036	7.188E-11	.033	6.671E-11	.041	8.807E-11	.034
6	1.280E+01	6.765E-11	.035	8.566E-11	.034	7.404E-11	.031	6.673E-11	.040	8.535E-11	.034
7	1.220E+01	6.644E-11	.033	8.857E-11	.037	7.835E-11	.034	7.572E-11	.036	8.687E-11	.032
8	1.110E+01	6.543E-11	.035	8.491E-11	.032	7.532E-11	.038	7.268E-11	.034	8.742E-11	.033
9	1.000E+01	5.753E-11	.044	7.255E-11	.040	6.012E-11	.038	6.370E-11	.039	8.124E-11	.040
10	9.050E+00	5.306E-11	.040	6.887E-11	.048	5.881E-11	.040	5.762E-11	.044	7.196E-11	.044
11	8.190E+00	4.623E-11	.049	6.364E-11	.044	5.287E-11	.042	5.620E-11	.044	6.751E-11	.051
12	7.410E+00	2.689E-11	.067	4.323E-11	.062	3.404E-11	.081	4.169E-11	.062	4.089E-11	.066
13	6.380E+00	1.628E-11	.120	3.050E-11	.091	2.294E-11	.096	3.021E-11	.085	2.699E-11	.088
14	4.970E+00	9.530E-12	.198	2.349E-11	.135	1.210E-11	.167	1.359E-11	.136	2.801E-11	.106
15	4.720E+00	1.429E-11	.206	2.559E-11	.125	1.484E-11	.176	1.856E-11	.142	2.655E-11	.124
16	4.070E+00	8.690E-12	.207	3.048E-11	.108	1.537E-11	.151	1.661E-11	.157	3.941E-11	.099
17	3.010E+00	1.079E-11	.154	3.636E-11	.098	2.319E-11	.155	1.832E-11	.146	3.642E-11	.104
18	2.390E+00	1.489E-11	.191	3.958E-11	.096	2.444E-11	.134	1.947E-11	.136	4.891E-11	.093
19	2.310E+00	1.711E-11	.160	4.640E-11	.089	2.216E-11	.123	2.258E-11	.135	5.138E-11	.104
20	1.830E+00	1.707E-11	.152	4.676E-11	.092	2.855E-11	.154	3.331E-11	.119	5.486E-11	.082
21	1.110E+00	2.282E-11	.124	6.256E-11	.084	3.072E-11	.111	3.715E-11	.097	5.681E-11	.078
22	5.500E-01	3.244E-11	.112	6.544E-11	.066	3.997E-11	.130	4.316E-11	.095	6.699E-11	.076
23	1.580E-01	3.774E-11	.101	6.647E-11	.084	4.722E-11	.097	5.813E-11	.099	6.162E-11	.100
24	1.110E-01	4.476E-11	.101	6.958E-11	.083	5.321E-11	.107	4.370E-11	.106	6.283E-11	.081
25	5.250E-02	4.126E-11	.116	7.604E-11	.089	3.981E-11	.112	5.952E-11	.098	6.888E-11	.083
26	2.480E-02	3.868E-11	.132	7.959E-11	.098	4.197E-11	.126	5.075E-11	.103	6.657E-11	.098
27	2.190E-02	4.716E-11	.122	8.145E-11	.094	4.930E-11	.107	5.982E-11	.103	6.065E-11	.092
28	1.030E-02	5.197E-11	.102	8.404E-11	.089	4.737E-11	.120	5.500E-11	.098	7.256E-11	.077
29	3.350E-03	5.290E-11	.107	7.940E-11	.083	5.370E-11	.108	5.321E-11	.103	7.693E-11	.077
30	1.230E-03	5.169E-11	.102	8.496E-11	.091	6.017E-11	.098	6.551E-11	.096	6.968E-11	.104
31	5.830E-04	5.463E-11	.096	8.007E-11	.073	5.705E-11	.101	6.477E-11	.088	7.668E-11	.084
32	1.010E-04	5.582E-11	.107	7.970E-11	.089	6.019E-11	.104	6.676E-11	.092	7.472E-11	.080
33	2.900E-05	5.795E-11	.122	8.790E-11	.084	5.767E-11	.109	6.011E-11	.111	7.583E-11	.091
34	1.070E-05	5.568E-11	.106	8.176E-11	.090	6.483E-11	.099	7.147E-11	.092	7.352E-11	.086
35	3.060E-06	5.711E-11	.115	7.426E-11	.098	6.531E-11	.111	6.359E-11	.111	8.192E-11	.094
36	1.130E-06	6.205E-11	.131	8.170E-11	.126	5.589E-11	.115	6.666E-11	.128	6.507E-11	.113
37	4.140E-07	4.647E-11	.034	5.138E-11	.030	5.036E-11	.032	4.674E-11	.032	4.976E-11	.030

Table A-6. 2 PI (back) integrated adjoint leakage neutron-gamma ray fluence (rads / n/cm**2) (FSD)

Energy Group	Upper Energy (MeV)	Complex Mid-Head	Complex Mid-Thorax	Complex Marrow	Simple Mid-Head	Simple Mid-Thorax
1	1.960E+01	4.610E-11 .037	6.148E-11 .039	5.118E-11 .038	4.924E-11 .041	6.437E-11 .036
2	1.690E+01	5.783E-11 .038	6.869E-11 .035	6.230E-11 .037	5.171E-11 .041	7.952E-11 .034
3	1.490E+01	6.328E-11 .035	8.026E-11 .034	6.868E-11 .035	6.151E-11 .042	8.838E-11 .030
4	1.420E+01	6.598E-11 .032	7.945E-11 .032	6.549E-11 .030	6.025E-11 .035	8.589E-11 .034
5	1.380E+01	6.631E-11 .038	8.153E-11 .031	6.748E-11 .031	6.183E-11 .036	8.295E-11 .031
6	1.280E+01	6.686E-11 .035	7.861E-11 .036	6.630E-11 .038	6.832E-11 .036	8.709E-11 .032
7	1.220E+01	7.014E-11 .036	8.399E-11 .032	6.995E-11 .032	7.727E-11 .039	9.226E-11 .033
8	1.110E+01	6.479E-11 .039	8.206E-11 .042	6.545E-11 .034	6.933E-11 .038	7.789E-11 .033
9	1.000E+01	5.271E-11 .037	7.061E-11 .041	5.793E-11 .039	6.166E-11 .039	7.119E-11 .036
10	9.050E+00	5.073E-11 .046	6.159E-11 .043	5.594E-11 .050	5.289E-11 .045	6.698E-11 .047
11	8.190E+00	4.498E-11 .048	6.144E-11 .058	4.873E-11 .046	5.742E-11 .046	6.309E-11 .056
12	7.410E+00	2.481E-11 .067	3.934E-11 .072	2.949E-11 .067	3.653E-11 .068	3.911E-11 .072
13	6.380E+00	1.882E-11 .098	3.393E-11 .094	1.954E-11 .092	3.000E-11 .085	3.552E-11 .091
14	4.970E+00	1.129E-11 .202	2.702E-11 .120	1.347E-11 .237	1.332E-11 .161	2.676E-11 .112
15	4.720E+00	8.671E-12 .200	2.529E-11 .119	1.319E-11 .180	1.190E-11 .166	2.977E-11 .109
16	4.070E+00	1.201E-11 .189	2.747E-11 .114	1.450E-11 .200	1.249E-11 .150	3.410E-11 .113
17	3.010E+00	8.605E-12 .190	3.469E-11 .104	2.193E-11 .152	1.872E-11 .149	3.747E-11 .099
18	2.390E+00	1.535E-11 .159	4.060E-11 .104	1.900E-11 .127	1.654E-11 .140	4.716E-11 .095
19	2.310E+00	1.429E-11 .187	4.413E-11 .096	2.461E-11 .138	2.447E-11 .116	4.728E-11 .098
20	1.830E+00	2.395E-11 .141	5.079E-11 .099	2.148E-11 .132	2.646E-11 .113	4.675E-11 .094
21	1.110E+00	2.081E-11 .122	5.781E-11 .088	3.143E-11 .116	2.916E-11 .110	5.295E-11 .085
22	5.500E-01	2.772E-11 .099	5.446E-11 .081	3.035E-11 .107	4.523E-11 .091	5.521E-11 .073
23	1.580E-01	3.260E-11 .128	6.136E-11 .084	3.306E-11 .109	4.184E-11 .095	5.951E-11 .084
24	1.110E-01	4.480E-11 .104	6.166E-11 .085	4.318E-11 .127	4.770E-11 .120	6.642E-11 .082
25	5.250E-02	3.991E-11 .122	5.700E-11 .094	3.700E-11 .122	4.950E-11 .111	6.456E-11 .089
26	2.480E-02	3.727E-11 .134	5.862E-11 .118	4.085E-11 .116	5.297E-11 .111	6.128E-11 .087
27	2.190E-02	4.010E-11 .112	5.214E-11 .112	3.846E-11 .125	4.710E-11 .118	7.286E-11 .088
28	1.030E-02	4.121E-11 .110	6.470E-11 .088	3.869E-11 .110	5.273E-11 .091	6.659E-11 .082
29	3.350E-03	4.919E-11 .102	6.389E-11 .091	4.802E-11 .107	4.996E-11 .095	6.134E-11 .086
30	1.230E-03	4.876E-11 .112	7.100E-11 .094	3.669E-11 .121	5.074E-11 .101	6.318E-11 .097
31	5.830E-04	4.864E-11 .103	7.034E-11 .084	4.928E-11 .090	5.501E-11 .090	6.582E-11 .082
32	1.010E-04	6.121E-11 .116	5.757E-11 .103	5.014E-11 .124	6.096E-11 .098	6.858E-11 .094
33	2.900E-05	5.652E-11 .117	6.415E-11 .096	4.975E-11 .112	6.617E-11 .106	6.648E-11 .091
34	1.070E-05	5.382E-11 .109	5.844E-11 .108	5.015E-11 .119	6.686E-11 .099	6.083E-11 .103
35	3.060E-06	6.162E-11 .108	6.655E-11 .111	5.668E-11 .119	6.396E-11 .112	6.679E-11 .108
36	1.130E-06	6.155E-11 .132	5.903E-11 .121	7.306E-11 .153	5.800E-11 .126	5.254E-11 .144
37	4.140E-07	4.055E-11 .038	4.109E-11 .037	3.641E-11 .039	3.811E-11 .035	3.779E-11 .038

Table A-7. 4 PI integrated adjoint leakage neutron-gamma ray fluence (rads / n/cm**2) (FSD)

Energy Group	Upper Energy (MeV)	Complex Mid-Head	Complex Mid-Thorax	Complex Marrow	Simple Mid-Head	Simple Mid-Thorax
1	1.960E+01	9.844E-11 .029	1.272E-10 .030	1.076E-10 .030	9.729E-11 .033	1.333E-10 .025
2	1.690E+01	1.189E-10 .027	1.467E-10 .027	1.291E-10 .028	1.009E-10 .033	1.618E-10 .024
3	1.490E+01	1.288E-10 .027	1.684E-10 .027	1.375E-10 .025	1.215E-10 .032	1.796E-10 .022
4	1.420E+01	1.327E-10 .024	1.663E-10 .025	1.323E-10 .024	1.200E-10 .028	1.770E-10 .024
5	1.380E+01	1.367E-10 .028	1.636E-10 .025	1.393E-10 .024	1.285E-10 .029	1.710E-10 .024
6	1.280E+01	1.345E-10 .025	1.643E-10 .027	1.403E-10 .026	1.351E-10 .030	1.724E-10 .025
7	1.220E+01	1.366E-10 .026	1.726E-10 .026	1.483E-10 .026	1.530E-10 .029	1.791E-10 .025
8	1.110E+01	1.302E-10 .027	1.670E-10 .028	1.408E-10 .027	1.420E-10 .029	1.653E-10 .025
9	1.000E+01	1.102E-10 .031	1.432E-10 .030	1.180E-10 .030	1.254E-10 .030	1.524E-10 .028
10	9.050E+00	1.038E-10 .032	1.305E-10 .033	1.147E-10 .032	1.105E-10 .034	1.389E-10 .034
11	8.190E+00	9.121E-11 .036	1.251E-10 .038	1.016E-10 .034	1.136E-10 .036	1.306E-10 .039
12	7.410E+00	5.170E-11 .049	8.257E-11 .050	6.353E-11 .055	7.822E-11 .047	8.000E-11 .051
13	6.380E+00	3.510E-11 .077	6.443E-11 .069	4.248E-11 .069	6.020E-11 .063	6.251E-11 .071
14	4.970E+00	2.082E-11 .154	5.051E-11 .096	2.557E-11 .149	2.691E-11 .114	5.477E-11 .083
15	4.720E+00	2.296E-11 .154	5.088E-11 .089	2.803E-11 .135	3.046E-11 .115	5.632E-11 .087
16	4.070E+00	2.070E-11 .142	5.796E-11 .080	2.987E-11 .128	2.910E-11 .113	7.350E-11 .078
17	3.010E+00	1.940E-11 .131	7.105E-11 .073	4.511E-11 .117	3.704E-11 .101	7.389E-11 .073
18	2.390E+00	3.024E-11 .125	8.019E-11 .079	4.344E-11 .104	3.600E-11 .100	9.606E-11 .071
19	2.310E+00	3.140E-11 .131	9.053E-11 .073	4.677E-11 .099	4.705E-11 .094	9.866E-11 .077
20	1.830E+00	4.102E-11 .111	9.755E-11 .075	5.004E-11 .112	5.976E-11 .088	1.016E-10 .065
21	1.110E+00	4.362E-11 .090	1.204E-10 .071	6.216E-11 .086	6.631E-11 .077	1.098E-10 .059
22	5.500E-01	6.016E-11 .082	1.199E-10 .058	7.032E-11 .089	8.839E-11 .069	1.222E-10 .059
23	1.580E-01	7.034E-11 .086	1.278E-10 .063	8.027E-11 .077	9.997E-11 .075	1.211E-10 .069
24	1.110E-01	8.956E-11 .078	1.312E-10 .065	9.641E-11 .085	9.141E-11 .088	1.293E-10 .063
25	5.250E-02	8.117E-11 .091	1.330E-10 .071	7.681E-11 .084	1.090E-10 .079	1.334E-10 .064
26	2.480E-02	7.595E-11 .105	1.382E-10 .080	8.282E-11 .089	1.037E-10 .078	1.279E-10 .066
27	2.190E-02	8.725E-11 .095	1.336E-10 .083	8.777E-11 .085	1.069E-10 .082	1.335E-10 .065
28	1.030E-02	9.318E-11 .079	1.487E-10 .066	8.604E-11 .088	1.077E-10 .069	1.392E-10 .059
29	3.350E-03	1.021E-10 .079	1.433E-10 .064	1.017E-10 .082	1.032E-10 .072	1.383E-10 .061
30	1.230E-03	1.005E-10 .082	1.560E-10 .066	9.685E-11 .085	1.163E-10 .078	1.329E-10 .075
31	5.830E-04	1.033E-10 .074	1.504E-10 .061	1.063E-10 .077	1.198E-10 .069	1.425E-10 .067
32	1.010E-04	1.170E-10 .085	1.373E-10 .071	1.103E-10 .085	1.277E-10 .071	1.433E-10 .066
33	2.900E-05	1.145E-10 .086	1.521E-10 .065	1.074E-10 .081	1.263E-10 .085	1.423E-10 .070
34	1.070E-05	1.095E-10 .076	1.402E-10 .073	1.150E-10 .085	1.383E-10 .071	1.343E-10 .070
35	3.060E-06	1.187E-10 .082	1.408E-10 .077	1.220E-10 .087	1.276E-10 .090	1.487E-10 .074
36	1.130E-06	1.236E-10 .100	1.407E-10 .096	1.289E-10 .102	1.247E-10 .097	1.176E-10 .094
37	4.140E-07	8.701E-11 .029	9.246E-11 .026	8.678E-11 .027	8.485E-11 .027	8.754E-11 .026

Table A-8. 4 PI integrated adjoint leakage neutron-gamma ray fluence by marrow region (rads / g/cm**2) (FSD)

Energy Group	Upper Energy (MeV)	Skull	Clavicles	Scapulae	Upper Limgs	Ribs
1	1.960E+01	7.969E-11 .071	9.540E-11 .072	1.005E-10 .069	9.625E-11 .059	1.024E-10 .060
2	1.690E+01	1.077E-10 .084	1.163E-10 .054	1.233E-10 .061	1.208E-10 .062	1.153E-10 .057
3	1.490E+01	1.004E-10 .066	1.250E-10 .057	1.412E-10 .063	1.242E-10 .060	1.480E-10 .052
4	1.420E+01	1.035E-10 .070	1.394E-10 .051	1.484E-10 .060	1.185E-10 .058	1.694E-10 .056
5	1.380E+01	1.069E-10 .067	1.328E-10 .053	1.450E-10 .063	1.424E-10 .055	1.386E-10 .057
6	1.280E+01	1.015E-10 .061	1.429E-10 .055	1.524E-10 .054	1.310E-10 .070	1.435E-10 .051
7	1.220E+01	1.100E-10 .068	1.493E-10 .051	1.348E-10 .060	1.368E-10 .060	1.398E-10 .050
8	1.110E+01	1.084E-10 .078	1.322E-10 .064	1.313E-10 .057	1.315E-10 .059	1.360E-10 .064
9	1.000E+01	8.656E-11 .071	1.328E-10 .060	1.210E-10 .075	1.072E-10 .069	1.233E-10 .061
10	9.050E+00	7.612E-11 .084	1.023E-10 .068	1.111E-10 .076	1.146E-10 .070	1.083E-10 .069
11	8.190E+00	7.577E-11 .100	1.085E-10 .085	1.009E-10 .078	9.667E-11 .074	1.081E-10 .080
12	7.410E+00	4.251E-11 .128	5.555E-11 .127	5.067E-11 .118	5.676E-11 .102	6.759E-11 .134
13	6.380E+00	2.954E-11 .207	4.257E-11 .180	3.386E-11 .157	3.743E-11 .167	3.734E-11 .141
14	4.970E+00	5.475E-12 .348	2.598E-11 .333	2.780E-11 .294	1.298E-11 .321	2.312E-11 .222
15	4.720E+00	4.039E-12 .490	2.076E-11 .290	1.326E-11 .367	1.565E-11 .304	3.006E-11 .287
16	4.070E+00	1.025E-11 .340	1.136E-11 .385	2.042E-11 .328	2.111E-11 .282	3.765E-11 .231
17	3.010E+00	2.230E-11 .353	3.214E-11 .246	3.013E-11 .257	2.527E-11 .237	3.185E-11 .248
18	2.390E+00	1.845E-11 .338	1.575E-11 .297	3.950E-11 .224	2.661E-11 .307	4.532E-11 .206
19	2.310E+00	1.939E-11 .272	1.750E-11 .266	3.087E-11 .334	3.652E-11 .218	4.438E-11 .202
20	1.830E+00	1.336E-11 .298	2.890E-11 .254	4.388E-11 .244	3.968E-11 .296	4.979E-11 .193
21	1.110E+00	3.968E-11 .286	4.532E-11 .248	2.681E-11 .203	6.085E-11 .172	6.824E-11 .169
22	5.500E-01	4.032E-11 .237	5.726E-11 .180	6.425E-11 .182	6.082E-11 .192	8.584E-11 .155
23	1.580E-01	3.964E-11 .258	7.231E-11 .190	7.372E-11 .196	8.963E-11 .179	1.016E-10 .177
24	1.110E-01	3.120E-11 .254	8.278E-11 .186	9.135E-11 .182	8.273E-11 .181	9.417E-11 .165
25	5.250E-02	4.757E-11 .225	7.037E-11 .188	7.674E-11 .196	9.132E-11 .192	1.155E-10 .157
26	2.480E-02	4.582E-11 .241	8.429E-11 .213	1.195E-10 .160	8.603E-11 .186	9.303E-11 .173
27	2.190E-02	3.126E-11 .278	8.299E-11 .222	1.033E-10 .179	6.091E-11 .189	9.491E-11 .185
28	1.030E-02	4.747E-11 .266	7.467E-11 .206	1.185E-10 .149	8.546E-11 .171	1.147E-10 .144
29	3.350E-03	5.366E-11 .237	7.718E-11 .182	8.524E-11 .197	8.672E-11 .177	1.015E-10 .167
30	1.230E-03	5.571E-11 .262	8.219E-11 .211	9.135E-11 .214	7.185E-11 .223	1.206E-10 .203
31	5.830E-04	7.470E-11 .222	1.060E-10 .184	1.212E-10 .169	1.079E-10 .171	1.179E-10 .166
32	1.010E-04	7.880E-11 .195	8.313E-11 .172	1.557E-10 .157	6.381E-11 .217	1.059E-10 .188
33	2.900E-05	9.354E-11 .209	7.194E-11 .235	1.232E-10 .169	1.170E-10 .168	1.471E-10 .155
34	1.070E-05	7.315E-11 .215	9.956E-11 .192	9.739E-11 .181	1.157E-10 .188	1.405E-10 .178
35	3.060E-06	8.478E-11 .253	1.144E-10 .191	1.620E-10 .197	1.383E-10 .192	1.693E-10 .176
36	1.130E-06	1.102E-10 .247	1.383E-10 .198	1.377E-10 .173	1.237E-10 .202	1.484E-10 .183
37	4.140E-07	7.444E-11 .070	9.481E-11 .062	9.199E-11 .057	8.620E-11 .067	9.670E-11 .055

Table A-8. 4 PI integrated adjoint leakage neutron-gamma ray fluence by marrow region (rads / g/cm**2) (FSD)

Energy Group	Upper Energy (MeV)	Vertebrae	Pelvis	Upper Femur	Lower Limbs	Average
1	1.960E+01	1.225E-10 .063	1.267E-10 .078	1.248E-10 .075	8.176E-11 .063	1.076E-10 .030
2	1.690E+01	1.439E-10 .061	1.366E-10 .051	1.348E-10 .063	1.160E-10 .070	1.291E-10 .028
3	1.490E+01	1.515E-10 .054	1.464E-10 .057	1.469E-10 .057	1.263E-10 .068	1.375E-10 .025
4	1.420E+01	1.362E-10 .052	1.441E-10 .056	1.332E-10 .053	1.245E-10 .063	1.323E-10 .024
5	1.380E+01	1.522E-10 .052	1.445E-10 .053	1.389E-10 .055	1.254E-10 .056	1.393E-10 .024
6	1.280E+01	1.561E-10 .058	1.546E-10 .049	1.484E-10 .056	1.184E-10 .068	1.403E-10 .026
7	1.220E+01	1.641E-10 .056	1.585E-10 .063	1.571E-10 .054	1.445E-10 .060	1.483E-10 .026
8	1.110E+01	1.564E-10 .061	1.620E-10 .057	1.393E-10 .057	1.225E-10 .065	1.408E-10 .027
9	1.000E+01	1.240E-10 .070	1.371E-10 .065	1.334E-10 .067	1.086E-10 .068	1.180E-10 .030
10	9.050E+00	1.355E-10 .069	1.233E-10 .072	1.178E-10 .070	8.984E-11 .076	1.147E-10 .032
11	8.190E+00	1.067E-10 .078	1.139E-10 .071	1.097E-10 .101	9.550E-11 .071	1.016E-10 .034
12	7.410E+00	7.871E-11 .115	6.748E-11 .133	6.611E-11 .103	4.631E-11 .095	6.353E-11 .055
13	6.380E+00	5.212E-11 .138	4.260E-11 .132	4.926E-11 .153	3.512E-11 .209	4.248E-11 .069
14	4.970E+00	4.353E-11 .249	2.882E-11 .263	2.457E-11 .226	6.728E-12 .405	2.557E-11 .149
15	4.720E+00	4.675E-11 .219	3.558E-11 .288	3.093E-11 .254	7.396E-12 .401	2.803E-11 .135
16	4.070E+00	4.023E-11 .250	3.919E-11 .248	2.480E-11 .243	2.174E-11 .305	2.987E-11 .128
17	3.010E+00	7.350E-11 .200	4.457E-11 .220	5.034E-11 .204	2.062E-11 .310	4.511E-11 .117
18	2.390E+00	6.101E-11 .191	4.202E-11 .215	5.327E-11 .205	3.378E-11 .301	4.344E-11 .104
19	2.310E+00	6.374E-11 .176	5.989E-11 .279	5.221E-11 .178	2.826E-11 .262	4.677E-11 .099
20	1.830E+00	7.535E-11 .201	5.032E-11 .188	5.801E-11 .209	2.534E-11 .325	5.004E-11 .112
21	1.110E+00	8.704E-11 .162	5.922E-11 .187	6.468E-11 .161	2.979E-11 .232	6.216E-11 .086
22	5.500E-01	9.825E-11 .174	6.551E-11 .162	8.190E-11 .163	2.806E-11 .245	7.032E-11 .089
23	1.580E-01	9.687E-11 .155	6.736E-11 .189	9.300E-11 .171	6.202E-11 .208	8.027E-11 .077
24	1.110E-01	1.388E-10 .158	9.163E-11 .180	8.808E-11 .163	6.900E-11 .212	9.641E-11 .085
25	5.250E-02	9.043E-11 .175	5.622E-11 .206	8.775E-11 .192	5.006E-11 .263	7.681E-11 .084
26	2.480E-02	9.336E-11 .204	8.997E-11 .166	9.854E-11 .170	5.341E-11 .231	8.282E-11 .089
27	2.190E-02	1.158E-10 .166	1.070E-10 .186	1.137E-10 .198	4.953E-11 .228	8.777E-11 .085
28	1.030E-02	1.028E-10 .193	7.894E-11 .185	1.052E-10 .162	5.120E-11 .248	8.604E-11 .088
29	3.350E-03	1.259E-10 .170	1.037E-10 .168	1.277E-10 .191	8.583E-11 .196	1.017E-10 .082
30	1.230E-03	1.225E-10 .170	8.608E-11 .184	1.084E-10 .164	8.542E-11 .209	9.685E-11 .085
31	5.830E-04	1.386E-10 .149	8.798E-11 .201	9.391E-11 .157	6.477E-11 .211	1.063E-10 .077
32	1.010E-04	1.383E-10 .179	1.333E-10 .153	1.060E-10 .182	7.946E-11 .190	1.103E-10 .085
33	2.900E-05	1.140E-10 .194	7.598E-11 .179	1.645E-10 .153	7.395E-11 .198	1.074E-10 .081
34	1.070E-05	1.226E-10 .187	1.597E-10 .203	1.056E-10 .199	8.491E-11 .194	1.150E-10 .085
35	3.060E-06	1.378E-10 .193	1.093E-10 .198	1.221E-10 .172	7.668E-11 .212	1.220E-10 .087
36	1.130E-06	1.614E-10 .215	9.286E-11 .238	1.225E-10 .222	9.435E-11 .229	1.289E-10 .102
37	4.140E-07	9.213E-11 .062	8.668E-11 .061	8.995E-11 .053	7.593E-11 .067	8.678E-11 .027

Table A-9. 2 PI (front) integrated adjoint leakage gamma ray fluence (rads / g/cm**2) (FSD)

Energy Group	Upper Energy (MeV)	Complex Mid-Head	Complex Mid-Thorax	Complex Marrow	Simple Mid-Head	Simple Mid-Thorax
1	1.400E+01	1.368E-09 .020	1.271E-09 .021	1.356E-09 .019	1.299E-09 .021	1.222E-09 .019
2	1.000E+01	1.043E-09 .020	1.033E-09 .022	1.032E-09 .020	1.052E-09 .022	1.000E-09 .021
3	8.000E+00	9.369E-10 .021	8.679E-10 .019	9.040E-10 .021	8.920E-10 .020	8.458E-10 .021
4	7.000E+00	8.308E-10 .021	7.620E-10 .021	7.945E-10 .021	7.893E-10 .023	7.663E-10 .022
5	6.000E+00	7.210E-10 .020	7.135E-10 .021	7.044E-10 .019	6.979E-10 .021	6.861E-10 .021
6	5.000E+00	6.259E-10 .021	5.869E-10 .020	6.427E-10 .021	6.140E-10 .020	5.755E-10 .021
7	4.000E+00	5.112E-10 .022	4.966E-10 .022	5.368E-10 .020	4.879E-10 .022	4.856E-10 .021
8	3.000E+00	4.491E-10 .021	4.321E-10 .021	4.262E-10 .020	4.213E-10 .023	4.084E-10 .022
9	2.500E+00	3.670E-10 .023	3.607E-10 .022	3.675E-10 .020	3.844E-10 .021	3.491E-10 .023
10	2.000E+00	3.104E-10 .023	3.024E-10 .022	3.160E-10 .021	3.143E-10 .022	2.853E-10 .021
11	1.500E+00	2.448E-10 .023	2.260E-10 .022	2.338E-10 .021	2.375E-10 .021	2.266E-10 .023
12	1.000E+00	1.692E-10 .023	1.591E-10 .023	1.689E-10 .023	1.668E-10 .022	1.537E-10 .025
13	7.000E-01	1.129E-10 .022	1.120E-10 .024	1.173E-10 .022	1.100E-10 .022	1.049E-10 .024
14	4.500E-01	7.248E-11 .026	6.719E-11 .028	7.699E-11 .023	7.019E-11 .027	6.715E-11 .026
15	3.000E-01	4.334E-11 .023	4.339E-11 .022	4.274E-11 .020	4.321E-11 .022	4.115E-11 .021
16	1.500E-01	2.182E-11 .022	2.133E-11 .021	2.145E-11 .021	2.133E-11 .022	2.144E-11 .019
17	1.000E-01	1.612E-11 .021	1.563E-11 .022	1.549E-11 .020	1.499E-11 .022	1.581E-11 .019
18	7.000E-02	1.403E-11 .020	1.270E-11 .019	1.216E-11 .021	1.164E-11 .020	1.368E-11 .022
19	4.500E-02	1.223E-11 .025	9.368E-12 .030	1.041E-11 .031	8.631E-12 .031	1.027E-11 .028
20	3.000E-02	5.736E-12 .057	2.975E-12 .085	4.533E-12 .067	2.171E-12 .110	3.930E-12 .075
21	2.000E-02	0.000E-01 .000	0.000E-01 .000	4.168E-13 .413	0.000E-01 .000	0.000E-01 .000

Table A-10. 2 PI (back) integrated adjoint leakage gamma ray fluence (rads / g/cm**2) (FSD)

Energy Group	Upper Energy (MeV)	Complex Mid-Head		Complex Mid-Thorax		Complex Marrow		Simple Mid-Head		Simple Mid-Thorax	
1	1.400E+01	1.336E-09	.021	1.261E-09	.023	1.312E-09	.019	1.321E-09	.021	1.223E-09	.023
2	1.000E+01	1.047E-09	.019	9.916E-10	.021	9.670E-10	.021	9.944E-10	.021	9.741E-10	.021
3	8.000E+00	8.799E-10	.020	8.536E-10	.022	8.926E-10	.020	8.883E-10	.024	8.531E-10	.020
4	7.000E+00	8.218E-10	.022	7.770E-10	.021	8.157E-10	.019	8.250E-10	.019	7.682E-10	.021
5	6.000E+00	7.249E-10	.020	6.645E-10	.020	7.116E-10	.019	6.922E-10	.021	6.730E-10	.019
6	5.000E+00	6.269E-10	.023	5.743E-10	.024	6.022E-10	.019	6.262E-10	.019	5.747E-10	.022
7	4.000E+00	5.362E-10	.021	4.995E-10	.021	5.035E-10	.020	5.094E-10	.020	4.813E-10	.020
8	3.000E+00	4.107E-10	.021	3.947E-10	.023	4.142E-10	.021	4.235E-10	.020	4.036E-10	.023
9	2.500E+00	3.671E-10	.021	3.426E-10	.024	3.456E-10	.020	3.654E-10	.023	3.466E-10	.021
10	2.000E+00	3.110E-10	.022	2.750E-10	.022	2.887E-10	.022	3.148E-10	.022	2.809E-10	.023
11	1.500E+00	2.250E-10	.022	2.089E-10	.022	2.169E-10	.021	2.366E-10	.022	2.122E-10	.022
12	1.000E+00	1.638E-10	.023	1.408E-10	.023	1.518E-10	.022	1.603E-10	.022	1.522E-10	.025
13	7.000E-01	1.114E-10	.023	9.846E-11	.025	1.074E-10	.022	1.125E-10	.026	1.045E-10	.023
14	4.500E-01	7.184E-11	.026	6.257E-11	.029	6.292E-11	.024	7.069E-11	.026	6.546E-11	.027
15	3.000E-01	4.042E-11	.022	3.729E-11	.024	3.983E-11	.021	4.171E-11	.022	3.751E-11	.024
16	1.500E-01	2.091E-11	.021	1.853E-11	.021	2.033E-11	.019	2.108E-11	.022	2.043E-11	.020
17	1.000E-01	1.512E-11	.023	1.417E-11	.023	1.343E-11	.022	1.459E-11	.021	1.459E-11	.023
18	7.000E-02	1.323E-11	.022	1.107E-11	.022	1.096E-11	.020	1.170E-11	.022	1.206E-11	.020
19	4.500E-02	1.224E-11	.026	8.461E-12	.033	8.417E-12	.029	8.456E-12	.034	8.958E-12	.031
20	3.000E-02	4.365E-12	.068	2.661E-12	.098	4.259E-12	.058	1.854E-12	.103	3.107E-12	.076
21	2.000E-02	0.000E-01	.000	0.000E-01	.000	1.656E-13	.496	0.000E-01	.000	0.000E-01	.000

Table A-11. 4 PI integrated adjoint leakage gamma ray fluence (rads / g/cm**2) (FSD)

Energy Group	Upper Energy (MeV)	Complex Mid-Head	Complex Mid-Thorax	Complex Marrow	Simple Mid-Head	Simple Mid-Thorax
1	1.400E+01	2.704E-09 .014	2.532E-09 .015	2.669E-09 .013	2.620E-09 .014	2.445E-09 .015
2	1.000E+01	2.090E-09 .014	2.024E-09 .016	1.999E-09 .015	2.047E-09 .015	1.975E-09 .015
3	8.000E+00	1.817E-09 .015	1.722E-09 .015	1.797E-09 .014	1.780E-09 .016	1.699E-09 .014
4	7.000E+00	1.653E-09 .014	1.539E-09 .015	1.610E-09 .014	1.614E-09 .014	1.535E-09 .015
5	6.000E+00	1.446E-09 .015	1.378E-09 .014	1.416E-09 .013	1.390E-09 .015	1.359E-09 .014
6	5.000E+00	1.253E-09 .015	1.161E-09 .015	1.245E-09 .013	1.240E-09 .014	1.150E-09 .015
7	4.000E+00	1.047E-09 .015	9.961E-10 .015	1.040E-09 .015	9.973E-10 .015	9.669E-10 .014
8	3.000E+00	8.598E-10 .015	8.268E-10 .015	8.404E-10 .014	8.448E-10 .015	8.120E-10 .016
9	2.500E+00	7.341E-10 .016	7.034E-10 .016	7.130E-10 .014	7.498E-10 .015	6.958E-10 .015
10	2.000E+00	6.214E-10 .014	5.774E-10 .015	6.047E-10 .015	6.292E-10 .014	5.663E-10 .015
11	1.500E+00	4.697E-10 .017	4.349E-10 .015	4.507E-10 .015	4.740E-10 .016	4.388E-10 .016
12	1.000E+00	3.330E-10 .016	2.998E-10 .016	3.207E-10 .016	3.271E-10 .016	3.059E-10 .017
13	7.000E-01	2.243E-10 .016	2.104E-10 .018	2.247E-10 .015	2.225E-10 .018	2.094E-10 .017
14	4.500E-01	1.443E-10 .018	1.298E-10 .020	1.399E-10 .016	1.409E-10 .018	1.326E-10 .019
15	3.000E-01	8.377E-11 .015	8.068E-11 .015	8.257E-11 .015	8.492E-11 .016	7.866E-11 .015
16	1.500E-01	4.273E-11 .015	3.986E-11 .015	4.178E-11 .014	4.241E-11 .015	4.186E-11 .013
17	1.000E-01	3.124E-11 .016	2.980E-11 .015	2.891E-11 .015	2.957E-11 .016	3.039E-11 .016
18	7.000E-02	2.726E-11 .015	2.377E-11 .015	2.311E-11 .014	2.334E-11 .015	2.574E-11 .015
19	4.500E-02	2.447E-11 .017	1.783E-11 .022	1.882E-11 .021	1.709E-11 .022	1.923E-11 .020
20	3.000E-02	1.010E-11 .043	5.635E-12 .065	8.791E-12 .045	4.025E-12 .077	7.036E-12 .053
21	2.000E-02	0.000E-01 .000	0.000E-01 .000	5.824E-13 .328	0.000E-01 .000	0.000E-01 .000

Table A-12. 4 PI integrated adjoint leakage gamma ray fluence by marrow region (rads / g/cm**2) (FSD)

Energy Group	Upper Energy (MeV)	Skull	Clavicles	Scapulae	Upper Limbs	Ribs
1	1.400E+01	2.703E-09 .035	2.691E-09 .029	2.625E-09 .032	2.772E-09 .033	2.770E-09 .031
2	1.000E+01	2.107E-09 .033	2.062E-09 .033	2.017E-09 .033	2.016E-09 .031	1.890E-09 .035
3	8.000E+00	1.896E-09 .030	1.875E-09 .034	1.723E-09 .029	1.728E-09 .030	1.752E-09 .034
4	7.000E+00	1.643E-09 .032	1.622E-09 .031	1.642E-09 .032	1.602E-09 .032	1.521E-09 .033
5	6.000E+00	1.497E-09 .030	1.440E-09 .031	1 403E-09 .032	1.438E-09 .031	1.375E-09 .035
6	5.000E+00	1.284E-09 .031	1.231E-09 .031	1.201E-09 .031	1.278E-09 .030	1.262E-09 .031
7	4.000E+00	1.113E-09 .032	1.045E-09 .032	1.034E-09 .033	1.055E-09 .033	1.012E-09 .030
8	3.000E+00	8.533E-10 .033	8.251E-10 .034	8.560E-10 .034	8.578E-10 .033	8.367E-10 .035
9	2.500E+00	7.368E-10 .036	7.388E-10 .035	7.048E-10 .032	7.010E-10 .035	7.482E-10 .033
10	2.000E+00	6.301E-10 .034	6.122E-10 .032	6.368E-10 .031	5.963E-10 .034	5.670E-10 .033
11	1.500E+00	4.627E-10 .034	4.361E-10 .032	4.282E-10 .036	4.462E-10 .036	4.468E-10 .036
12	1.000E+00	3.434E-10 .036	3.310E-10 .038	3.288E-10 .038	3.335E-10 .035	3.095E-10 .038
13	7.000E-01	2.388E-10 .037	2.173E-10 .039	2.253E-10 .040	2.172E-10 .038	2.234E-10 .040
14	4.500E-01	1.439E-10 .037	1.381E-10 .038	1.431E-10 .038	1.496E-10 .037	1.431E-10 .039
15	3.000E-01	9.083E-11 .035	8.432E-11 .033	8.773E-11 .035	8.313E-11 .033	8.324E-11 .033
16	1.500E-01	4.449E-11 .032	4.516E-11 .034	4.349E-11 .035	4.198E-11 .036	3.982E-11 .034
17	1.000E-01	3.195E-11 .034	3.163E-11 .034	3.003E-11 .036	3.024E-11 .037	2.907E-11 .035
18	7.000E-02	2.728E-11 .028	2.540E-11 .031	2.574E-11 .032	2.554E-11 .034	2.451E-11 .035
19	4.500E-02	2.708E-11 .041	2.312E-11 .043	1.939E-11 .047	2.098E-11 .049	2.006E-11 .049
20	3.000E-02	1.991E-11 .073	1.520E-11 .084	9.988E-12 .107	1.138E-11 .105	6.641E-12 .129
21	2.000E-02	1.519E-12 .496	0.000E-01 .000	0.000E-01 .000	3.797E-13 ****	0.000E-01 .000

Table A-12. 4 PI integrated adjoint leakage gamma ray fluence by marrow region (RADS / g/cm**2) (FSD)

Energy Group	Upper Energy (MeV)	Vertebrae	Pelvis	Upper Femur	Lower Limbs	Average
1	1.400E+01	2.682E-09 .030	2.671E-09 .034	2.571E-09 .035	2.523E-09 .034	2.669E-09 .013
2	1.000E+01	1.908E-09 .036	2.029E-09 .034	2.110E-09 .034	2.081E-09 .033	1.999E-09 .015
3	8.000E+00	1.777E-09 .033	1.811E-09 .031	1.733E-09 .032	1.883E-09 .035	1.797E-09 .014
4	7.000E+00	1.631E-09 .034	1.519E-09 .034	1.585E-09 .034	1.672E-09 .032	1.610E-09 .014
5	6.000E+00	1.373E-09 .031	1.402E-09 .033	1.456E-09 .034	1.452E-09 .034	1.416E-09 .013
6	5.000E+00	1.204E-09 .031	1.213E-09 .033	1.222E-09 .034	1.333E-09 .032	1.245E-09 .013
7	4.000E+00	1.022E-09 .035	9.925E-10 .037	9.913E-10 .035	1.099E-09 .032	1.040E-09 .015
8	3.000E+00	8.266E-10 .032	8.120E-10 .032	8.411E-10 .034	8.733E-10 .032	8.404E-10 .014
9	2.500E+00	6.813E-10 .033	7.319E-10 .031	7.493E-10 .035	7.315E-10 .032	7.130E-10 .014
10	2.000E+00	6.146E-10 .035	5.798E-10 .036	5.698E-10 .037	6.164E-10 .038	6.047E-10 .015
11	1.500E+00	4.594E-10 .035	4.208E-10 .034	4.133E-10 .036	4.804E-10 .034	4.507E-10 .015
12	1.000E+00	3.108E-10 .038	3.099E-10 .041	3.265E-10 .035	3.247E-10 .035	3.207E-10 .016
13	7.000E-01	2.216E-10 .036	2.204E-10 .038	2.159E-10 .034	2.372E-10 .036	2.247E-10 .015
14	4.500E-01	1.307E-10 .041	1.370E-10 .040	1.372E-10 .039	1.525E-10 .035	1.399E-10 .016
15	3.000E-01	7.688E-11 .036	7.840E-11 .037	8.607E-11 .035	8.983E-11 .032	8.257E-11 .015
16	1.500E-01	4.010E-11 .034	4.214E-11 .034	4.229E-11 .035	4.319E-11 .033	4.178E-11 .014
17	1.000E-01	2.677E-11 .037	2.857E-11 .035	3.017E-11 .035	2.970E-11 .034	2.891E-11 .015
18	7.000E-02	2.029E-11 .038	2.178E-11 .035	2.252E-11 .037	2.455E-11 .032	2.311E-11 .014
19	4.500E-02	1.495E-11 .062	1.577E-11 .052	1.936E-11 .049	2.141E-11 .048	1.882E-11 .021
20	3.000E-02	5.644E-12 .148	6.203E-12 .127	6.099E-12 .146	9.330E-12 .108	8.791E-12 .045
21	2.000E-02	3.797E-13 ****	1.898E-12 .443	0.000E-01 .000	0.000E-01 .000	5.824E-13 .328

Table A-13. ER1 scalar neutron fluence (n/cm**2 / kw-min) at 100 cm from core centerline (FSD)

Energy Group	Upper Energy (MeV)	Free Field	Complex Mid-Head	Complex Mid-Thorax	Complex Marrow	Simple Mid-Head	Simple Mid-Thorax
1	1.960E+01	1.808E+04	1.127E+04 .11	1.103E+04 .11	1.413E+04 .10	1.289E+04 .12	1.073E+04 .13
2	1.690E+01	8.108E+04	5.414E+04 .11	6.153E+04 .11	5.927E+04 .12	6.006E+04 .11	5.814E+04 .11
3	1.490E+01	7.538E+04	4.922E+04 .12	4.779E+04 .13	5.069E+04 .12	5.483E+04 .12	5.018E+04 .13
4	1.420E+01	5.365E+04	2.811E+04 .12	3.372E+04 .13	2.695E+04 .13	2.908E+04 .12	3.206E+04 .12
5	1.380E+01	3.111E+05	2.005E+05 .13	1.714E+05 .13	1.936E+05 .11	2.185E+05 .12	2.290E+05 .11
6	1.280E+01	2.737E+05	1.630E+05 .12	1.967E+05 .13	2.068E+05 .10	1.804E+05 .12	2.102E+05 .12
7	1.220E+01	1.101E+06	8.347E+05 .11	8.005E+05 .11	7.530E+05 .12	8.146E+05 .11	8.070E+05 .11
8	1.110E+01	2.354E+06	1.470E+06 .12	1.616E+06 .12	1.539E+06 .12	1.414E+06 .12	1.383E+06 .13
9	1.000E+01	4.390E+06	3.039E+06 .13	2.451E+06 .13	2.470E+06 .11	2.565E+06 .12	2.449E+06 .13
10	9.050E+00	7.210E+06	3.928E+06 .13	4.656E+06 .12	4.748E+06 .11	4.693E+06 .12	3.828E+0.12
11	8.190E+00	1.159E+07	8.710E+06 .11	7.335E+06 .12	7.612E+06 .12	7.964E+06 .12	7.072E+06 .12
12	7.410E+00	2.881E+07	2.035E+07 .11	1.981E+07 .11	1.666E+07 .11	2.054E+07 .11	1.987E+07 .11
13	6.380E+00	8.765E+07	4.816E+07 .12	5.332E+07 .10	5.903E+07 .11	5.079E+07 .11	5.373E+07 .11
14	4.970E+00	2.240E+07	1.383E+07 .12	1.499E+07 .10	1.533E+07 .10	1.254E+07 .11	1.297E+07 .11
15	4.720E+00	7.700E+07	4.304E+07 .11	4.874E+07 .12	4.293E+07 .10	4.468E+07 .11	4.621E+07 .10
16	4.070E+00	2.045E+08	1.517E+08 .10	1.012E+08 .12	1.298E+08 .09	9.369E+07 .11	1.091E+08 .11
17	3.010E+00	2.510E+08	1.514E+08 .09	1.282E+08 .11	1.492E+08 .09	1.405E+08 .10	1.252E+08 .11
18	2.390E+00	4.268E+07	2.411E+07 .10	2.308E+07 .10	3.221E+07 .09	2.260E+07 .10	2.164E+07 .09
19	2.310E+00	2.781E+08	1.483E+08 .09	1.617E+08 .10	1.786E+08 .09	1.465E+08 .10	1.324E+08 .10
20	1.830E+00	5.864E+08	3.321E+08 .09	3.422E+08 .09	3.661E+08 .08	2.950E+08 .09	3.259E+08 .10
21	1.110E+00	6.955E+08	3.876E+08 .09	3.341E+08 .10	4.423E+08 .07	3.880E+08 .09	3.716E+08 .10
22	5.500E-01	5.733E+08	4.734E+08 .09	3.869E+08 .10	5.168E+08 .08	3.719E+08 .10	3.192E+08 .10
23	1.580E-01	1.188E+08	7.773E+07 .09	8.969E+07 .09	1.112E+08 .07	8.945E+07 .08	7.390E+07 .09
24	1.110E-01	1.658E+08	1.536E+08 .11	1.452E+08 .10	2.045E+08 .10	1.271E+08 .10	1.538E+08 .10
25	5.250E-02	1.216E+08	1.395E+08 .11	1.349E+08 .11	1.766E+08 .09	1.231E+08 .10	1.312E+08 .12
26	2.480E-02	2.222E+07	2.133E+07 .10	2.025E+07 .11	2.518E+07 .10	2.024E+07 .11	1.689E+07 .11
27	2.190E-02	1.148E+08	1.020E+08 .13	1.232E+08 .13	1.502E+08 .11	1.057E+08 .13	1.282E+08 .13
28	1.030E-02	1.576E+08	1.763E+08 .13	1.510E+08 .12	2.123E+08 .10	1.815E+08 .15	1.462E+08 .13
29	3.350E-03	1.350E+08	1.064E+08 .09	1.906E+08 .15	2.107E+08 .12	1.541E+08 .15	1.372E+08 .13
30	1.230E-03	9.848E+07	9.790E+07 .13	1.148E+08 .12	1.426E+08 .09	1.367E+08 .11	1.374E+08 .17
31	5.830E-04	2.130E+08	2.359E+08 .09	3.071E+08 .10	3.410E+08 .07	2.743E+08 .08	2.781E+08 .13
32	1.010E-04	1.315E+08	1.909E+08 .09	2.237E+08 .11	2.581E+08 .11	2.039E+08 .10	1.939E+08 .12
33	2.900E-05	8.390E+07	1.798E+08 .11	1.478E+08 .10	2.133E+08 .13	1.621E+08 .11	1.561E+08 .12
34	1.070E-05	7.532E+07	1.391E+08 .08	2.437E+08 .12	2.312E+08 .08	1.849E+08 .11	2.445E+08 .15
35	3.060E-06	3.676E+07	1.734E+08 .14	1.544E+08 .12	1.745E+08 .08	1.582E+08 .11	1.428E+08 .11
36	1.130E-06	2.125E+07	1.399E+08 .09	1.632E+08 .09	2.295E+08 .14	1.771E+08 .12	1.551E+08 .12
37	4.140E-07	4.633E+07	4.710E+09 .03	7.161E+09 .03	4.262E+09 .04	5.363E+09 .04	7.021E+09 .03

Table A-14. ER1 scalar neutron fluence by marrow region
(n/cm**2 / kw-min) at 100 cm from core centerline (FSD)

Energy Group	Upper Energy (MeV)	Free Field	Skull	Clavicles	Scapulae	Upper Limbs	Ribs
1	1.960E+01	1.808E+04	1.341E+04 .23	2.080E+04 .20	9.079E+03 .27	2.018E+04 .22	1.037E+04 .27
2	1.690E+01	8.108E+04	5.486E+04 .27	4.023E+04 .29	6.440E+04 .25	7.175E+04 .25	4.597E+04 .30
3	1.490E+01	7.538E+04	2.655E+04 .30	4.939E+04 .29	3.681E+04 .30	4.283E+04 .31	4.259E+04 .26
4	1.420E+01	5.365E+04	2.572E+04 .28	3.049E+04 .27	3.661E+04 .25	3.459E+04 .29	3.767E+04 .26
5	1.380E+01	3.111E+05	2.575E+05 .26	2.459E+05 .24	3.091E+05 .21	2.302E+05 .25	2.643E+05 .24
6	1.280E+01	2.737E+05	1.948E+05 .25	9.325E+04 .31	2.076E+05 .23	2.494E+05 .24	3.318E+05 .21
7	1.220E+01	1.101E+06	4.885E+05 .30	8.785E+05 .24	6.300E+05 .27	6.812E+05 .27	5.011E+05 .26
8	1.110E+01	2.354E+06	1.394E+06 .26	1.710E+06 .25	1.321E+06 .28	1.028E+06 .30	2.141E+06 .23
9	1.000E+01	4.390E+06	1.482E+06 .32	2.617E+06 .26	2.424E+06 .26	1.822E+06 .29	2.268E+06 .28
10	9.050E+00	7.210E+06	2.417E+06 .31	6.026E+06 .23	6.430E+06 .24	5.739E+06 .24	3.678E+06 .27
11	8.190E+00	1.159E+07	7.318E+06 .26	7.305E+06 .26	7.038E+06 .27	6.361E+06 .33	7.141E+06 .27
12	7.410E+00	2.881E+07	1.626E+07 .27	1.412E+07 .33	1.000E+07 .34	2.285E+07 .24	1.647E+07 .26
13	6.380E+00	8.765E+07	5.295E+07 .26	7.028E+07 .24	7.274E+07 .23	5.599E+07 .25	3.247E+07 .26
14	4.970E+00	2.240E+07	1.226E+07 .26	1.507E+07 .23	1.039E+07 .26	1.686E+07 .25	1.709E+07 .21
15	4.720E+00	7.700E+07	3.406E+07 .28	3.781E+07 .24	4.198E+07 .24	3.849E+07 .24	3.664E+07 .24
16	4.070E+00	2.045E+08	1.297E+08 .21	2.202E+08 .19	1.037E+08 .23	1.708E+08 .19	1.457E+08 .21
17	3.010E+00	2.510E+08	9.106E+07 .24	1.673E+08 .20	1.213E+08 .25	1.635E+08 .21	1.696E+08 .20
18	2.390E+00	4.268E+07	2.381E+07 .20	2.514E+07 .22	2.274E+07 .24	2.513E+07 .21	2.762E+07 .19
19	2.310E+00	2.781E+08	1.197E+08 .24	1.774E+08 .22	1.780E+08 .21	1.298E+08 .24	1.283E+08 .22
20	1.830E+00	5.864E+08	2.385E+08 .23	3.353E+08 .20	4.618E+08 .20	2.277E+08 .23	4.126E+08 .18
21	1.110E+00	6.955E+08	2.924E+08 .22	3.910E+08 .20	3.555E+08 .22	3.603E+08 .20	5.650E+08 .16
22	5.500E-01	5.733E+08	3.999E+08 .22	4.919E+08 .18	3.996E+08 .20	5.794E+08 .19	4.847E+08 .17
23	1.580E-01	1.188E+08	8.217E+07 .23	1.303E+08 .17	7.886E+07 .17	9.233E+07 .18	9.527E+07 .17
24	1.110E-01	1.658E+08	1.030E+08 .16	1.459E+08 .21	1.712E+08 .22	1.516E+08 .27	1.700E+08 .17
25	5.250E-02	1.216E+08	1.022E+08 .19	1.600E+08 .20	1.111E+08 .21	1.220E+08 .18	2.049E+08 .22
26	2.480E-02	2.222E+07	1.447E+07 .27	1.825E+07 .25	2.145E+07 .27	2.069E+07 .20	2.263E+07 .15
27	2.190E-02	1.148E+08	4.816E+07 .19	1.672E+08 .33	1.334E+08 .24	1.154E+08 .25	6.515E+07 .19
28	1.030E-02	1.576E+08	1.703E+08 .32	2.087E+08 .31	2.517E+08 .30	3.203E+08 .34	2.088E+08 .23
29	3.350E-03	1.350E+08	7.493E+07 .21	8.614E+07 .20	1.681E+08 .19	1.736E+08 .22	2.916E+08 .28
30	1.230E-03	9.848E+07	6.399E+07 .22	7.947E+07 .21	1.429E+08 .28	1.028E+08 .19	1.947E+08 .33
31	5.830E-04	2.130E+08	2.268E+08 .28	2.196E+08 .15	2.769E+08 .15	2.989E+08 .18	3.428E+08 .18
32	1.010E-04	1.315E+08	1.476E+08 .21	1.480E+08 .17	1.731E+08 .17	1.611E+08 .26	1.687E+08 .16
33	2.900E-05	8.390E+07	9.373E+07 .16	1.434E+08 .21	2.177E+08 .23	1.399E+08 .26	2.171E+08 .23
34	1.070E-05	7.532E+07	1.114E+08 .16	1.584E+08 .14	1.983E+08 .32	1.536E+08 .18	2.833E+08 .19
35	3.060E-06	3.676E+07	1.082E+08 .18	1.637E+08 .30	1.825E+08 .17	1.258E+08 .16	2.650E+08 .25
36	1.130E-06	2.125E+07	1.314E+08 .27	1.262E+08 .20	1.356E+08 .16	1.550E+08 .17	1.848E+08 .19
37	4.140E-07	4.633E+07	1.702E+09 .13	3.262E+09 .09	3.064E+09 .09	3.196E+09 .10	4.556E+09 .08

Table A-14. ER1 scalar neutron fluence by marrow region
(n/cm**2 / kw-min) at 100 cm from core centerline (FSD)

Energy Group	Upper Energy (MeV)	Free Field	Vertebrae	Pelvis	Upper Femur	Lower Limbs	Average
1	1.960E+01	1.808E+04	1.400E+04 .22	1.601E+04 .23	1.423E+04 .22	1.057E+04 .26	1.414E+04 .10
2	1.690E+01	8.108E+04	6.939E+04 .25	6.932E+04 .23	4.372E+04 .25	3.015E+04 .35	5.927E+04 .12
3	1.490E+01	7.538E+04	6.177E+04 .25	7.390E+04 .23	5.869E+04 .23	3.153E+04 .32	5.069E+04 .12
4	1.420E+01	5.365E+04	2.683E+04 .34	1.988E+04 .29	3.548E+04 .24	1.570E+04 .36	2.695E+04 .13
5	1.380E+01	3.111E+05	1.397E+05 .35	2.169E+05 .24	2.575E+05 .23	1.167E+05 .35	1.936E+05 .11
6	1.280E+01	2.737E+05	2.178E+05 .23	1.962E+05 .26	2.094E+05 .23	1.055E+05 .31	2.068E+05 .10
7	1.220E+01	1.101E+06	9.851E+05 .23	8.545E+05 .26	8.901E+05 .26	4.386E+05 .33	7.529E+05 .12
8	1.110E+01	2.354E+06	1.776E+06 .27	2.098E+06 .22	1.684E+06 .25	6.867E+05 .36	1.539E+06 .12
9	1.000E+01	4.390E+06	2.871E+06 .24	3.784E+06 .23	3.893E+06 .22	9.875E+05 .29	2.470E+06 .11
10	9.050E+00	7.210E+06	5.579E+06 .23	4.915E+06 .24	3.934E+06 .27	3.863E+06 .29	4.746E+06 .11
11	8.190E+00	1.159E+07	9.079E+06 .24	1.053E+07 .21	9.157E+06 .22	2.158E+06 .35	7.613E+06 .12
12	7.410E+00	2.881E+07	1.789E+07 .26	1.824E+07 .25	2.243E+07 .22	5.958E+06 .41	1.666E+07 .11
13	6.380E+00	8.765E+07	6.819E+07 .23	8.125E+07 .20	6.717E+07 .21	2.644E+07 .36	5.905E+07 .11
14	4.970E+00	2.240E+07	1.751E+07 .22	2.205E+07 .19	1.651E+07 .25	4.539E+06 .29	1.533E+07 .10
15	4.720E+00	7.700E+07	3.804E+07 .23	8.327E+07 .20	6.536E+07 .20	1.949E+07 .34	4.292E+07 .10
16	4.070E+00	2.045E+08	1.273E+08 .20	1.569E+08 .20	1.462E+08 .20	5.924E+07 .31	1.298E+08 .09
17	3.010E+00	2.510E+08	1.783E+08 .19	1.770E+08 .18	1.734E+08 .18	6.990E+07 .28	1.492E+08 .09
18	2.390E+00	4.268E+07	4.239E+07 .17	4.615E+07 .17	3.078E+07 .20	1.280E+07 .28	3.221E+07 .09
19	2.310E+00	2.781E+08	1.941E+08 .19	3.092E+08 .16	2.969E+08 .18	7.127E+07 .29	1.786E+08 .09
20	1.830E+00	5.864E+08	3.791E+08 .19	6.888E+08 .15	5.004E+08 .15	1.365E+08 .27	3.661E+08 .08
21	1.110E+00	6.955E+08	4.358E+08 .17	7.206E+08 .15	6.973E+08 .15	2.295E+08 .24	4.425E+08 .07
22	5.500E-01	5.733E+08	6.238E+08 .15	6.529E+08 .14	5.161E+08 .15	2.087E+08 .34	5.169E+08 .08
23	1.580E-01	1.188E+08	1.135E+08 .15	1.744E+08 .14	1.877E+08 .14	6.266E+07 .25	1.112E+08 .07
24	1.110E-01	1.658E+08	2.928E+08 .19	2.621E+08 .16	2.036E+08 .16	9.014E+07 .32	2.045E+08 .10
25	5.250E-02	1.216E+08	2.307E+08 .18	2.385E+08 .14	2.142E+08 .15	8.098E+07 .36	1.766E+08 .09
26	2.480E-02	2.222E+07	3.620E+07 .18	2.859E+07 .13	3.021E+07 .17	7.493E+06 .18	2.518E+07 .10
27	2.190E-02	1.148E+08	1.891E+08 .23	2.829E+08 .21	1.987E+08 .20	6.002E+07 .24	1.502E+08 .11
28	1.030E-02	1.576E+08	2.241E+08 .17	2.236E+08 .15	2.760E+08 .16	6.580E+07 .20	2.123E+08 .10
29	3.350E-03	1.350E+08	2.447E+08 .28	3.124E+08 .15	2.263E+08 .12	1.457E+08 .37	2.107E+08 .12
30	1.230E-03	9.848E+07	1.834E+08 .19	1.919E+08 .13	1.381E+08 .14	7.523E+07 .23	1.426E+08 .09
31	5.830E-04	2.130E+08	3.931E+08 .14	4.891E+08 .13	4.847E+08 .17	1.519E+08 .30	3.410E+08 .07
32	1.010E-04	1.315E+08	3.671E+08 .22	3.634E+08 .12	3.049E+08 .19	1.140E+08 .17	2.581E+08 .11
33	2.900E-05	8.390E+07	2.921E+08 .27	2.781E+08 .12	1.984E+08 .11	1.276E+08 .25	2.133E+08 .13
34	1.070E-05	7.532E+07	2.852E+08 .17	3.177E+08 .16	2.801E+08 .13	1.466E+08 .22	2.312E+08 .08
35	3.060E-06	3.676E+07	2.185E+08 .16	1.774E+08 .14	2.077E+08 .16	9.988E+07 .21	1.745E+08 .08
36	1.130E-06	2.125E+07	3.130E+08 .28	2.555E+08 .13	2.500E+08 .12	1.890E+08 .38	2.295E+08 .14
37	4.140E-07	4.633E+07	6.289E+09 .08	5.090E+09 .09	4.167E+09 .09	1.812E+09 .11	4.263E+09 .04

Table A-15. ER1 scalar neutron-gamma ray fluence (g/cm**2 / kw-min) at 100 cm from core centerline (FSD)

Energy Group	Upper Energy (MeV)	Free Field	Complex Mid-Head		Complex Mid-Thorax		Complex Marrow		Simple Mid-Head		Simple Mid-Thorax	
1	1.400E+01	1.502E+04	8.094E+04	.80	6.703E+02	***	5.138E+02	.78	3.141E+05	.98	6.433E+04	.96
2	1.000E+01	7.308E+06	4.874E+03	.53	6.563E+03	.51	8.532E+04	.90	3.332E+03	.64	2.540E+03	.78
3	8.000E+00	1.979E+07	1.664E+06	.75	4.180E+06	.46	1.186E+07	.43	1.520E+05	.87	1.150E+05	.21
4	7.000E+00	1.947E+07	5.421E+06	.40	8.716E+06	.27	7.277E+06	.39	6.368E+06	.85	3.386E+06	.51
5	6.000E+00	3.153E+07	1.390E+06	.50	7.171E+06	.44	2.044E+06	.50	3.719E+06	.74	8.070E+06	.47
6	5.000E+00	7.633E+07	3.012E+06	.21	6.327E+06	.25	5.845E+06	.18	1.023E+07	.52	2.143E+06	.13
7	4.000E+00	1.820E+08	9.595E+05	.29	4.799E+06	.49	1.937E+06	.57	2.235E+06	.47	1.571E+06	.65
8	3.000E+00	2.061E+08	1.112E+06	.63	5.455E+06	.48	6.156E+06	.50	1.698E+05	.41	2.660E+05	.45
9	2.500E+00	4.739E+08	2.946E+08	.08	6.471E+08	.06	3.123E+08	.06	4.283E+08	.07	6.857E+08	.05
10	2.000E+00	5.193E+08	1.052E+07	.24	1.784E+07	.21	2.010E+07	.25	1.830E+07	.54	2.082E+07	.21
11	1.500E+00	7.007E+08	1.689E+07	.32	1.688E+07	.23	1.423E+07	.28	7.899E+06	.43	2.083E+07	.22
12	1.000E+00	4.023E+08	4.515E+06	.28	1.527E+07	.39	6.361E+06	.27	4.748E+06	.37	1.567E+07	.24
13	7.000E-01	3.134E+08	1.048E+07	.27	2.375E+07	.24	1.137E+07	.24	1.401E+07	.28	1.478E+07	.26
14	4.500E-01	9.542E+07	7.944E+06	.38	4.013E+07	.30	1.496E+07	.26	1.813E+07	.50	3.736E+07	.28
15	3.000E-01	1.241E+08	2.857E+07	.51	4.587E+07	.29	2.559E+07	.23	3.304E+07	.34	3.746E+07	.27
16	1.500E-01	5.936E+07	6.084E+06	.49	1.496E+07	.32	2.810E+06	.52	9.031E+06	.24	1.727E+07	.40
17	1.000E-01	4.972E+07	6.423E+06	.62	9.820E+06	.42	4.768E+06	.35	1.727E+06	.36	6.932E+06	.50
18	7.000E-02	4.633E+07	7.541E+05	.55	4.184E+06	.57	5.657E+05	.50	3.743E+05	.56	5.466E+06	.57
19	4.500E-02	1.646E+07	7.913E+03	.62	1.194E+05	.88	9.181E+04	.59	5.671E+04	.51	6.300E+05	.79
20	3.000E-02	1.429E+06	3.504E+05	***	5.391E+03	.89	7.021E+05	.74	1.344E+04	.82	1.359E+03	.55
21	2.000E-02	1.167E+04	2.331E-03	***	0.000E-01	.00	1.900E+02	.69	3.569E+00	.97	1.104E-01	***

Table A-16. ER1 scalar neutron-gamma fluence by marrow region (g/cm**2 / kw-min) at 100 cm from core centerline (FSD)

Energy Group	Upper Energy (MeV)	Free Field	Skull	Clavicles	Scapulae	Upper Limbs	Ribs
1	1.400E+01	1.502E+04	0.000E-01 .00	7.988E+02 ***	1.302E+04 .79	0.000E-01 .00	0.000E-01 .00
2	1.000E+01	7.308E+06	9.978E+03 ***	6.936E+04 .83	2.075E+06 .95	2.001E+04 .62	2.155E+03 .97
3	8.000E+00	1.979E+07	8.525E+06 .81	1.927E+05 .47	2.010E+05 .38	1.340E+05 .65	1.346E+06 .76
4	7.000E+00	1.947E+07	2.927E+06 .48	3.469E+06 .44	2.083E+06 .70	1.080E+07 .68	4.054E+06 .39
5	6.000E+00	3.153E+07	6.344E+05 .68	1.263E+06 .60	2.267E+06 .56	1.764E+05 .65	1.359E+05 .59
6	5.000E+00	7.633E+07	4.751E+06 .54	3.767E+06 .32	4.044E+06 .30	5.134E+06 .26	4.967E+06 .66
7	4.000E+00	1.820E+08	4.553E+05 .42	4.915E+05 .45	6.853E+05 .55	8.959E+05 .68	8.494E+05 .34
8	3.000E+00	2.061E+08	5.599E+05 .74	2.450E+06 .85	4.269E+06 .93	6.166E+04 .61	8.761E+06 .99
9	2.500E+00	4.739E+08	1.559E+08 .23	2.619E+08 .14	3.149E+08 .15	2.719E+08 .16	3.337E+08 .15
10	2.000E+00	5.193E+08	8.228E+06 .80	2.117E+07 .48	5.455E+06 .36	1.147E+07 .47	3.996E+07 .38
11	1.500E+00	7.007E+08	1.490E+07 .78	1.416E+07 .62	2.280E+06 .44	1.289E+07 .66	5.059E+06 .52
12	1.000E+00	4.023E+08	1.115E+07 .79	6.307E+05 .54	4.450E+06 .62	6.211E+06 .49	1.183E+07 .55
13	7.000E-01	3.134E+08	1.318E+07 .87	1.990E+06 .46	1.970E+07 .51	3.589E+06 .55	8.142E+06 .41
14	4.500E-01	9.542E+07	6.091E+06 .55	2.372E+07 .57	1.545E+07 .57	2.539E+06 .50	2.968E+07 .53
15	3.000E-01	1.241E+08	4.987E+06 .87	3.521E+05 .35	1.914E+07 .57	1.429E+07 .65	9.116E+07 .40
16	1.500E-01	5.936E+07	2.777E+05 .41	1.403E+07 .53	7.568E+06 .99	1.145E+07 .98	4.936E+05 .92
17	1.000E-01	4.972E+07	8.036E+05 .98	2.549E+04 .56	3.069E+06 .99	1.824E+07 .61	1.174E+07 .79
18	7.000E-02	4.633E+07	6.218E+03 .99	2.166E+07 ***	3.333E+05 .62	1.648E+04 .79	2.696E+06 .99
19	4.500E-02	1.646E+07	1.561E+02 .80	2.280E+03 .61	7.995E+03 .71	1.546E+03 .92	4.368E+05 .97
20	3.000E-02	1.429E+06	8.269E+01 .77	1.442E+02 .99	4.129E-01 ***	3.596E+02 .65	7.318E+02 ***
21	2.000E-02	1.167E+04	0.000E-01 .00	0.000E-01 .00	0.000E-01 .00	2.783E-03 ***	6.754E+01 ***

Table A-16. ER1 scalar gamma ray fluence (g/cm**2 / kw-min) at 100 cm from core centerline (FSD)

Energy Group	Upper Energy (MeV)	Free Field	Vertebrae	Pelvis	Upper Femur	Lower Limbs	Average
1	1.400E+01	1.502E+04	2.226E-01 ***	9.978E-02 ***	0.000E-01 .00	0.000E-01 .00	5.136E+02 .78
2	1.000E+01	7.308E+06	3.098E+00 ***	9.950E+02 .93	1.492E+02 .94	5.982E+02 .63	8.530E+04 .90
3	8.000E+00	1.979E+07	2.340E+07 .62	1.429E+07 .62	5.049E+06 .62	6.758E+06 .99	1.187E+07 .43
4	7.000E+00	1.947E+07	7.158E+06 .87	2.091E+07 .65	2.089E+06 .33	5.500E+05 .38	7.277E+06 .39
5	6.000E+00	3.153E+07	2.884E+06 .94	5.387E+06 .70	2.884E+06 .81	3.435E+04 .50	2.044E+06 .50
6	5.000E+00	7.633E+07	7.175E+06 .31	4.464E+06 .30	1.227E+07 .78	3.242E+06 .27	5.846E+06 .18
7	4.000E+00	1.820E+08	3.815E+06 .86	7.356E+05 .30	7.137E+05 .39	2.173E+06 .80	1.937E+06 .57
8	3.000E+00	2.061E+08	1.272E+07 .70	4.457E+06 .84	6.525E+06 .90	9.752E+05 .91	6.155E+06 .50
9	2.500E+00	4.739E+08	3.921E+08 .12	3.500E+08 .18	4.129E+08 .18	1.832E+08 .16	3.123E+08 .06
10	2.000E+00	5.193E+08	3.334E+07 .43	1.915E+07 .41	8.494E+06 .56	6.409E+06 .58	2.010E+07 .25
11	1.500E+00	7.007E+08	1.555E+07 .36	7.346E+06 .50	1.330E+07 .41	2.661E+07 .84	1.423E+07 .28
12	1.000E+00	4.023E+08	3.517E+06 .44	1.459E+07 .65	4.228E+06 .64	1.017E+06 .44	6.361E+06 .27
13	7.000E-01	3.134E+08	2.961E+06 .55	2.505E+07 .40	3.531E+07 .56	1.219E+07 .88	1.137E+07 .24
14	4.500E-01	9.542E+07	2.194E+07 .46	1.590E+07 .46	2.752E+07 .66	1.463E+06 .79	1.496E+07 .26
15	3.000E-01	1.241E+08	1.647E+07 .57	2.391E+07 .63	1.153E+08 .46	4.153E+06 .89	2.559E+07 .23
16	1.500E-01	5.936E+07	1.321E+06 .55	3.160E+05 .77	6.925E+06 .80	1.229E+05 .56	2.811E+06 .52
17	1.000E-01	4.972E+07	2.120E+06 .85	2.514E+06 .76	1.171E+06 .80	3.705E+06 .69	4.769E+06 .35
18	7.000E-02	4.633E+07	7.380E+04 .68	1.445E+06 .89	2.664E+05 .71	2.724E+02 .85	5.658E+05 .50
19	4.500E-02	1.646E+07	1.405E+05 .99	1.265E+05 .74	1.368E+04 .99	2.755E+02 .97	9.182E+04 .59
20	3.000E-02	1.429E+06	5.599E-01 ***	5.442E+06 .74	********* ***	9.513E+02 .95	7.022E+05 .74
21	2.000E-02	1.167E+04	6.939E-01 ***	2.375E-01 ***	2.760E+03 .71	4.310E+00 ***	1.900E+02 .69

Table A-17. ER1 scalar gamma ray fluence (g/cm**2 / kw-min) at 100 cm from core centerline (FSD)

Energy Group	Upper Energy (MeV)	Free Field	Complex Mid-Head	Complex Mid-Thorax	Complex Marrow	Simple Mid-Head	Simple Mid-Thorax
1	1.400E+01	1.502E+04	1.320E+04 .02	1.223E+04 .02	1.302E+04 .02	1.263E+04 .02	1.174E+04 .02
2	1.000E+01	7.308E+06	6.430E+06 .10	7.317E+06 .09	5.991E+06 .09	6.189E+06 .10	7.364E+06 .09
3	8.000E+00	1.979E+07	1.820E+07 .09	1.822E+07 .10	1.483E+07 .09	1.692E+07 .09	1.749E+07 .10
4	7.000E+00	1.947E+07	1.694E+07 .09	1.700E+07 .08	2.102E+07 .08	1.710E+07 .09	1.725E+07 .09
5	6.000E+00	3.153E+07	2.517E+07 .08	2.620E+07 .08	2.457E+07 .08	2.467E+07 .08	2.875E+07 .09
6	5.000E+00	7.633E+07	5.382E+07 .09	7.368E+07 .09	8.383E+07 .08	7.326E+07 .08	6.378E+07 .09
7	4.000E+00	1.820E+08	1.572E+08 .09	1.499E+08 .09	1.565E+08 .09	1.712E+08 .09	1.666E+08 .09
8	3.000E+00	2.061E+08	1.578E+08 .09	1.644E+08 .08	1.566E+08 .08	1.741E+08 .08	1.749E+08 .08
9	2.500E+00	4.739E+08	3.940E+08 .07	4.114E+08 .08	3.657E+08 .07	4.019E+08 .08	3.212E+08 .09
10	2.000E+00	5.193E+08	4.140E+08 .08	4.788E+08 .07	4.337E+08 .08	5.364E+08 .07	4.414E+08 .07
11	1.500E+00	7.007E+08	6.793E+08 .07	6.326E+08 .07	6.274E+08 .06	6.543E+08 .06	6.557E+08 .07
12	1.000E+00	4.023E+08	4.078E+08 .06	3.855E+08 .06	4.417E+08 .06	4.046E+08 .07	4.055E+08 .06
13	7.000E-01	3.134E+08	3.757E+08 .07	4.171E+08 .07	3.779E+08 .07	3.696E+08 .07	3.831E+08 .08
14	4.500E-01	9.542E+07	2.775E+08 .09	2.956E+08 .08	3.103E+08 .08	2.582E+08 .08	3.462E+08 .09
15	3.000E-01	1.241E+08	4.159E+08 .09	5.458E+08 .08	4.313E+08 .09	4.046E+08 .08	6.161E+08 .09
16	1.500E-01	5.936E+07	1.372E+08 .13	2.309E+08 .12	1.705E+08 .09	1.686E+08 .12	2.306E+08 .12
17	1.000E-01	4.972E+07	7.958E+07 .06	1.201E+08 .14	8.449E+07 .06	1.057E+08 .13	1.239E+08 .13
18	7.000E-02	4.633E+07	7.378E+07 .11	9.463E+07 .12	6.147E+07 .05	6.401E+07 .07	9.364E+07 .15
19	4.500E-02	1.646E+07	2.557E+07 .17	2.798E+07 .14	1.580E+07 .04	1.930E+07 .12	2.449E+07 .04
20	3.000E-02	1.429E+06	1.607E+06 .04	1.921E+06 .05	8.590E+05 .03	9.755E+05 .06	2.491E+06 .18
21	2.000E-02	1.167E+04	1.882E+04 .11	3.970E+04 .56	2.993E+03 .16	6.057E+03 .20	1.936E+04 .10

Table A-18. ER1 scalar gamma ray fluence by marrow region (g/cm**2 / kw-min) at 100 cm from core centerline (FSD)

Energy Group	Upper Energy (MeV)	Free Field	Skull	Clavicles	Scapulae	Upper Limbs	Ribs
1	1.400E+01	1.502E+04	1.299E+04 .04	1.309E+04 .03	1.295E+04 .04	1.349E+04 .04	1.372E+04 .04
2	1.000E+01	7.308E+06	3.619E+06 .26	6.213E+06 .22	7.472E+06 .18	5.948E+06 .21	5.892E+06 .22
3	8.000E+00	1.979E+07	2.073E+07 .17	1.410E+07 .21	1.372E+07 .21	1.460E+07 .21	1.347E+07 .21
4	7.000E+00	1.947E+07	1.829E+07 .19	1.701E+07 .19	2.074E+07 .16	2.359E+07 .17	1.969E+07 .18
5	6.000E+00	3.153E+07	2.520E+07 .19	1.660E+07 .23	2.351E+07 .20	2.420E+07 .19	2.740E+07 .20
6	5.000E+00	7.633E+07	9.354E+07 .18	7.085E+07 .18	3.878E+07 .23	6.901E+07 .18	8.302E+07 .16
7	4.000E+00	1.820E+08	1.717E+08 .18	1.434E+08 .20	1.264E+08 .20	1.355E+08 .20	1.514E+08 .21
8	3.000E+00	2.061E+08	1.343E+08 .20	1.745E+08 .20	1.887E+08 .19	1.748E+08 .17	1.595E+08 .19
9	2.500E+00	4.739E+08	3.279E+08 .20	3.768E+08 .18	4.915E+08 .16	3.854E+08 .18	3.880E+08 .17
10	2.000E+00	5.193E+08	3.192E+08 .18	3.569E+08 .19	5.524E+08 .15	4.675E+08 .16	3.774E+08 .17
11	1.500E+00	7.007E+08	3.052E+08 .17	5.203E+08 .16	5.198E+08 .14	6.099E+08 .15	5.581E+08 .15
12	1.000E+00	4.023E+08	4.363E+08 .14	5.241E+08 .12	5.312E+08 .14	4.114E+08 .13	4.594E+08 .13
13	7.000E-01	3.134E+08	2.824E+08 .14	3.660E+08 .15	3.271E+08 .16	3.541E+08 .24	4.307E+08 .17
14	4.500E-01	9.542E+07	2.378E+08 .20	2.432E+08 .22	3.404E+08 .22	3.500E+08 .21	3.366E+08 .19
15	3.000E-01	1.241E+08	2.952E+08 .16	2.155E+08 .12	4.991E+08 .20	3.589E+08 .21	4.517E+08 .18
16	1.500E-01	5.936E+07	9.515E+07 .09	1.145E+08 .21	1.396E+08 .23	2.336E+08 .26	1.661E+08 .26
17	1.000E-01	4.972E+07	7.477E+07 .15	1.507E+08 .36	8.449E+07 .19	6.930E+07 .08	9.595E+07 .18
18	7.000E-02	4.633E+07	5.463E+07 .05	1.256E+08 .31	6.670E+07 .13	7.029E+07 .18	6.524E+07 .06
19	4.500E-02	1.646E+07	1.635E+07 .04	1.713E+07 .07	1.612E+07 .04	1.490E+07 .03	1.680E+07 .07
20	3.000E-02	1.429E+06	1.206E+06 .04	1.290E+06 .05	1.082E+06 .05	1.089E+06 .06	9.335E+05 .04
21	2.000E-02	1.167E+04	5.302E+03 .25	4.022E+03 .34	7.703E+03 .57	4.835E+03 .44	5.406E+03 .39

Table A-18. ER1 scalar gamma ray fluence by marrow region
(g/cm**2 / kw-min) at 100 cm from core centerline (FSD)

Energy Group	Upper Energy (MeV)	Free Field	Vertebrae	Pelvis	Upper Femur	Lower Limbs	Average
1	1.400E+01	1.502E+04	1.308E+04 .04	1.311E+04 .04	1.275E+04 .04	1.226E+04 .04	1.303E+04 .02
2	1.000E+01	7.308E+06	6.566E+06 .22	7.425E+06 .18	7.788E+06 .19	3.847E+06 .26	5.991E+06 .09
3	8.000E+00	1.979E+07	1.334E+07 .21	1.323E+07 .23	1.699E+07 .20	1.537E+07 .21	1.483E+07 .09
4	7.000E+00	1.947E+07	2.269E+07 .17	2.030E+07 .19	2.369E+07 .17	1.703E+07 .18	2.102E+07 .08
5	6.000E+00	3.153E+07	2.296E+07 .21	2.868E+07 .18	3.092E+07 .17	2.058E+07 .22	2.457E+07 .08
6	5.000E+00	7.633E+07	1.051E+08 .17	6.887E+07 .19	7.675E+07 .17	6.892E+07 .19	8.384E+07 .08
7	4.000E+00	1.820E+08	1.699E+08 .20	1.760E+08 .18	1.630E+08 .20	1.198E+08 .21	1.565E+08 .09
8	3.000E+00	2.061E+08	1.630E+08 .18	1.931E+08 .17	1.552E+08 .20	9.609E+07 .23	1.566E+08 .08
9	2.500E+00	4.739E+08	3.846E+08 .17	4.036E+08 .17	3.623E+08 .18	2.483E+08 .19	3.657E+08 .07
10	2.000E+00	5.193E+08	5.274E+08 .16	4.168E+08 .17	3.674E+08 .18	3.090E+08 .18	4.337E+08 .08
11	1.500E+00	7.007E+08	8.024E+08 .13	5.505E+08 .14	7.350E+08 .14	5.609E+08 .15	6.272E+08 .06
12	1.000E+00	4.023E+08	4.508E+08 .13	4.845E+08 .13	4.953E+08 .11	3.438E+08 .16	4.417E+08 .06
13	7.000E-01	3.134E+08	4.184E+08 .14	4.366E+08 .16	4.180E+08 .15	2.903E+08 .18	3.778E+08 .07
14	4.500E-01	9.542E+07	2.779E+08 .17	3.312E+08 .17	4.276E+08 .20	3.163E+08 .24	3.102E+08 .08
15	3.000E-01	1.241E+08	4.977E+08 .19	5.373E+08 .20	4.424E+08 .15	3.176E+08 .21	4.313E+08 .09
16	1.500E-01	5.936E+07	1.493E+08 .18	2.084E+08 .24	2.099E+08 .22	1.844E+08 .21	1.705E+08 .09
17	1.000E-01	4.972E+07	9.826E+07 .14	7.472E+07 .07	7.529E+07 .10	7.732E+07 .09	8.449E+07 .06
18	7.000E-02	4.633E+07	5.864E+07 .07	5.873E+07 .08	8.076E+07 .31	5.222E+07 .04	6.146E+07 .05
19	4.500E-02	1.646E+07	1.646E+07 .11	1.527E+07 .16	1.380E+07 .03	1.541E+07 .04	1.580E+07 .04
20	3.000E-02	1.429E+06	6.062E+05 .06	5.887E+05 .10	1.021E+06 .24	1.049E+06 .12	8.589E+05 .03
21	2.000E-02	1.167E+04	1.091E+03 .45	6.765E+02 .57	3.699E+03 .64	3.459E+03 .43	2.993E+03 .16

Table A-19. ER1 scalar total gamma ray fluence
(g/cm**2 / kw-min) at 100 cm from core centerline (FSD)

Energy Group	Upper Energy (MeV)	Free Field	Complex Mid-Head		Complex Mid-Thorax		Complex Marrow		Simple Mid-Head		Simple Mid-Thorax	
1	1.400E+01	1.502E+04	9.415E+04	.72	1.290E+04	.07	1.354E+04	.04	3.267E+05	.95	7.607E+04	.85
2	1.000E+01	7.308E+06	6.435E+06	.10	7.323E+06	.09	6.076E+06	.09	6.192E+06	.10	7.366E+06	.09
3	8.000E+00	1.979E+07	1.986E+07	.11	2.240E+07	.13	2.669E+07	.23	1.707E+07	.09	1.761E+07	.10
4	7.000E+00	1.947E+07	2.237E+07	.14	2.572E+07	.12	2.830E+07	.14	2.346E+07	.29	2.064E+07	.13
5	6.000E+00	3.153E+07	2.656E+07	.09	3.338E+07	.14	2.661E+07	.09	2.839E+07	.14	3.682E+07	.15
6	5.000E+00	7.633E+07	5.684E+07	.09	8.001E+07	.08	8.967E+07	.08	8.349E+07	.11	6.592E+07	.09
7	4.000E+00	1.820E+08	1.581E+08	.08	1.547E+08	.08	1.585E+08	.09	1.734E+08	.09	1.681E+08	.09
8	3.000E+00	2.061E+08	1.590E+08	.09	1.699E+08	.08	1.628E+08	.08	1.742E+08	.08	1.752E+08	.08
9	2.500E+00	4.739E+08	6.887E+08	.06	1.059E+09	.05	6.779E+08	.05	8.302E+08	.05	1.007E+09	.05
10	2.000E+00	5.193E+08	4.246E+08	.08	4.966E+08	.07	4.538E+08	.07	5.547E+08	.07	4.622E+08	.07
11	1.500E+00	7.007E+08	6.962E+08	.07	6.495E+08	.07	6.416E+08	.06	6.622E+08	.06	6.765E+08	.06
12	1.000E+00	4.023E+08	4.123E+08	.06	4.008E+08	.06	4.480E+08	.06	4.093E+08	.07	4.212E+08	.06
13	7.000E-01	3.134E+08	3.862E+08	.07	4.409E+08	.07	3.892E+08	.07	3.836E+08	.07	3.979E+08	.07
14	4.500E-01	9.542E+07	2.854E+08	.09	3.357E+08	.08	3.252E+08	.07	2.763E+08	.09	3.836E+08	.09
15	3.000E-01	1.241E+08	4.445E+08	.09	5.917E+08	.08	4.569E+08	.08	4.377E+08	.08	6.535E+08	.08
16	1.500E-01	5.936E+07	1.433E+08	.13	2.459E+08	.11	1.733E+08	.09	1.777E+08	.11	2.479E+08	.12
17	1.000E-01	4.972E+07	8.600E+07	.08	1.299E+08	.14	8.925E+07	.06	1.074E+08	.13	1.308E+08	.13
18	7.000E-02	4.633E+07	7.453E+07	.11	9.881E+07	.12	6.203E+07	.05	6.439E+07	.07	9.910E+07	.14
19	4.500E-02	1.646E+07	2.558E+07	.17	2.810E+07	.14	1.589E+07	.04	1.936E+07	.12	2.512E+07	.04
20	3.000E-02	1.429E+06	1.957E+06	.23	1.927E+06	.05	1.561E+06	.39	9.890E+05	.06	2.493E+06	.18
21	2.000E-02	1.167E+04	1.882E+04	.11	3.970E+04	.56	3.183E+03	.16	6.061E+03	.20	1.936E+04	.10

Table A-20. ER1 scalar total gamma fluence by marrow region (g/cm**2 / kw-min) at 100 cm from core centerline (FSD)

Energy Group	Upper Energy (MeV)	Free Field	Skull	Clavicles	Scapulae	Upper Limbs	Ribs
1	1.400E+01	1.502E+04	1.299E+04 .04	1.388E+04 .08	2.598E+04 .46	1.349E+04 .04	1.372E+04 .04
2	1.000E+01	7.308E+06	3.629E+06 .26	6.282E+06 .22	9.547E+06 .29	5.969E+06 .21	5.894E+06 .22
3	8.000E+00	1.979E+07	2.926E+07 .31	1.429E+07 .21	1.392E+07 .21	1.474E+07 .20	1.481E+07 .21
4	7.000E+00	1.947E+07	2.122E+07 .18	2.048E+07 .18	2.282E+07 .17	3.439E+07 .28	2.374E+07 .17
5	6.000E+00	3.153E+07	2.584E+07 .18	1.786E+07 .21	2.578E+07 .18	2.438E+07 .19	2.753E+07 .20
6	5.000E+00	7.633E+07	9.829E+07 .17	7.462E+07 .17	4.282E+07 .20	7.415E+07 .16	8.799E+07 .16
7	4.000E+00	1.820E+08	1.722E+08 .18	1.439E+08 .20	1.271E+08 .20	1.364E+08 .20	1.523E+08 .21
8	3.000E+00	2.061E+08	1.349E+08 .20	1.769E+08 .20	1.930E+08 .19	1.748E+08 .17	1.683E+08 .19
9	2.500E+00	4.739E+08	4.838E+08 .15	6.387E+08 .12	8.065E+08 .11	6.574E+08 .12	7.217E+08 .11
10	2.000E+00	5.193E+08	3.274E+08 .18	3.781E+08 .18	5.578E+08 .15	4.790E+08 .16	4.173E+08 .16
11	1.500E+00	7.007E+08	3.201E+08 .16	5.345E+08 .15	5.221E+08 .14	6.228E+08 .15	5.631E+08 .15
12	1.000E+00	4.023E+08	4.474E+08 .13	5.247E+08 .12	5.356E+08 .14	4.176E+08 .13	4.712E+08 .13
13	7.000E-01	3.134E+08	2.956E+08 .15	3.680E+08 .15	3.468E+08 .15	3.577E+08 .24	4.388E+08 .16
14	4.500E-01	9.542E+07	2.439E+08 .19	2.669E+08 .20	3.559E+08 .21	3.526E+08 .21	3.663E+08 .17
15	3.000E-01	1.241E+08	3.001E+08 .16	2.159E+08 .12	5.182E+08 .19	3.732E+08 .20	5.428E+08 .17
16	1.500E-01	5.936E+07	9.543E+07 .09	1.286E+08 .19	1.472E+08 .22	2.451E+08 .26	1.666E+08 .26
17	1.000E-01	4.972E+07	7.557E+07 .15	1.507E+08 .36	8.756E+07 .19	8.754E+07 .17	1.077E+08 .19
18	7.000E-02	4.633E+07	5.463E+07 .05	1.472E+08 .32	6.704E+07 .13	7.030E+07 .18	6.794E+07 .08
19	4.500E-02	1.646E+07	1.635E+07 .04	1.713E+07 .07	1.613E+07 .04	1.490E+07 .03	1.724E+07 .07
20	3.000E-02	1.429E+06	1.206E+06 .04	1.290E+06 .05	1.082E+06 .05	1.089E+06 .06	9.343E+05 .04
21	2.000E-02	1.167E+04	5.302E+03 .25	4.022E+03 .34	7.703E+03 .57	4.835E+03 .44	5.474E+03 .38

Table A-20. ER1 scalar total gamma fluence by marrow region (g/cm**2 / kw-min) at 100 cm from core centerline (FSD)

Energy Group	Upper Energy (MeV)	Free Field	Vertebrae	Pelvis	Upper Femur	Lower Limbs	Average
1	1.400E+01	1.502E+04	1.308E+04 .04	1.311E+04 .04	1.275E+04 .04	1.226E+04 .04	1.354E+04 .04
2	1.000E+01	7.308E+06	6.566E+06 .22	7.426E+06 .18	7.788E+06 .19	3.848E+06 .26	6.076E+06 .09
3	8.000E+00	1.979E+07	3.673E+07 .44	2.752E+07 .38	2.204E+07 .23	2.213E+07 .40	2.669E+07 .23
4	7.000E+00	1.947E+07	2.984E+07 .29	4.121E+07 .39	2.578E+07 .15	1.758E+07 .17	2.830E+07 .14
5	6.000E+00	3.153E+07	2.584E+07 .22	3.407E+07 .21	3.380E+07 .18	2.061E+07 .22	2.661E+07 .09
6	5.000E+00	7.633E+07	1.123E+08 .16	7.334E+07 .17	8.902E+07 .20	7.216E+07 .18	8.968E+07 .08
7	4.000E+00	1.820E+08	1.737E+08 .20	1.767E+08 .18	1.637E+08 .20	1.219E+08 .20	1.584E+08 .09
8	3.000E+00	2.061E+08	1.757E+08 .18	1.975E+08 .16	1.618E+08 .19	9.707E+07 .23	1.628E+08 .08
9	2.500E+00	4.739E+08	7.767E+08 .10	7.536E+08 .12	7.752E+08 .13	4.315E+08 .12	6.779E+08 .05
10	2.000E+00	5.193E+08	5.607E+08 .15	4.359E+08 .16	3.759E+08 .17	3.154E+08 .18	4.538E+08 .07
11	1.500E+00	7.007E+08	8.180E+08 .12	5.579E+08 .14	7.483E+08 .14	5.875E+08 .15	6.414E+08 .06
12	1.000E+00	4.023E+08	4.543E+08 .13	4.991E+08 .13	4.995E+08 .11	3.448E+08 .16	4.481E+08 .06
13	7.000E-01	3.134E+08	4.213E+08 .14	4.616E+08 .15	4.533E+08 .14	3.025E+08 .18	3.892E+08 .07
14	4.500E-01	9.542E+07	2.999E+08 .16	3.471E+08 .16	4.551E+08 .19	3.178E+08 .24	3.252E+08 .07
15	3.000E-01	1.241E+08	5.141E+08 .18	5.612E+08 .19	5.576E+08 .16	3.217E+08 .21	4.569E+08 .08
16	1.500E-01	5.936E+07	1.507E+08 .17	2.087E+08 .24	2.168E+08 .22	1.846E+08 .21	1.733E+08 .09
17	1.000E-01	4.972E+07	1.004E+08 .14	7.724E+07 .08	7.646E+07 .09	8.102E+07 .10	8.926E+07 .06
18	7.000E-02	4.633E+07	5.871E+07 .07	6.017E+07 .08	8.103E+07 .31	5.222E+07 .04	6.203E+07 .05
19	4.500E-02	1.646E+07	1.660E+07 .11	1.540E+07 .16	1.382E+07 .03	1.541E+07 .04	1.589E+07 .04
20	3.000E-02	1.429E+06	6.062E+05 .06	6.030E+06 .69	1.021E+06 .24	1.050E+06 .12	1.561E+06 .39
21	2.000E-02	1.167E+04	1.091E+03 .45	6.767E+02 .57	6.459E+03 .48	3.463E+03 .43	3.183E+03 .16

Table A-21. ER2 scalar neutron fluence
(n/cm**2 / kw-min) at 100 cm from core centerline (FSD)

Energy Group	Upper Energy (MeV)	Free Field	Complex Mid-Head	Complex Mid-Thorax	Complex Marrow	Simple Mid-Head	Simple Mid-Thorax
1	1.960E+01	3.741E+04	2.325E+04 .12	2.265E+04 .12	2.918E+04 .11	2.703E+04 .12	2.230E+04 .13
2	1.690E+01	1.697E+05	1.140E+05 .12	1.322E+05 .12	1.252E+05 .13	1.269E+05 .12	1.240E+05 .12
3	1.490E+01	1.598E+05	1.048E+05 .13	1.022E+05 .14	1.061E+05 .13	1.186E+05 .12	1.075E+05 .13
4	1.420E+01	1.143E+05	5.859E+04 .13	7.177E+04 .14	5.664E+04 .15	6.104E+04 .14	6.810E+04 .13
5	1.380E+01	6.595E+05	4.316E+05 .14	3.644E+05 .14	4.118E+05 .12	4.658E+05 .13	4.967E+05 .12
6	1.280E+01	5.829E+05	3.480E+05 .12	4.261E+05 .14	4.472E+05 .11	3.867E+05 .13	4.591E+05 .13
7	1.220E+01	2.343E+06	1.807E+06 .11	1.750E+06 .11	1.631E+06 .13	1.765E+06 .12	1.750E+06 .11
8	1.110E+01	5.008E+06	3.125E+06 .13	3.473E+06 .13	3.292E+06 .13	3.028E+06 .13	2.960E+06 .14
9	1.000E+01	9.317E+06	6.565E+06 .13	5.191E+06 .13	5.123E+06 .12	5.440E+06 .13	5.195E+06 .14
10	9.050E+00	1.533E+07	8.403E+06 .14	1.003E+07 .13	1.016E+07 .12	1.006E+07 .13	8.234E+06 .13
11	8.190E+00	2.452E+07	1.873E+07 .12	1.579E+07 .13	1.630E+07 .12	1.717E+07 .12	1.520E+07 .13
12	7.410E+00	6.070E+07	4.350E+07 .12	4.274E+07 .12	3.531E+07 .12	4.434E+07 .12	4.307E+07 .12
13	6.380E+00	1.835E+08	1.012E+08 .13	1.129E+08 .12	1.265E+08 .12	1.064E+08 .12	1.148E+08 .12
14	4.970E+00	4.829E+07	3.042E+07 .13	3.306E+07 .12	3.351E+07 .12	2.640E+07 .13	2.868E+07 .12
15	4.720E+00	1.614E+08	9.244E+07 .13	1.080E+08 .14	9.097E+07 .12	9.980E+07 .13	1.032E+08 .12
16	4.070E+00	3.826E+08	3.135E+08 .11	2.067E+08 .13	2.583E+08 .10	1.834E+08 .13	2.237E+08 .12
17	3.010E+00	4.012E+08	2.711E+08 .11	2.394E+08 .12	2.586E+08 .11	2.556E+08 .11	2.373E+08 .13
18	2.390E+00	6.676E+07	4.231E+07 .13	4.141E+07 .12	5.766E+07 .10	4.038E+07 .12	3.810E+07 .11
19	2.310E+00	3.579E+08	2.342E+08 .12	2.601E+08 .12	2.770E+08 .11	2.297E+08 .13	2.092E+08 .12
20	1.830E+00	6.549E+08	4.688E+08 .11	5.250E+08 .11	4.899E+08 .10	4.224E+08 .12	4.958E+08 .11
21	1.110E+00	6.534E+08	4.848E+08 .11	4.612E+08 .11	5.339E+08 .10	4.933E+08 .12	5.301E+08 .12
22	5.500E-01	5.777E+08	5.998E+08 .11	5.127E+08 .12	6.615E+08 .10	4.459E+08 .13	4.169E+08 .12
23	1.580E-01	1.187E+08	9.130E+07 .11	1.278E+08 .11	1.419E+08 .09	1.117E+08 .10	9.743E+07 .12
24	1.110E-01	1.951E+08	1.915E+08 .13	2.037E+08 .13	2.484E+08 .13	1.565E+08 .13	2.000E+08 .13
25	5.250E-02	1.533E+08	1.820E+08 .13	1.896E+08 .13	2.220E+08 .11	1.656E+08 .13	1.885E+08 .13
26	2.480E-02	2.740E+07	2.704E+07 .13	2.602E+07 .15	3.147E+07 .12	2.541E+07 .14	2.069E+07 .14
27	2.190E-02	1.536E+08	1.095E+08 .18	1.624E+08 .16	1.996E+08 .14	1.391E+08 .17	1.721E+08 .15
28	1.030E-02	2.133E+08	2.208E+08 .17	1.820E+08 .15	2.606E+08 .12	2.296E+08 .19	1.881E+08 .16
29	3.350E-03	1.861E+08	1.120E+08 .11	2.493E+08 .18	2.779E+08 .15	1.941E+08 .19	1.818E+08 .16
30	1.230E-03	1.390E+08	1.118E+08 .18	1.376E+08 .15	1.887E+08 .11	1.646E+08 .14	1.848E+08 .18
31	5.830E-04	3.255E+08	2.782E+08 .12	4.240E+08 .12	4.455E+08 .09	3.361E+08 .11	3.559E+08 .16
32	1.010E-04	2.334E+08	2.248E+08 .12	3.112E+08 .13	3.319E+08 .13	2.613E+08 .12	2.627E+08 .15
33	2.900E-05	1.874E+08	2.348E+08 .14	1.856E+08 .13	3.022E+08 .13	1.960E+08 .15	2.039E+08 .15
34	1.070E-05	2.343E+08	1.721E+08 .11	3.318E+08 .14	3.511E+08 .10	2.420E+08 .14	3.410E+08 .16
35	3.060E-06	1.867E+08	2.226E+08 .16	2.037E+08 .15	2.750E+08 .09	2.099E+08 .15	1.904E+08 .13
36	1.130E-06	1.856E+08	1.968E+08 .10	2.307E+08 .11	3.869E+08 .12	2.383E+08 .14	2.139E+08 .14
37	4.140E-07	2.266E+09	8.615E+09 .03	1.289E+10 .03	1.036E+10 .04	9.946E+09 .04	1.230E+10 .03

Table A-22. ER2 scalar neutron fluence by marrow region (n/cm**2 / kw-min) at 100 cm from core centerline (FSD)

Energy Group	Upper Energy (MeV)	Free Field	Group Skull		Clavicles		Scapulae		Upper Limbs		Ribs	
1	1.960E+01	3.741E+04	2.728E+04	.25	4.536E+04	.21	1.847E+04	.30	4.261E+04	.23	2.092E+04	.30
2	1.690E+01	1.697E+05	1.159E+05	.28	8.179E+04	.32	1.375E+05	.26	1.549E+05	.27	9.350E+04	.32
3	1.490E+01	1.598E+05	5.229E+04	.34	1.043E+05	.31	7.799E+04	.32	9.105E+04	.33	8.801E+04	.28
4	1.420E+01	1.143E+05	5.318E+04	.31	6.395E+04	.29	7.917E+04	.26	7.389E+04	.32	8.175E+04	.27
5	1.380E+01	6.595E+05	5.681E+05	.27	5.347E+05	.26	6.772E+05	.23	4.941E+05	.27	5.774E+05	.25
6	1.280E+01	5.829E+05	4.224E+05	.27	1.838E+05	.36	4.476E+05	.25	5.449E+05	.25	7.389E+05	.22
7	1.220E+01	2.343E+06	1.019E+06	.33	1.908E+06	.26	1.325E+06	.30	1.468E+06	.28	1.012E+06	.30
8	1.110E+01	5.008E+06	2.990E+06	.28	3.728E+06	.26	2.797E+06	.30	2.150E+06	.33	4.709E+06	.24
9	1.000E+01	9.317E+06	3.014E+06	.35	5.571E+06	.28	5.110E+06	.28	3.665E+06	.32	4.730E+06	.31
10	9.050E+00	1.533E+07	4.764E+06	.36	1.305E+07	.24	1.397E+07	.26	1.248E+07	.25	7.647E+06	.29
11	8.190E+00	2.452E+07	1.556E+07	.28	1.552E+07	.28	1.529E+07	.28	1.386E+07	.35	1.542E+07	.28
12	7.410E+00	6.070E+07	3.380E+07	.30	2.965E+07	.36	2.090E+07	.37	4.984E+07	.25	3.425E+07	.29
13	6.380E+00	1.835E+08	1.123E+08	.29	1.519E+08	.26	1.628E+08	.24	1.213E+08	.28	6.256E+07	.32
14	4.970E+00	4.829E+07	2.617E+07	.30	3.355E+07	.26	2.187E+07	.31	3.791E+07	.28	3.810E+07	.24
15	4.720E+00	1.614E+08	7.418E+07	.33	8.162E+07	.30	9.350E+07	.28	7.998E+07	.30	7.338E+07	.30
16	4.070E+00	3.826E+08	2.599E+08	.25	4.747E+08	.20	2.047E+08	.28	3.651E+08	.21	2.976E+08	.24
17	3.010E+00	4.012E+08	1.397E+08	.33	3.101E+08	.24	2.187E+08	.29	3.110E+08	.24	3.163E+08	.24
18	2.390E+00	6.676E+07	3.882E+07	.26	4.633E+07	.26	3.945E+07	.30	4.476E+07	.25	4.950E+07	.23
19	2.310E+00	3.579E+08	1.685E+08	.33	2.764E+08	.27	3.245E+08	.24	1.863E+08	.31	1.931E+08	.29
20	1.830E+00	6.549E+08	3.025E+08	.31	4.810E+08	.24	6.658E+08	.22	2.776E+08	.32	5.787E+08	.22
21	1.110E+00	6.534E+08	3.137E+08	.30	5.305E+08	.23	4.320E+08	.26	4.248E+08	.25	7.207E+08	.20
22	5.500E-01	5.777E+08	5.017E+08	.27	6.429E+08	.22	5.461E+08	.23	8.433E+08	.21	6.209E+08	.22
23	1.580E-01	1.187E+08	9.802E+07	.29	1.844E+08	.20	9.456E+07	.22	1.277E+08	.23	1.186E+08	.22
24	1.110E-01	1.951E+08	9.185E+07	.26	1.655E+08	.27	1.934E+08	.27	1.628E+08	.35	2.009E+08	.22
25	5.250E-02	1.533E+08	1.158E+08	.29	2.138E+08	.24	1.379E+08	.26	1.405E+08	.23	2.715E+08	.26
26	2.480E-02	2.740E+07	1.672E+07	.35	2.247E+07	.34	2.753E+07	.32	2.357E+07	.26	2.893E+07	.18
27	2.190E-02	1.536E+08	4.941E+07	.26	2.201E+08	.38	1.635E+08	.30	1.471E+08	.28	6.763E+07	.24
28	1.030E-02	2.133E+08	2.101E+08	.41	2.578E+08	.36	3.324E+08	.33	4.612E+08	.38	2.668E+08	.29
29	3.350E-03	1.861E+08	8.987E+07	.26	1.025E+08	.25	2.163E+08	.22	2.310E+08	.28	4.041E+08	.32
30	1.230E-03	1.390E+08	6.531E+07	.31	9.633E+07	.29	1.791E+08	.34	1.229E+08	.23	2.699E+08	.37
31	5.830E-04	3.255E+08	3.120E+08	.40	2.578E+08	.21	3.092E+08	.18	4.000E+08	.23	4.476E+08	.22
32	1.010E-04	2.334E+08	1.650E+08	.29	1.844E+08	.21	2.251E+08	.23	2.049E+08	.29	2.075E+08	.21
33	2.900E-05	1.874E+08	1.060E+08	.22	1.975E+08	.27	3.076E+08	.24	2.092E+08	.29	3.261E+08	.26
34	1.070E-05	2.343E+08	1.605E+08	.21	2.049E+08	.19	2.790E+08	.33	2.166E+08	.23	4.527E+08	.20
35	3.060E-06	1.867E+08	1.487E+08	.20	2.493E+08	.30	2.407E+08	.20	2.055E+08	.19	4.303E+08	.27
36	1.130E-06	1.856E+08	2.016E+08	.27	1.877E+08	.23	2.026E+08	.19	2.361E+08	.20	2.855E+08	.24
37	4.140E-07	2.266E+09	4.413E+09	.11	6.860E+09	.09	7.334E+09	.09	8.036E+09	.09	1.025E+10	.08

Table A-22. ER2 scalar neutron fluence by marrow region (N/cm**2 / kw-min) at 100 cm from core centerline (FSD)

Energy Group	Upper Energy (MeV)	Free Field	Vertebrae	Pelvis	Upper Femur	Lower Limbs	Average
1	1.960E+01	3.741E+04	2.837E+04 .25	3.340E+04 .24	2.966E+04 .24	2.231E+04 .27	2.918E+04 .11
2	1.690E+01	1.697E+05	1.487E+05 .27	1.438E+05 .25	8.424E+04 .29	6.383E+04 .38	1.252E+05 .13
3	1.490E+01	1.598E+05	1.288E+05 .27	1.577E+05 .24	1.203E+05 .25	6.696E+04 .34	1.061E+05 .13
4	1.420E+01	1.143E+05	5.711E+04 .36	3.908E+04 .33	7.363E+04 .26	3.217E+04 .40	5.665E+04 .15
5	1.380E+01	6.595E+05	2.862E+05 .39	4.502E+05 .26	5.550E+05 .25	2.485E+05 .38	4.118E+05 .12
6	1.280E+01	5.829E+05	4.705E+05 .25	4.240E+05 .27	4.443E+05 .25	2.190E+05 .34	4.471E+05 .11
7	1.220E+01	2.343E+06	2.180E+06 .24	1.842E+06 .28	1.941E+06 .27	9.232E+05 .36	1.631E+06 .13
8	1.110E+01	5.008E+06	3.804E+06 .29	4.536E+06 .24	3.567E+06 .27	1.419E+06 .39	3.292E+06 .13
9	1.000E+01	9.317E+06	5.943E+06 .26	8.099E+06 .24	8.331E+06 .23	1.811E+06 .36	5.123E+06 .12
10	9.050E+00	1.533E+07	1.208E+07 .25	1.031E+07 .26	8.255E+06 .29	8.382E+06 .30	1.016E+07 .12
11	8.190E+00	2.452E+07	1.967E+07 .26	2.245E+07 .23	1.926E+07 .24	4.096E+06 .41	1.631E+07 .12
12	7.410E+00	6.070E+07	3.837E+07 .28	3.779E+07 .28	4.755E+07 .24	1.207E+07 .46	3.531E+07 .12
13	6.380E+00	1.835E+08	1.469E+08 .25	1.764E+08 .22	1.386E+08 .24	5.563E+07 .41	1.265E+08 .12
14	4.970E+00	4.829E+07	3.919E+07 .25	4.781E+07 .22	3.531E+07 .30	7.820E+06 .37	3.351E+07 .12
15	4.720E+00	1.614E+08	7.393E+07 .30	1.922E+08 .23	1.449E+08 .23	3.980E+07 .44	9.095E+07 .12
16	4.070E+00	3.826E+08	2.427E+08 .24	3.161E+08 .23	2.862E+08 .24	1.134E+08 .37	2.583E+08 .10
17	3.010E+00	4.012E+08	3.037E+08 .24	3.013E+08 .24	2.866E+08 .24	1.217E+08 .36	2.586E+08 .11
18	2.390E+00	6.676E+07	7.786E+07 .20	8.408E+07 .20	5.182E+07 .25	2.165E+07 .35	5.764E+07 .10
19	2.310E+00	3.579E+08	2.973E+08 .24	4.950E+08 .19	4.853E+08 .21	1.080E+08 .39	2.770E+08 .11
20	1.830E+00	6.549E+08	4.844E+08 .24	9.697E+08 .17	6.848E+08 .20	1.945E+08 .37	4.898E+08 .10
21	1.110E+00	6.534E+08	5.318E+08 .24	8.306E+08 .19	8.331E+08 .18	3.231E+08 .32	5.339E+08 .10
22	5.500E-01	5.777E+08	8.124E+08 .19	7.638E+08 .18	5.821E+08 .20	2.452E+08 .44	6.615E+08 .10
23	1.580E-01	1.187E+08	1.409E+08 .20	2.225E+08 .17	2.660E+08 .16	7.537E+07 .33	1.419E+08 .09
24	1.110E-01	1.951E+08	3.801E+08 .24	3.379E+08 .20	2.296E+08 .21	9.312E+07 .43	2.484E+08 .13
25	5.250E-02	1.533E+08	2.987E+08 .21	3.059E+08 .17	2.730E+08 .18	8.729E+07 .47	2.220E+08 .11
26	2.480E-02	2.740E+07	4.844E+07 .23	3.318E+07 .19	3.637E+07 .23	7.313E+06 .27	3.148E+07 .12
27	2.190E-02	1.536E+08	2.663E+08 .28	3.904E+08 .23	2.336E+08 .24	7.507E+07 .32	1.996E+08 .14
28	1.030E-02	2.133E+08	2.531E+08 .22	2.946E+08 .23	3.184E+08 .21	5.085E+07 .27	2.606E+08 .12
29	3.350E-03	1.861E+08	3.147E+08 .35	4.561E+08 .17	2.790E+08 .16	1.780E+08 .44	2.779E+08 .15
30	1.230E-03	1.390E+08	2.570E+08 .22	2.788E+08 .16	1.611E+08 .20	7.587E+07 .28	1.887E+08 .11
31	5.830E-04	3.255E+08	4.946E+08 .18	6.818E+08 .16	7.211E+08 .20	1.564E+08 .46	4.456E+08 .09
32	1.010E-04	2.334E+08	4.815E+08 .25	5.229E+08 .15	3.494E+08 .26	1.168E+08 .24	3.319E+08 .13
33	2.900E-05	1.874E+08	4.164E+08 .28	4.257E+08 .14	2.750E+08 .14	1.509E+08 .31	3.022E+08 .13
34	1.070E-05	2.343E+08	4.248E+08 .20	5.508E+08 .19	4.295E+08 .15	1.950E+08 .31	3.511E+08 .10
35	3.060E-06	1.867E+08	3.535E+08 .17	3.226E+08 .18	3.263E+08 .20	1.124E+08 .23	2.750E+08 .09
36	1.130E-06	1.856E+08	5.339E+08 .24	5.110E+08 .13	4.459E+08 .12	2.737E+08 .42	3.869E+08 .12
37	4.140E-07	2.266E+09	1.433E+10 .07	1.440E+10 .08	1.181E+10 .08	3.932E+09 .10	1.036E+10 .04

Table A-23. ER2 scalar neutron-gamma ray fluence
(G/cm**2 / kw-min) at 100 cm from core centerline (FSD)

Energy Group	Upper Energy (MeV)	Free Field	Complex Mid-Head		Complex Mid-Thorax		Complex Marrow		Simple Mid-Head		Simple Mid-Thorax	
1	1.400E+01	1.318E+05	1.446E+05	.75	1.459E+03	***	2.190E+03	.88	2.362E+05	.86	1.188E+05	.92
2	1.000E+01	9.731E+07	1.656E+04	.68	4.523E+05	.94	6.886E+05	.96	1.319E+04	.77	1.121E+04	.90
3	8.000E+00	2.246E+08	2.772E+06	.72	6.493E+06	.47	1.980E+07	.35	8.319E+04	.55	2.614E+05	.22
4	7.000E+00	1.612E+08	1.076E+07	.40	1.753E+07	.26	1.611E+07	.35	1.027E+07	.82	5.787E+06	.46
5	6.000E+00	2.399E+08	1.554E+06	.46	2.005E+07	.37	4.971E+06	.50	3.742E+06	.65	1.751E+07	.46
6	5.000E+00	5.925E+08	4.975E+06	.15	1.772E+07	.33	1.349E+07	.18	1.905E+07	.43	3.948E+06	.13
7	4.000E+00	1.297E+09	2.183E+06	.27	7.359E+06	.42	6.522E+06	.33	3.818E+06	.48	4.481E+06	.74
8	3.000E+00	1.308E+09	2.582E+06	.44	1.526E+07	.48	8.454E+06	.46	3.349E+05	.36	1.062E+06	.70
9	2.500E+00	3.473E+09	7.025E+08	.07	1.343E+09	.05	8.099E+08	.06	9.333E+08	.06	1.378E+09	.05
10	2.000E+00	3.336E+09	2.623E+07	.24	5.470E+07	.18	5.690E+07	.19	3.259E+07	.49	5.711E+07	.19
11	1.500E+00	5.489E+09	3.396E+07	.27	4.548E+07	.27	3.282E+07	.25	2.532E+07	.36	3.752E+07	.22
12	1.000E+00	5.058E+09	1.949E+07	.32	3.339E+07	.33	1.489E+07	.21	1.709E+07	.31	4.476E+07	.25
13	7.000E-01	6.723E+09	2.392E+07	.27	6.379E+07	.21	3.813E+07	.26	5.449E+07	.29	4.087E+07	.29
14	4.500E-01	4.507E+09	2.417E+07	.31	8.145E+07	.26	3.091E+07	.19	4.123E+07	.37	6.915E+07	.25
15	3.000E-01	5.065E+09	8.069E+07	.43	1.245E+08	.24	8.496E+07	.25	6.218E+07	.33	9.553E+07	.24
16	1.500E-01	2.151E+09	1.165E+07	.50	3.746E+07	.32	1.277E+07	.44	1.854E+07	.27	4.793E+07	.37
17	1.000E-01	1.328E+09	9.046E+06	.68	2.159E+07	.40	8.289E+06	.38	2.613E+06	.44	8.479E+06	.44
18	7.000E-02	8.671E+08	1.676E+06	.46	7.173E+06	.61	2.586E+06	.61	9.202E+05	.58	1.023E+07	.50
19	4.500E-02	2.443E+08	2.026E+05	.94	2.754E+05	.63	1.562E+05	.54	7.845E+04	.59	9.972E+05	.74
20	3.000E-02	2.047E+07	3.640E+05	.99	1.448E+04	.89	9.976E+05	.79	1.658E+05	.85	6.374E+03	.65
21	2.000E-02	1.529E+05	8.796E-03	***	0.000E-01	.00	3.111E+02	.88	2.098E+00	***	1.176E+00	***

Table A-24. ER2 scalar neutron-gamma fluence by marrow region (g/cm**2 / kw-min) at 100 cm from core centerline (FSD)

Energy Group	Upper Energy (MeV)	Free Field	Skull	Clavicles	Scapulae	Upper Limbs	Ribs
1	1.400E+01	1.318E+05	0.000E-01 .00	5.947E+02 ***	5.605E+04 .88	0.000E-01 .00	0.000E-01 .00
2	1.000E+01	9.731E+07	7.363E+04 ***	1.543E+05 .72	1.706E+07 .99	1.090E+05 .80	4.840E+03 .99
3	8.000E+00	2.246E+08	1.179E+07 .96	5.013E+05 .45	5.191E+05 .39	3.103E+05 .63	3.709E+06 .65
4	7.000E+00	1.612E+08	3.876E+06 .40	8.847E+06 .39	2.832E+06 .51	1.769E+07 .56	1.121E+07 .39
5	6.000E+00	2.399E+08	1.568E+06 .63	2.870E+06 .57	1.310E+06 .45	2.277E+06 .93	1.235E+06 .74
6	5.000E+00	5.925E+08	7.448E+06 .31	2.303E+07 .74	6.725E+06 .29	9.790E+06 .28	2.513E+07 .57
7	4.000E+00	1.297E+09	1.329E+06 .41	1.145E+06 .50	1.556E+07 .92	1.843E+06 .74	2.206E+06 .32
8	3.000E+00	1.308E+09	4.709E+05 .47	2.745E+06 .53	6.209E+06 .70	1.130E+06 .92	1.241E+07 .98
9	2.500E+00	3.473E+09	4.603E+08 .16	7.177E+08 .12	9.299E+08 .13	7.465E+08 .14	8.927E+08 .12
10	2.000E+00	3.336E+09	1.567E+07 .68	4.823E+07 .37	2.356E+07 .53	3.612E+07 .51	8.894E+07 .38
11	1.500E+00	5.489E+09	1.874E+07 .63	4.684E+07 .50	2.857E+07 .53	4.903E+07 .44	1.901E+07 .80
12	1.000E+00	5.058E+09	2.942E+07 .60	1.278E+06 .53	3.899E+07 .55	9.587E+06 .43	2.473E+07 .49
13	7.000E-01	6.723E+09	2.510E+07 .59	3.910E+07 .67	5.212E+07 .45	1.545E+07 .45	9.705E+06 .37
14	4.500E-01	4.507E+09	1.572E+07 .55	5.284E+07 .56	7.803E+07 .38	4.371E+06 .44	5.313E+07 .45
15	3.000E-01	5.065E+09	4.354E+07 .89	1.909E+06 .43	5.525E+07 .56	3.823E+07 .70	2.090E+08 .36
16	1.500E-01	2.151E+09	6.776E+06 .67	6.598E+07 .65	2.794E+07 .82	1.670E+07 .86	1.087E+06 .92
17	1.000E-01	1.328E+09	2.842E+06 .79	1.127E+05 .64	1.105E+06 .80	3.382E+07 .65	2.563E+07 .79
18	7.000E-02	8.671E+08	1.121E+04 ***	3.976E+07 ***	1.630E+07 .96	6.095E+04 .97	1.350E+06 .94
19	4.500E-02	2.443E+08	8.475E+01 ***	3.071E+03 .71	3.025E+05 .80	2.691E+03 .96	1.266E+06 .90
20	3.000E-02	2.047E+07	1.411E+02 ***	3.713E+01 ***	********* ***	2.085E+02 .98	6.421E+03 ***
21	2.000E-02	1.529E+05	0.000E-01 .00	0.000E-01 .00	0.000E-01 .00	1.014E-02 ***	7.414E+01 ***

Table A-24. ER2 scalar neutron-gamma fluence by marrow region (g/cm**2 / kw-min) at 100 cm from core centerline (FSD)

Energy Group	Upper Energy (MeV)	Free Field	Vertebrae	Pelvis	Upper Femur	Lower Limbs	Average
1	1.400E+01	1.318E+05	8.014E-01 ***	3.255E-01 ***	0.000E-01 .00	0.000E-01 .00	2.190E+03 .88
2	1.000E+01	9.731E+07	********* ***	1.711E+03 .98	3.370E+02 .96	9.502E+02 .61	6.884E+05 .96
3	8.000E+00	2.246E+08	3.293E+07 .53	3.533E+07 .60	5.174E+06 .56	1.817E+07 .99	1.980E+07 .35
4	7.000E+00	1.612E+08	1.962E+07 .70	4.383E+07 .53	3.763E+06 .29	1.889E+06 .49	1.611E+07 .35
5	6.000E+00	2.399E+08	4.041E+06 .95	2.098E+07 .79	4.582E+06 .57	1.545E+05 .54	4.969E+06 .50
6	5.000E+00	5.925E+08	1.067E+07 .24	2.421E+07 .53	2.830E+07 .57	6.987E+06 .30	1.349E+07 .18
7	4.000E+00	1.297E+09	1.087E+07 .51	2.045E+06 .46	1.570E+07 .91	3.655E+06 .74	6.524E+06 .33
8	3.000E+00	1.308E+09	1.498E+07 .70	2.556E+06 .58	2.565E+07 .91	1.594E+06 .87	8.453E+06 .46
9	2.500E+00	3.473E+09	9.769E+08 .12	9.266E+08 .13	9.917E+08 .15	4.637E+08 .14	8.098E+08 .06
10	2.000E+00	3.336E+09	9.249E+07 .32	5.449E+07 .30	4.540E+07 .38	2.449E+07 .43	5.691E+07 .19
11	1.500E+00	5.489E+09	3.310E+07 .39	2.023E+07 .54	2.204E+07 .44	5.347E+07 .84	3.282E+07 .25
12	1.000E+00	5.058E+09	1.082E+07 .41	1.842E+07 .62	9.422E+06 .55	6.302E+06 .51	1.489E+07 .21
13	7.000E-01	6.723E+09	3.702E+07 .67	4.072E+07 .34	1.011E+08 .40	4.747E+07 .69	3.813E+07 .26
14	4.500E-01	4.507E+09	2.750E+07 .39	5.102E+07 .39	8.158E+07 .55	5.673E+06 .64	3.091E+07 .19
15	3.000E-01	5.065E+09	1.125E+08 .50	3.340E+07 .63	2.559E+08 .39	1.135E+07 .54	8.496E+07 .25
16	1.500E-01	2.151E+09	1.635E+07 .90	6.607E+05 .69	3.281E+07 .80	5.068E+06 .95	1.277E+07 .44
17	1.000E-01	1.328E+09	3.263E+06 .80	3.779E+06 .64	4.333E+06 .61	2.516E+06 .59	8.288E+06 .38
18	7.000E-02	8.671E+08	1.794E+05 .70	1.154E+07 .96	4.569E+05 .73	6.011E+02 ***	2.586E+06 .61
19	4.500E-02	2.443E+08	1.208E+05 .97	1.744E+05 .84	2.652E+04 ***	3.712E+02 ***	1.562E+05 .54
20	3.000E-02	2.047E+07	********* ***	7.727E+06 .79	********* ***	1.102E+03 .90	9.974E+05 .79
21	2.000E-02	1.529E+05	5.250E+00 .84	8.653E-01 ***	4.510E+03 .91	1.818E+01 ***	3.111E+02 .88

Table A-25. ER2 scalar gamma ray fluence
(g/cm**2 / kw-min) at 100 cm from core centerline (FSD)

Energy Group	Upper Energy (MeV)	Free Field	Complex Mid-Head	Complex Mid-Thorax	Complex Marrow	Simple Mid-Head	Simple Mid-Thorax
1	1.400E+01	1.318E+05	1.175E+05 .02	1.083E+05 .02	1.150E+05 .02	1.114E+05 .02	1.053E+05 .02
2	1.000E+01	9.731E+07	8.508E+07 .09	9.569E+07 .08	8.013E+07 .09	8.209E+07 .09	9.615E+07 .08
3	8.000E+00	2.246E+08	2.041E+08 .08	2.040E+08 .09	1.706E+08 .08	1.928E+08 .08	1.956E+08 .09
4	7.000E+00	1.612E+08	1.419E+08 .09	1.425E+08 .08	1.741E+08 .07	1.445E+08 .09	1.445E+08 .08
5	6.000E+00	2.399E+08	1.938E+08 .08	2.020E+08 .08	1.880E+08 .08	1.916E+08 .08	2.180E+08 .09
6	5.000E+00	5.925E+08	4.214E+08 .09	5.737E+08 .09	6.458E+08 .08	5.703E+08 .08	4.936E+08 .09
7	4.000E+00	1.297E+09	1.117E+09 .08	1.073E+09 .08	1.117E+09 .09	1.217E+09 .08	1.179E+09 .09
8	3.000E+00	1.308E+09	1.007E+09 .09	1.059E+09 .09	9.944E+08 .08	1.119E+09 .08	1.124E+09 .08
9	2.500E+00	3.473E+09	2.941E+09 .08	3.079E+09 .08	2.719E+09 .08	2.990E+09 .09	2.373E+09 .09
10	2.000E+00	3.336E+09	2.671E+09 .09	3.134E+09 .07	2.820E+09 .08	3.540E+09 .08	2.894E+09 .08
11	1.500E+00	5.489E+09	5.381E+09 .08	4.985E+09 .08	4.889E+09 .08	5.215E+09 .07	5.265E+09 .08
12	1.000E+00	5.058E+09	4.852E+09 .08	4.311E+09 .08	5.364E+09 .07	4.690E+09 .08	4.789E+09 .07
13	7.000E-01	6.723E+09	5.800E+09 .08	6.860E+09 .08	5.866E+09 .08	5.700E+09 .08	6.228E+09 .09
14	4.500E-01	4.507E+09	5.318E+09 .08	5.594E+09 .08	5.973E+09 .06	5.401E+09 .07	6.172E+09 .07
15	3.000E-01	5.065E+09	9.127E+09 .07	1.123E+10 .07	8.994E+09 .07	8.990E+09 .07	1.251E+10 .07
16	1.500E-01	2.151E+09	3.722E+09 .08	5.740E+09 .09	4.769E+09 .07	4.135E+09 .08	5.574E+09 .09
17	1.000E-01	1.328E+09	2.386E+09 .08	3.450E+09 .08	2.921E+09 .07	2.938E+09 .08	3.410E+09 .08
18	7.000E-02	8.671E+08	2.001E+09 .12	2.336E+09 .10	1.520E+09 .05	1.785E+09 .09	2.362E+09 .08
19	4.500E-02	2.443E+08	4.839E+08 .11	6.720E+08 .13	4.005E+08 .14	4.972E+08 .15	8.003E+08 .09
20	3.000E-02	2.047E+07	3.533E+07 .06	5.285E+07 .09	2.067E+07 .16	2.112E+07 .06	5.786E+07 .12
21	2.000E-02	1.529E+05	4.650E+05 .23	5.703E+05 .34	6.185E+04 .28	1.177E+05 .26	3.606E+05 .14

Table A-26. ER2 scalar gamma ray fluence by marrow region (g/cm**2 / kw-min) at 100 cm from core centerline (FSD)

Energy Group	Upper Energy (MeV)	Free Field	Skull	Clavicles	Scapulae	Upper Limbs	Ribs
1	1.400E+01	1.318E+05	1.112E+05 .05	1.152E+05 .04	1.182E+05 .05	1.181E+05 .05	1.241E+05 .05
2	1.000E+01	9.731E+07	5.248E+07 .22	8.213E+07 .20	9.854E+07 .17	7.927E+07 .19	7.751E+07 .20
3	8.000E+00	2.246E+08	2.298E+08 .16	1.630E+08 .19	1.545E+08 .20	1.664E+08 .18	1.617E+08 .18
4	7.000E+00	1.612E+08	1.511E+08 .19	1.411E+08 .18	1.746E+08 .16	1.928E+08 .16	1.656E+08 .17
5	6.000E+00	2.399E+08	1.886E+08 .18	1.272E+08 .22	1.759E+08 .19	1.881E+08 .18	2.106E+08 .19
6	5.000E+00	5.925E+08	7.149E+08 .17	5.487E+08 .17	3.179E+08 .21	5.471E+08 .17	6.454E+08 .16
7	4.000E+00	1.297E+09	1.214E+09 .17	1.024E+09 .20	9.014E+08 .20	9.692E+08 .19	1.082E+09 .20
8	3.000E+00	1.308E+09	8.538E+08 .21	1.120E+09 .21	1.211E+09 .20	1.119E+09 .18	1.006E+09 .20
9	2.500E+00	3.473E+09	2.406E+09 .21	2.768E+09 .19	3.719E+09 .17	2.881E+09 .18	2.878E+09 .18
10	2.000E+00	3.336E+09	2.085E+09 .20	2.280E+09 .21	3.659E+09 .16	3.060E+09 .18	2.373E+09 .19
11	1.500E+00	5.489E+09	1.850E+09 .24	4.151E+09 .19	3.928E+09 .18	4.912E+09 .18	4.297E+09 .18
12	1.000E+00	5.058E+09	5.118E+09 .17	6.684E+09 .15	6.534E+09 .17	4.720E+09 .17	5.361E+09 .16
13	7.000E-01	6.723E+09	3.882E+09 .19	5.943E+09 .17	4.580E+09 .19	4.696E+09 .24	6.604E+09 .18
14	4.500E-01	4.507E+09	3.166E+09 .20	5.374E+09 .17	6.255E+09 .17	7.894E+09 .15	5.590E+09 .16
15	3.000E-01	5.065E+09	7.252E+09 .16	6.009E+09 .15	9.974E+09 .15	7.900E+09 .17	9.130E+09 .17
16	1.500E-01	2.151E+09	2.652E+09 .11	3.862E+09 .17	4.304E+09 .17	5.285E+09 .20	4.567E+09 .17
17	1.000E-01	1.328E+09	2.693E+09 .21	3.430E+09 .15	3.064E+09 .26	2.048E+09 .10	4.141E+09 .24
18	7.000E-02	8.671E+08	1.247E+09 .11	1.946E+09 .17	1.502E+09 .08	1.836E+09 .15	1.734E+09 .09
19	4.500E-02	2.443E+08	3.676E+08 .17	5.108E+08 .35	4.108E+08 .14	3.188E+08 .09	3.327E+08 .08
20	3.000E-02	2.047E+07	2.510E+07 .12	3.096E+07 .22	1.895E+07 .09	2.377E+07 .17	1.759E+07 .12
21	2.000E-02	1.529E+05	7.518E+04 .24	5.760E+04 .34	3.573E+05 .87	5.913E+04 .40	1.079E+05 .40

Table A-26. ER2 scalar gamma ray fluence by marrow region
(g/cm**2 / kw-min) at 100 cm from core centerline (FSD)

Energy Group	Upper Energy (MeV)	Free Field	Vertebrae	Pelvis	Upper Femur	Lower Limbs	Average
1	1.400E+01	1.318E+05	1.154E+05 .05	1.169E+05 .05	1.145E+05 .06	1.076E+05 .05	1.150E+05 .02
2	1.000E+01	9.731E+07	8.761E+07 .19	9.662E+07 .17	1.030E+08 .17	5.321E+07 .23	8.013E+07 .09
3	8.000E+00	2.246E+08	1.565E+08 .19	1.546E+08 .20	1.963E+08 .18	1.729E+08 .20	1.706E+08 .08
4	7.000E+00	1.612E+08	1.872E+08 .16	1.689E+08 .19	1.980E+08 .16	1.417E+08 .18	1.741E+08 .07
5	6.000E+00	2.399E+08	1.787E+08 .20	2.196E+08 .18	2.336E+08 .17	1.534E+08 .22	1.881E+08 .08
6	5.000E+00	5.925E+08	7.973E+08 .17	5.354E+08 .18	5.903E+08 .17	5.391E+08 .18	6.458E+08 .08
7	4.000E+00	1.297E+09	1.204E+09 .20	1.271E+09 .18	1.179E+09 .20	8.605E+08 .20	1.117E+09 .09
8	3.000E+00	1.308E+09	1.031E+09 .19	1.222E+09 .17	9.745E+08 .21	6.169E+08 .24	9.944E+08 .08
9	2.500E+00	3.473E+09	2.878E+09 .18	3.047E+09 .17	2.660E+09 .19	1.768E+09 .21	2.719E+09 .08
10	2.000E+00	3.336E+09	3.433E+09 .17	2.731E+09 .18	2.333E+09 .20	2.004E+09 .20	2.820E+09 .08
11	1.500E+00	5.489E+09	6.408E+09 .15	4.164E+09 .18	5.979E+09 .17	4.337E+09 .18	4.890E+09 .08
12	1.000E+00	5.058E+09	5.567E+09 .17	5.943E+09 .17	6.551E+09 .14	4.075E+09 .20	5.363E+09 .07
13	7.000E-01	6.723E+09	7.176E+09 .16	7.408E+09 .16	5.793E+09 .17	3.862E+09 .22	5.865E+09 .08
14	4.500E-01	4.507E+09	5.610E+09 .15	7.860E+09 .13	7.684E+09 .15	4.839E+09 .21	5.971E+09 .06
15	3.000E-01	5.065E+09	1.029E+10 .15	1.029E+10 .18	1.235E+10 .14	5.059E+09 .23	8.995E+09 .07
16	1.500E-01	2.151E+09	5.098E+09 .14	5.836E+09 .15	6.189E+09 .18	3.732E+09 .21	4.768E+09 .07
17	1.000E-01	1.328E+09	3.417E+09 .14	3.410E+09 .12	2.571E+09 .10	1.733E+09 .13	2.921E+09 .07
18	7.000E-02	8.671E+08	1.519E+09 .10	1.603E+09 .11	1.815E+09 .20	1.109E+09 .12	1.520E+09 .05
19	4.500E-02	2.443E+08	5.225E+08 .31	3.669E+08 .11	3.278E+08 .07	2.912E+08 .09	4.005E+08 .14
20	3.000E-02	2.047E+07	1.367E+07 .11	1.120E+07 .09	2.915E+07 .41	3.796E+07 .60	2.067E+07 .16
21	2.000E-02	1.529E+05	4.856E+04 .72	1.053E+04 .49	2.717E+04 .62	4.550E+04 .42	6.185E+04 .28

Table A-27. ER2 scalar total gamma ray fluence
(g/cm**2 / kw-min) at 100 cm from core centerline (FSD)

Energy Group	Upper Energy (MeV)	Free Field	Complex Mid-Head	Complex Mid-Thorax	Complex Marrow	Simple Mid-Head	Simple Mid-Thorax
1	1.400E+01	1.318E+05	2.621E+05 .37	1.098E+05 .03	1.172E+05 .02	3.477E+05 .54	2.241E+05 .43
2	1.000E+01	9.731E+07	8.510E+07 .09	9.614E+07 .08	8.082E+07 .08	8.211E+07 .09	9.616E+07 .08
3	8.000E+00	2.246E+08	2.068E+08 .08	2.105E+08 .09	1.904E+08 .08	1.929E+08 .08	1.959E+08 .09
4	7.000E+00	1.612E+08	1.526E+08 .09	1.600E+08 .08	1.902E+08 .07	1.547E+08 .09	1.503E+08 .08
5	6.000E+00	2.399E+08	1.953E+08 .08	2.220E+08 .08	1.930E+08 .08	1.954E+08 .08	2.355E+08 .09
6	5.000E+00	5.925E+08	4.264E+08 .09	5.914E+08 .08	6.593E+08 .08	5.894E+08 .08	4.975E+08 .09
7	4.000E+00	1.297E+09	1.119E+09 .08	1.080E+09 .08	1.124E+09 .09	1.221E+09 .08	1.183E+09 .09
8	3.000E+00	1.308E+09	1.010E+09 .09	1.074E+09 .08	1.003E+09 .08	1.120E+09 .08	1.125E+09 .08
9	2.500E+00	3.473E+09	3.644E+09 .07	4.422E+09 .06	3.529E+09 .06	3.924E+09 .07	3.751E+09 .06
10	2.000E+00	3.336E+09	2.697E+09 .08	3.189E+09 .07	2.877E+09 .08	3.572E+09 .07	2.951E+09 .08
11	1.500E+00	5.489E+09	5.415E+09 .08	5.031E+09 .08	4.922E+09 .08	5.240E+09 .07	5.302E+09 .08
12	1.000E+00	5.058E+09	4.872E+09 .08	4.344E+09 .08	5.379E+09 .07	4.707E+09 .08	4.834E+09 .07
13	7.000E-01	6.723E+09	5.824E+09 .08	6.924E+09 .08	5.904E+09 .08	5.754E+09 .08	6.269E+09 .09
14	4.500E-01	4.507E+09	5.342E+09 .08	5.675E+09 .07	6.003E+09 .06	5.442E+09 .07	6.241E+09 .07
15	3.000E-01	5.065E+09	9.207E+09 .07	1.135E+10 .07	9.079E+09 .07	9.053E+09 .07	1.261E+10 .07
16	1.500E-01	2.151E+09	3.734E+09 .08	5.777E+09 .09	4.782E+09 .07	4.153E+09 .08	5.622E+09 .09
17	1.000E-01	1.328E+09	2.395E+09 .08	3.471E+09 .08	2.930E+09 .07	2.941E+09 .08	3.418E+09 .08
18	7.000E-02	8.671E+08	2.003E+09 .12	2.344E+09 .09	1.522E+09 .05	1.786E+09 .09	2.372E+09 .08
19	4.500E-02	2.443E+08	4.841E+08 .11	6.723E+08 .13	4.007E+08 .14	4.973E+08 .15	8.013E+08 .09
20	3.000E-02	2.047E+07	3.569E+07 .06	5.286E+07 .09	2.167E+07 .15	2.129E+07 .06	5.787E+07 .12
21	2.000E-02	1.529E+05	4.650E+05 .23	5.703E+05 .34	6.216E+04 .28	1.177E+05 .26	3.606E+05 .14

Table A-28. ER2 scalar total gamma fluence by marrow region (g/cm**2 / kw-min) at 100 cm from core centerline (FSD)

Energy Group	Upper Energy (MeV)	Free Field	Skull	Clavicles	Scapulae	Upper Limbs	Ribs
1	1.400E+01	1.318E+05	1.112E+05 .05	1.158E+05 .04	1.742E+05 .24	1.181E+05 .05	1.241E+05 .05
2	1.000E+01	9.731E+07	5.255E+07 .22	8.228E+07 .20	1.156E+08 .19	7.938E+07 .19	7.751E+07 .20
3	8.000E+00	2.246E+08	2.416E+08 .16	1.635E+08 .19	1.550E+08 .20	1.667E+08 .18	1.654E+08 .18
4	7.000E+00	1.612E+08	1.550E+08 .18	1.499E+08 .18	1.775E+08 .16	2.105E+08 .16	1.768E+08 .17
5	6.000E+00	2.399E+08	1.902E+08 .18	1.300E+08 .22	1.772E+08 .19	1.904E+08 .18	2.118E+08 .19
6	5.000E+00	5.925E+08	7.224E+08 .17	5.718E+08 .17	3.247E+08 .21	5.569E+08 .17	6.706E+08 .15
7	4.000E+00	1.297E+09	1.215E+09 .17	1.025E+09 .20	9.169E+08 .19	9.710E+08 .19	1.084E+09 .20
8	3.000E+00	1.308E+09	8.543E+08 .21	1.123E+09 .21	1.217E+09 .20	1.120E+09 .18	1.019E+09 .20
9	2.500E+00	3.473E+09	2.867E+09 .18	3.486E+09 .16	4.649E+09 .14	3.628E+09 .15	3.771E+09 .14
10	2.000E+00	3.336E+09	2.101E+09 .20	2.328E+09 .21	3.683E+09 .16	3.096E+09 .18	2.462E+09 .18
11	1.500E+00	5.489E+09	1.869E+09 .24	4.198E+09 .19	3.957E+09 .18	4.961E+09 .18	4.316E+09 .18
12	1.000E+00	5.058E+09	5.148E+09 .17	6.685E+09 .15	6.573E+09 .17	4.729E+09 .17	5.386E+09 .16
13	7.000E-01	6.723E+09	3.907E+09 .19	5.982E+09 .17	4.632E+09 .19	4.712E+09 .24	6.614E+09 .18
14	4.500E-01	4.507E+09	3.182E+09 .20	5.427E+09 .17	6.333E+09 .16	7.898E+09 .15	5.643E+09 .16
15	3.000E-01	5.065E+09	7.296E+09 .16	6.011E+09 .15	1.003E+10 .15	7.938E+09 .17	9.339E+09 .16
16	1.500E-01	2.151E+09	2.659E+09 .11	3.928E+09 .16	4.332E+09 .16	5.301E+09 .20	4.568E+09 .17
17	1.000E-01	1.328E+09	2.696E+09 .21	3.430E+09 .15	3.065E+09 .26	2.082E+09 .10	4.167E+09 .24
18	7.000E-02	8.671E+08	1.247E+09 .11	1.985E+09 .17	1.518E+09 .08	1.836E+09 .15	1.735E+09 .09
19	4.500E-02	2.443E+08	3.676E+08 .17	5.108E+08 .35	4.111E+08 .14	3.188E+08 .09	3.340E+08 .08
20	3.000E-02	2.047E+07	2.510E+07 .12	3.096E+07 .22	1.895E+07 .09	2.377E+07 .17	1.760E+07 .12
21	2.000E-02	1.529E+05	7.518E+04 .24	5.760E+04 .34	3.573E+05 .87	5.913E+04 .40	1.080E+05 .40

Table A-28. ER2 scalar total gamma fluence by marrow region (g/cm**2 / kw-min) at 100 cm from core centerline (FSD)

Energy Group	Upper Energy (MeV)	Free Field	Vertebrae	Pelvis	Upper Femur	Lower Limbs	Average
1	1.400E+01	1.318E+05	1.154E+05 .05	1.169E+05 .05	1.145E+05 .06	1.076E+05 .05	1.172E+05 .02
2	1.000E+01	9.731E+07	8.761E+07 .19	9.662E+07 .17	1.030E+08 .17	5.321E+07 .23	8.082E+07 .08
3	8.000E+00	2.246E+08	1.894E+08 .18	1.899E+08 .19	2.014E+08 .18	1.910E+08 .20	1.904E+08 .08
4	7.000E+00	1.612E+08	2.068E+08 .16	2.127E+08 .18	2.017E+08 .16	1.436E+08 .17	1.902E+08 .07
5	6.000E+00	2.399E+08	1.828E+08 .20	2.406E+08 .18	2.382E+08 .16	1.535E+08 .22	1.930E+08 .08
6	5.000E+00	5.925E+08	8.080E+08 .17	5.596E+08 .18	6.186E+08 .17	5.461E+08 .18	6.593E+08 .08
7	4.000E+00	1.297E+09	1.215E+09 .20	1.273E+09 .18	1.195E+09 .19	8.641E+08 .20	1.123E+09 .09
8	3.000E+00	1.308E+09	1.046E+09 .19	1.225E+09 .17	1.000E+09 .20	6.185E+08 .24	1.003E+09 .08
9	2.500E+00	3.473E+09	3.855E+09 .14	3.974E+09 .14	3.652E+09 .15	2.232E+09 .18	3.528E+09 .06
10	2.000E+00	3.336E+09	3.526E+09 .17	2.786E+09 .18	2.378E+09 .19	2.029E+09 .20	2.877E+09 .08
11	1.500E+00	5.489E+09	6.441E+09 .15	4.185E+09 .18	6.001E+09 .17	4.391E+09 .18	4.922E+09 .08
12	1.000E+00	5.058E+09	5.578E+09 .17	5.961E+09 .17	6.560E+09 .14	4.081E+09 .20	5.378E+09 .07
13	7.000E-01	6.723E+09	7.213E+09 .16	7.449E+09 .16	5.894E+09 .16	3.909E+09 .22	5.903E+09 .08
14	4.500E-01	4.507E+09	5.638E+09 .15	7.911E+09 .13	7.766E+09 .15	4.845E+09 .21	6.002E+09 .06
15	3.000E-01	5.065E+09	1.041E+10 .15	1.032E+10 .18	1.261E+10 .14	5.070E+09 .23	9.080E+09 .07
16	1.500E-01	2.151E+09	5.115E+09 .14	5.837E+09 .15	6.221E+09 .18	3.737E+09 .21	4.781E+09 .07
17	1.000E-01	1.328E+09	3.420E+09 .14	3.414E+09 .12	2.575E+09 .10	1.735E+09 .13	2.930E+09 .07
18	7.000E-02	8.671E+08	1.519E+09 .10	1.614E+09 .11	1.815E+09 .20	1.109E+09 .12	1.522E+09 .05
19	4.500E-02	2.443E+08	5.226E+08 .31	3.671E+08 .11	3.278E+08 .07	2.912E+08 .09	4.006E+08 .14
20	3.000E-02	2.047E+07	1.367E+07 .11	1.893E+07 .29	2.915E+07 .41	3.796E+07 .60	2.167E+07 .15
21	2.000E-02	1.529E+05	4.856E+04 .72	1.053E+04 .49	3.168E+04 .55	4.552E+04 .42	6.216E+04 .28

DISTRIBUTION LIST

DEPARTMENT OF DEFENSE

Armed Forces Inst of Pathology
ATTN: Director
ATTN: Radiation Pathology Br

Armed Forces Radiobio Res Inst
ATTN: Deputy Director
ATTN: Director
ATTN: Scientific Director
ATTN: Technical Library

Assistant to the Secy of Defense
Atomic Energy
ATTN: J. Morrison

Assistant Secy of Defense, Public Affairs
ATTN: ASD(PA)

Assistant Secy of Defense, Manpower Installations
ATTN: ASD(MI&L)

Assistant Secy of Defense, Health Affairs
ATTN: ASD(HA)

Defense Intelligence Agency
ATTN: RTS-2B

Defense Nuclear Agency
ATTN: Director
ATTN: GC
ATTN: PAO
5 cy ATTN: STBE
54 cy ATTN: STTI-CA

Defense Technical Information Center
12 cy ATTN: DD

Deputy Under Secy of Defense Res & Eng
ATTN: DUSDRE, Rsch & Adv Tech

Deputy Asst Secy of Defense
Energy, Environment & Safety
ATTN: DASD(EE&S)

Field Command, DNA, Det 2
Lawrence Livermore National Lab
ATTN: FC-1

Field Command, DNA, Det 3, Los Alamos National Lab
ATTN: MS-635 FC-2

Field Command, DNA
ATTN: FCL
ATTN: FCPR
ATTN: FCTT, W. Summa
ATTN: FCTXE
ATTN: FCTXE, Maj Evinrude
2 cy ATTN: FCLS

Interservice Nuclear Weapons School
ATTN: TTV

DEPARTMENT OF THE ARMY

Headquarters
Department of the Army
5 cy ATTN: DAAG-ESG-N, NTPR

DEPARTMENT OF THE ARMY (Continued)

Harry Diamond Laboratories
ATTN: DELHD-TA-L, 81100, Tech Lib

Office of the Chief of Staff
ATTN: DACS-DMZ-A, T. Green

US Army Center of Military History
ATTN: Library

USA Ballistic Research Labs
ATTN: DRDAR-BLV-R, J. Maloney

USA Medical Research & Dev Cmd
ATTN: SGRD-SD

USA Nuclear & Chemical Agency
ATTN: MONA-ZB, C. Davidson

Walter Reed Army Medical Center
ATTN: Library

DEPARTMENT OF THE NAVY

Bureau of Medicine and Surgery
ATTN: NM&S-00
ATTN: NM&S-09
ATTN: NM&S-3C22

Marine Corps History & Museums
ATTN: Historical Division

National Naval Medical Center
ATTN: Dept of Radiology
ATTN: Medical Library

Naval Medical Rsch Institute
ATTN: Tech Ref Library

Naval Ocean Systems Center
ATTN: Research Library

Naval Sea Systems Command
ATTN: SEA-08, M. Miles

Naval Surface Weapons Center
ATTN: Code F31, D. Levine

Naval Weapons Evaluation Facility
ATTN: G. Binns

Office of the Deputy Chief of Naval Ops
ATTN: NOP 0455
ATTN: NOP 098

Operational Archives Branch
ATTN: DD Allard

US Marine Corps
ATTN: MGNTPR

DEPARTMENT OF THE AIR FORCE

Aerospace Medical Div
ATTN: Library SCL-4

DEPARTMENT OF THE AIR FORCE (Continued)

Air Force Historical Rsch Center
ATTN: Library

Air Force Inst of Technology
ATTN: ENP, J. Bridgeman
ATTN: Library

Air Force Weapons Lab
ATTN: DYT
ATTN: NT
ATTN: SUL

Air University Library
ATTN: AUL-LSE

HQ USAF/SG
ATTN: M. Chesney

USAF Nuclear Test Personnel Review
4 cy ATTN: Col Gibbons

USAF Occupational & Env Health
ATTN: CC
4 cy ATTN: AFNTPR

DEPARTMENT OF ENERGY

Department of Energy
Albuquerque Operations Office
ATTN: R. Cuddihy

Department of Energy
Office of Military Application, GTN
ATTN: OMA, C. Morris
ATTN: OMA, DP-22

Department of Energy
Nevada Operations Office
ATTN: B. Church
ATTN: Health Physics Div
ATTN: L. O'Neal
ATTN: Public Affairs

Department of Energy
Human Health & Assess Div
ATTN: C. Edington, EV-31
ATTN: H. Hollister, EV-4
ATTN: J. Blair, EV-32
ATTN: J. Thiesen, EV-32
ATTN: J. Whitnah, EV-50
ATTN: N. Barr, EV-32
ATTN: Tech Info Center, E-201
ATTN: W, Burr, EV-2

OTHER GOVERNMENT AGENCIES

Cancer Center, NIH
ATTN: A. Knudson

Centers for Disease Control
ATTN: Consolidated Surveillance
ATTN: K. Choi
2 cy ATTN: G. Caldwell

Central Intelligence Agency
ATTN: Office of Medical Services

Consumer Product Safety Comm
ATTN: M. Bloom
ATTN: P. Pruess

OTHER GOVERNMENT AGENCIES (Continued)

Dep of Health & Human Svcs
ATTN: Ofc of Regulation Review

Department of Agriculture
ATTN: M. Carter

Department of Agriculture
ATTN: R. Jarrett

Department of Commerce
National Bureau of Standards
ATTN: C. Kuyatt
ATTN: J. Hubell
ATTN: M. Ehrlich

Department of Labor
ATTN: S. Weiner

Department of Transportation
Federal Aviation Administration
ATTN: H. Reighard

Department of Health & Human Services
Bureau of Radiological Health
ATTN: C. Silverman, HFX-101
ATTN: G. Johnson, HFX-4
ATTN: J. Villforth, HFX-1

National Center for Health Statistics
ATTN: R. Murphy

Environmental Protection Agency
ATTN: P. Magno
ATTN: T. Thorslund, RD-689

Environmental Protection Agency
ATTN: J. Knelson

Environmental Protection Agency
ATTN: D. Rosendaum, ANR-458
ATTN: N. Nelson, ANR-460
ATTN: W. Ellett, ANR-460
ATTN: W. Mills, ANR-460

Federal Emergency Management Agency
ATTN: Asst Assoc Dir for Rsch, J. Kerr
ATTN: C. Siebentritt
ATTN: Ofc of Rsch/NP, D. Bensen

Library of Congress
ATTN: Science & Technology Div

NASA Headquarters
ATTN: M/S SBR-3, P. Rambaut

National Cancer Institute
ATTN: B. Wacholz
ATTN: E. Stonehill
ATTN: G. Beebe
ATTN: M. Knipmayer
ATTN: V. Zeve

National Cancer Institute
ATTN: C. Land
ATTN: J. Fraumeni
ATTN: W. Blot

National Cancer Institute
ATTN: J. Gart

OTHER GOVERNMENT AGENCIES (Continued)

National Cancer Institute
ATTN: A. Rabson
ATTN: D. Pistenmaa
ATTN: J. Wyngaarden

National Institute for Occupational Safety & Health
ATTN: W. Murray

National Institutes of Health
ATTN: Library, Acquisition Unit

National Science Foundation
ATTN: Kin-Ping Wong
ATTN: P. Haarlman

Natl Heart, Lung & Blood Institute
ATTN: W. Zukel

National Library of Medicine
ATTN: Library

Office of Technology Assessment
ATTN: M. Gough

Office on Smoking & Health
ATTN: J. Pinney

US Senate
Subcommittee of Nucl Reg Comm for Envir & Public Works
ATTN: J. Curtiss

US House of Representatives
Committee on Armed Services
ATTN: Subcommittee on Mil Per & Comp

US House of Representatives
Committee on Veteran's Affairs
ATTN: C. Graves
ATTN: C. Moore
ATTN: F. Stover
ATTN: M. Fleming
ATTN: R. Wilson

US Public Health Service
ATTN: Library

US Senate
Committee on Armed Services
ATTN: J. McGovern

US Senate
Committee on Veterans Affairs
ATTN: J. Steinberb
ATTN: J. Susman
ATTN: K. Burdick
ATTN: T. Principi
ATTN: V. Raymond
ATTN: W. Brew

US Senate
Committee on Governmental Affairs
ATTN: S. Ulm

US Nuclear Regulatory Commission
ATTN: R. Whipp for F. Arsenault
ATTN: R. Whipp fpr R. Minogue
ATTN: R. Whipp for W. Mills

US Public Health Service Hospital
ATTN: E. Nishimura

OTHER GOVERNMENT AGENCIES (Continued)

Veterans Adm Wadsworth Hospital Center
ATTN: T. Makinodan

Veterans Admin Medical Center
ATTN: K. Lee

Veterans Admin Medical Center
ATTN: D. McGregor

Veterans Admin Medical Center
ATTN: C. Tessmer

Veterans Administration
ATTN: B. Polcari
ATTN: D. Bosch
ATTN: J. Donsbach
ATTN: J. Smith
ATTN: L. Hobson
2 cy ATTN: D. Starbuck

Veterans Administration
ATTN: Director

Veterans Administration
ATTN: Director

Veterans Administration
ATTN: Director

Veterans Administration
ATTN: Director

Veterans Administration
ATTN: Director

Veterans Administration
ATTN: Director

Veterans Adminstration
ATTN: Director

Veterans Administration
ATTN: Director

Veterans Administration
ATTN: Director

Veterans Administration
ATTN: Director

Veterans Administration
ATTN: Director

Veterans Administration
ATTN: Director

Veterans Administration
ATTN: Director

Veterans Administration
ATTN: Director

Veterans Administration
ATTN: Director

OTHER GOVERNMENT AGENCIES (Continued)

Veterans Administration
ATTN: Director

Veterans Administration
ATTN: Director

Veterans Administration
ATTN: Director

Veterans Administration
ATTN: Director

Veterans Administration
ATTN: Director

Veterans Administration
ATTN: Director

Veterans Administration
ATTN: Director

Veterans Administration
ATTN: Director

Veterans Administration
ATTN: Director

Veterans Administration
ATTN: Director

Veterans Administration
ATTN: Director

Veterans Administration
ATTN: Director

Veterans Administration
ATTN: Director

Veterans Administration
ATTN: Director

Veterans Administration
ATTN: Director

Veterans Administration
ATTN: Director

Veterans Administration
ATTN: Director

Veterans Administration
ATTN: Director

Veterans Administration
ATTN: Director

Veterans Administration
ATTN: Director

Veterans Administration
ATTN: Director

Veterans Administration
ATTN: Director

Veterans Administration
ATTN: Director

OTHER GOVERNMENT AGENCIES (Continued)

Veterans Administration
ATTN: Director

Veterans Administration
ATTN: Director

Veterans Administration
ATTN: Director

Veterans Administration
ATTN: Director

Veterans Administration
ATTN: Director

Veterans Administration
ATTN: Director

Veterans Administration
ATTN: Director

Veterans Administration
ATTN: Director

Veterans Administration
ATTN: Director

Veterans Administration
ATTN: Director

Veterans Administration
ATTN: Director

Veterans Administration
ATTN: Director

Veterans Administration
ATTN: Director

Veterans Administration
ATTN: Director

The White House
ATTN: Ofc of Policy Dev (DP)

US House of Representatives
Committee on Interstate & Foreign Commerce
ATTN: Subcommittee on Health & Envir

FOREIGN AGENCIES

Canadian Embassy
ATTN: Library

EDF-RETN 1
French Engr Bureau
ATTN: Library

Medical Enclave, Ansari Nagar
ATTN: A. Taskar

Japan-Hawaii Cancer Study
ATTN: G. Glober

French Engineering Bureau
ATTN: M. Delpla

McGill University
ATTN: R. O'Seasohn

FOREIGN AGENCIES (Continued)

Comitato Nazionale Per L'Energia Nucleare
ATTN: Library

Puerto Rico School of Medicine
ATTN: Library

United Kingdom Scientific Miss
ATTN: Military Liaison for D. Fakley
2 cy ATTN: Publications (for MRC) SO 128

OTHER

Brookhaven National Laboratory
ATTN: A. Brill, Medical Dept
ATTN: E. Cronkite, Medical Dept
ATTN: M. Bender, Medical Dept
ATTN: Technical Library
ATTN: V. Bond

California Institute of Technology
ATTN: E. Lewis
ATTN: R. Christy

University of Chicago
ATTN: P. Meier

University of Colorado
ATTN: Library

Columbia University
ATTN: A. Bloom
ATTN: Library

Columbia University
ATTN: Div of Biostatistics

Cornell University
ATTN: W. Federer

University of Drew
ATTN: Library

Medical College of Georgia
ATTN: L. Stoddard

Harvard School of Public Health
ATTN: J. Bailor
ATTN: Library
ATTN: R. Reed

Harvard School of Public Health
ATTN: B. MacMahon

Harvard University
ATTN: W. Cochran

University of Hawaii
ATTN: Y. Matsumoto

Indiana University
ATTN: F. Putnam

Iowa State University
ATTN: T. Brancroft

Johns Hopkins University
ATTN: A. Kimball
ATTN: A. Lilienfield
ATTN: R. Seltser

Kansas University, Agri & Applied Sci
ATTN: H. Fryer

OTHER (Continued)

Kingston Hospital
ATTN: K. Johnson

Memorial Hospital for Cancer and Allied Diseases
ATTN: P. Lieberman

Memorial Sloan-Kettering Cancer Center
ATTN: J. Laughlin
ATTN: P. Marks

Merck, Sharp & Dohme Intl
ATTN: A. Bearn

University of Miami
ATTN: P. Hodes

University of Michigan Medical School
ATTN: J. Neel

University of Michigan
ATTN: R. Cornell

University of Michigan
ATTN: F. Moore

Minnesota Dept of Health
ATTN: D. Lilienfield

University of Minnesota
ATTN: J. Bearman
ATTN: L. Schuman
ATTN: Library

Natl Council on Radiation Protection & Measurements
ATTN: W. Sinclair

University of New Mexico
ATTN: C. Key
ATTN: R. Anderson

New York University Medical Center
ATTN: N. Nelson

New York University
ATTN: A. Upton
ATTN: B. Posternack
ATTN: Library
ATTN: M. Eisenbud

University of North Carolina
ATTN: B. Greenberg
ATTN: Library for Dean

Northwestern University
ATTN: H. Cember

Oak Ridge Assoc Universities
ATTN: D. Lushbaugh
ATTN: E. Tompkins
ATTN: J. Totter

University of Oaklahoma
ATTN: P. Anderson

University of Oregon
ATTN: B. Pirofsky

Pacific Northwest Laboratory
ATTN: S. Marks

OTHER (Continued)

Pennsylvania University Hospital
ATTN: S. Baum

University of Pennsylvania
ATTN: P. Nowell

University of Pittsburgh
ATTN: E. Radford
ATTN: Library

University of Pittsburgh
ATTN: N. Wald

Rochester University Medical Center
ATTN: C. Odoroff
ATTN: G. Casarett

University of Rochester
ATTN: L. Hempelmann

Saint Francis Hospital
ATTN: R. Blaisdell

Medical University of South Carolina
ATTN: P. Liu

University of Southern California
ATTN: J. Birren

Stanford University Medical Center
ATTN: J. Brown

Stanford University
ATTN: L. Moses

Stanford University Hospital
ATTN: D. Dorfman

Texas A & M University
ATTN: R. Stone

University of Texas at Austin
ATTN: H. Sutton

University of Texas
ATTN: C. Cook

University of Texas
ATTN: R. Stallones

University of Texas
ATTN: W. Sutow

University of Texas
ATTN: G. Taylor

University of Utah
ATTN: Library

University of Utah
ATTN: C. Mays
ATTN: E. Wrenn
ATTN: L. Lyons
ATTN: Library

Vanderbilt University
ATTN: R. Quinn

University of Washington
ATTN: D. Thompson

OTHER (Continued)

University of Washington
ATTN: A. Motulsky

University of Wisconsin
ATTN: J. Crow

Yale University School of Medicine
ATTN: J. Meigs
ATTN: Library

DEPARTMENT OF ENERGY CONTRACTORS

University of California
Lawrence Livermore National Lab
ATTN: L. Anspaugh
ATTN: Tech Info Dept Library
ATTN: Y. Ng

Los Alamos National Laboratory
ATTN: J. Dummer
ATTN: Library
ATTN: M/S634, T. Dowler
ATTN: MS218, P. Whalen

Oak Ridge National Laboratory
ATTN: C. Richmond
ATTN: G. Kerr
ATTN: J. Auxier

Oak Ridge National Laboratory
ATTN: T. Jones

Reynolds Electrical & Eng Co, Inc
ATTN: J. Brady
ATTN: LST
2 cy ATTN: CIC

Sandia National Laboratories
ATTN: Div 1314, S. Durpee

DEPARTMENT OF DEFENSE CONTRACTORS

Advanced Res & Applications Corp
ATTN: R. Armistead

BDM Corp
ATTN: J. Braddock

Colorado State University
ATTN: M. Zelle

Energy Systems, Inc
ATTN: T. Gates

JAYCOR
ATTN: A. Nelson

Kaman Tempo
ATTN: DASIAC

LA Univ School of Medicine, Shreveport
ATTN: Library

National Academy of Sciences
ATTN: National Materials Advisory Board
ATTN: S. Jablon
ATTN: S. McKee
7 cy ATTN: C. Robinette

DEPARTMENT OF DEFENSE CONTRACTORS (Continued)

University of Nebraska
ATTN: Library

Ohio State University
ATTN: Library

Pacific-Sierra Research Corp
ATTN: H. Brode, Chairman SAGE

R&D Associates
ATTN: C. Lee
ATTN: P. Haas

R&D Associates
ATTN: A. Deverill

Radiation Research Associates, Inc
ATTN: N. Schaeffer

Rand Corp
ATTN: Library
ATTN: P. Davis

DEPARTMENT OF DEFENSE CONTRACTORS (Continued)

Rand Corp
ATTN: B. Bennett

Science Applications Intl Corp
ATTN: C. Thomas
ATTN: J. Klemm
ATTN: W. McRaney
2 cy ATTN: J. Goetz
5 cy ATTN: J. McGahan

Science Applications, Inc
ATTN: J. Striegal

Science Applications, Inc
2 cy ATTN: D. Kaul
2 cy ATTN: S. Egbert
2 cy ATTN: J. Roberts

Scientific Info Svcs, Inc
ATTN: Library

Varian Associates, Inc
ATTN: E. Tochilin, Radiation Div C-063

END

FILMED

1-86

DTIC